IN-SILICO GUIDED SYNTHESIS AND CHARACTERIZATION OF NOVEL ELECTROPHILIC CARBENES

by

M. Brenton Gildner B.S.

A thesis submitted to the Graduate Council of
Texas State University in partial fulfillment
of the requirements for the degree of
Master of Science
with a Major in Chemistry
August 2018

Committee Members:

Todd Hudnall

Debra Feakes

William Brittain

FAIR USE AND AUTHOR'S PERMISSION STATEMENT

Fair Use

Duplication Permission

ACKNOWLEDGEMENTS

I want to start by thanking my advisor Dr. Todd Hudnall for giving me the opportunity to work in his lab my graduate and undergraduate research. He always pushed me to question everything and be a better scientist. I am thankful that he allowed me the freedom to take my own path with my project and guiding me when I needed help with a part of my project. I always enjoyed our brainstorming sessions trying to figure out how to synthesize a new molecule.

I also want to thank all the Hudnall group members for their support and for making being in the lab so fun. I've really enjoyed going through my masters together with one of my best friends, Isaac Blythe. We've learned so much from each other over the years and our late-night D&D sessions were the best. I also want to thank our former post-doc Dr. Tharushi Perera; she taught me so much about DFT and photochemistry. I want to thank Dr. Ben Shoulders for all his help with NMR. I also want to thank Dr. Chris Dorsey for his help when I had questions about synthesis or fixing equipment.

Lastly, I need to thank my amazing wife, Laura, I would not be here without her. Her motivation inspired me to always work harder and push myself to be the best I can. I could not have made it through this without her love and support. She always encouraged and convinced me to push through even when it seemed like I would never get my chemistry to work. I can never thank her enough for going through this with me.

TABLE OF CONTENTS

Page

LIST OF TABLES

Table **Page**

LIST OF FIGURES

Figure **Page**

LIST OF ABBREVIATIONS

Abbreviation	Description
Ad	Adamantyl
aDAC	abnormal diamido carbene
CAAC	cyclic(alkyl)amino carbene
CAAmC	cyclic(alkyl)amido carbene
CAArC	cyclic(alkyl)aryl carbene
CAmArY	cyclic(amido)aryl carbene
COD	cyclooctadiene
DAAC	diamido(alkenyl)carbene
DAC	six-membered diamido carbene
DAC5	five-membered diamido carbene
DCM	dichloromethane
DFT	density functional theory
DIBAL-H	diisobutyl aluminum hydride
DIC	six-membered diimino carbene
DIC5	five-membered diimino carbene
Dipp	2,6-diisopropylphenyl
DMF	N,N-dimethylformamide
DMMC	dimethylmalonyl dichloride
DMSO	dimethylsufoxide
HOMO	highest occupied molecular orbital
IC	indole-derived carbene
IMes	N,N’dimesitylimidizolylidene
IPr	N,N’bis(dipp)imidazolylidene
iPr	isopropyl
KOtBu	potassium tert-butoxide
LDA	lithium diisopropyl amide
LUMO	lowest unoccupied molecular orbital
MAAC	mono(amido)amino carbene
Mes	2,4,6-trimethylphenyl
MO	molecular orbital
NaHMDS	sodium hexamethyldisilyl amide
nBuLi	n-butyl lithium
NHC	N-heterocyclic carbene
NMR	nuclear magnetic resonance
OTf	triflate

TEP	Tolman electronic parameter
THF	tetrahydrofuran
TMS	trimethylsilyl or tetramethylsilane
XRD	X-ray diffraction

ABSTRACT

The synthesis and electronic characterization of two new electrophilic carbenes is described. The synthesized carbenes were selected based on computational studies investigating the HOMO and LUMO energies of various new carbenes.

The cyclic(amido)arylcarbene (CAmArY) could not be isolated due to rapid dimerization when the carbene was generated. The carbene dimer was characterized through NMR, mass spectrometry, and X-ray crystallography. A sulfur trapping experiment was performed to confirm the generation of the carbene. The π-accepting ability of CAmArY was studied via selenium NMR. As of this writing, the CAmArY selenium adduct is the most π-accepting carbene with a selenium NMR shift of 1240 ppm. Tolman Electronic Parameter (TEP) studies could not be completed due to decomposition of the iridium and rhodium metal complexes which is discussed in further detail below.

A series of diiminocarbenes (DICs) were synthesized in good yields. DICs were isolated successfully and characterized through NMR and a single crystal X-ray structure of one free DIC was obtained. The π-accepting ability of the DICs were also studied via ^{77}Se NMR. The DIC selenium adducts displayed ^{77}Se NMR shifts ranging from 640 - 699 ppm, which suggests a π-accepting ability greater than CAAC but less than the DACs. TEP studies were performed by synthesizing the iridium (I) dicarbonyl chloride complex of the parent DIC and examining the stretching frequencies of the metal carbonyls via IR spectroscopy. The TEP value of the DIC was determined to be 2046

cm^{-1} which places its overall donating ability very similar to CAAC. To determine the effect of *para*-substitution of the arylimino substituents, DFT calculations were performed and a Hammett analysis was performed which showed that the level of the LUMO energy was more effected than the HOMO energy level. The selenium adducts of some of these DIC derivatives were prepared to conduct a Hammett analysis by plotting the ^{77}Se NMR chemical shift versus the respective LUMO level. This Hammett analysis revealed a direct correlation of the LUMO energy level to the ^{77}Se NMR shift.

The synthesis of two other carbenes, an abnormal diamidocarbene (aDAC) and an indole derived carbene (IC) has been started. The synthetic routes currently being employed to synthesize the carbene precursors is described herein along with future efforts to prepare and characterize these carbenes.

I. INTRODUCTION

General Introduction

A carbene is a molecule that contains a neutral divalent carbon atom and six valence electrons. There are two ground state electronic configurations possible for a carbene, a singlet or a triplet carbene (Figure 1). The triplet carbene has two unpaired electrons and is sp-hybridized, they are usually acyclic and linear.[1] Triplet carbenes are considered biradicals. Due to their biradical nature, they are incredibly reactive and are short-lived intermediates generated *in-situ* for reactions. Hideo Tomioka has recently synthesized some relatively stable triplet carbenes with half-lives of up to a week in solution.[2–4] Singlet carbenes are much more stable than triplet carbenes. Many singlet carbenes are stable enough in the solid state to be stored indefinitely under inert atmosphere. Singlet carbenes have a lone pair of electrons, an empty orbital, and are sp^2-hybridized. Singlet carbenes are typically cyclic, but there are some stable acyclic carbenes reported.[1,5–8] Singlet carbenes are unreactive toward oxygen, but are sensitive to water.

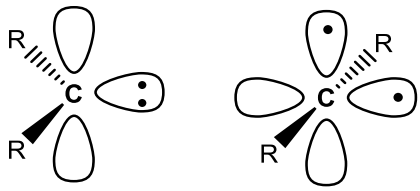

Figure 1 A singlet and triplet carbene

History of Carbenes

Although stable carbenes are a relatively recent discovery, they have an interesting history. The first attempt to synthesize a carbene was by Dumas in 1835. It was common knowledge that alcohols could be dehydrated, and so Dumas began his

attempts to dehydrate methanol using P_2O_5 (Figure 2).[9] This would have resulted in the formation of methylene, a neutral divalent carbon with two hydrogen atoms, but his attempts to dehydrate methanol were unsuccessful. At this time it was not known that carbon was tetravalent; that discovery was not made until 1931 by Linus Pauling.[10] As others would later learn, additional stabilization to the carbon center is required to generate a stable carbene.

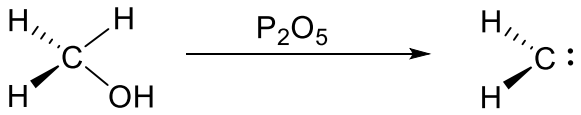

Figure 2 Reaction showing the potential product of Dumas's dehydration of methanol

The modern idea of a carbene was first introduced by Büchner in 1903. He was studying the reactivity of diazoesters which release elemental nitrogen and a carbene upon photolyzing or heating.[11] By refluxing diazoethylacetate with toluene, the triplet carbene generated inserts into the carbon–carbon bond of toluene to form a cycloheptatriene, a seven-membered ring, shown in Figure 3. This reaction is now known as the Büchner ring expansion and is a reaction that is exclusively accomplished by triplet carbenes.[12]

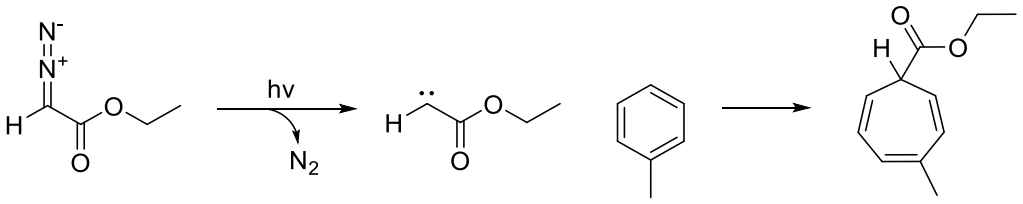

Figure 3 Büchner ring expansion of a triplet carbene with toluene

In the late 1950's, Breslow was studying the reactivity of thiamine molecules, a coenzyme used in biochemical reactions. Based on known reactivity of alkyl-pyridinium compounds and the similarity to N-ethylthiazole, Breslow expected the reaction of one

equivalent of base and one equivalent of benzaldehyde to form the condensation product shown on the left in Figure 4. Instead the thiazolium was deprotonated to form the thiazole carbene *in situ* which catalytically reacted with benzaldehyde to form benzoin, shown on the right in Figure 4.[13] The catalytic mechanism of the role of the thiazolylidene is shown in Figure 5. During the catalytic cycle, the neutral molecule that was suspected to be formed is known as the Breslow intermediate. Isolation of the Breslow intermediate eluded scientists for over 60 years until, in 2012 DiRocco, isolated the intermediate using a similar thiazoleylidene.[14]

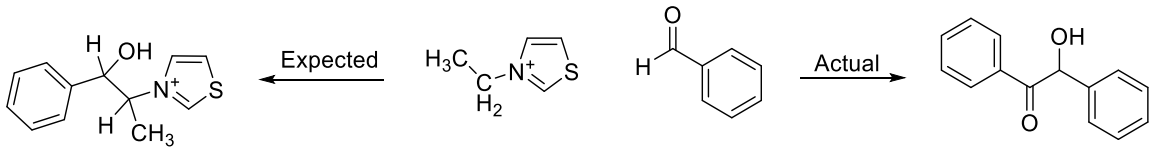

Figure 4 Expected and actual reaction products of Breslow's thiazole studies. On the left was the expected formation of the alcohol with benzaldehyde. On the right is the actual product of the catalytic formation of benzoin.

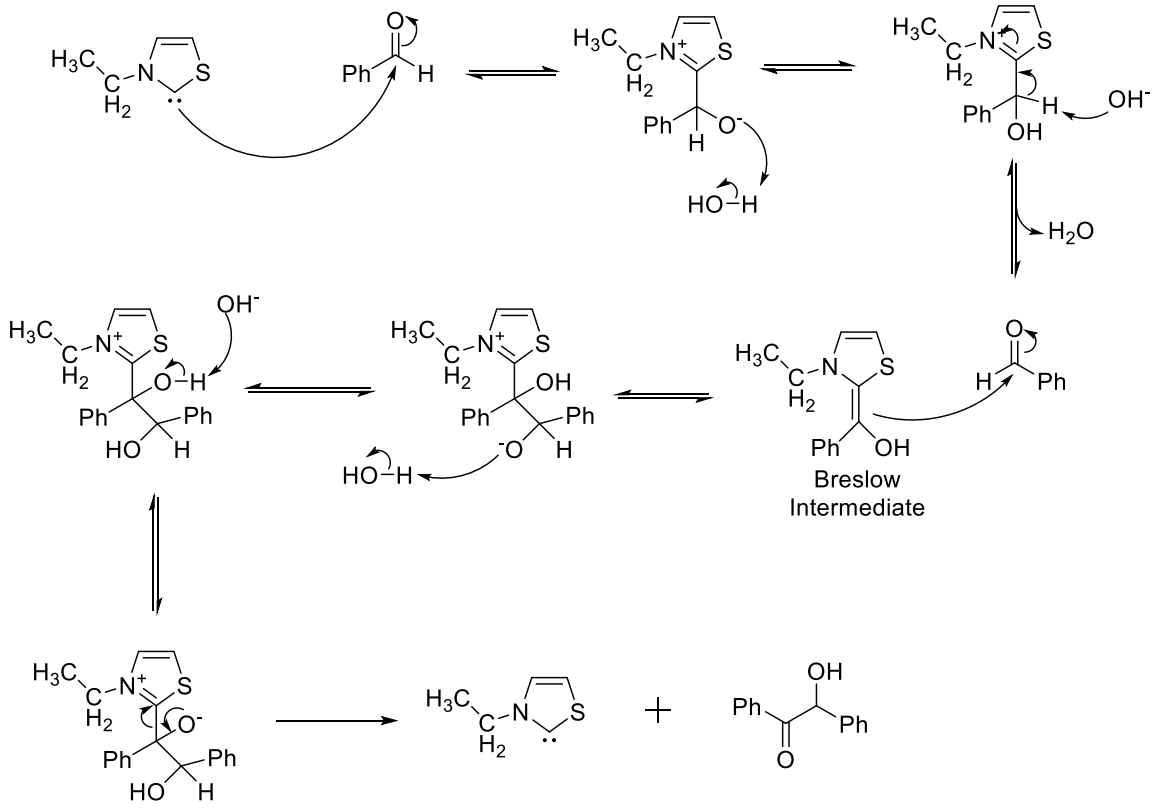

Figure 5 Catalytic mechanism of the condensation of benzaldehyde to benzoin with Breslow's thiazoleylidene. The Breslow intermediate is shown also.

In 1961, Wanzlick synthesized the first *N*-heterocyclic carbene, commonly referred to as an NHC, but could not isolate the free carbene. He found that his NHC would dimerize but was in equilibrium with the free carbene.[15] If an acid such as HCl was added to the carbene dimer, two equivalents of the carbene HCl salt were formed. This is now known as the Wanzlick equilibrium, carbenes without sufficient steric protection can dimerize. For carbenes that have an aromatic heterocycle, the equilibrium is pushed toward the free carbene since the aromaticity is broken when the dimer is formed (Figure 6).[16]

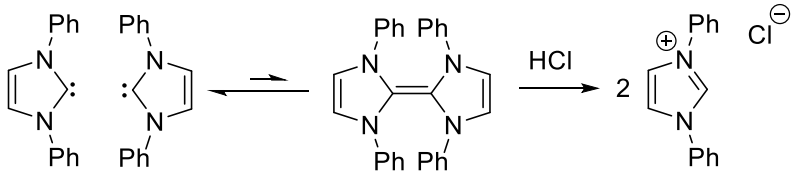

Figure 6 Wanzlick equilibrium of carbene dimers

It wasn't until 1988 when Bertrand synthesized the phosphinosilylcarbene (Figure 7). It was the first carbene to be isolated, but it couldn't be fully characterized because it was a liquid that would decompose slowly even under inert atmosphere.[17] His carbene had greater stability through steric protection from the trimethylsilyl group and better electronic stabilization from the phosphorous. Finally, in 1991, Arduengo synthesized the first stable, solid, isolable carbene.[18] Arduengo's NHC differs from Wanzlick's NHC by substituting the phenyl groups with adamantyl groups (Figure 7). This increased steric protection kinetically stabilizes the carbene from dimerization.[19] Since then many derivatives of NHCs have been isolated and studied.[20]

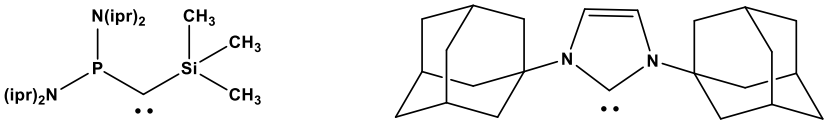

Figure 7 Bertrand's phosphinosilylcarbene[17] (left) and Arduengo's *N,N'*-diadamantyl n-heterocyclic carbene (right)[18].

Stabilizing Carbenes

For a carbene to be stable, it needs to be stabilized through kinetics (sterics) and thermodynamics (electronics).[20] Carbenes can be resonance stabilized electronically by having electron donating and withdrawing atoms adjacent to the carbon atom. Typically nitrogen atoms are used as electron donating atoms adjacent to the carbene.[6,18–21] Phosphorus has also been used, as seen in Bertrand's phosphinosilylcarbene.[17] The nitrogen atoms can use their lone pairs to donate electron density into the empty p-orbital

on the carbon. (Figure 8).[1,18,22] The resonance structure shown on the left in Figure 8 shows the carbene as an ylide, with a formal negative charge on the carbene atom and a positive charge on the adjacent atom. If one of the adjacent atoms has an empty orbital, it can be used to stabilize the carbene lone pair through delocalization. For example, an sp^2-hybridized boryl substituent would feature an empty p-orbital at boron which can be used to stabilize the lone pair on the carbon atom.[23] There are computations that show a carbene that is flanked on both sides with an atom that has an empty orbital could also be resonance stabilized. Structurally this one would be different than other carbenes since the resonance structure would be with a positive charge on the carbene carbon and a negative charge on one of the adjacent atoms.[24] None of these have been isolated, but are theoretically possible.

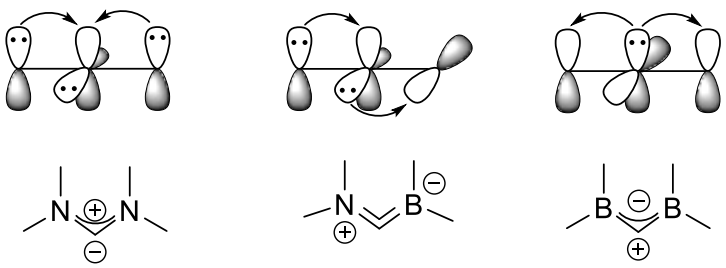

Figure 8 The three electronic methods of resonance stabilization of carbenes with two heteroatoms

Carbenes are also stabilized through inductive effects. Atoms adjacent to the carbene center that are more electronegative than carbon will inductively pull electron density away from the carbene. So, while the nitrogen atom adjacent to the carbene stabilizes the empty p-orbital, it also pulls electron density away inductively. This has the effect of further stabilizing the lone pair on the carbene carbon. Atoms that are more electropositive than carbon have the opposite effect. They will push electron density into and destabilize the carbene carbon. These inductive effects can be categorized in three

ways: push-push, push-pull, and pull-pull, depending on the nature of the substituents on the carbene carbon.[1]

Stability of carbenes is further increased if the ring is aromatic.[19] Usually carbenes require kinetic stabilization to prevent dimerization, there are only a few examples of stable carbenes without any protection from bulky groups.[25,21] Common protecting groups include 2,6-diisopropylphenyl (or Dipp), 2,4,6-trimethylphenyl, (or mesityl, Mes), *t*-butyl, and adamantyl (or Ad).

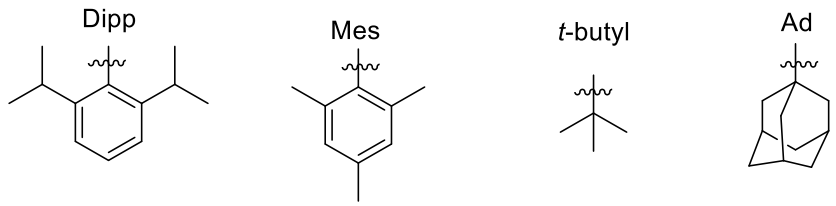

Figure 9 Common carbene protecting groups: Dipp, Mes, *t*-butyl, and Ad.

Molecular Orbital Theory

Molecular orbital (MO) theory is a method for describing the bonding in molecules where electrons are not confined to a single atom or bond, but are connected throughout the molecule.[26] MO theory can be used to estimate the relative highest occupied molecular orbital (HOMO) and lowest unoccupied molecular orbital (LUMO) energies of carbenes, these are known as the frontier orbitals. The energies of the HOMO and LUMO are important in understanding carbene reactivity. In a carbene, the HOMO is usually the lone pair located on the carbene carbon; the LUMO is usually the empty p-orbital on the carbene carbon. Singlet carbenes are one of the strongest neutral bases, this is due to the very high energy HOMO.[1] A high energy HOMO will result in a carbene that can donate more electron density, this is also referred to as its σ-donating ability. A somewhat unique feature of carbenes is the ability to act as a Lewis acid and a Lewis

base at the same time, on the same atom. The relative energy of the LUMO will determine the carbene's ability to engage in π-backbonding with other atoms, also called π-accepting ability or π-acidity. The HOMO-LUMO gap is another important aspect for carbenes. A smaller HOMO-LUMO gap relates to a smaller singlet-triplet gap. The singlet-triple gap of a carbene increases as electronegative atoms are installed adjacent to the carbene.[27] Electronegative groups will also have the effect of lowering the HOMO energy through the inductive pull effect. Electropositive atoms will raise the HOMO energy of the carbene. A smaller gap should allow easier excitation to a triplet carbene through photolysis or other methods. If the HOMO-LUMO gap for a carbene gets too small, it will be in a triplet ground-state and so it won't be stable enough to isolate. The longest half-life for a triplet carbene is reported to be about a week.[28]

Types of Carbenes

By comparing the different types of carbenes, we can see what effects the different functional groups have on the stability and reactivity of the carbene. NHCs (Figure 10) are one of the most nucleophilic of all the carbenes, they have a higher lying HOMO making them better sigma donor ligands.[20] They are such good sigma donors because they have two nitrogen atoms that can donate into the carbene and do not feature any electron withdrawing groups. The heterocyclic rings of some NHCs are also aromatic which additionally stabilizes the LUMO. This has the effect of also raising the energy level of the LUMO, which causes the NHCs to be the least electrophilic, but one of the most stable, of the carbenes. NHCs are one of the few examples of a carbene that can be stabilized purely through electronic stabilization.[21] There is even an example of an NHC that is completely air stable, which has replaced the protons in the backbone of the

carbene with chlorines.[29] Typically NHCs are used as a ligand in transition metals and for stabilizing reactive main group complexes, but are also used as organocatalysts.[30–32]

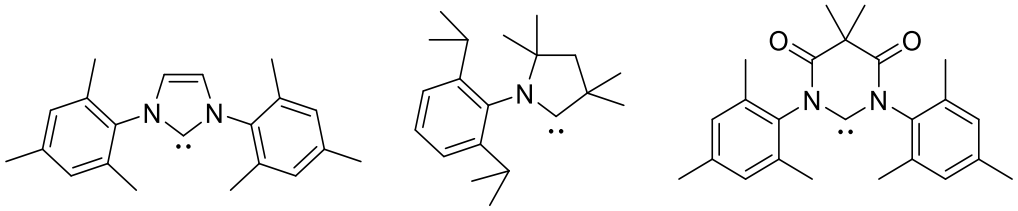

Figure 10 An NHC[18], CAAC[22], and DAC[33]

The cyclic alkyl amino carbene, or CAAC, is the most nucleophilic of the known carbenes.[22] CAACs were synthesized by replacing one of the nitrogen atoms in the NHCs with a quaternary carbon adjacent to the carbene carbon. Since carbon is a less electronegative atom when compared to nitrogen, it raises the level of the HOMO without really changing the level of the LUMO. The removal of one of the electronegative nitrogen atoms also has the effect of decreasing the singlet-triplet gap. CAAC has a smaller singlet-triplet gap than any of the other nucleophilic carbenes. The combination of a high-lying HOMO and a small singlet-triplet gap allows CAAC to do some unique chemistry compared to other carbenes that typically is only seen in reactions with transition metals, most notably that CAAC is the only singlet carbene to date that is able to split hydrogen.[34]

Diamidocarbenes (DACs) are similar to the NHCs in that they have two nitrogen atoms adjacent to the carbene but they are changed from amino to amido moieties.[33] This causes the lone pair on the nitrogen atoms to be delocalized into the electron withdrawing carbonyl groups. The carbonyl groups reduce the nitrogen atom's ability to stabilize the empty p-orbital of the carbene. The resonance structure shown in Figure 11 shows why the nitrogen cannot donate into the carbene as well. This causes the energy of the LUMO

to drop drastically when compared to CAAC and the NHCs, resulting in a very electrophilic or π-accepting carbene. The addition of the carbonyl groups into the heterocyclic rings causes a lowering of the HOMO through inductive effects resulting in DAC also being a weak σ-donor. DAC has roughly the same σ-donating ability as a trialkylphosphine.[20]

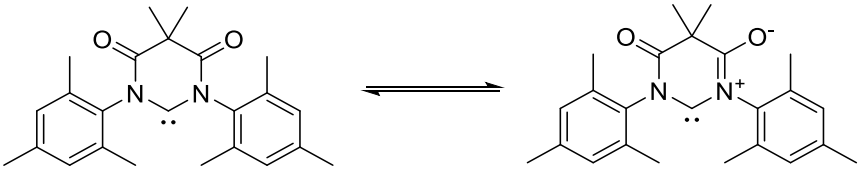

Figure 11 Resonance structure of DAC demonstrating why DAC is more electrophilic

Synthesis of Carbene Precursors

Carbenes are generated from a variety of different precursors. The most common precursors are iminium salts and hydrohalic compounds. The aromatic NHCs are synthesized through a condensation reaction with 2 equivalents of a primary amine and glyoxal to generate the diazabutadiene. The diazabutadiene is then treated with formaldehyde and acid in a ring closing condensation reaction to generate the imidazolium precursor.[18] (Figure 12)

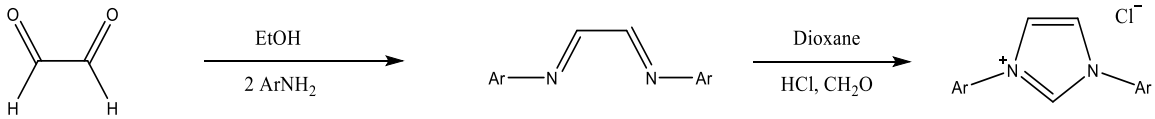

Figure 12 Synthesis of an n-heterocyclic carbene (NHC) precursor

The synthetic route for CAACs begins similarly to the NHC synthesis, through a condensation reaction of an aldehyde and an amine to give an acyclic imine. The imine is then treated with n-BuLi and a chloroalkene to add a terminal alkene to the chain. Under strong acidic conditions, the alkene is protonated to generate a tertiary carbocation which

then reacts with the imine in a ring closing reaction. This results in the cyclic iminium salt (Figure 13).[5]

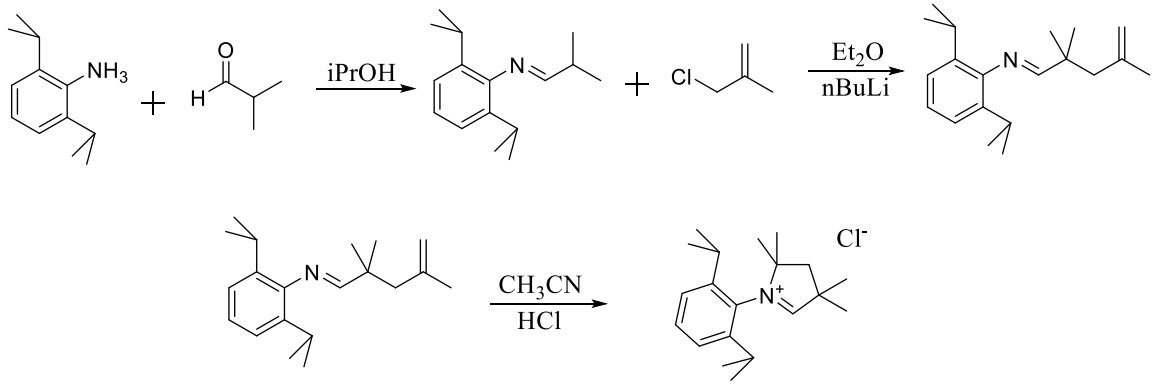

Figure 13 Synthesis of the cyclic alkyl amino carbene (CAAC) precursor

There are two commonly used DACs which have a five-membered or six-membered ring. The six-membered ring DAC can be synthesized by doing a triple condensation reaction with two equivalents of 2,4,6-trimethylaniline and triethyl orthoformate to generate the *N,N'*-dimesitylformamidine. The HCl precursor is generated by treating the formamidine with one equivalent of dimethylmalonyl dichloride (DMMC) and 1 equivalent of triethylamine.[33] The addition of the triethylamine is necessary to capture the HCl released during the reaction. In this case, the iminium salt is not obtained and instead the chloride is bound directly to the carbene carbon. This is likely due to the increased electrophilicity of the DAC.

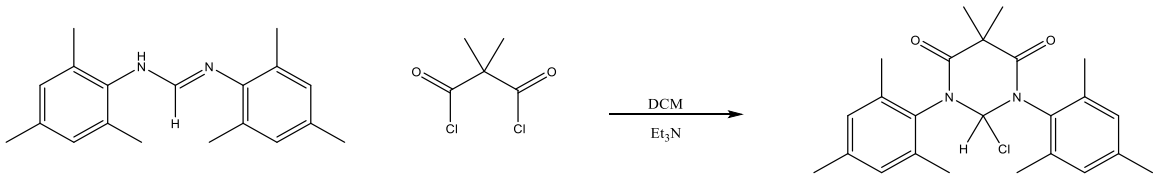

Figure 14 Synthesis of the six-membered diamido carbene (DAC) precursor

The precursor for a stable five-membered DAC is synthesized similarly to the six-membered DAC precursor, but instead uses oxalyl chloride and tert-butyl carbodiimide to

generate the dichloro precursor. The five-membered DAC can only be isolated by starting with the dichloro precursor, using the HCl precursor generates the carbene in solution but quickly dimerizes. Bielawski suggests that this is due to an acid catalyzed dimerization.[35]

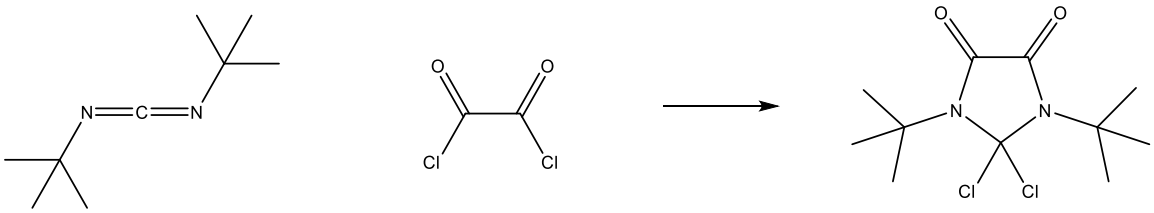

Figure 15 Synthesis of the five-membered diamido carbene (DAC5) precursor

Synthesis of Carbenes

Once the carbene precursors have been synthesized, a few common methods are used to generate the free carbene. The iminium salts and HX carbene precursors can be deprotonated using a strong base to generate the carbene.[5,18,36] Use of non-nucleophilic bases is important so that you avoid addition of the base onto the carbene carbon. The most common base for generation of carbenes is sodium hexamethyldisilamide (NaHMDS), other bases include potassium hydride, lithium diisopropylamide (LDA) and potassium tert-butoxide (KOtBu) (Figure 16).

Figure 16 Reaction schemes of deprotonation of an iminium salt and a reduction of a dichloro carbene precursor

The dichloro and thiourea precursors can be reduced to the carbene using alkali metals, typically lithium or potassium metal.[35] Reduction of the thioureas sometimes requires high temperatures and long reaction times, these reaction conditions will not work for some carbenes because of thermal decomposition.[6] Carbenes can also be generated from their diazo parent compounds through photolysis or heating to generate

N_2 gas and the carbene, shown in Figure 17.[37] These are very clean and high yielding reactions since the only byproduct is an inert gas but are typically used to generate triplet carbenes.[2,3] These are used not usually used for singlet carbenes because they are more difficult to synthesize and the diazo compounds tend to be explosive and shock sensitive.

Figure 17 Reaction scheme of the reduction of a thiourea and photolysis of a diazo carbene precursor

Reactions of Carbenes

Carbenes have many different uses but the most well-known is probably in the Grubb's generation II catalyst, which includes a carbene coordinated to a ruthenium catalyst.[31,38] The Grubb's catalyst is used for ring opening metathesis polymerization, ring closing metathesis, alkene metathesis, and other polymerization reactions. It was an improvement on the previous version of the catalyst by replacing one of the phosphine ligands with an NHC (Figure 18). The increased activity and stability of the catalyst is due to the NHC being a much better electron donor than the phosphine and is a less labile ligand than the phosphine which results in a more robust catalyst.[31] NHCs are also used as a ligand in catalytic aryl amination reactions.[7,30]

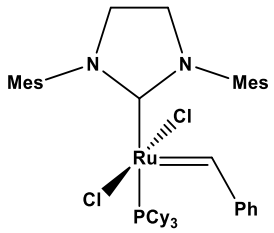

Figure 18 Grubb's generation II catalyst used in various olefin metathesis reactions

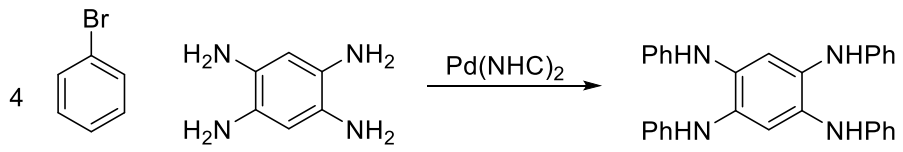

Figure 19 Catalytic aryl amination using a palladium NHC catalyst

Sometimes the carbene itself can act as a catalyst. The thiazolylidene that Breslow was studying in the 1960's would catalytically form benzoin from excess benzaldehyde (Figure 4).[13] Carbenes are also used as organocatalysts in the reactions of aldehydes with olefins to form ketones, known as the Stetter reaction.[39,40] More recently, James Hedrick has developed the use of NHCs as organocatalysts in the formation of polymers.[32] In 2003 he reported that NHCs are able to catalytically polymerize lactides.[41]

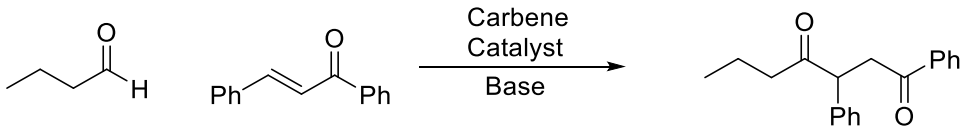

Figure 20 Carbene used as organocatalyst in the Stetter reaction

Carbenes are also very good at stabilizing reactive transition metal and main group elements. Since carbenes are neutral ligands, they do not change the oxidation state of the atom they are coordinated to. To additionally stabilize the carbene complexes, the metal can also engage in π-backbonding with the carbene, resulting in a stronger bond between the metal and carbene. Carbenes are also good at stabilizing radicals of reactive main group complexes. Our group synthesized a stable borylene radical using DAC to stabilize the radical.[42]

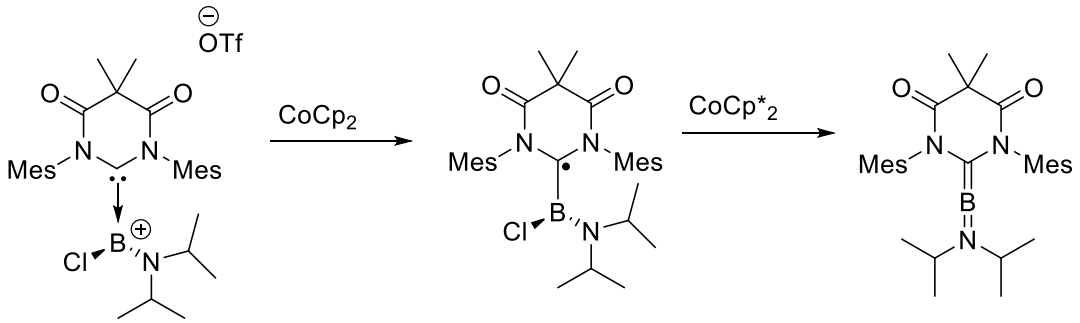

Figure 21 Carbene stabilized borylene radical

Carbenes are also known to activate small molecules. For example CAACs and DACs can fix carbon monoxide to generate ketenes.[43,44] These are usually fairly stable molecules, but some are only stable under high pressure atmospheres of carbon monoxide.[44] Moreover, both CAACs and DACs can also split ammonia, and CAACs can split dihydrogen, feats typically reserved for transition metals.[34,44] The ability of CAACs to split hydrogen is due to it being very nucleophilic and having a smaller singlet-triplet gap than other nucleophilic carbenes (Figure 22).[34]

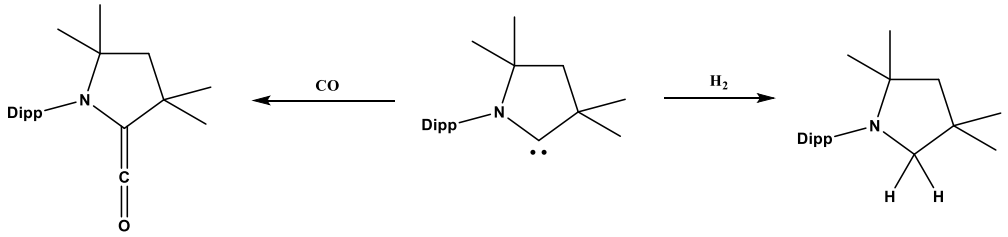

Figure 22 Small molecule activation of H_2 and CO by CAAC

Both singlet and triplet carbenes undergo cycloaddition reactions with alkenes and alkynes (Figure 23). For the former, singlet carbenes give a single cyclopropane isomer because the reaction proceeds through a concerted 2+2 cycloaddition.[5,45–48] Triplet carbenes however, can give multiple isomers because the reaction mechanism is multistep.[49] Figure 23 shows the mechanisms of cycloaddition. The intermediate in the

reaction of the triplet carbene with an olefin has freedom of rotation which gives rise to the multiple isomers seen in those reactions.

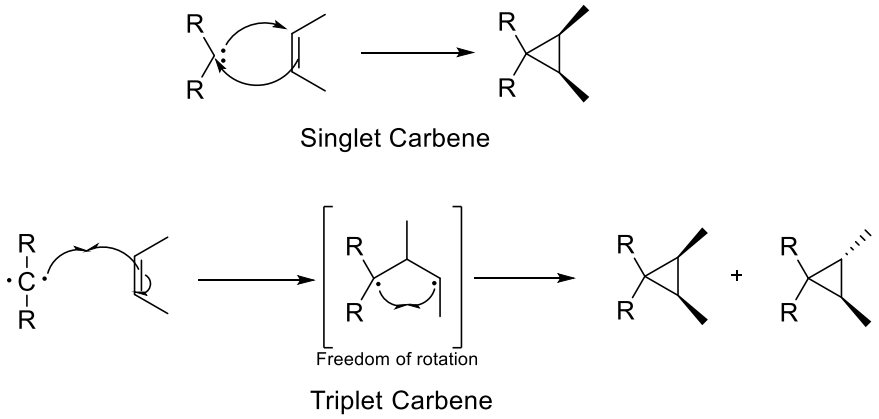

Figure 23 Cycloaddition reactions of singlet and triplet carbenes

Some carbenes can also undergo C–H and C–F insertion reactions. Usually C–H insertions are intramolecular. For example, DACs have been shown to insert into the methyl substituent on the mesityl ring under high temperatures (Figure 24).[33]

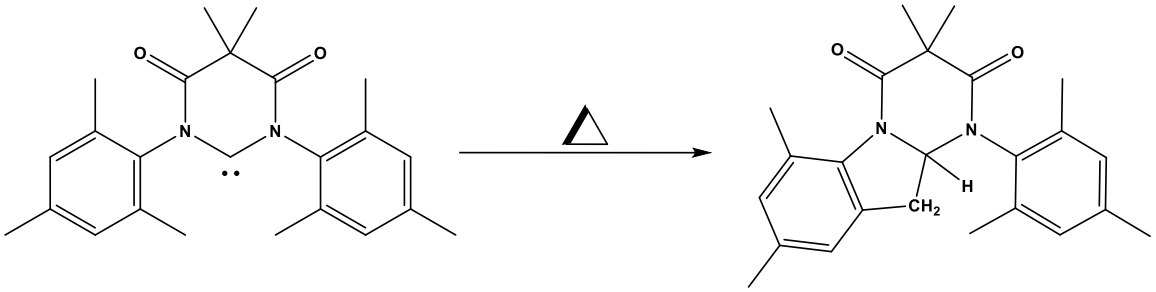

Figure 24 Thermally activated intramolecular C–H insertion by DAC

Recently our group discovered that DAC can be excited to a triplet state using UV light. This excitation to the triplet state causes the DAC to insert into the carbon–carbon bond in aromatic rings forming a cycloheptatriene (Figure 25). This is the first instance of a singlet carbene reported that is capable of achieving triplet carbene reactivity. The Büchner ring expansion product is thermally reversible, giving the DAC free carbene and benzene.[50] Other carbenes tested by our group including: CAACs, NHCs, and

mono(amido)amino carbenes (MAACs) exhibit similar photochemistry, and showed no triplet reactivity. We suspect that DAC is able to do this due to its small singlet-triplet gap and its low lying LUMO. In order to determine the reasons behind DAC's ability to undergo photochemical Büchner ring expansions – we began a systematic study geared toward the synthesis of novel electrophilic carbenes that may be photoactive.

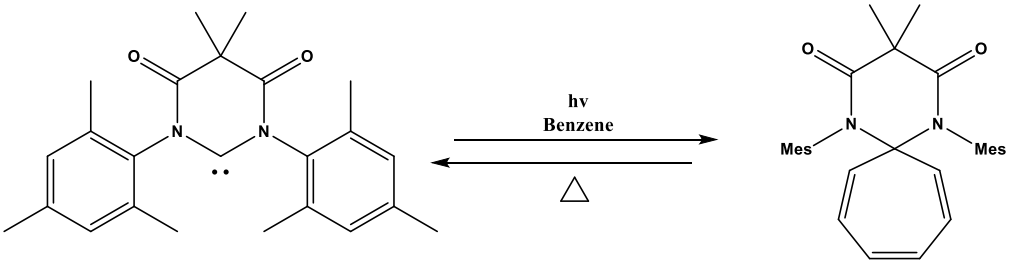

Figure 25 Photochemically activated Büchner ring-expansion of benzene by DAC

Designing New Carbenes

Density functional theory (DFT) is a computational method that can be used to investigate the electronic properties of molecules. DFT calculates the electron density within molecules and uses that information to model orbitals and orbital energies.[51] DFT analysis has been used to estimate and compare the frontier orbital energies of carbenes. All calculations were completed using B3LYP/6-31G+(d). The structure of potential new carbenes were selected by incremental changes to known carbenes. Initially we explored making changes to DAC. Changing the carbonyl groups to thiones, selenones and tellurones resulted in significant increases in HOMO-LUMO gaps, so the synthesis of those is not being pursued. Replacing the carbonyls in DAC to arylimine groups, we see a slight increase in the HOMO and LUMO energies. This carbene also has the potential to be tuned further by changing the aryl groups in the imine moiety. We expected this one to be relatively straightforward to synthesize and it will be described more in chapter 4. In our attempts to synthesize carbenes more electrophilic than DAC, we found two potential

carbenes. The diamidoalkenylcarbene (DAAC) replaces the dimethyl group in the backbone of DAC with an alkene group. This actually increased the HOMO and lowered the LUMO relative to DAC.[35] The cyclicamidoaryl carbene (CAmArY) is one of the most electrophilic carbene we have found through DFT calculations. As Bertrand saw with his CAArC, an aryl group adjacent to the carbene increases electrophilicity of the carbene significantly when compared to his CAACs.[23] To increase the electrophilicity further we changed the amino group to an amide. The synthesis and characterization of this carbene is described later in chapter 3. Other less electrophilic carbenes are also being explored currently. In an attempt to make a more electrophilic CAAC type carbene, we are exploring the synthesis of an indole derived carbene. Structurally it is very similar to Bertrand's CAArC just with the aryl group moved away from the carbene. Another interesting carbene we are currently exploring is the abnormal DAC (ADAC), which is the structural isomer of DAC. The location of the carbene carbon and one of the carbonyls are swapped resulting in a carbene very similar to Bielawski's cyclic alkyl amido carbene.[48] The indole carbene (IC) and the ADAC synthetic progress are described in chapter 5. The energies of the frontier orbitals of potential new carbenes were calculated and are shown in Table 1. The results of the DFT analysis were used as the basis for selecting which carbenes would be synthesized for this thesis. The frontier orbital energies of CAAC, DAC, and an NHC are shown for comparison to the new carbenes. In order to experimentally compare the electrophilicity and nucleophilicity of new carbenes, we can synthesize a few complexes and analyze them spectroscopically.

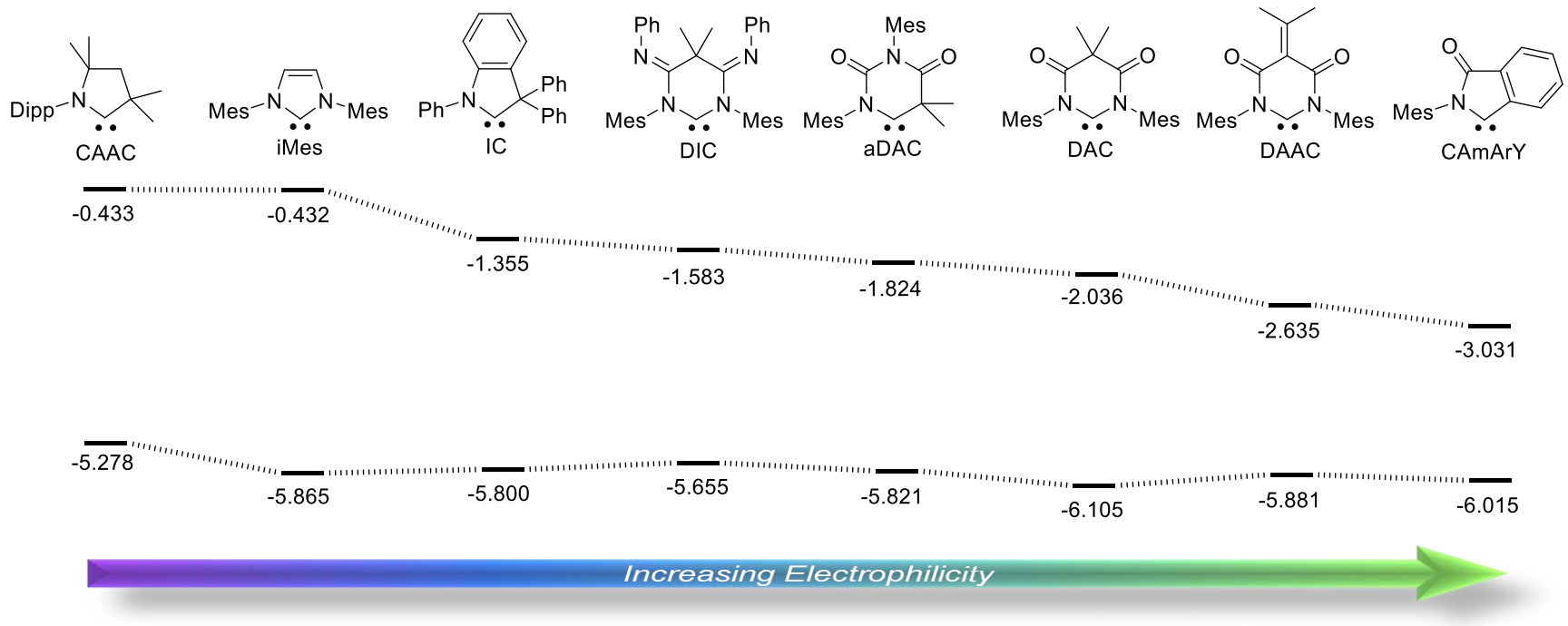

Figure 26 Various carbenes sorted by electrophilicity from left to right. All carbenes calculated using Gaussian 09. B3LYP/6-31G+d(p)

Table 1 HOMO and LUMO energies, and HOMO-LUMO gap of various carbenes sorted by decreasing LUMO energy

Carbene	HOMO (eV)	LUMO (eV)	Delta (kcal/mol)
NHC	-5.865	-0.432	125.282
CAAC	-5.278	-0.433	111.728
IC	-5.800	-1.355	102.504
DIC	-5.655	-1.583	93.882
aDAC	-5.701	-1.782	90.361
DAC	-6.105	-2.036	93.844
DSAC	-6.886	-2.069	111.100
DASi	-6.950	-2.298	107.260
DAGe	-7.148	-2.595	105.001
DAAC	-5.881	-2.635	74.837
DIC5	-5.667	-2.643	69.729
CAmArY	-6.015	-3.031	68.813

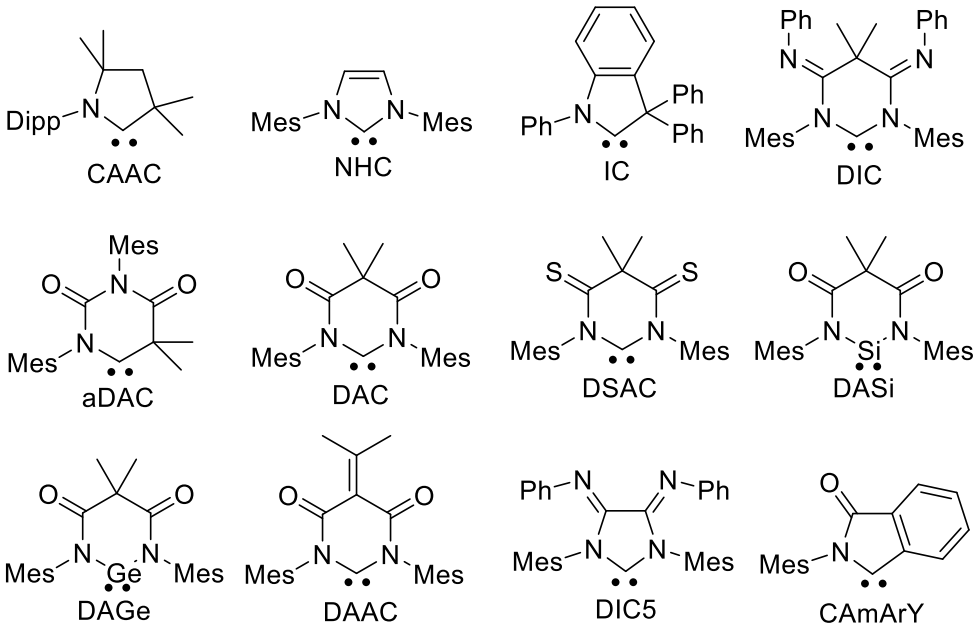

Figure 27 Structures of carbenes listed in Table 1

Measuring the Electronic Properties of Carbenes

The electronic properties of carbenes can be measured in a lot of different ways. The Tolman electronic parameter (TEP), developed by Chadwick Tolman in 1977, is a method of measuring the overall electron donating ability of ligands in nickel carbonyl complexes by measuring the CO stretching frequencies in IR.[52] Carbonyl groups in metal complexes are capable of π-backbonding with the metal. A strongly donating ligand will result in a more electron rich nickel center. An electron rich nickel atom can donate into the π*-orbital of the CO bond from the d-orbital of the nickel (Figure 28). More electron density being donated to the carbonyl groups will shift the CO stretching frequency to a lower wavenumber relative to a weaker donating ligand. This shift to a lower wavenumber is because donating electron density into the π* orbital of the CO bond weakens the triple bond between the carbon and oxygen giving it more of a double bond character.

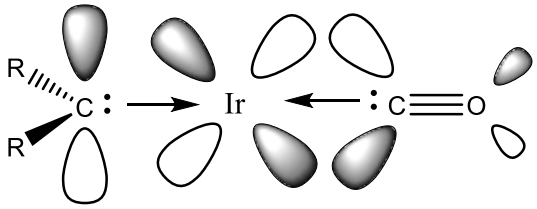

Figure 28 Diagram showing orbitals of iridium carbonyl complexes with a carbene.

Subsequently, Nolan and Crabtree developed similar methods using iridium (I) and rhodium (I) carbonyl complexes respectively. Nolan's method has many advantages over Tolman's because $Ni(CO)_4$ is an air sensitive incredibly toxic volatile oil, and the iridium complex is usually an air stable solid that is relatively safe to work with. The same phosphines were complexed with $Ir(CO)_2Cl$ and an average of the two carbonyl stretches were used for the comparison. The stretching frequencies of the nickel

complexes were plotted as compared to the iridium complexes and a linear regression was performed to relate the two complexes, and to develop a method of comparing other ligands. The linear regression equation determined by Nolan will be used for the determination of TEP values.

$$y = 0.847x + 336$$

Equation 1 Linear regression used to determine TEP values of carbene iridium complexes, where x = ν_{CO} (avg) and y = TEP.

Based on TEP, most carbenes are much stronger σ-donors than phosphines, and in fact are one of the strongest neutral bases. If the ligand being evaluated is also strongly π-accepting, the carbonyl stretching frequencies will shift back to a higher frequency since the metal has less electron density than what it would have just from the σ-donation from the ligand. One downside to this study is that there is a small range for the TEP values, only a range of about 50 cm^{-1}, so carbenes that are very different electronically can still have similar TEP values. Because of this, there is no way to separate the σ-donating and π-accepting abilities of the ligand and so other methods must be used to learn more about the π-accepting ability of the carbenes.

NMR can also be used to evaluate the π-accepting ability of carbenes. Since NMR shifts are related to the electron density around an atom, it can give us some insight into the electronic environment around the carbene. Phosphorus and selenium are both very sensitive to changes in electronic environment. Bertrand showed that carbene–phosphinidine compounds can take on multiple resonance structures depending on the π-accepting ability of the carbene being studied.[53,54] With a weakly π-accepting carbene, the adduct is a carbene stabilized phosphinidine. With a strong π-accepting carbene, the adduct is like a phosphaalkene (Figure 29). The π-acidity of the carbenes are evaluated by

their ^{31}P NMR shifts with strongly π-acidic carbenes having downfield NMR shifts.[54] Crystallographic data of the carbene phosphorus adducts can also be used to evaluate the bond order between the carbene and phosphorus. Due to the difficulty of the synthesis and purification the phosphinidine complexes will not be studied.

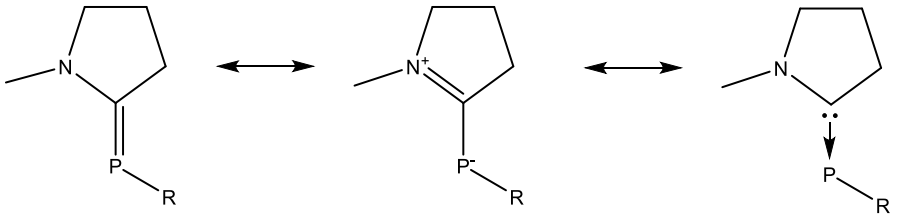

Figure 29 Resonance structures of phosphinidine carbene adducts

Table 2 Carbene selenium NMR shifts

Carbene	HOMO ev	LUMO ev	Delta (kcal/mol)	Se shift (ppm)
A	-5.865	-0.432	125.282	35
B	-5.683	-0.985	-0.985	472
C	-5.270	-1.270	92.244	616
D	-5.571	-1.515	-1.515	652
E	-5.655	-1.583	93.882	669
F	-5.837	-1.830	-1.830	698
G	-6.105	-2.036	93.844	847
H	-6.015	-3.031	68.813	1240

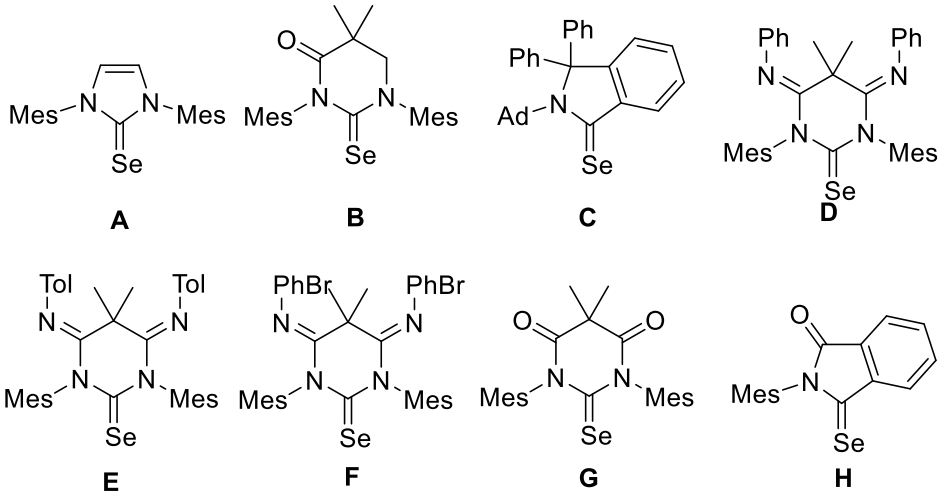

Figure 30 Structures of selected carbenes in Table 2

Selenium NMR can be used similarly to phosphorus NMR to evaluate π-acidity of carbenes. Ganter published an analysis of the HOMO and LUMO energies' relation to the ^{77}Se NMR shift.[51,55] His analysis showed that the energy of the HOMO did not have a direct effect on the selenium shift, but the energy of the LUMO showed a strong correlation. Based on the analysis by Ganter, the σ-donor ability of a carbene does not have much effect on the NMR shifts of the selenium adducts. A weakly π-accepting carbene forms a zwitterion with a positive charge on the nitrogen, and a negative charge on the selenium. A strongly π-accepting carbene will have a double bond between the carbene carbon and selenium (Figure 31).[51,55]

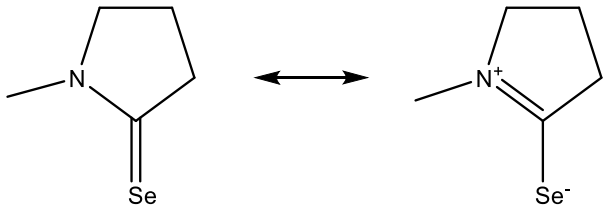

Figure 31 Resonance structures of selenium carbene adducts

General Procedures

All procedures were performed using standard Schlenk techniques under an atmosphere of nitrogen or in a nitrogen-filled glove box unless otherwise noted. Benzene, toluene, THF, and hexanes were dried over sodium, then distilled and degassed by three freeze-pump-thaw cycles. All dried and degassed solvents were stored over 3 Å molecular sieves in a nitrogen filled glove box. All EPR spectra were recorded on an X-band Active Spectrum Benchtop Micro ESR spectrometer (9.5 GHz, 300 Gauss sweep range). Field calibration was accomplished by using a standard of solid 2,2-diphenyl-1-picrylhydrazyl (DPPH), g = 2.0036.

Instrumentation

NMR spectra were recorded on Bruker Avance 400 MHz and Bruker Avance 500 MHz spectrometers. Chemical shifts are given in δ with positive values downfield of TMS. and are reported in ppm relative to the residual solvent signal for for ^{1}H and ^{13}C (^{1}H: C_6D_6, δ 7.16; $CDCl_3$, δ 7.26; CD_2Cl_2, δ 5.32; d-DMSO, δ 2.50; d-DMF, δ 8.05; d-THF, δ 3.58; ^{13}C: C_6D_6, δ 128.06; $CDCl_3$, δ 77.16; CD_2Cl_2, δ 53.84; d-DMSO, δ 39.52; d-DMF, δ 163.15; d-THF, δ 67.21). $CDCl_3$, C_6D_6, CD_2Cl_2, d-DMSO, d-DMF, or d-THF, or to an external reference (Me_2Se) for ^{77}Se. Coupling constant magnitudes, J, are given in Hz. Melting point (Mp) or decomposition points (Dp) were obtained on samples in glass capillaries using a MEL-TEMP II laboratory device, USA apparatus and are uncorrected. UV-Vis spectra were recorded on a PerkinElmer Lambda 365 Uv-Vis spectrophotometer in a benzene solution. IR spectra were recorded on a Bruker Tensor II FTIR-ATR spectrometer

Theoretical Methods

All the calculations were performed using Gaussian09.[56] Geometry optimizations have been calculated using density functional theory (DFT). DFT calculations used the B3LYP functional and the 6-31G+d basis set for all molecules. Geometry optimizations were confirmed to have zero imaginary frequencies. The computed structures were compared to the respective X-ray structures when available to ensure that the experimental and calculated data were in good agreement.

X-ray Crystallography

Crystals were obtained by slow evaporation or vapor diffusion at room temperature. Data was collected using CrystalClear software on a Rigaku SCX-Mini with

Mercury 2 CCD detector with a Mo radiation source. Data reduction was performed using CrysAlisPro software. The structures were solved by intrinsic phasing using OLEX2 and refined by least squares using SHELXL.

II. SYNTHESIS AND CHARACTERIZATION OF THE CYCLICARYLAMIDOCARBENE

The ability of DACs and CAACs to do certain small molecule activation may be due to the small singlet-triplet gap relative to NHCs.[22,36] As the singlet-triplet gap gets smaller, carbenes are able to engage in more reactions associated with triplet carbenes. Our group has been interested in expanding the variety of carbenes which exhibit varying levels of nucleophilic or electrophilic character. The DACs exhibit a very low energy LUMO due to the amide groups incorporated into the carbene.[36] The amide groups also have the effect of drastically lowering the HOMO, which makes DAC a very weak σ-donor relative to other carbenes. This can make reactions with DAC difficult to accomplish as their nucleophilicity is similar to that of triaryl phosphines. Bielawski's cyclic(alkyl)amidocarbene (CAAmC) (Figure 32) was an attempt to increase the nucleophilicity of an amido carbene by replacing one of the amide groups with a quaternary alkyl group, similar to CAAC.[48] Recently Bertrand synthesized the cyclic(alkyl)arylcarbene (CAArC) (Figure 32) which increased the π-acidity relative to CAAC.[23] The replacement of the quaternary alkyl group with an aryl group into the heterocyclic ring of the CAArC pulls electron density from the carbene carbon into the aryl group. This results in lowering the LUMO relative to CAAC but it retains a HOMO energy similar to CAAC and consequently lowers the singlet-triplet gap. Based on the reactivity of these new carbenes, we hypothesized that the π-accepting properties of carbenes can be increased even further. The cyclic(amido)arylcarbene (CAmArY) incorporates both an amide and aryl moiety into the heterocyclic ring resulting in a very electrophilic carbene.

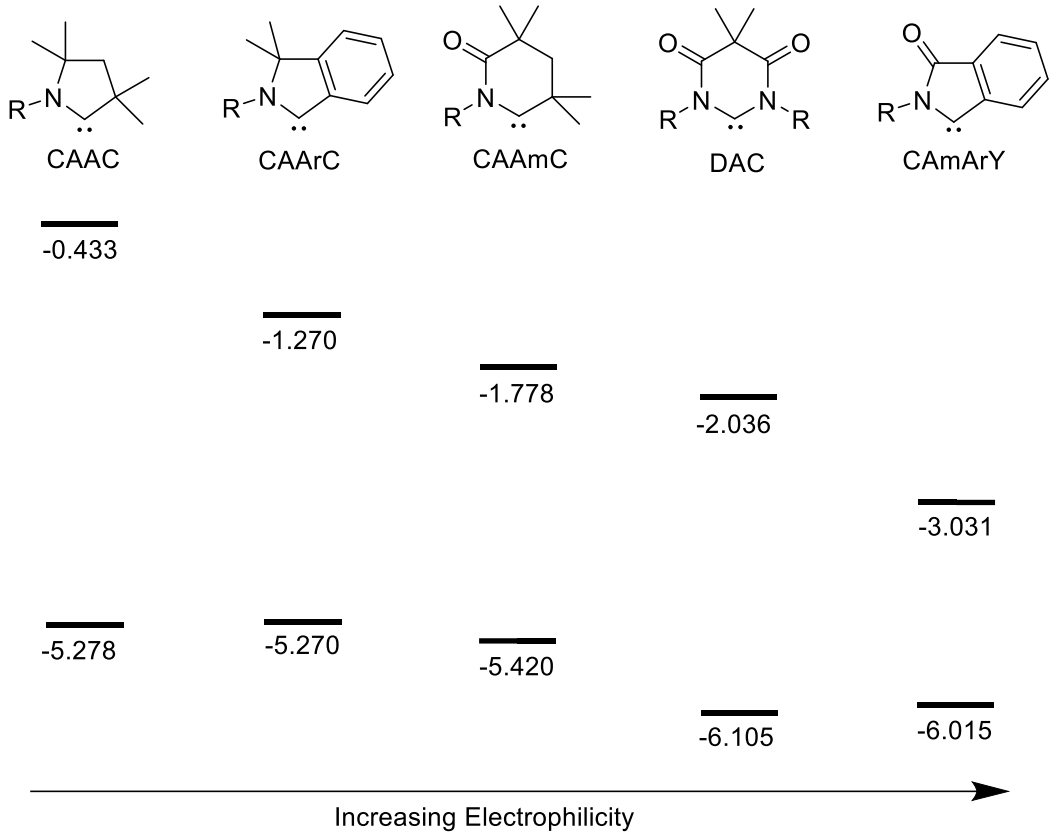

Figure 32 HOMO-LUMO diagram showing CAAC, CAArC, CAAmC, DAC, and CAmArY. Calculated using B3LYP/6-31G+(d).

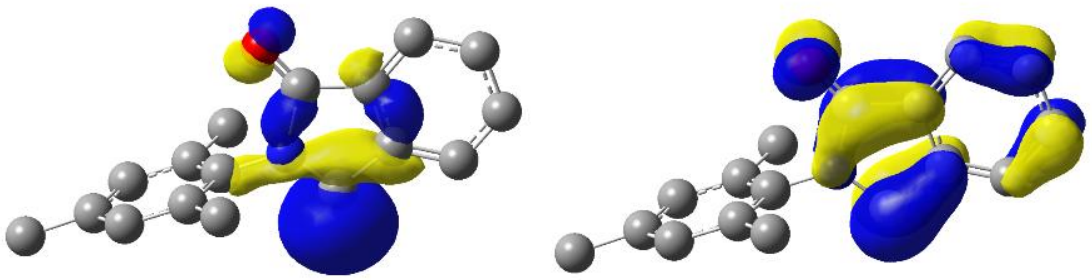

Figure 33 HOMO and LUMO orbitals of CAmArY

DFT calculations suggest that CAmArY is a very electrophilic carbene with a LUMO energy of -3.00 eV which is significantly less than other reported carbenes. DAC's LUMO is -2.06 eV and CAAC's LUMO is -0.433 eV. CAmArY's HOMO energy is slightly higher than DAC with an energy of -6.01 eV, DAC's HOMO is -6.10 eV. The

singlet-triplet gap of CAmArY is also very small, only about 19.1 kcal/mol. The singlet-triplet gap is approaching what is seen with triplet ground state carbenes, usually triplet carbene singlet-triplet gaps are less than 10 kcal/mol.[4,24,27] As expected, the HOMO of CAmArY looks like a lone pair of electrons on the carbene carbon. Interestingly, the LUMO of CAmArY shows delocalization of the LUMO throughout the aryl substituent and the carbonyl group. The delocalization of the LUMO into the aryl group was also seen in Bertrand's CAArC.[23] Typically, the LUMO of a carbene looks like a p-orbital localized on the carbene carbon. Based on these results, we attempted the synthesis of CAmArY and subsequently studied its electronic properties.

The N-mesityliminomethyl benzoic acid **1** was synthesized via condensation of 2-carboxybenzaldehyde with 2,4,6-trimethylaniline. Cyclization of **1** was achieved via chlorination with thionyl chloride in refluxing acetonitrile. Thionyl chloride was used to generate the acid chloride *in situ* which spontaneously ring closed with the imino group to form 3-chloro-2-mesitylisoindolin-1-one **2**, which was isolated in nearly quantitative yield. The ^{1}H NMR ($CDCl_3$) featured a peak at 6.5 ppm which was assigned to the proton on the carbon adjacent to the amide nitrogen (Figure 50 in the experimental section of this chapter). This is similar to what is observed in the ^{1}H NMR of the DAC-HCl, suggesting that the chloride is directly bound to the carbon adjacent to the amide nitrogen instead of forming the iminium salt like with the CAACs and NHCs.[36] This is likely due to the increased electrophilicity of the carbene and formation of an amidinium salt is unlikely.

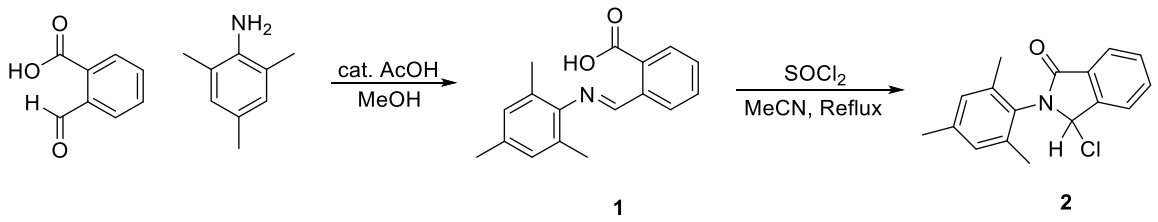

Figure 34 Reaction scheme of the synthesis of CAmArY HCl **2**

Generation of the carbene **3** was attempted in multiple solvents and with multiple bases, including NaH:KOtBu, and NaHMDS. Initially we believed that we had synthesized the free carbene due to disappearance of the proton signal at 6.5 ppm in the ^{1}H NMR. However, ^{13}C NMR did not show a signal past 200 ppm which is where carbene signals are expected to appear. Treating this molecule with various reagents known to react with carbenes resulted in no reaction. This led us to the conclusion that the carbene dimer **4** was isolated instead of the free carbene. Mass spectrometric data confirmed that the carbene dimer was formed. CAmArY cannot be isolated and instead results in the bright yellow air stable dimer **4** and a black/blue colored species which we have not been able to characterize fully when generating the carbene.

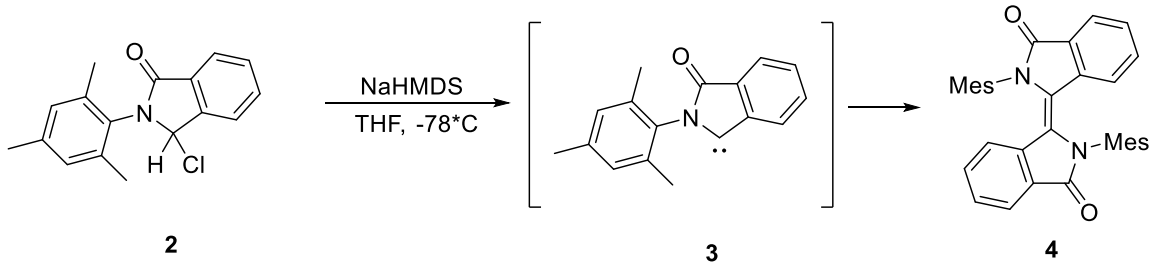

Figure 35 Synthesis of CAmArY dimer **4**

The blue colored molecule is suspected to be a sodium salt of the dimer (Figure 36) that features a single bond between the two CAmArY molecules, with a chloride bound to one carbon, and the other carbon being anionic. These structures were suggested

by Wanzlick as intermediates in the formation of the carbene dimer. If the dark colored molecule is left under vacuum, or washed with large amounts of solvent, more of the yellow dimer is formed. Unfortunately, at this point, we have not been able to characterize the suspected salt further but attempts to grow a single crystal for XRD are being made.

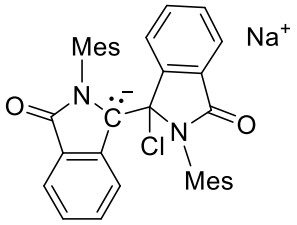

Figure 36 Suspected structure of the second product in the synthesis of the CAmArY dimer.

The dimerization occurs through the reaction of one CAmArY HOMO and another CAmArY LUMO. For this to happen the carbene acting as a base needs to attack the LUMO from above. The carbene dimerizes because the side of the ring with the aryl substituent offers no steric protection. A single crystal of **4** suitable for X-ray diffraction analysis was obtained by slow evaporation of hexanes. The heterocyclic rings of the monomers are planar. The N–C–C bond angles are both around 104.5° with C–N bond lengths of 1.395 Å. The C1–C3 bond has a length of 1.33 Å which makes sense for a carbon–carbon double bond. The dimer is not totally planar and has a N1–C1–C3–N2 torsion angle of 23.55°.

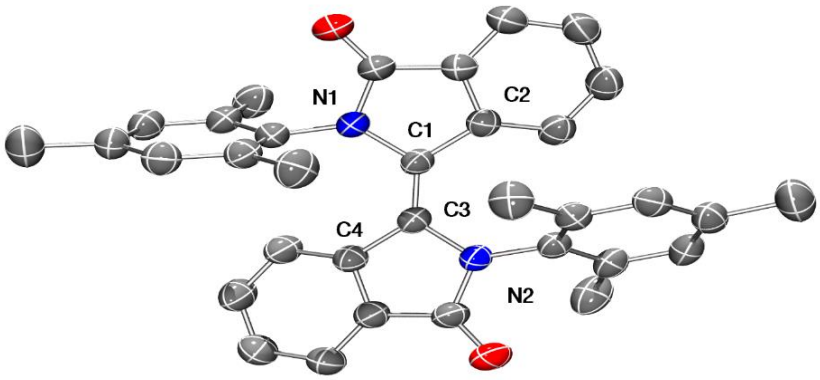

Figure 37 X-ray structure of **4** with thermal ellipsoids set at 50% probability. Hydrogen atoms are omitted for clarity. Selected bond lengths [Å] and angles [°]: C3–C1, 1.33(3); N1–C1, 1.39(7); N2–C3, 1.39(5); C3–C4, 1.44(2); C1–C2, 1.43(7); C2–C1–N1, 104.48(3); C4–C3–N2, 104.40(9); C3–C1–N1, 125.34(9); C1–C3–N2, 125.16(7)

Carbenes are known to react with elemental sulfur to form thioamides or thioureas. To confirm that the free carbene was being formed *in situ* at low temperatures, the CAmArY was generated in the presence of elemental sulfur. The expected thioamide **5** was formed and isolated via column chromatography as a bright pink, air stable solid in 50% yield. ^{1}H NMR ($CDCl_3$) of the compound shows that **2** was successfully deprotonated and the free carbene was formed transiently. The ^{13}C NMR ($CDCl_3$) shows a resonance at 197 ppm, which was assigned to the carbon bonded to sulfur and is consistent with other thioamides.[23,35,48] A single crystal of **5** suitable for X-ray diffraction analysis was obtained by slow evaporation of hexanes. The sulfur adduct **5** has a C1–S1 bond length of 1.51(7) Å which is consistent with a carbon sulfur double bond.[23] Similar to the dimer **4**, it has a C2–C1–N1 bond angle of 104.76(8) Å.

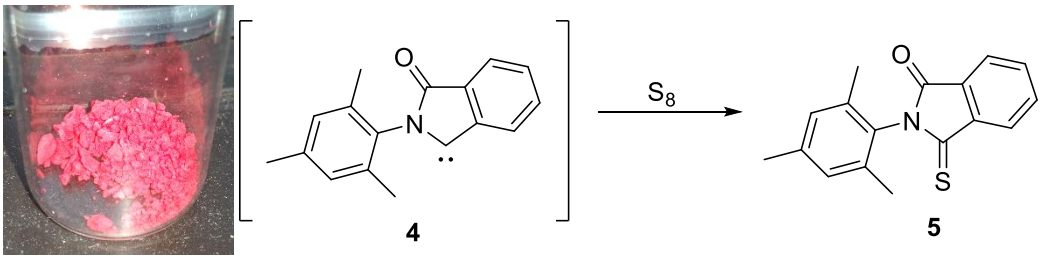

Figure 38 Synthesis of CAmArY sulfur adduct

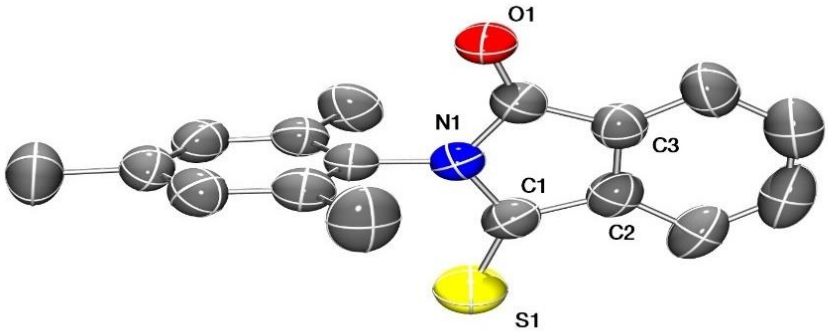

Figure 39 X-ray structure of **4** with thermal ellipsoids set at 50% probability. Hydrogen atoms are omitted for clarity. Selected bond lengths [Å] and angles [°]: C1–C2, 1.45(4); C1–N1, 1.34(8); C1–S1, 1.51(7); C4–O1, 1.21(2); C2–C1–N1, 104.76(8)

Now that we have confirmed the carbene is actually being generated, the selenium adduct was synthesized. As with elemental sulfur, carbenes will react with elemental selenium to form a selenoamide or selenourea. The product **6** was isolated via column chromatography as a teal solid, in 20% yield. As expected, the ^{77}Se NMR ($CDCl_3$) showed a peak very far downfield at 1240 ppm, significantly more downfield than other carbenes, DAC has a ^{77}Se shift of 847 ppm and CAAC shows a resonance at 493 ppm. To our knowledge, this is the most electrophilic carbene synthesized to date based on the selenium adduct. Bielawski's cyclicalkylamido carbene (CAAmC) previously held that record with a ^{77}Se shift of 1174 ppm. The ^{13}C NMR ($CDCl_3$) shows a signal at 201 ppm, consistent with other selenium carbene adducts.[51,55]

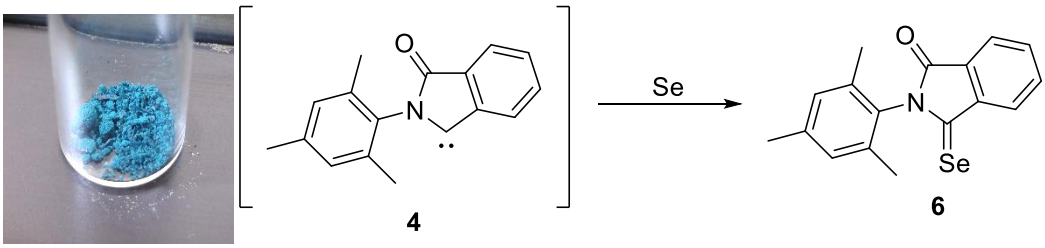

Figure 40 Synthesis of CAmArY selenium adduct.

A single crystal of **6** suitable for X-ray diffraction analysis was obtained by slow evaporation of hexanes. Most $C_{carbene}$–Se bonds have lengths of ca. 1.83 Å with the more π-accepting carbenes having bond lengths around 1.78 Å.[51] CAmArY has a much shorter bond length than even the five-membered DAC with a bond length of 1.73(8) Å.[51] A plot of the free carbene LUMO energy as compared to its selenium adduct's ^{77}Se NMR shift shows a strong correlation ($R^2 = 0.9683$) between the π-acidity of a carbene and its selenium NMR resonance (Figure 41). This information gives us a reliable method of testing the computational data we receive from DFT analysis and we could potentially use this to estimate the location of the selenium NMR resonance. The σ-donating ability of a carbene is not as easy to determine. Now that we have the π-accepting ability of CAmArY determined, we set out to study its overall electron donating ability.

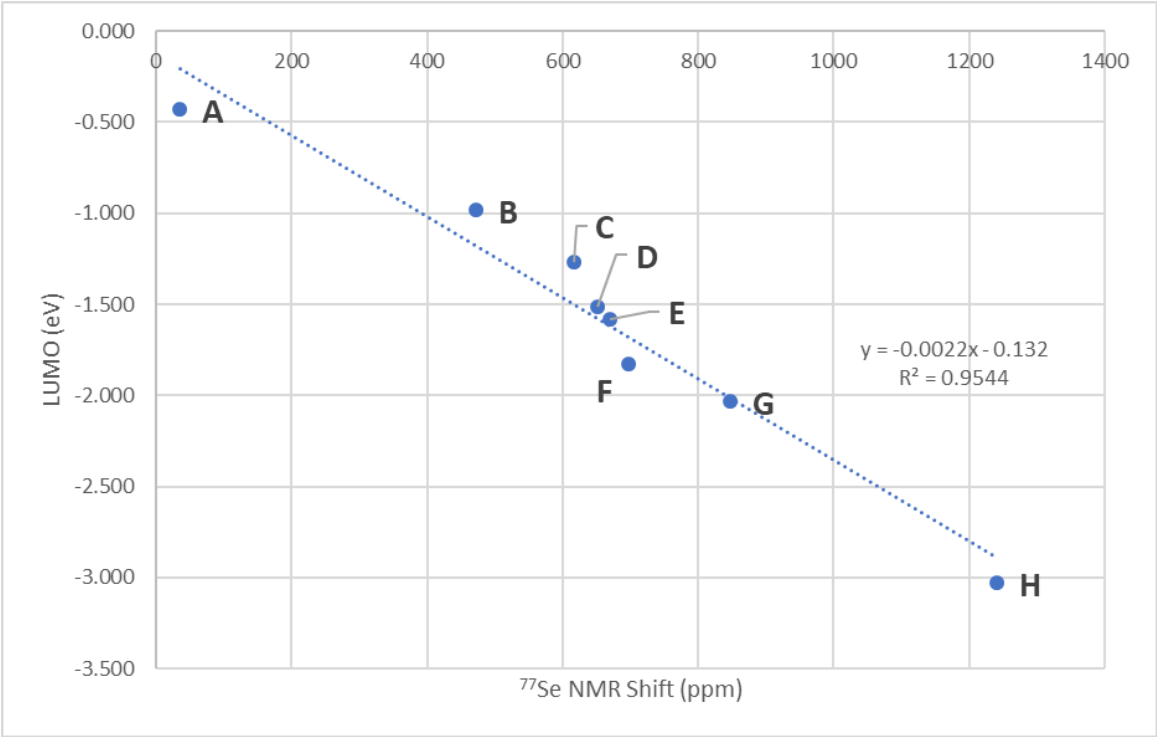

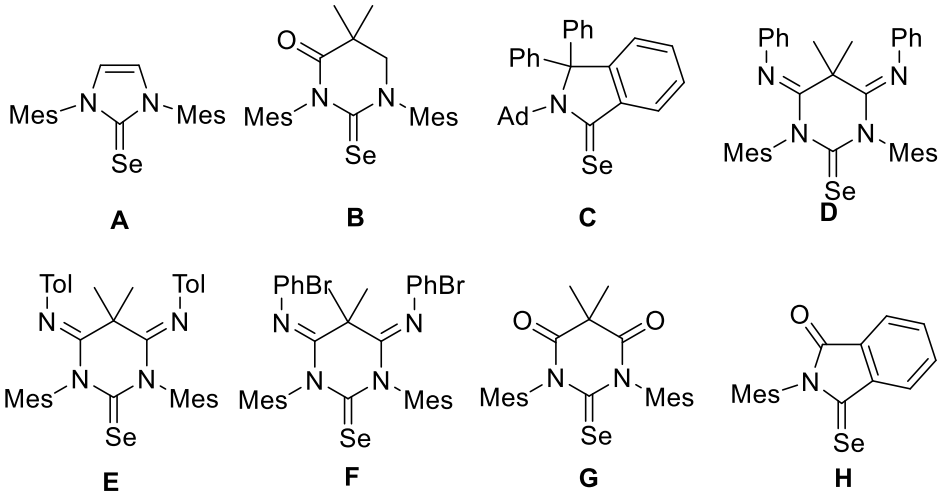

Figure 41 Plot of LUMO energies as compared to ^{77}Se NMR shifts of selected carbene selenium adducts.[23,51]

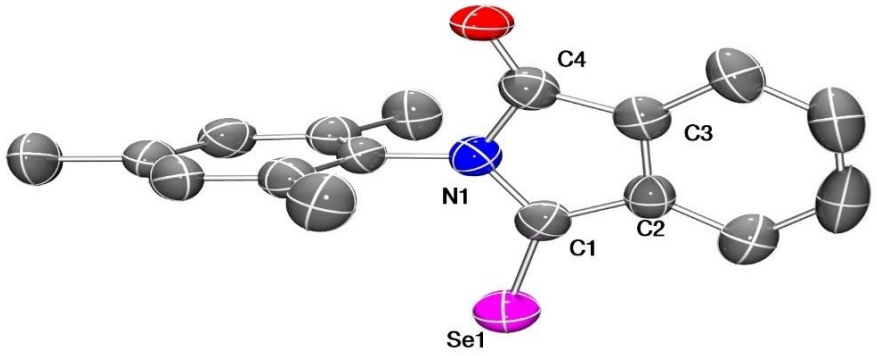

Figure 42 X-ray structure of **6** with thermal ellipsoids set at 50% probability. Hydrogen atoms are omitted for clarity. Selected bond lengths [Å] and angles [°]: C1–C2, 1.45(1); C1–N1, 1.35(9); C1–Se1, 1.73(8); C4–O1, 1.22(9); C2–C1–N1, 105.46(1)

In our attempts to study the overall donating ability of CAmArY, the iridium COD complex **7** was synthesized by adding $[Ir(COD)Cl]_2$ to the reaction when generating the carbene. The yield for the synthesis of the iridium complex was very low due to the rapid generation of the dimer even at very low temperatures. This complex is very fragile and decomposes quickly on silica and if left under vacuum in solid state.

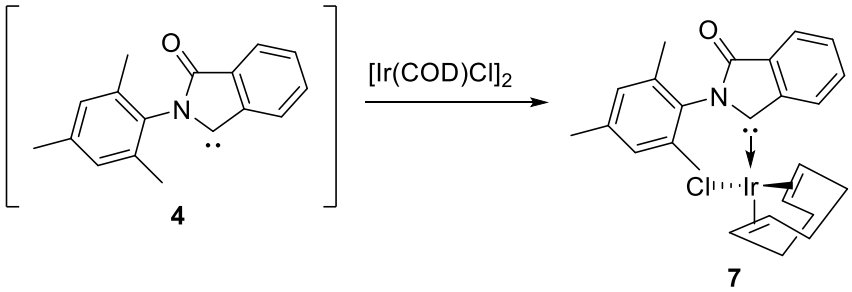

Figure 43 Synthesis of CAmArY–Ir(COD)Cl complex **7**

When carbonylation of the iridium cod complex was attempted, the complex decomposes and 2,4,6-trimethylphenyl phthalimide **9** was formed. To confirm that **9** was formed through this reaction, a single crystal of the product was grown and **9** was directly synthesized with 2,4,6-trimethylaniline and phthalic anhydride. To our knowledge, this is the only example where a carbene–Ir(COD)Cl complex decomposes in the presence of carbon monoxide to give and oxidized carbene.

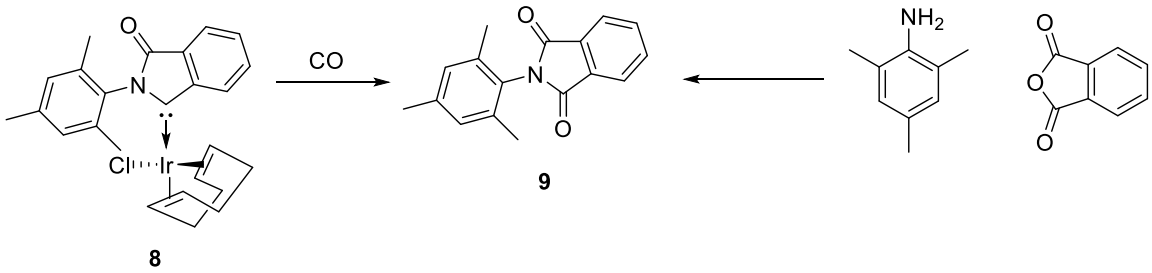

Figure 44 Reaction schemes of the formation of phthalimide

A single crystal of **9** suitable for X-ray diffraction analysis was obtained by slow evaporation of hexanes (Figure 45). Usually the rhodium carbonyl complexes are more stable than the iridium carbonyl complexes, but this complex also decomposes before characterization can be completed. Unfortunately, because of this, the TEP of the CAmArY carbene could not be measured to evaluate the overall donating properties of the carbene.

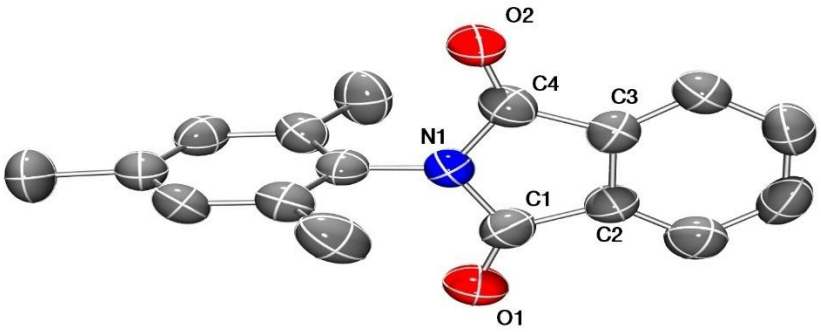

Figure 45 X-ray structure of **4** with thermal ellipsoids set at 50% probability. Hydrogen atoms are omitted for clarity. Selected bond lengths [Å] and angles [°]: N1–C1, 1.40(8); N1–C4, 1.41(1); C1–C2, 1.48(7); C3–C4, 1.49(8); C1–O1, 1.20(6); C4–O2, 1.20(7); N1–C1–C2, 105.73(1); N1–C4–C3, 105.18(2).

There are ongoing efforts to sterically protect CAmArY to prevent dimerization. The dimerization reaction is a stepwise process and begins with the HOMO of one carbene reacting with the LUMO of the second carbene. For this to happen, the first carbene must attack from above. Initially we attempted substituting the aryl group in the ring, specifically the ortho position. Attempting Friedel-Crafts alkylation with $AlCl_3$ and

t-butyl chloride resulted in a complex mixture of isomers which could not be separated. Further attempts to substitute that ring are not being made at this time.

Currently we are modifying the aniline starting material to provide more steric protection. The new aniline will be synthesized by performing a Suzuki cross coupling reaction of two equivalents of 3,5-bistrifluomethylphenyl boronic acid with 2,6-dibromoaniline with using tetrakis(triphenylphosphine) palladium (0) as the catalyst (Figure 46).

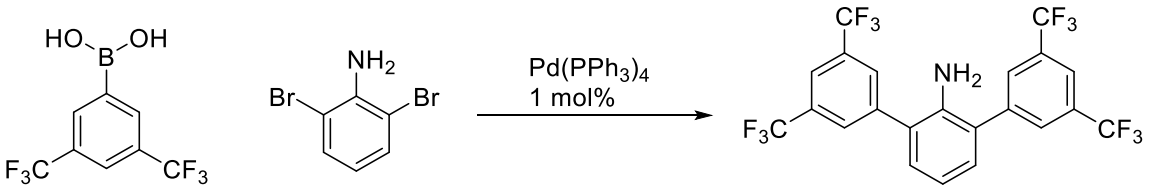

Figure 46 Synthesis of the modified protecting group for CAmArY

By replacing the methyl groups in the mesityl with 3,5-bistrifluoromethylphenyl groups, the empty p-orbital of the carbene carbon is protected above and below. Additionally, the trifluoromethyl groups protrude out in front of the carbene which should also prevent dimerization. We expect that this version of the carbene will be more stable and may be isolable.

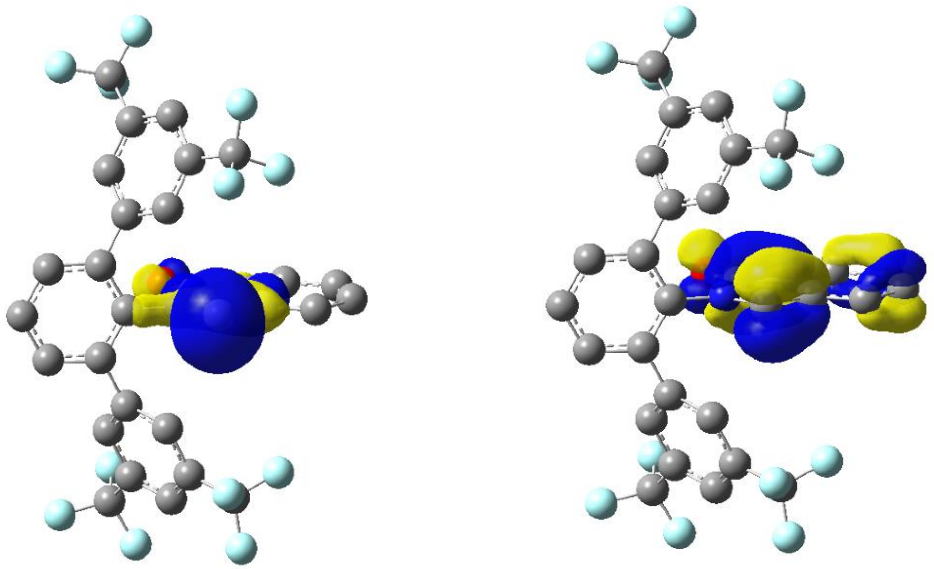

Figure 47 HOMO and LUMO orbital diagrams of modified CAmArY

Interestingly, modification of the aryl group changed the electronic properties more than expected. DFT calculations predict that the HOMO and LUMO energies are both lowered by about 0.5 eV. Because a plot of the LUMO energy of various carbenes as compared to their ^{77}Se NMR shift results in a linear trend (see Figure 41). The ^{77}Se chemical shifts of new carbenes can be estimated based on the LUMO energy value determined from DFT calculations. Using the linear regression from Figure 41, a value of -3.461 eV for the LUMO of this CAmArY derivative should give a selenium NMR shift of ca. 1470 ppm. If it is an isolable carbene, it will be by far the most electrophilic carbene isolated at this point.

In conclusion, we have described the synthesis and characterization of the cyclic(amido)arylylidene (CAmArY). The carbene precursor was synthesized in good yields in two steps. Building on the work of Bertrand's CAArC that increased electrophilicity relative to CAACs, and our work with the already electrophilic amido carbenes, we developed the most electrophilic carbene to date. Unfortunately, due to

insufficient steric protection, the carbene dimerizes. The TEP studies could not be completed due to the metal complex decomposing during carbonylation. We are currently exploring methods of increasing steric protection enough to allow for the isolation of CAmArY.

Experimental Section

1. Synthesis of (E)-2-((mesitylimino)methyl)benzoic acid **1**

The 2-carboxybenzaldehyde acid (5.0 g, 33 mmol) was dissolved in 75 mL isopropanol then 3 drops acetic acid was added and stirred for 1 hour. Then 4.5 g (33 mmol) of 2,4,6-trimethylaniline was added and refluxed for 1 hour. The reaction was allowed to cool to room temperature and was stirred at room temperature overnight. A white needlelike precipitate formed overnight. The solid was filtered and washed with cold methanol (6.76 g recovered, 76% yield). M.P. – 122-126 °C. ^{1}H NMR (400 MHz, $CDCl_3$) δ 7.92 (d, J = 7.0 Hz, 1H), 7.77 (dt, J = 14.7, 7.5 Hz, 2H), 7.63 (t, J = 7.3 Hz, 1H), 6.92 (s, 2H), 6.39 (s, 1H), 3.74 (s, 1H), 2.38 (s, 6H), 2.28 (s, 3H). ^{13}C NMR (101 MHz, $CDCl_3$) δ 169.17, 146.09, 137.91, 134.36, 134.15, 132.02, 130.61, 129.63, 128.26, 125.41, 123.62, 93.44, 77.27, 20.74, 18.56.

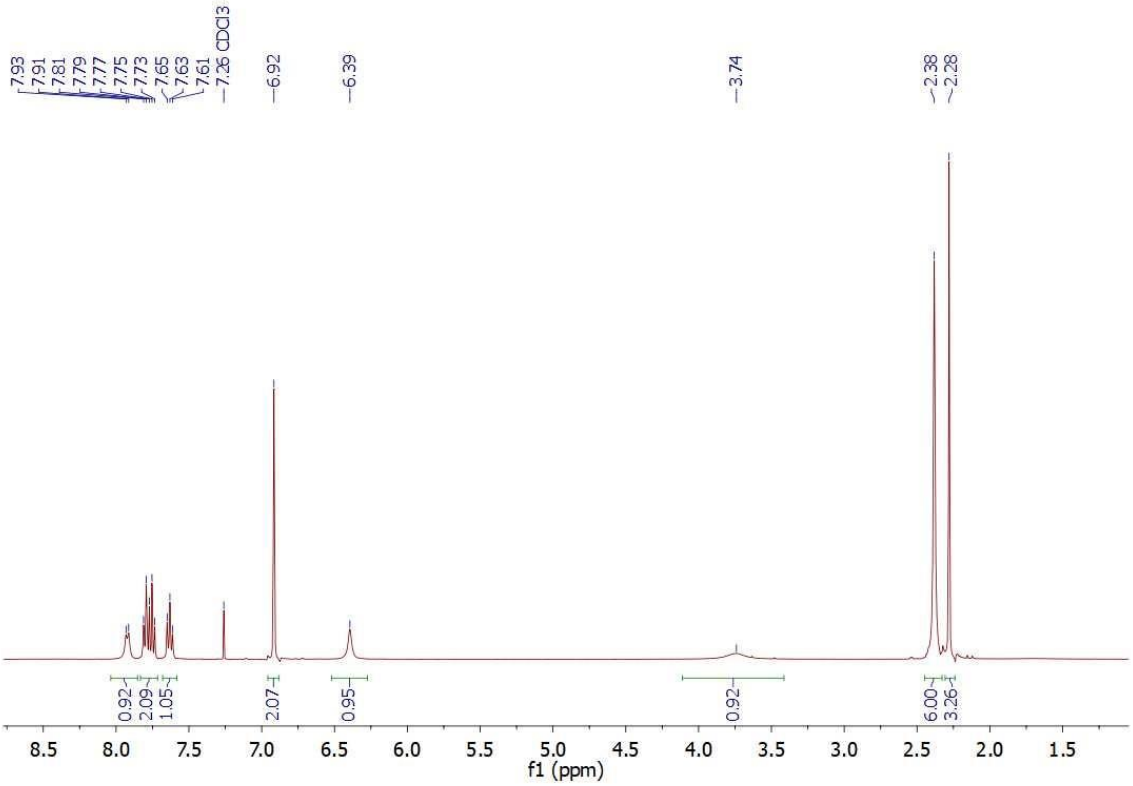

Figure 48 ^{1}H NMR of **1**

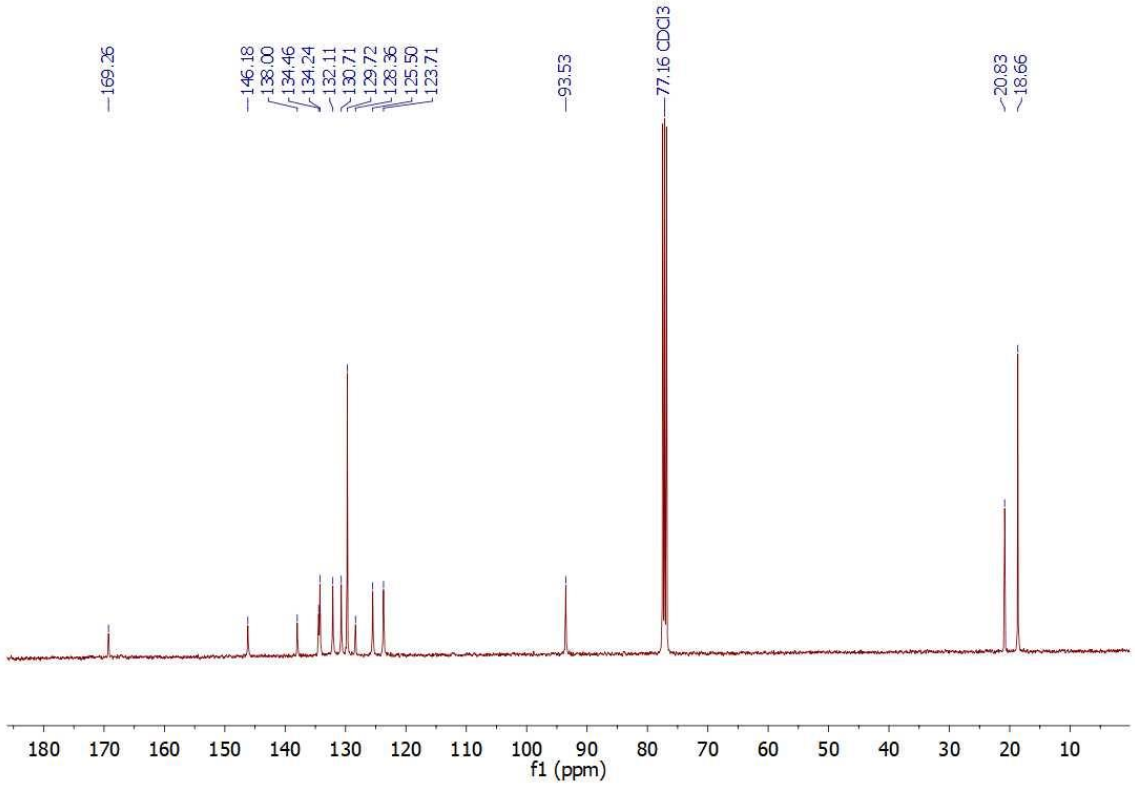

Figure 49 ^{13}C NMR of **1**

2. Synthesis of 3-chloro-2-mesitylisoindolin-1-one **2**

To a Schlenk flask, 1.0 g (3.74 mmol) of **1** dissolved in 20 mL of acetonitrile. Then 0.89 g (7.5 mmol) of thionyl chloride was added and refluxed for 3 hours. Volatiles were evaporated under reduced pressure overnight to afford the desired compound as an off white solid (1.07g, 3.74 mmol, 99% yield). M.P. = 146 – 148 °C. ^{1}H NMR (400 MHz, C_6D_6) δ 7.81 (d, J = 7.5 Hz, 1H), 7.25 (d, J = 7.6 Hz, 1H), 7.09 (t, J = 7.5 Hz, 1H), 6.99 (t, J = 7.5 Hz, 1H), 6.80 (s, 1H), 6.69 (s, 1H), 6.46 (s, 1H), 2.43 (s, 3H), 2.08 (s, 3H), 1.73 (s, 3H). ^{13}C NMR (101 MHz, C_6D_6) δ 166.01, 144.08, 138.92, 138.50, 135.83, 132.70, 131.04, 130.96, 130.41, 130.13, 129.57, 124.34, 124.14, 73.98, 20.97, 19.22, 17.68.

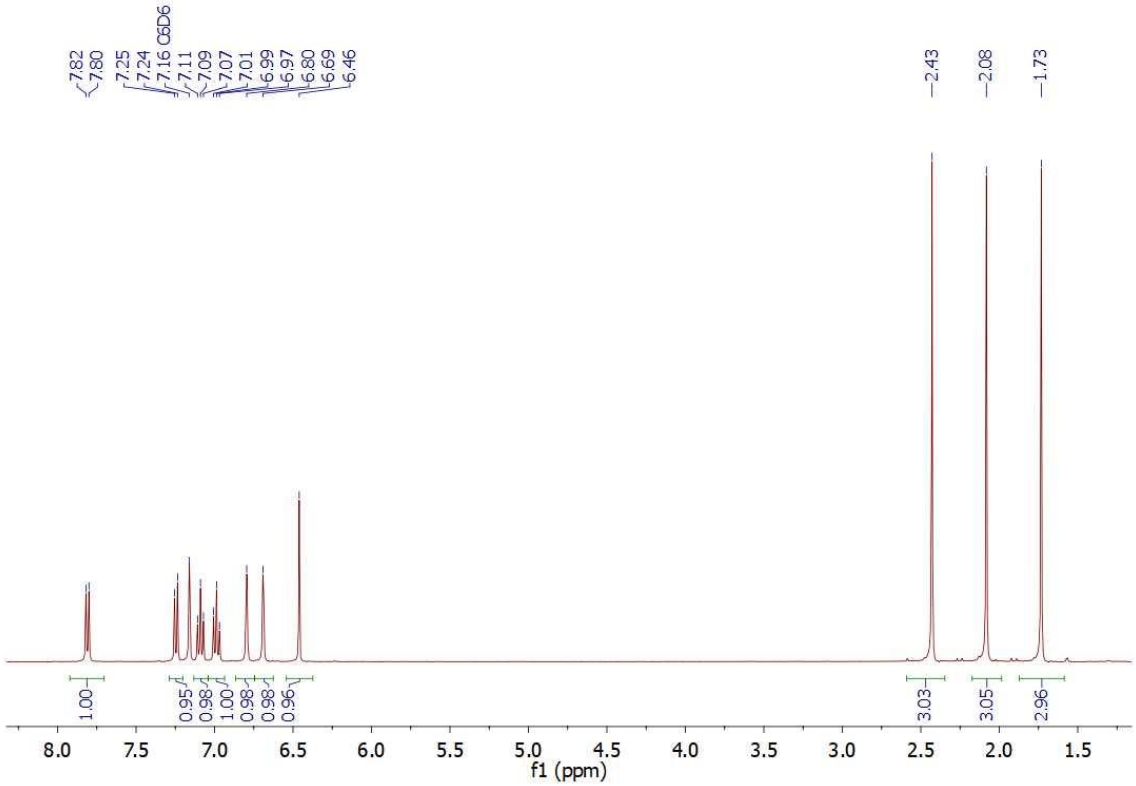

Figure 50 ^{1}H NMR of CAmArY HCl **2**

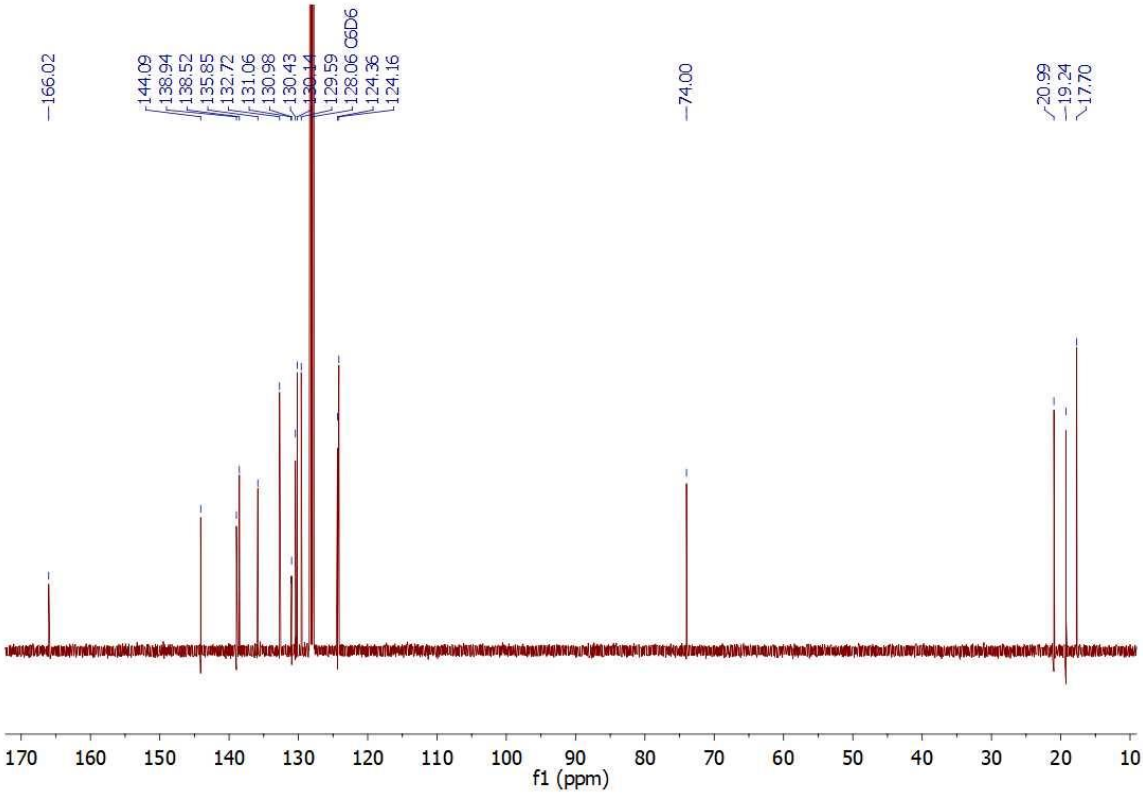

Figure 51 ^{13}C NMR of **2**

3. Synthesis of (E)-2,2'-dimesityl-[1,1'-biisoindolinylidene]-3,3'-dione **4**

Added 1.0 g (3.5 mmol) of **2** to schlenk flask, dissolved in 25 mL of dry THF and cooled to -78 °C. A solution of 0.68 g (3.7 mmol) NaHMDS in 10 mL of THF was added dropwise over 30 minutes. After 2 hours the solution was allowed to warm to room temperature. Solution turns black/green. The solution was filtered over celite and volatiles were evaporated under reduced pressure. The product was purified by column chromatography (80:20 DCM: Hexane). Recovered a yellow solid (0.75 g, 1.5 mmol, 86% yield). M.P. – 294-296 °C. ^{1}H NMR (400 MHz, $CDCl_3$) δ 8.40 (d, J = 8.0 Hz, 1H), 7.93 (d, J = 7.5 Hz, 1H), 7.55 (dt, J = 33.5, 7.2 Hz, 2H), 6.67 (s, 2H), 2.27 (s, 3H), 1.59 (s, 6H). ^{13}C NMR (101 MHz, $CDCl_3$) δ 166.80, 137.80, 136.68, 132.63, 132.00, 129.37, 129.16, 127.97, 124.46, 124.29, 20.93, 18.15, 14.11.

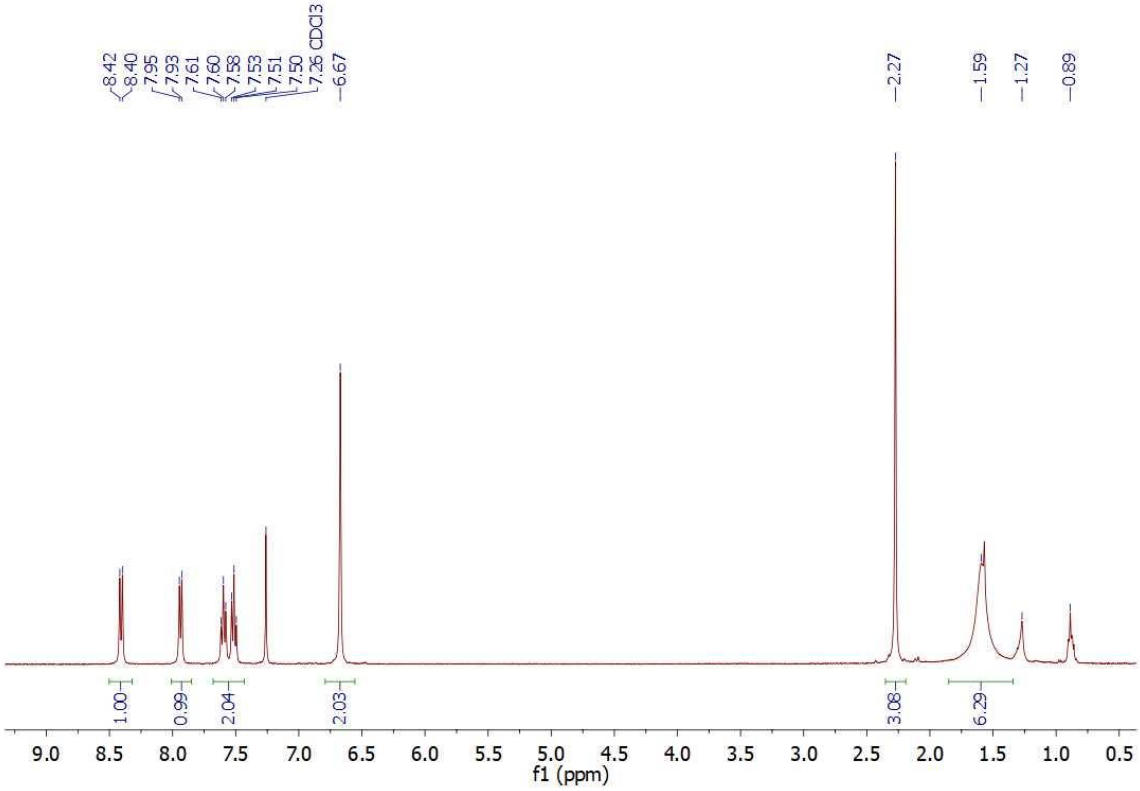

Figure 52 ^{1}H NMR of **4**

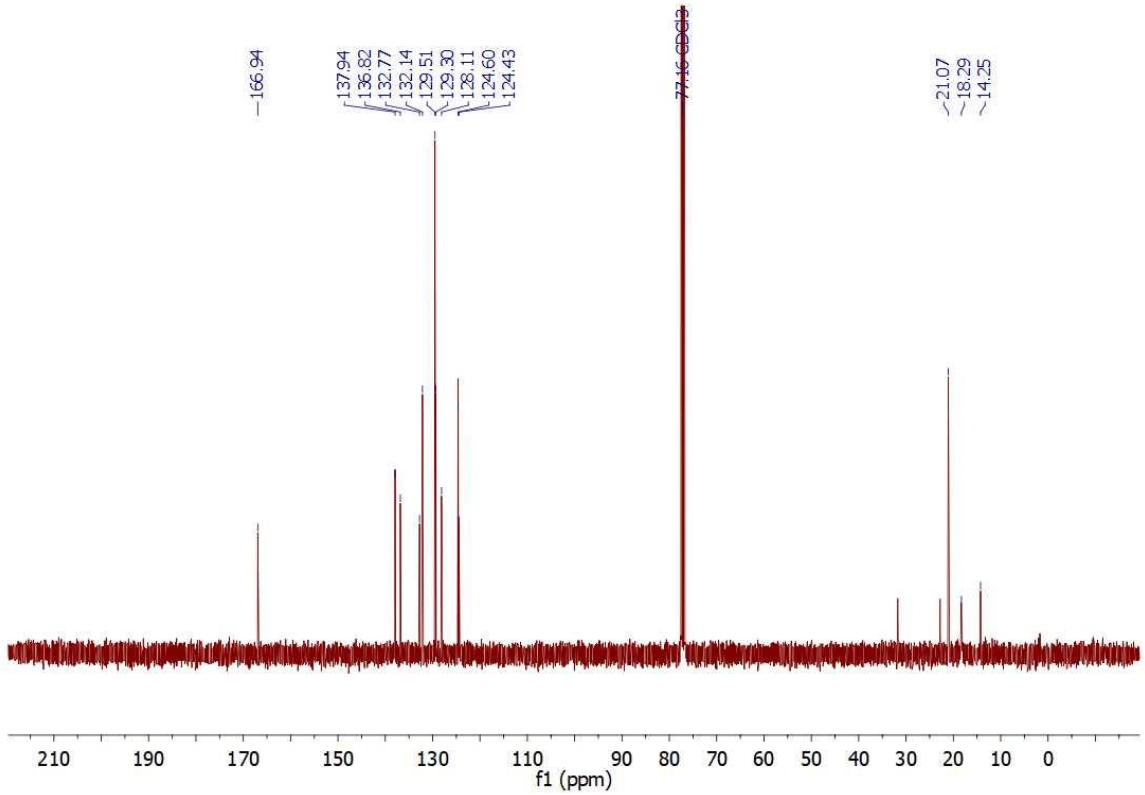

Figure 53 ^{13}C NMR of **4**

4. Synthesis of 2-mesityl-3-thioxoisoindolin-1-one **5**

Added 1.0 g (3.5 mmol) of **2** and 0.34 g (11 mmol) sulfur to a schlenk flask and dissolved in 25 mL of THF. The flask was then cooled to -78 °C. A solution of 0.83 g (4.5 mmol) NaHMDS in 10 mL of THF was added dropwise over 30 minutes. The reaction was allowed to warm to room temperature and was stirred overnight. The solution was filtered over celite and volatiles were evaporated under reduced pressure. Purified by column chromatography (80:20 DCM: Hexane). Recovered a bright pink solid (0.49 g, 1.7 mmol, 49% yield). M.P. – 137-139 °C. ^{1}H NMR (400 MHz, C6D6) δ 7.88 (ddd, J = 3.5, 2.0, 0.7 Hz, 1H), 7.53 (ddd, J = 5.7, 2.1, 0.7 Hz, 1H), 7.05 – 6.92 (m, 2H), 6.72 (dd, J = 1.2, 0.6 Hz, 2H), 2.05 (s, 3H), 1.97 (s, 6H). ^{13}C NMR (101 MHz, C6D6) δ 196.80, 169.12, 139.17, 137.59, 136.68, 134.16, 133.32, 130.28, 129.48, 124.27, 123.07, 21.04, 17.80.

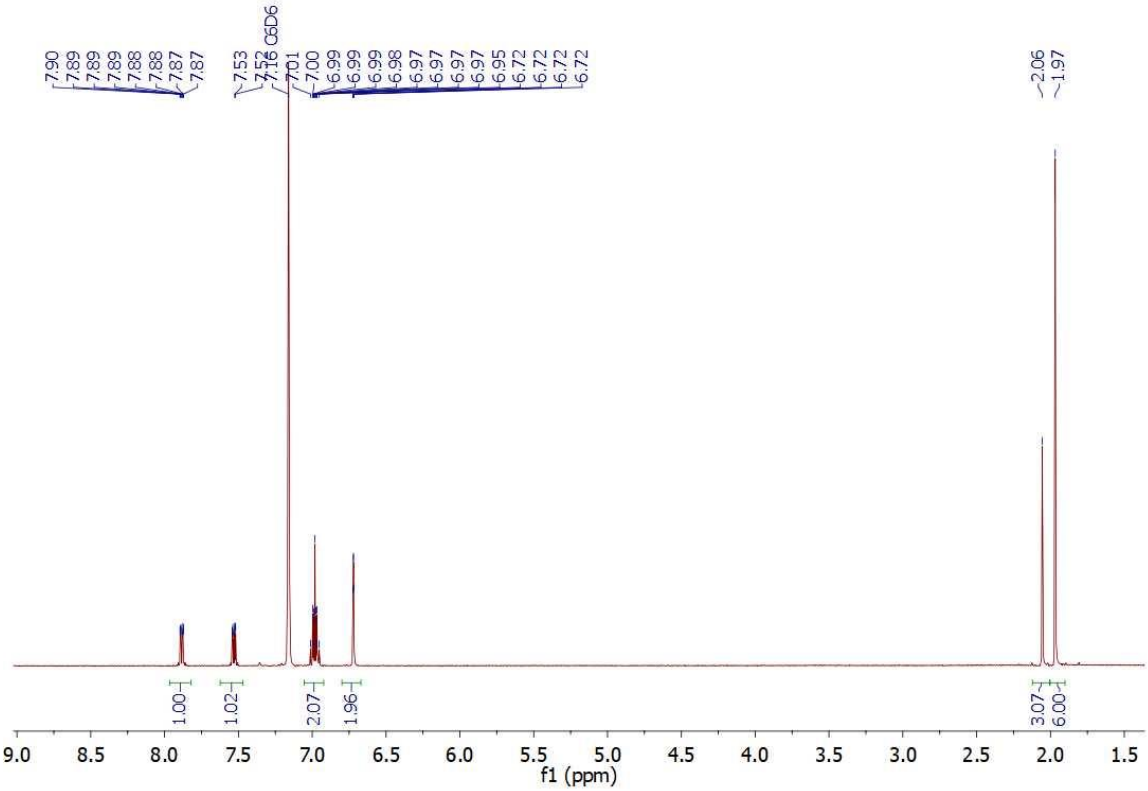

Figure 54 ^{1}H NMR of **5**

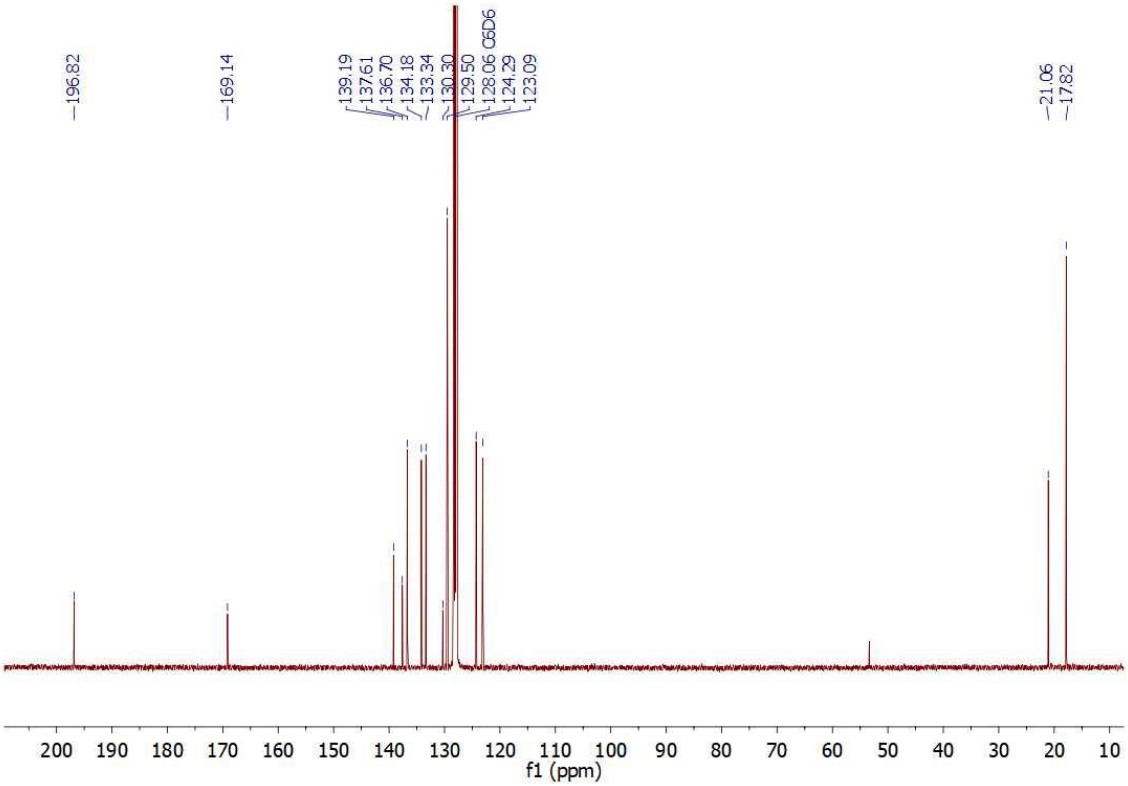

Figure 55 ^{13}C NMR of **5**

5. Synthesis of 2-mesityl-3-selenoxoisoindolin-1-one **6**

Added 100 mg (0.35 mmol) of **2** and 83 mg (1.05 mmol) of red selenium to schlenk flask, dissolved in 5 mL of THF, and cooled to -78 °C. A solution of 83 mg (0.45 mmol) of NaHMDS in 2 mL of THF was added dropwise over 30 minutes. The reaction was allowed to warm to room temperature and was stirred overnight. The solution was filtered over celite and volatiles were evaporated under reduced pressure. Purified by column chromatography (80:20 DCM: Hexanes). Recovered a teal solid (35 mg, 0.11 mmol, 15% yield). M.P. – 130-132 °C. 1H NMR (CDCl3, 400.13 MHz): δ 2.09 (s, 6H), 2.36 (s, 3H), 7.02 (s, 2H), 7.75 (t, J = 8.0 Hz, 2H), 7.87 (m, 2H), 8.09 (d, J = 8.0 Hz, 1H). 13C NMR (C6D6, 100.61 MHz): δ 18.05, 21.36, 123.55, 125.90, 126.52, 129.39, 130.66, 133.35, 134.50, 136.23, 139.66, 141.21, 169.93, 200.95. 77Se NMR (CDCl3, 76.31 MHz): δ 1240.86.

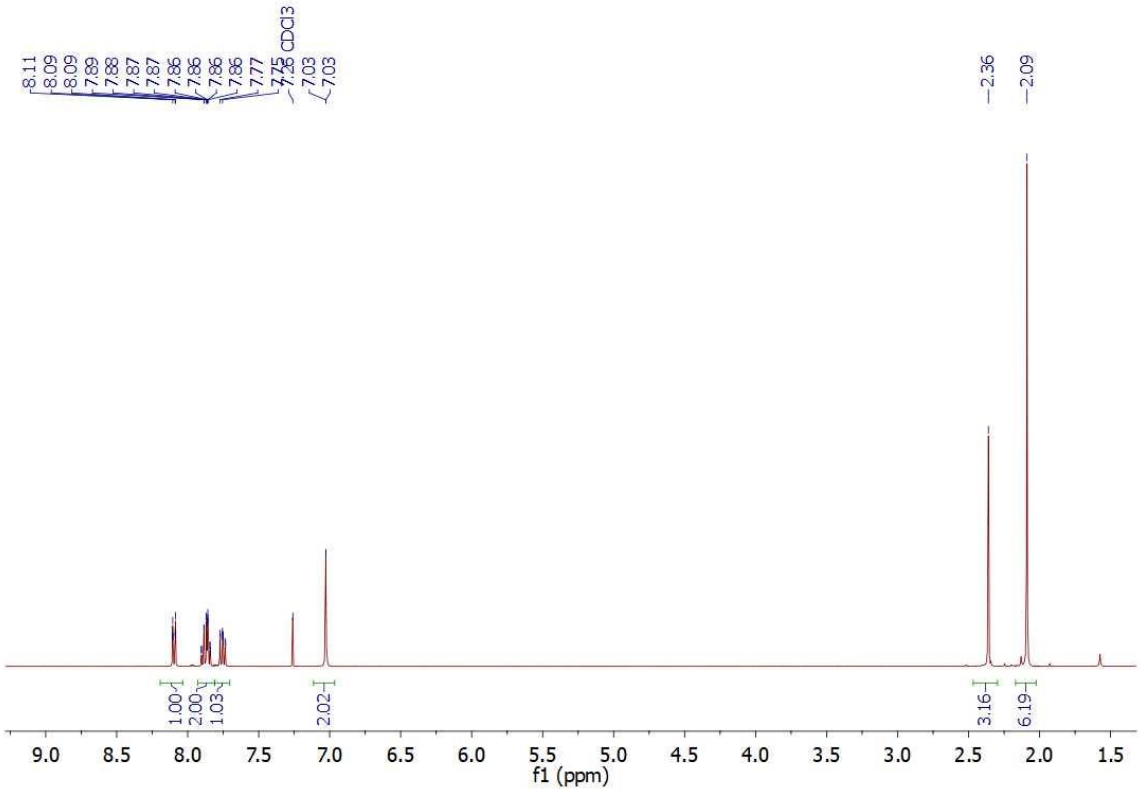

Figure 56 ^{1}H NMR of **6**

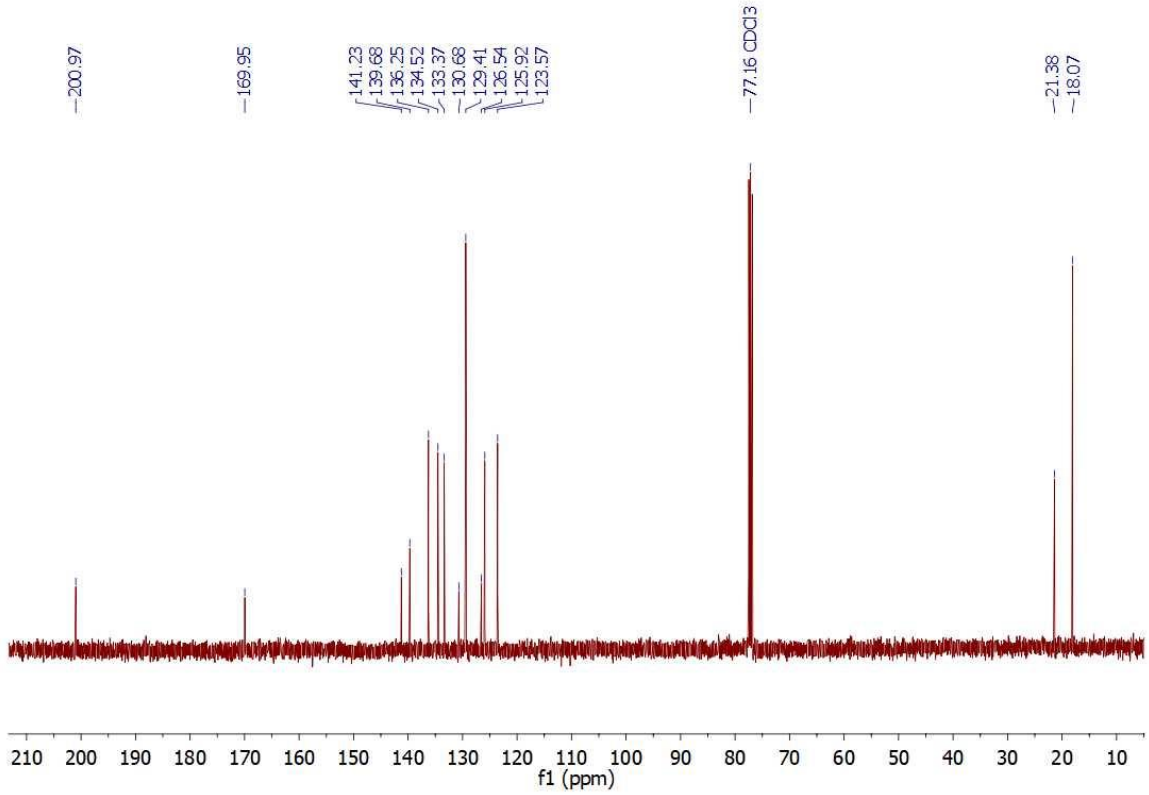

Figure 57 ^{13}C NMR of **6**

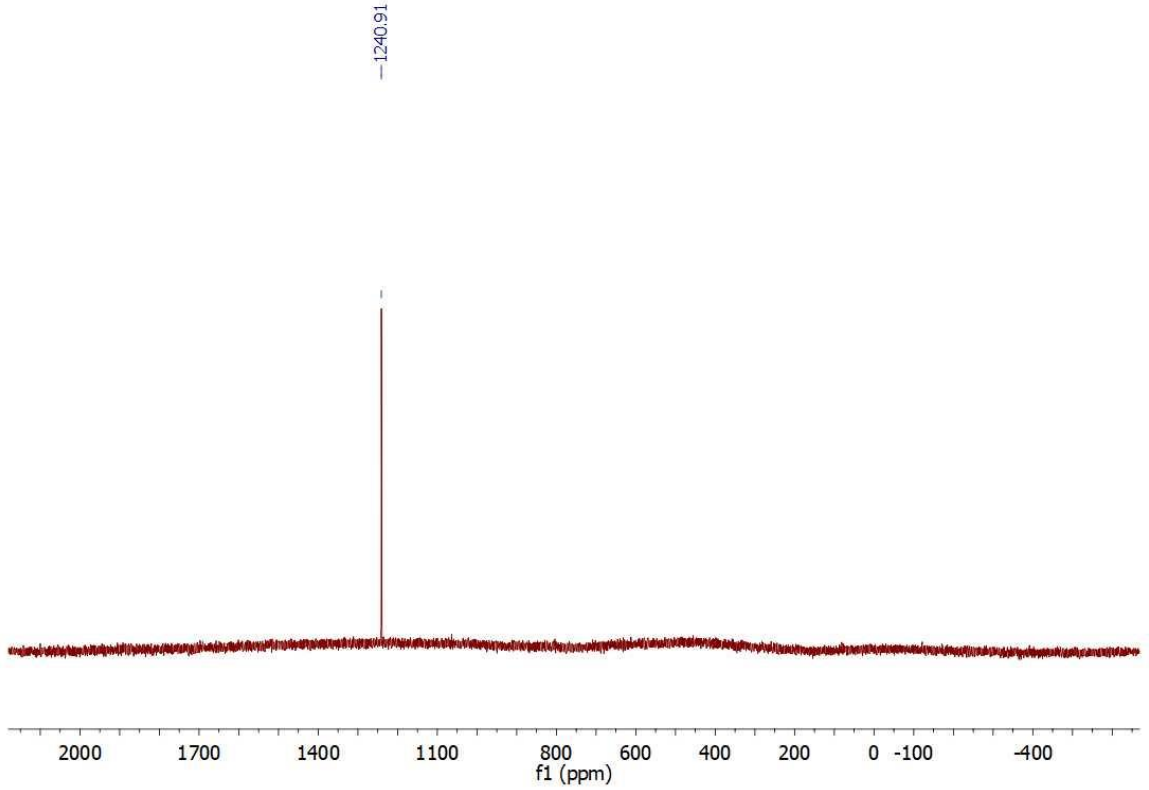

Figure 58 ^{77}Se NMR of **6**

6. Synthesis of CAmArY-Ir-COD-Cl **7**

Added 85 mg (0.30 mmol) of **2** and 100 mg (0.15 mmol) of $[Ir(COD)Cl]_2$ to Schlenk flask and dissolved in THF in glovebox. The flask was cooled to -78°C and 65 mg (0.35 mmol) of NaHMDS in 2 mL of THF was added dropwise over 30 minutes. After 1 hour the solution was allowed to warm to room temperature then stirred overnight. The solution was filtered over celite and volatiles were evaporated under reduced pressure. Purified by column chromatography (80:20 DCM: Hexanes). Recovered an orange solid (18 mg, 0.031 mmol, 10% yield). ^{1}H NMR (400 MHz, $CDCl_3$) δ 8.67 – 8.52 (m, 1H), 7.79 (ddd, J = 11.9, 5.5, 3.8 Hz, 2H), 7.75 – 7.67 (m, 1H), 7.09 (s, 1H), 6.97 (s, 1H), 5.56 – 5.42 (m, 1H), 5.13 (d, J = 4.8 Hz, 1H), 3.43 – 3.27 (m, 2H), 2.41 (d, J = 22.1 Hz, 7H), 2.22 (d, J = 5.1 Hz, 3H), 1.96 (s, 3H), 1.86 (ddd, J = 23.4, 16.2, 7.6 Hz, 5H). ^{13}C NMR (101 MHz, $CDCl_3$) δ 250.10, 169.55, 148.66, 138.96, 136.96, 135.55, 134.56, 133.90, 132.89, 132.72, 130.05, 128.27, 124.19, 123.23, 100.99, 99.17, 57.63, 56.72, 35.01, 32.01, 29.70, 27.29, 21.20, 19.66, 18.47.

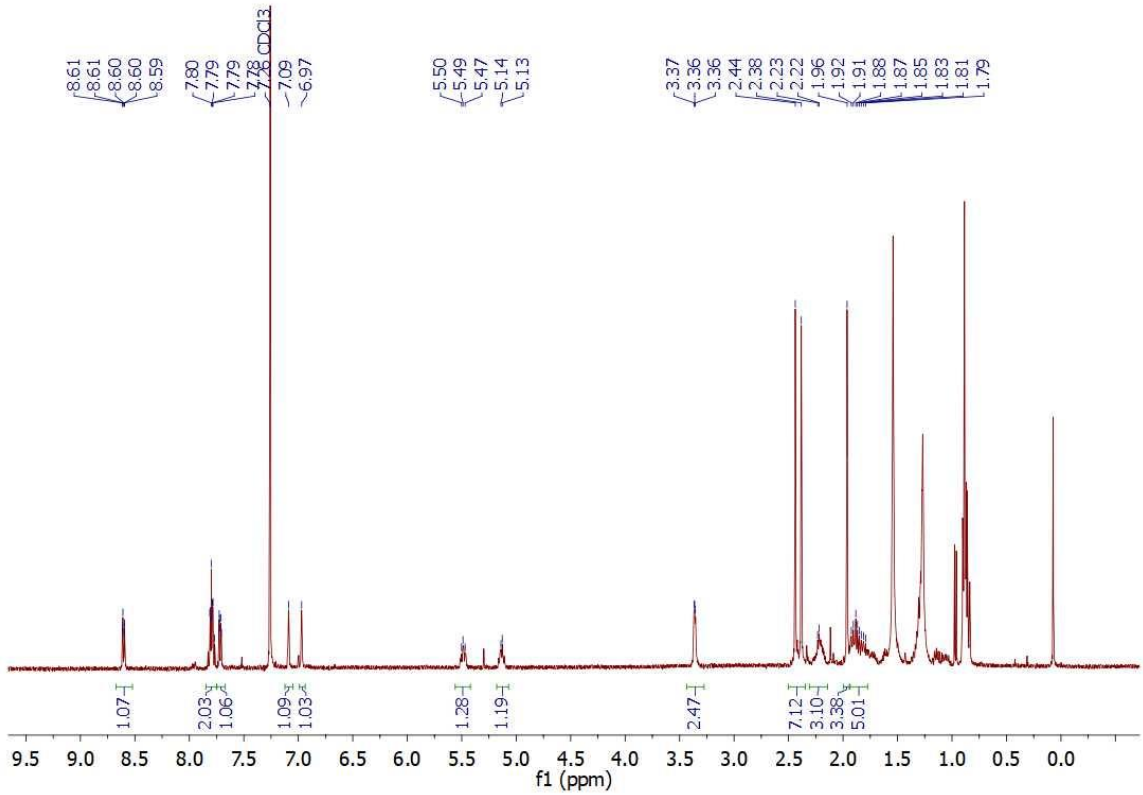

Figure 59 ^{1}H NMR of **7**

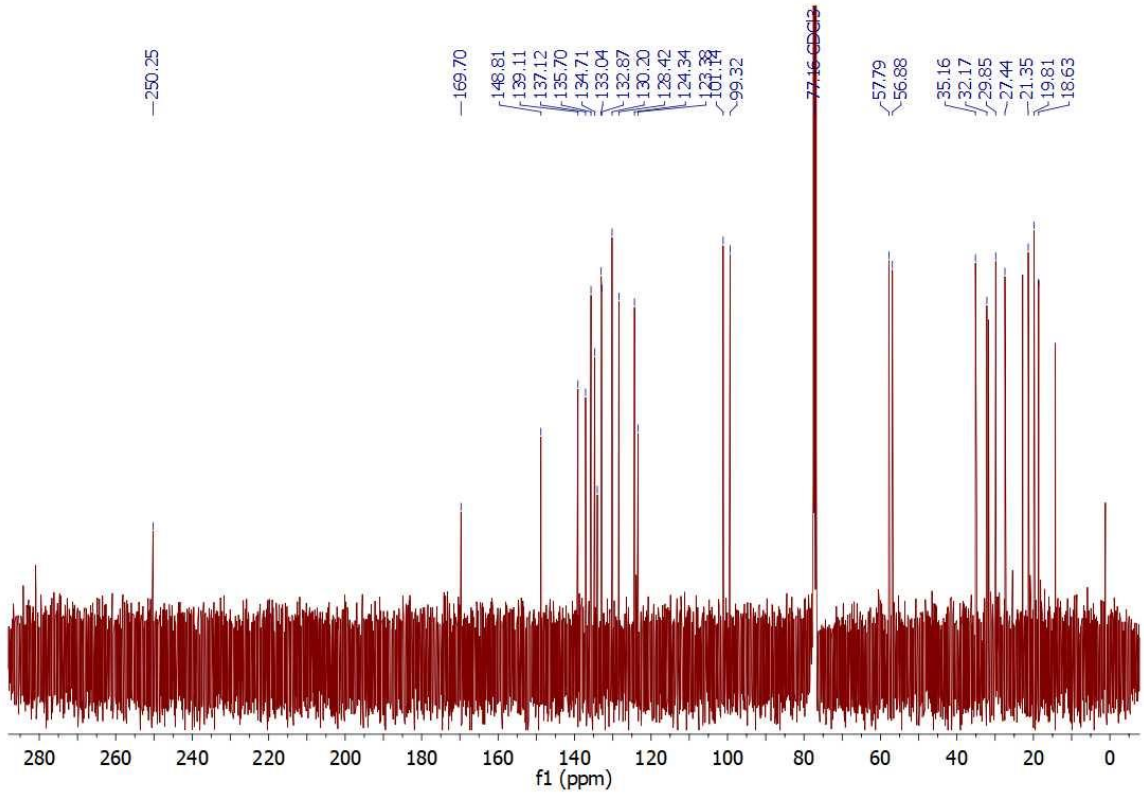

Figure 60 ^{13}C NMR of **7**

7. Synthesis of N-2,4,6-trimethylphenylphthalimide (method A) **9**

The phthalic anhydride (5.00 g, 33.8 mmol), 2,4,6-trimethylaniline (4.57 g, 33.8 mmol), and a few drops of glacial acetic acid were added to a round bottom flask equipped with a reflux condenser and heated to 150 °C for 2 hours. 100 mL of hexanes was added to the flask while still hot to precipitate the product as a white solid. The precipitate was filtered to isolate the product as a white solid (8.95 g, 33.7 mmol, 100% yield). ^{1}H NMR (400 MHz, $CDCl_3$) δ 7.98 (dd, J = 5.5, 3.0 Hz, 1H), 7.82 (dd, J = 5.5, 3.0 Hz, 1H), 7.03 (d, J = 0.6 Hz, 1H), 2.36 (s, 2H), 2.14 (s, 3H). ^{13}C NMR (101 MHz, $CDCl_3$) δ 167.29, 139.25, 136.35, 134.13, 131.97, 129.18, 126.97, 123.62, 77.21, 77.09, 76.89, 76.57, 53.28, 21.00, 17.84.

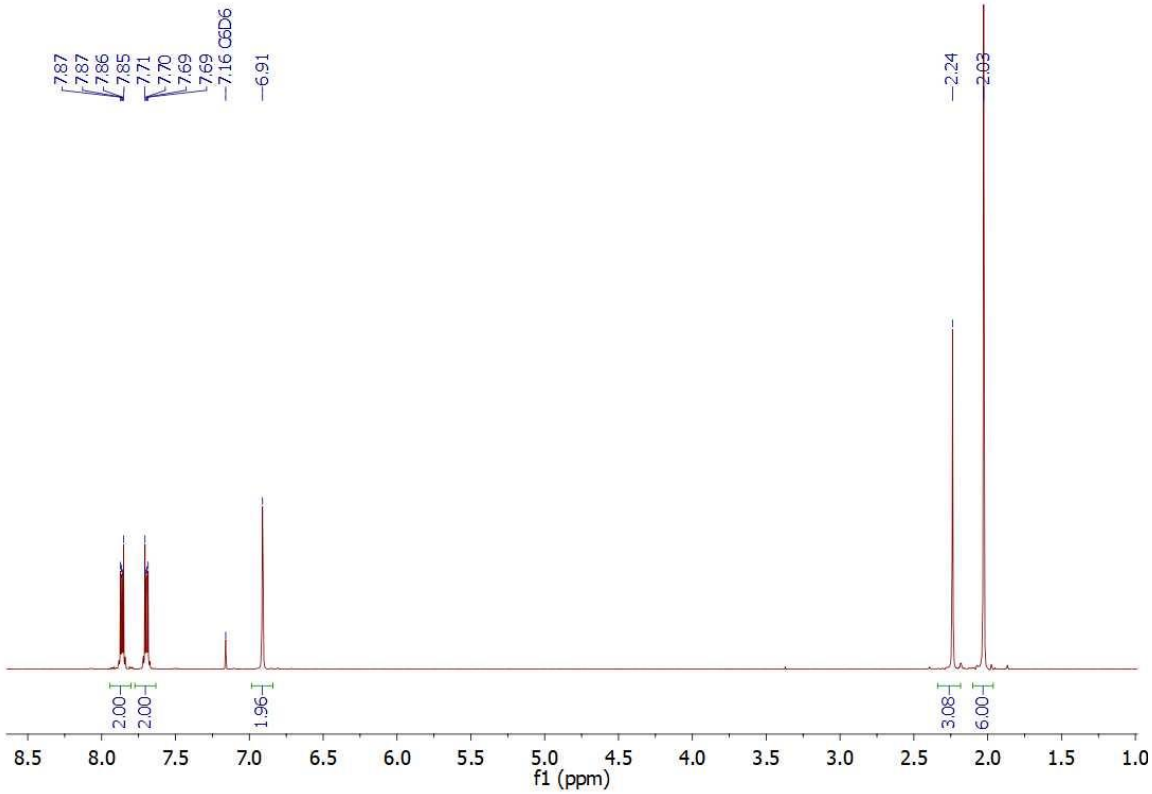

Figure 61 ^{1}H NMR of **9** direct synthesis

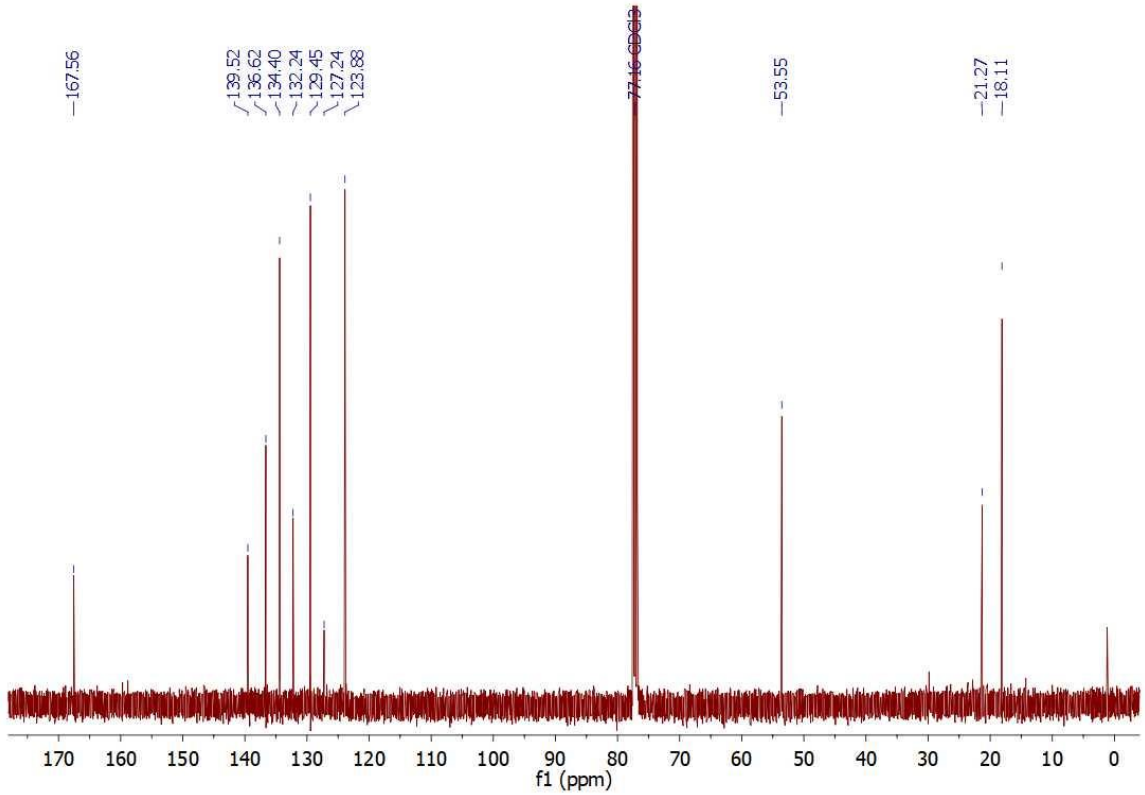

Figure 62 ^{13}C NMR of **9** direct synthesis

8. Synthesis of N-2,4,6-trimethylphenylphthalimide (method B) **9**

The CAmArY-Ir(COD)Cl **6** (50 mg, 0.081 mmol) was dissolved in 5 mL of DCM in a Schlenk flask and wrapped in foil and covered with a rubber septum. Carbon monoxide was bubbled directly into the solution until all solvent had evaporated. Then 5 mL of hexanes was added, and carbon monoxide was bubbled into the solution until all solvent had evaporated, this was repeated 2 more times. The residue was dissolved in 5 mL of hexanes again and filtered over celite to afford an off-white solid. ^{1}H NMR (400 MHz, $CDCl_3$) δ 7.98 (dd, J = 5.5, 3.0 Hz, 1H), 7.82 (dd, J = 5.5, 3.0 Hz, 1H), 7.03 (d, J = 0.6 Hz, 1H), 2.36 (s, 2H), 2.14 (s, 3H). ^{13}C NMR (101 MHz, $CDCl_3$) δ 167.29, 139.25, 136.35, 134.13, 131.97, 129.18, 126.97, 123.62, 77.21, 77.09, 76.89, 76.57, 53.28, 21.00, 17.84.

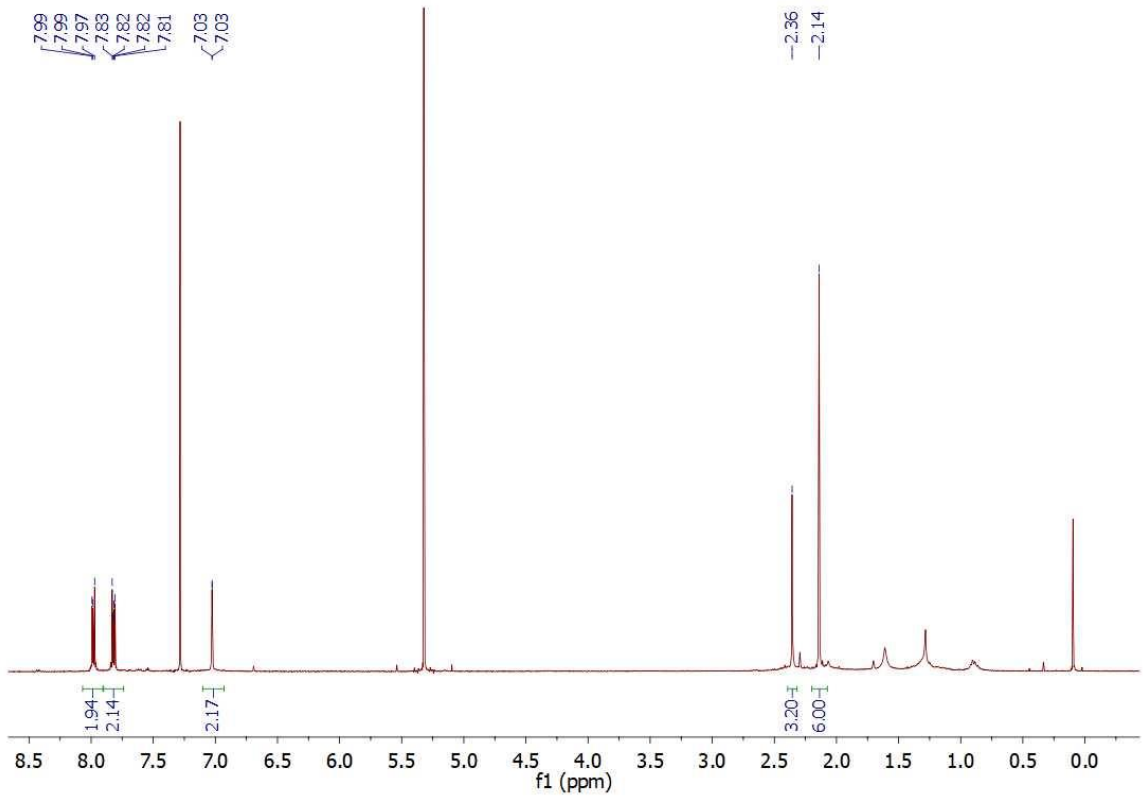

Figure 63 ^{1}H NMR of **9** carbonylation reaction

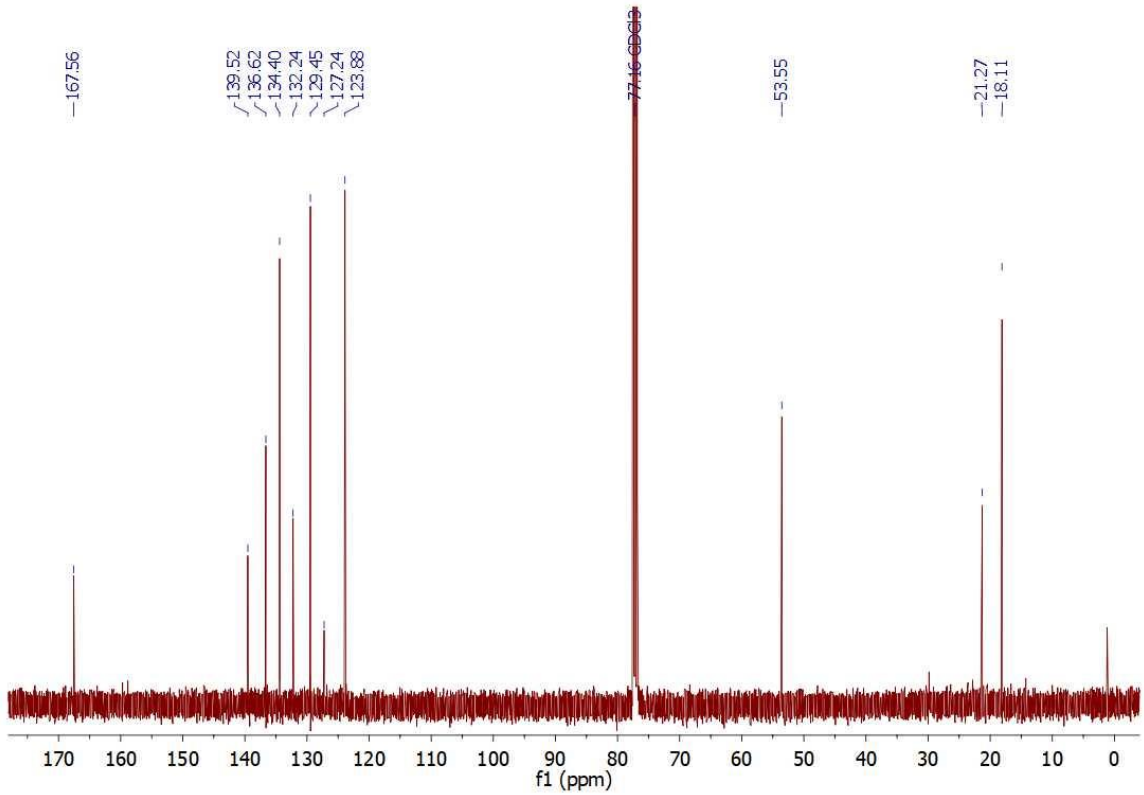

Figure 64 ^{13}C NMR of **9** carbonylation reaction

III. SYNTHESIS AND CHARACTERIZATION OF A SERIES OF DIIMINOCARBENES (DICs)

The diamidocarbene (DAC) is a very electrophilic carbene because of the inclusion of amide groups within the architecture of the ring. This also reduces the carbene's σ- donating properties. DAC's weak σ-donating makes some reactions difficult to achieve, but typically once DAC is coordinated to something it forms a stronger bond because of its strong π-accepting ability. DAC's weak σ-donating ability led our group to investigate the synthesis of various amido carbene derivatives. Small changes to the structure of DAC has resulted in large changes in its electronic properties. A few derivatives of DAC have been previously synthesized.[36,57,58] The mono(amino)amido carbene (MAAC)[57] replaces one of the carbonyl groups with an alkyl group. This allows the amino nitrogen atom to easily stabilize the carbene center, resulting in a large increase in the HOMO and LUMO energies. Unfortunately, the change to an amino group from an amide resulted in electrophilic character closer to an NHC. The cyclicalkylamido carbene (CAAmC) is another amido carbene but replaces one nitrogen atom with an alkyl group. It still retains its electrophilic character but is an unstable carbene. Bielawski reported that CAAmC rapidly undergoes C–H insertion into the methane C–H bond of one of the Dipp substituents' isopropyl groups.[48] Similarly, the cyclicamidoaryl carbene (CAmArY) is a very electrophilic amido carbene. But at this point we have not been able to stabilize it sufficiently to isolate the free carbene.

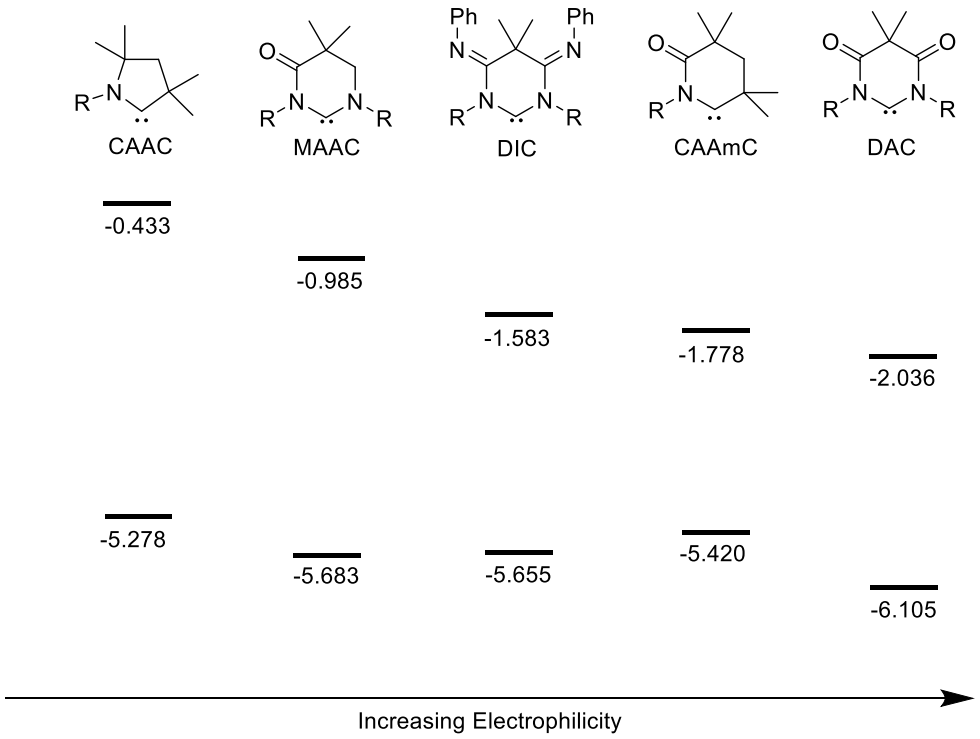

Figure 65 MO diagram of CAAC, MAAC, DIC, CAAmC, and DAC.

Our group is interested in synthesizing more isolable electrophilic carbenes. We hypothesized that if we replaced the carbonyl groups with imino substituents, it would increase the nucleophilicity of the carbene while still retaining its electrophilic character. Since nitrogen is a less electronegative element than oxygen, we thought that the nitrogen atoms adjacent to the carbene would be able to better stabilize the carbene center. Although there are reported imino carbene metal complexes[59], there seem to be no efforts to synthesize and isolate imino carbenes.

As expected, the substitution of the carbonyl groups with imino substituents raised the energy of the HOMO and LUMO. The HOMO of DIC raises to -5.655 eV from -6.01 eV for DAC (Figure 65). We expect this will increase the nucleophilicity relative to DAC and should have very similar nucleophilicity to MAAC (-5.683 eV). The energy of the LUMO is also raised to -1.583 eV from -2.036 eV for DAC (Figure 65). The

HOMO/LUMO gap for DIC remains the same as that of DAC. DFT shows similar delocalization of electron density of the HOMO and LUMO with DIC and DAC. The synthesis and characterization a series of diimino-carbenes (DICs), their precursors and selected iridium and selenium complexes is reported. An investigation of the tunability of the carbene's electronic properties through substitution of the iminoaryl group is also discussed.

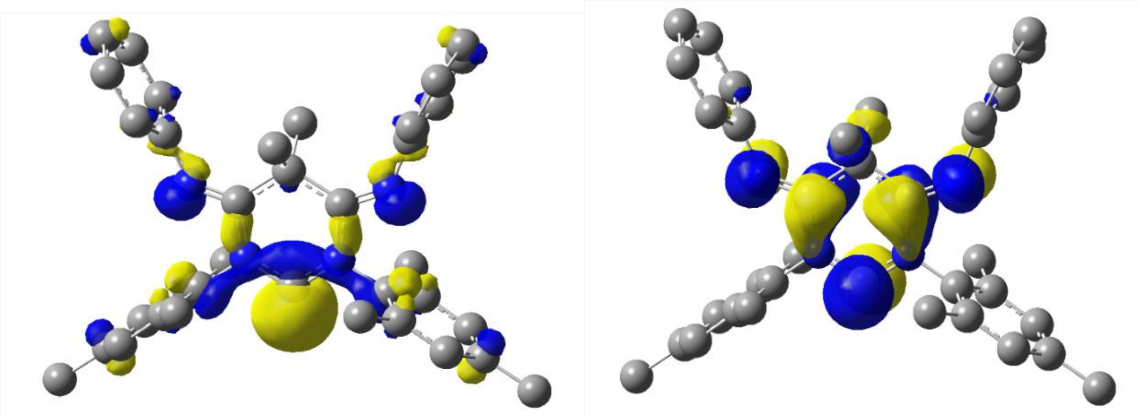

Figure 66 HOMO and LUMO orbital diagrams

The synthesis of DICs is a four-step procedure with good yields of all intermediates. First, condensation of dimethylmalonyl dichloride with aniline afforded the *N,N'*-diphenyldiamide **10a**. The diamide was doubly chlorinated with PCl_5 in refluxing toluene to afford the diimidoyl dichloride **11a** in 99% yield. The diimidoyl chloride is analogous to dimethylmalonyl dichloride which is used to synthesize DAC.

The synthesis of DICHCl **12a** was attempted in a similar way to how DACHCl is made, using one equivalent of triethylamine and *N*,*N*'-dimesitylformamidine, but this resulted in low yields (ca. 40%), and purification proved difficult because of the generation of multiple salts. To simplify purification and increase yields, **11a** was treated with the known compound *N*-trimethylsilyl-*N*,*N*'-dimesitylformamidine (TMS-

formamidine)[33] in refluxing chloroform for 5 hours. An additional base is no longer needed to remove HCl generated in the reaction because TMS–Cl is generated instead. TMS–Cl is a volatile liquid and can just be removed under vacuum after the reaction is finished. DICHCl **12a** was isolated as a bright yellow solid in nearly quantitative yield using this synthetic route.

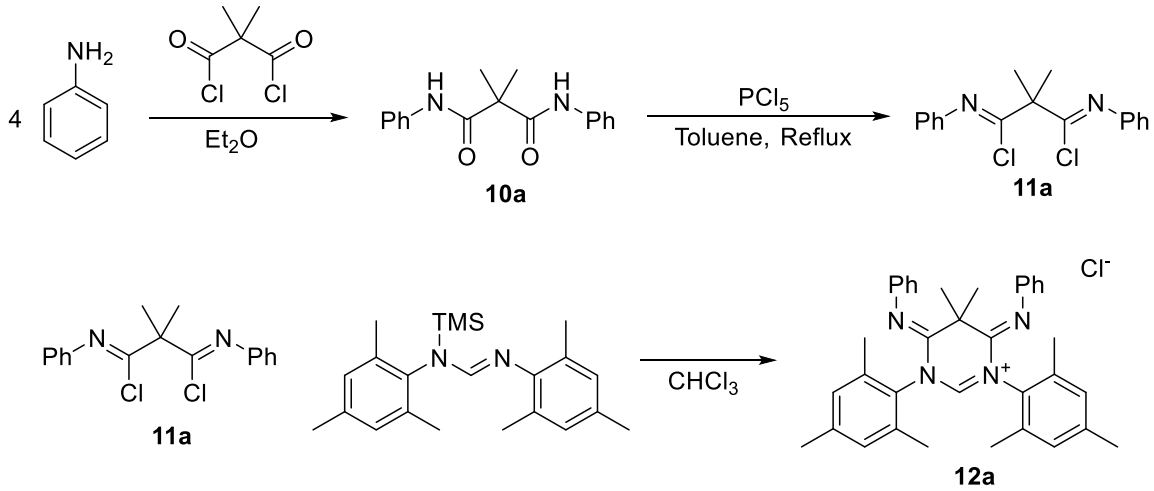

Figure 67 Synthesis of DICHCl **12a**

With the DICHCl salt **12a** in hand, attempts were made to prepare the free carbene **13a** by deprotonation with NaHMDS in benzene at room temperature. The imino groups are both in the E conformation initially in both the DICHCl and the free DIC. When dissolved in benzene however, the imino groups isomerize into a mixture of the *E-E*, *E-Z,* and *Z-Z* isomers which makes the NMR difficult to interpret. When deprotonated in toluene or THF, a single isomer (*E,E*) of the carbene can be isolated by filtration and is stable under inert atmosphere for at least a year. The ^{13}C NMR (C_6D_6) features a peak at 265.49 ppm which was assigned to the carbene carbon. The carbene resonance is upfield from DAC (278 ppm) and downfield from the NHCs (211 ppm). The calculated HOMO energy for DIC lies between DAC and NHCs. A higher HOMO energy suggests more

electron density on the carbene center. More electron density on the carbene center should correlate with an upfield shift in the carbon NMR relative to a carbene with a lower HOMO energy.

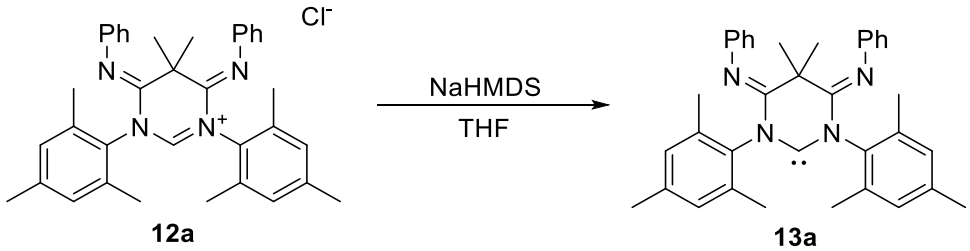

Figure 68 Synthesis of DIC free carbene

To measure the overall donating ability of DIC, the iridium carbonyl complex was synthesized and TEP studies were performed. When two equivalents of the free carbene were treated with $[Ir(COD)Cl]_2$ in THF, the iridium COD chloride complex **14a** was formed in good yield as a red solid. The *cis*-dicarbonylchloroiridium complex **15a** was synthesized by bubbling carbon monoxide through a dichloromethane (DCM)/Hexanes solution of DIC–Ir(COD)Cl. The IR spectrum of this complex shows two peaks at 1977.55 and 2060.31 cm^{-1}. Using Nolan's method, the TEP value was calculated using the average of the IR frequencies (2018.93), giving a TEP of 2046.03. This gives a very similar TEP value to CAAC (2041) which seems to be a slightly better overall donor of electron density. When compared to DAC (2057 cm^{-1}), DIC seems to be a better overall donor.

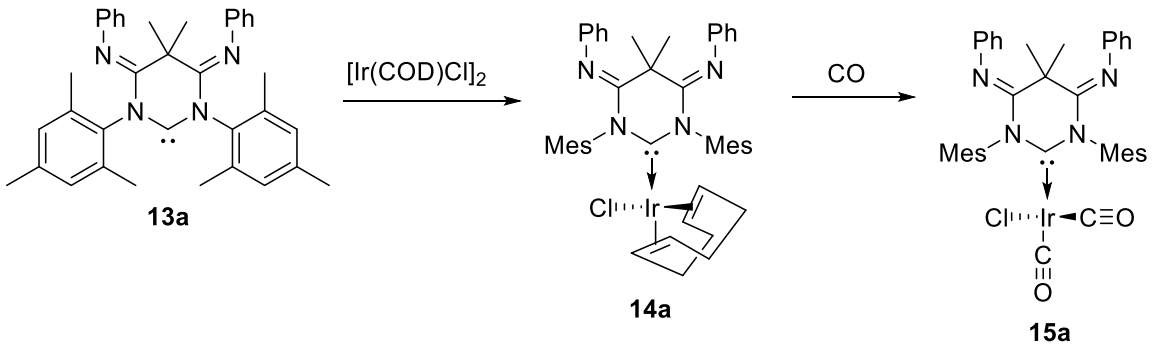

Figure 69 Synthesis of (DIC)Ir(CO)$_2$Cl **16a**

A single crystal of **15a** suitable for X-ray diffraction analysis was obtained by slow evaporation of chloroform. The N1–C1–N2 bond angle of 117.842° is within the expected range for a six-membered carbene complex.[36] Similar to what is seen with DAC, the heterocyclic ring of DIC is puckered with a torsion angle of 41.472° around N1–C4–C5–C6. The N1–C1 (1.334 Å) and N2–C1 (1.337 Å) bond lengths are within the range seen in other NHCs.[18,35,36] The N1–C4 (1.418 Å) and N2–C6 (1.412 Å) show a partial double-bond character suggesting some delocalization of the nitrogen lone-pair into those bonds. As expected the C1–Ir1–C3 bond angle is nearly linear with an angle of 174.253°.

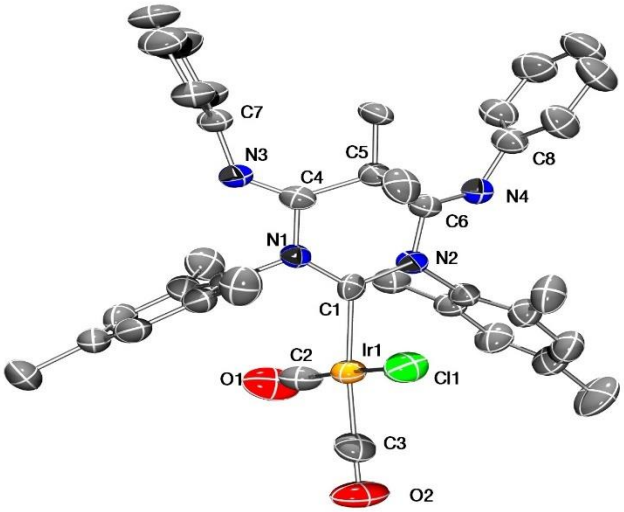

Figure 70 X-ray structure of **15a** with thermal ellipsoids set at 50% probability. Hydrogen atoms are omitted for clarity. Selected bond lengths [Å] and angles [°]: N1–C1, 1.33(4); N2–C1, 1.33(7); C1–Ir1,

2.07(0); C2–Ir1, 1.80(3); C3–Ir1, 1.84(8); Ir1–Cl, 2.34(0); C2–O1, 1.12(5); C3–O2, 1.13(3); C4–N3, 1.23(9); C6–N4, 1.24(5); C4–N1, 1.41(8); C6–N2, 1.41(2); C7–N3, 1.39(9); C8–N4, 1.40(3); N1–C1–N2, 117.84(2); C4–N3–C7, 131.12(1); C6–N4–C8, 130.23(6); N1–C4–N3, 113.65(7); N2–C6–N4, 114.06(1); C1–Ir1–C3, 174.25(3); C1–N1–C4–C5, 23.20(5); N1–C4–C5–C6, 42.44(6).

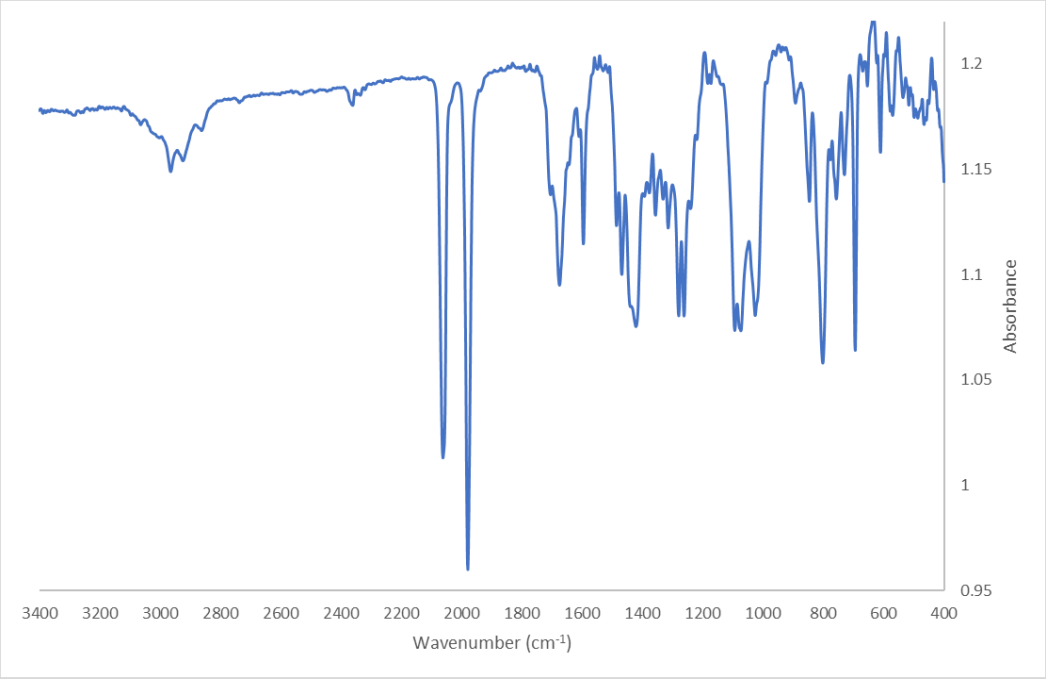

Figure 71 IR spectra of (DIC)Ir(CO)$_2$Cl **15a** showing two carbonyl resonances at 1977 and 2060 cm^{-1}

When the free carbene was treated with elemental selenium, the selenium carbene adduct **16a** was obtained. 16a exhibited a ^{77}Se NMR shift ($CDCl_3$) of 669 ppm suggesting that it is much more electrophilic than CAAC (492 ppm) and less electrophilic than DAC (847 ppm). A single crystal of **14a** suitable for X-ray diffraction analysis was obtained by slow evaporation of hexanes. The overall structure of the DIC in **14a** was isostructural with **16a**, with the back of the ring still twisted out of plane and the N1–C1–N2 bond angle was still in the expected range (117.236°). The C1–Se1 bond length of 1.762 Å is near the expected bond length for a π-acidic carbene.[51,55] One notable difference in the heterocyclic structure of the carbene is the shortening of the N1–C3 and N2–C5 bond lengths relative to complex **16a**. N1–C3 shortened from 1.418 Å to 1.378 Å and N2–C5 shortened from 1.412 Å to 1.381 Å.

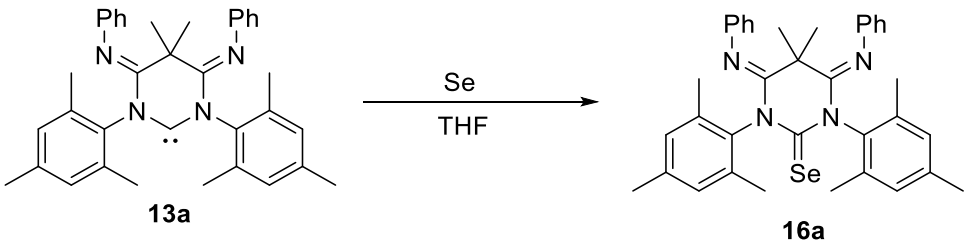

Figure 72 Synthesis of DIC selenium adduct

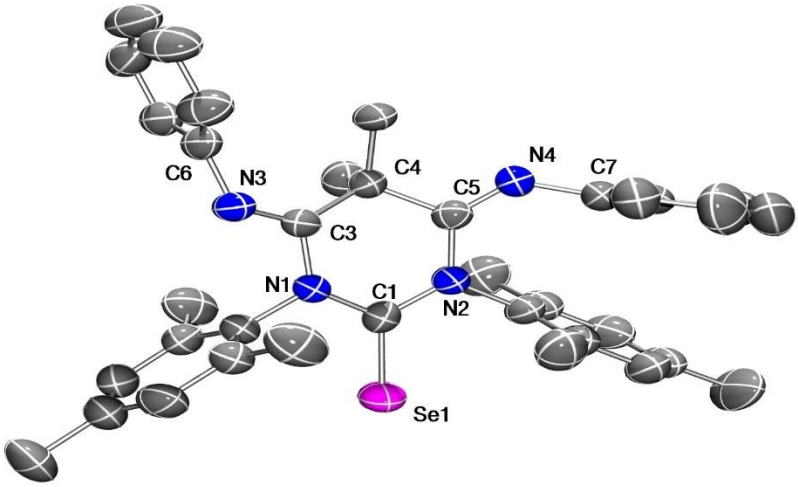

Figure 73 X-ray structure of **14a** with thermal ellipsoids set at 50% probability. Hydrogen atoms are omitted for clarity. Selected bond lengths [Å] and angles [°]: N1–C1, 1.35(5); N2–C2, 1.35(5); N1–C3, 1.37(8); N2–C5, 1.38(1); N3–C3, 1.23(8); N4–C5, 1.22(5); N3–C6, 1.36(6); N4–C7, 1.35(7); C1–Se1, 1.76(2); N1–C1–N2, 117.23(6); N3–C3–N1, 127.53(4); N4–C5–N2, 114.84(2); C6–N3–C3, 132.28(7); C7–N4–C5, 130.03(0); N1–C3–C4–C5, -41.47(2); C1–N1–C3–C4, 18.42(9).

We were also interested to see if we could further modify the electronic properties of a DIC by modification of the aryl groups in the imino substituents. DFT calculations were used to estimate the HOMO and LUMO energies of DIC derivatives with varying substitutions at the *para*-position of the imino aryl moieties. The effect of para-substitution was investigated since it should have a greater effect when compared to ortho-substitution. A plot of the HOMO and LUMO energy levels as compared to the Hammett parameters (σ_p) gave a linear relationship (Figure 74). As electron donating or withdrawing groups are substituted, the HOMO and LUMO energies are raised or

lowered, respectively. The energy values for the LUMO are slightly more affected than the HOMO energies. Figure 75 shows resonance structures of the most electron donating and withdrawing derivatives. These resonance structures give insight into what effects the substitution has on the nitrogen atom's ability to stabilize the p-orbital of the carbene atom. Electron withdrawing groups pull electron density away from the carbene causing the lone pair on the nitrogen atom to be pulled away from the carbene. The electron donating groups push electron density towards the carbene allowing the nitrogen atoms to easily donate into the empty orbital of the carbene.

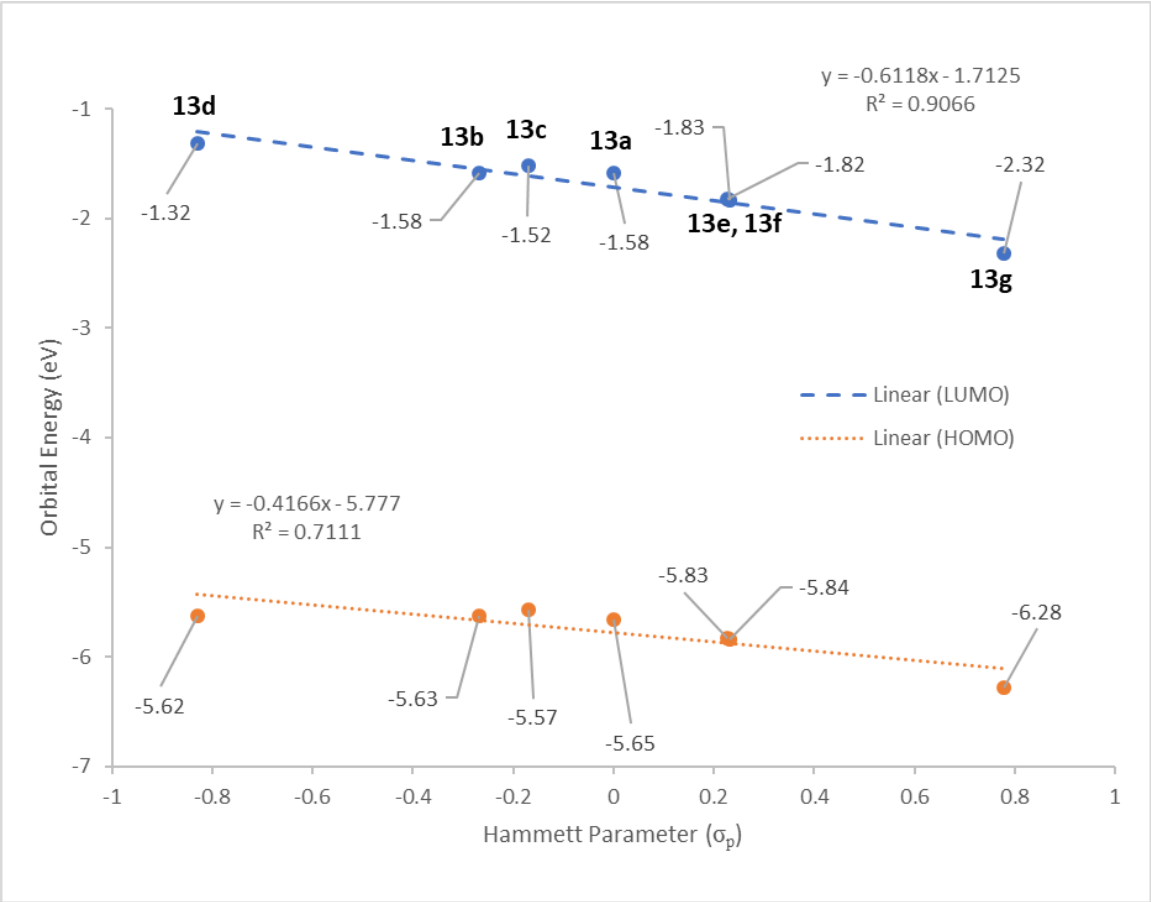

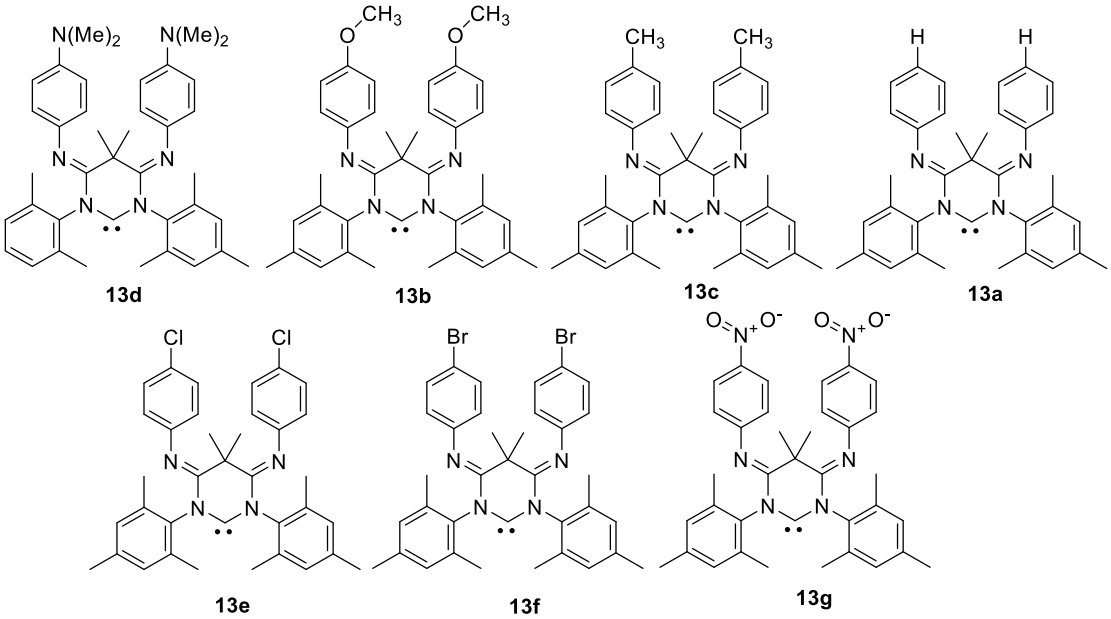

Figure 74 Hammett analysis of para-substituted DIC derivatives. Orange points are HOMO energies, Blue points are LUMO energies. Dashed line is the linear regression for LUMO energies, dotted line is the linear regression for the HOMO energies.

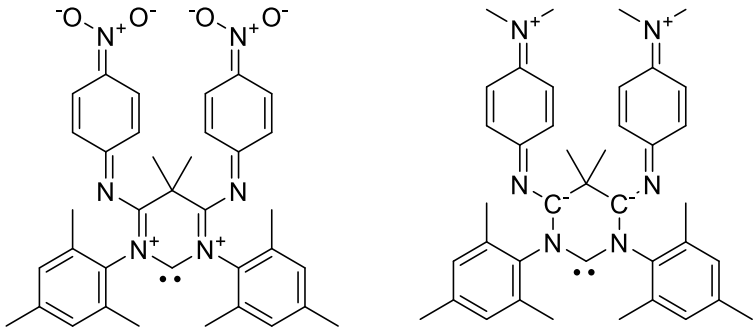

Figure 75 Resonance structures of substituted DIC derivatives demonstrating the effect of nucleophilicity of the carbenes.

A few of the substituted derivatives and their selenium adducts have been synthesized and studied via ^{77}Se NMR. The *para*-bromophenyl and *para*-tolyl derivatives were synthesized. Attempts to synthesize the other derivatives are ongoing and a more complete analysis will be performed then. A plot of the selenium adducts as compared to the energy value of the LUMO shows a linear correlation. This provides a relatively easy synthetic route to tune the carbene energy values over a range of about 1 eV for the LUMO and 0.66 eV for the HOMO. Interestingly, substitution of a nitro group results in a carbene that should be even more electrophilic than DAC. A TEP analysis was not performed for these derivatives because the very small range of possible values would have likely given very similar data.

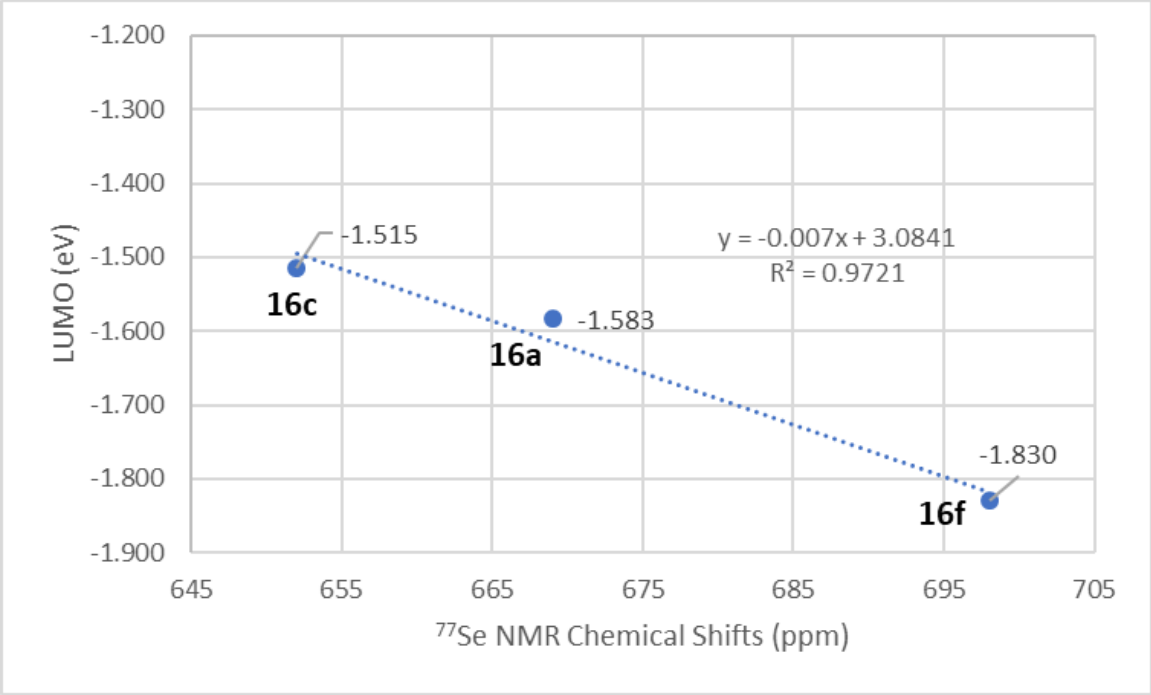

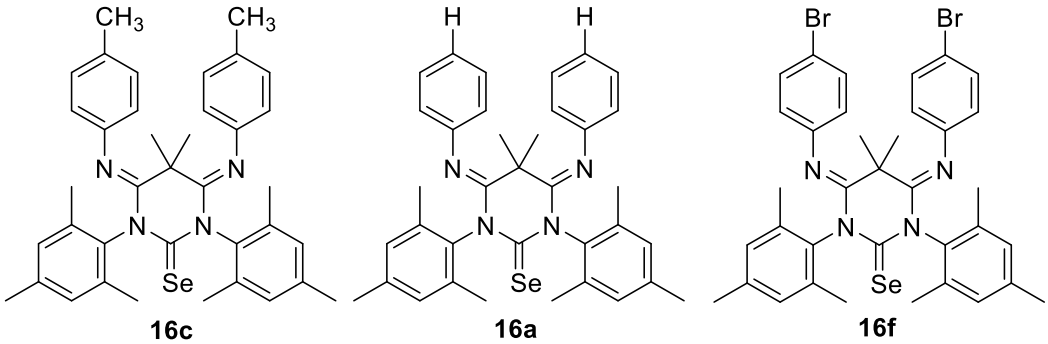

Figure 76 Plot of LUMO energies as compared to selenium NMR shifts of substituted DIC selenium adducts

Our group is also interested in the electronic properties of the five-membered analogue (DIC5) of the DIC. DFT calculations show that the DIC5 is both more nucleophilic and electrophilic than DAC. The proposed synthesis for DIC5 follows essentially the same synthetic route as the six-membered analogue, only changing the acid chloride to oxalyl chloride from dimethylmalonyl dichloride (Figure 77).

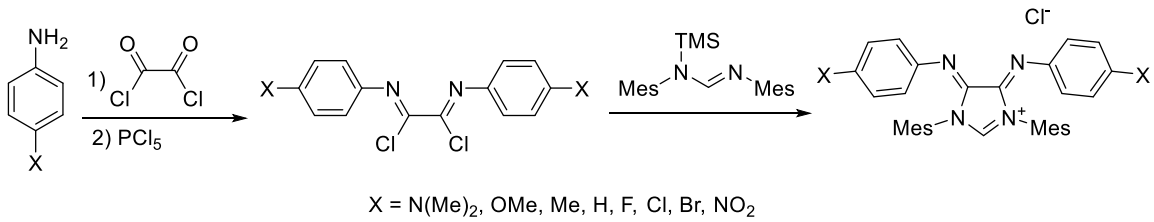

Figure 77 Proposed synthesis of five-membered DIC derivatives

Similar studies of the effect of substitution of the imino phenyl groups will also be performed. Computational studies show a much stronger linear relationship between the Hammett parameters (σ_p) and the frontier orbital energies. As with the six-membered DIC, the LUMO energy is more affected by substitution. The results of the Hammett analysis for the five-membered DIC derivatives are shown in Figure 78.

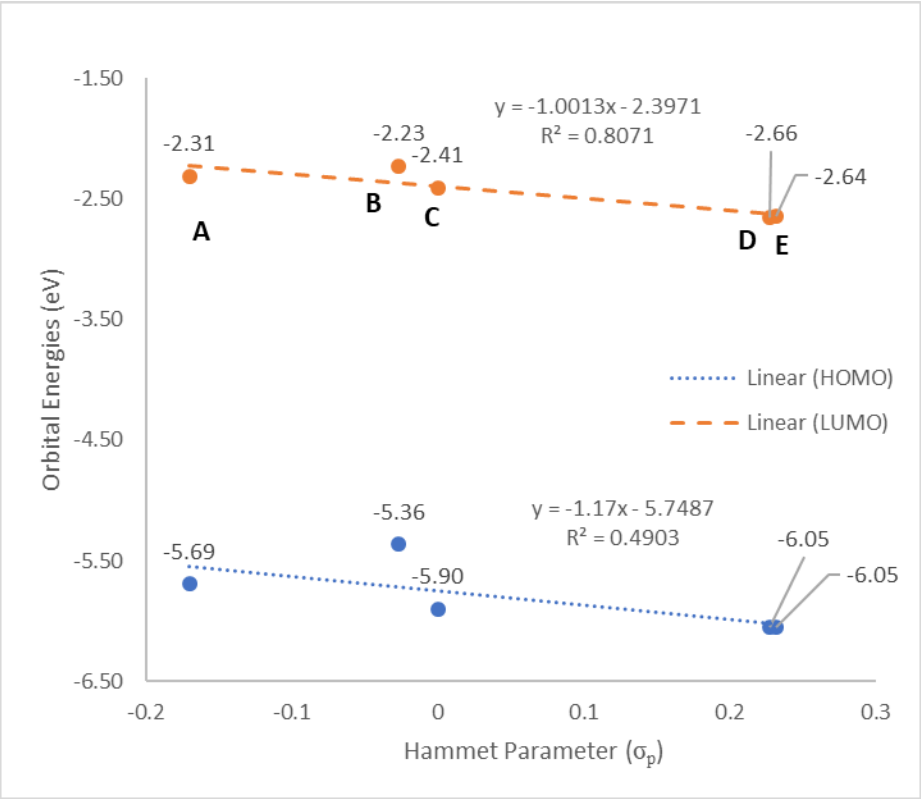

Figure 78 Hammett analysis of *para*-substituted DIC5 derivatives. Orange points are HOMO energies, Blue points are LUMO energies. Dashed line is the linear regression for LUMO energies, dotted line is the linear regression for the HOMO energies

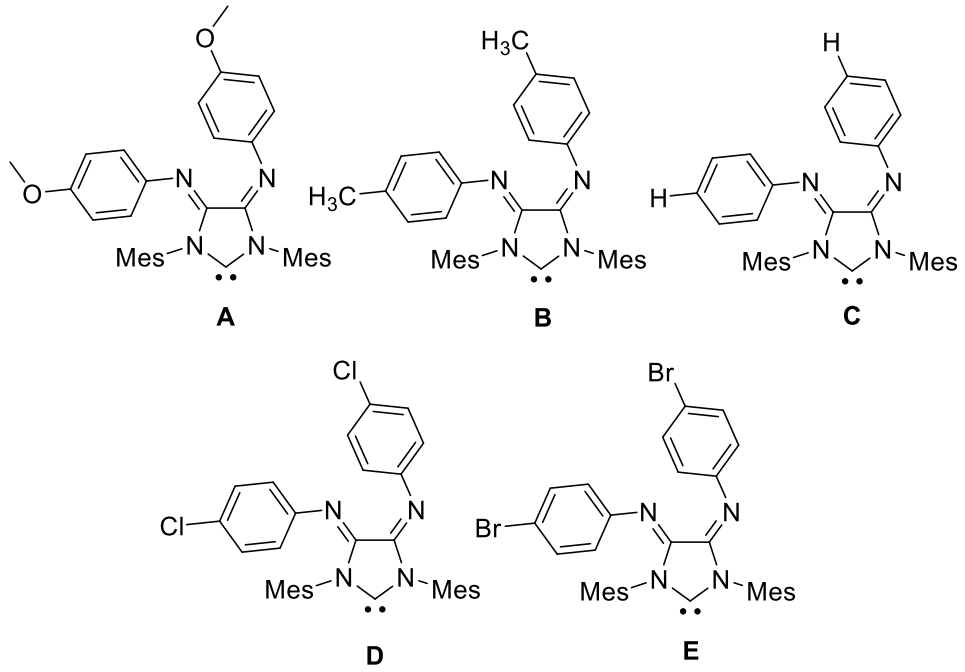

Figure 79 Structures of DIC5 derivatives studied in the Hammett analysis shown in **Figure 78**

In conclusion, we have described the synthesis and characterization of a diimino carbene. The carbene was synthesized in 4 steps with good yields. The TEP analysis indicated that DIC was indeed more nucleophilic than DAC as expected. Also, not surprisingly, the ^{77}Se NMR showed that while it is still more electrophilic than most carbenes, it is less electrophilic than DAC. We also demonstrated DIC's ability to easily be electronically tuned over a wide range of HOMO and LUMO energies, and in one case it is more electrophilic than DAC. The five-membered derivative (DIC5) is currently being explored. In other future experiments, our group will investigate the electronic properties of the phosphorus analogues of the DIC and DIC5.

Experimental Section

1. Synthesis of Diphenyldiamide **10a**

Aniline (2.6 mL, 28 mmol) was dissolved in 300 mL diethyl ether in a round bottom flask and purged with nitrogen and covered with a rubber septum. Then dimethylmalonyl dichloride (1.0 mL, 7.6 mmol) was added dropwise via a syringe; a large amount of white precipitate immediately forms. The reaction was stirred for 2 hours. Then 100 mL water was added to the flask and was stirred for 10 minutes. The solution was filtered and the precipitate was washed with another 50 mL water and 100 mL diethyl ether. The product was isolated as a white solid. Yield, 1.95 g, 91 %. ^{1}H NMR (400 MHz, $CDCl_3$) δ 8.46 (s, 1H), 7.59 – 7.47 (m, 2H), 7.34 (dd, J = 8.4, 7.6 Hz, 2H), 7.18 – 7.08 (m, 1H), 1.69 (s, 3H). ^{13}C NMR (101 MHz, DMSO) δ 172.26, 139.59, 128.89, 123.91, 120.84, 52.41, 23.92.

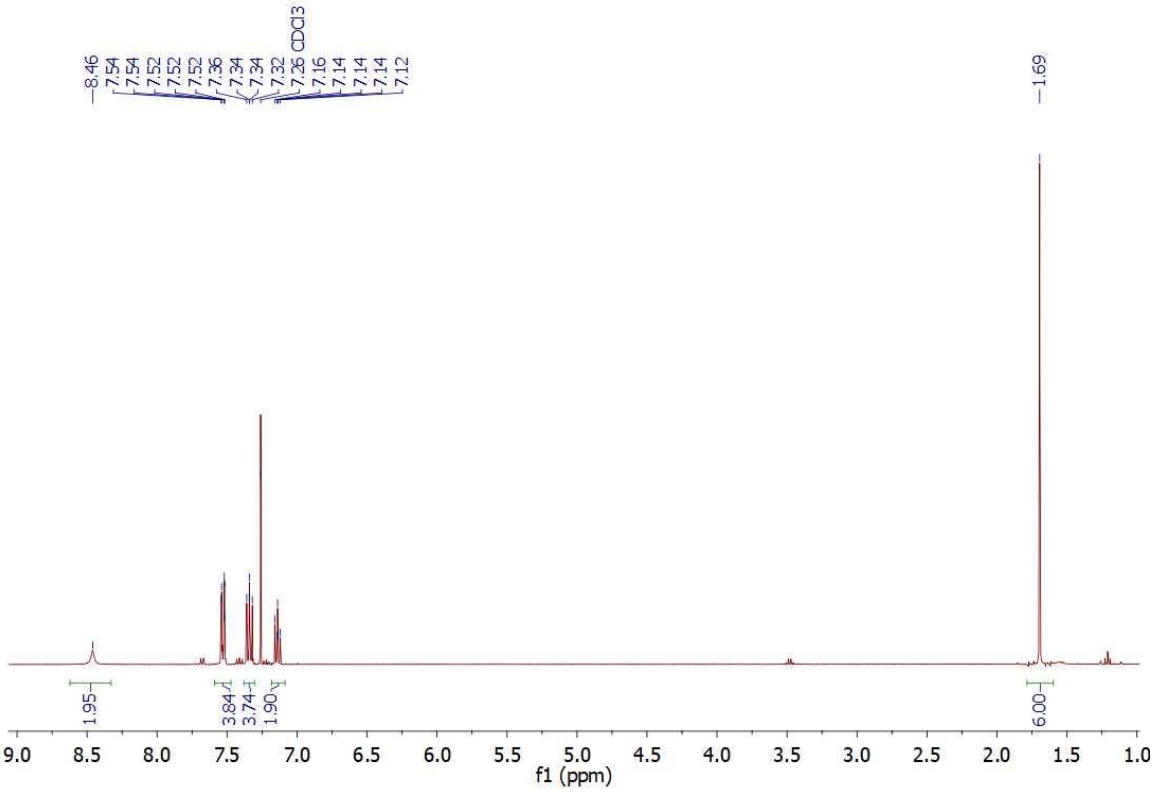

Figure 80 ^{1}H NMR of **10a**

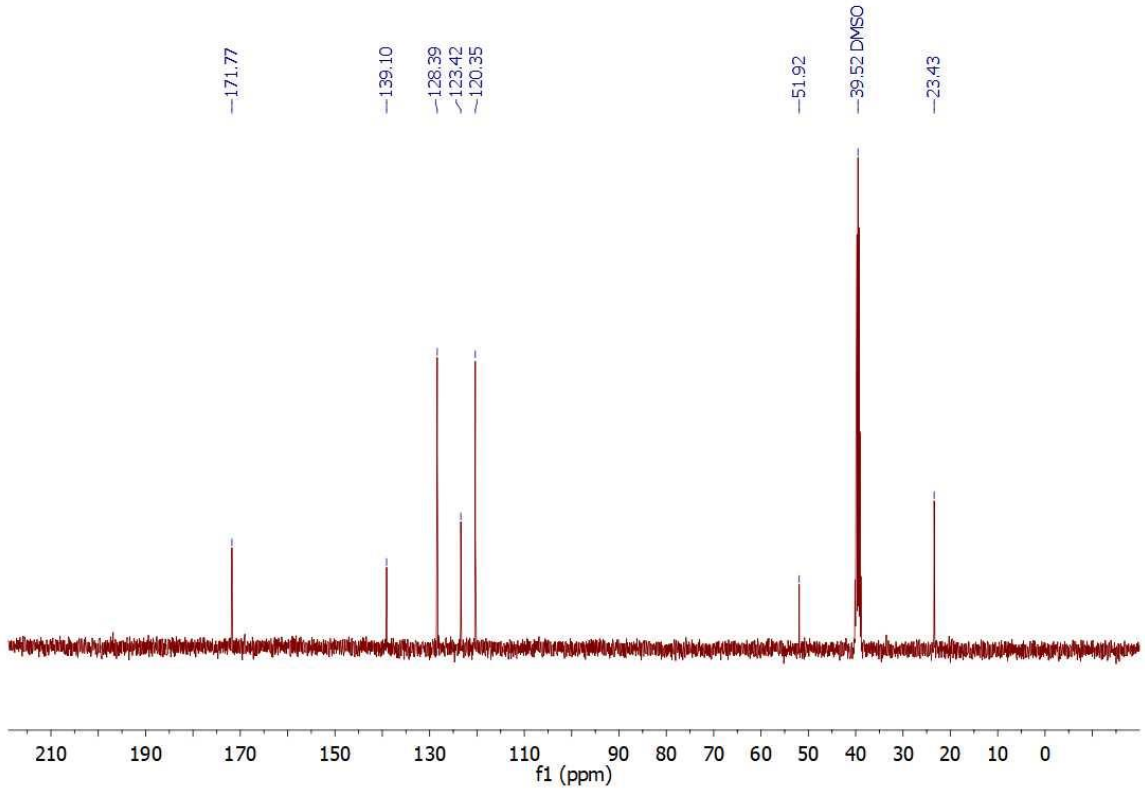

Figure 81 ^{13}C NMR of **10a**

2. Synthesis of Di-*p*-tolyldiamide **10c**

p-toluidine (3.24g, 30 mmol) was dissolved in 300 mL diethyl ether in a round bottom flask and purged with nitrogen and covered with a rubber septum. Then dimethylmalonyl dichloride (1.0 mL, 7.6 mmol) was added dropwise via a syringe A large amount of white precipitate immediately forms. The reaction was stirred for 2 hours. Then 100 mL water was added to the flask and was stirred for 10 minutes. The solution was filtered and the precipitate was washed with another 50 mL water and 100 mL diethyl ether. The product was isolated as a white solid. Yield, 1.70 g, 73%. ^{1}H NMR (400 MHz, $CDCl_3$) δ 8.43 (s, 1H), 7.39 (d, J = 8.5 Hz, 2H), 7.13 (d, J = 8.1 Hz, 2H), 2.31 (s, 3H), 1.66 (s, 3H). ^{13}C NMR (126 MHz, DMSO) δ 172.11, 130.56, 129.26, 123.37, 120.92, 52.24, 23.96, 20.92.

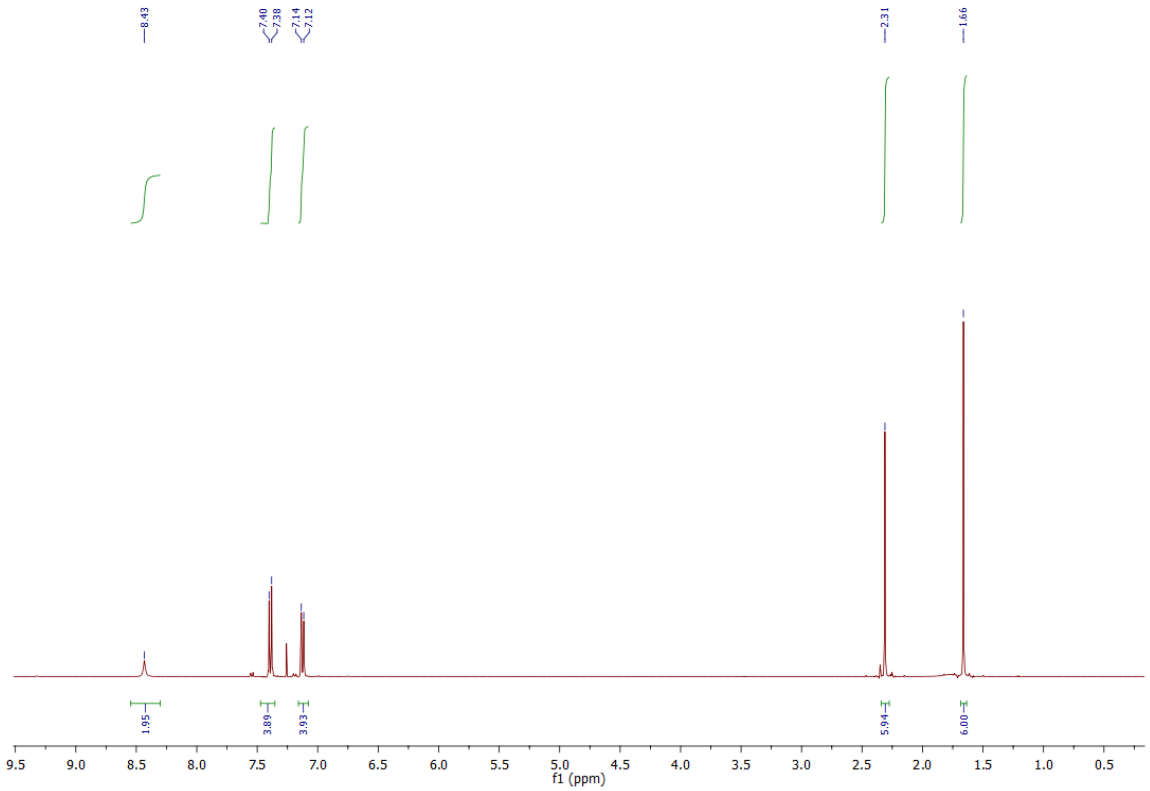

Figure 82 ^{1}H NMR of **10c**

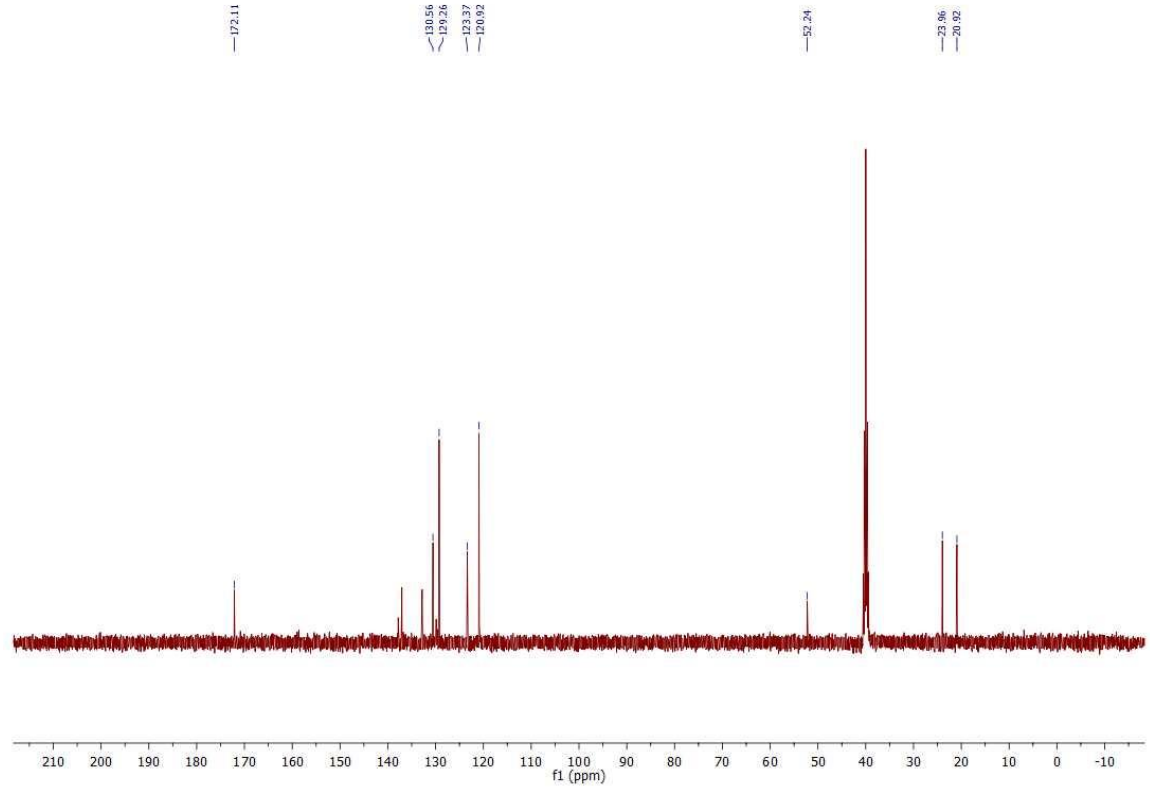

Figure 83 ^{13}C NMR of **10c**

3. Synthesis of Di-*p*-anisolediamide **10b**

p-anisidine (3.73 g, 30 mmol) was dissolved in 300 mL diethyl ether in a round bottom flask and purged with nitrogen and covered with a rubber septum. Then dimethylmalonyl dichloride (1.0 mL, 7.6 mmol) was added dropwise via a syringe and stirred for 2 hours. A large amount of white precipitate immediately forms. 100 mL water was added to the flask and was stirred for 10 minutes. The solution was filtered and the precipitate was washed with another 50 mL water and 100 mL diethyl ether. The product was isolated as a white solid. Yield, 2.2 g, 85%. ^{1}H NMR (400 MHz, DMF) δ 9.55 (s, 1H), 7.88 – 7.68 (m, 2H), 7.10 – 6.95 (m, 2H), 3.94 (s, 3H), 1.77 (s, 3H). ^{13}C NMR (126 MHz, DMSO) δ 171.98, 155.89, 132.61, 122.55, 114.01, 55.62, 51.90, 24.03.

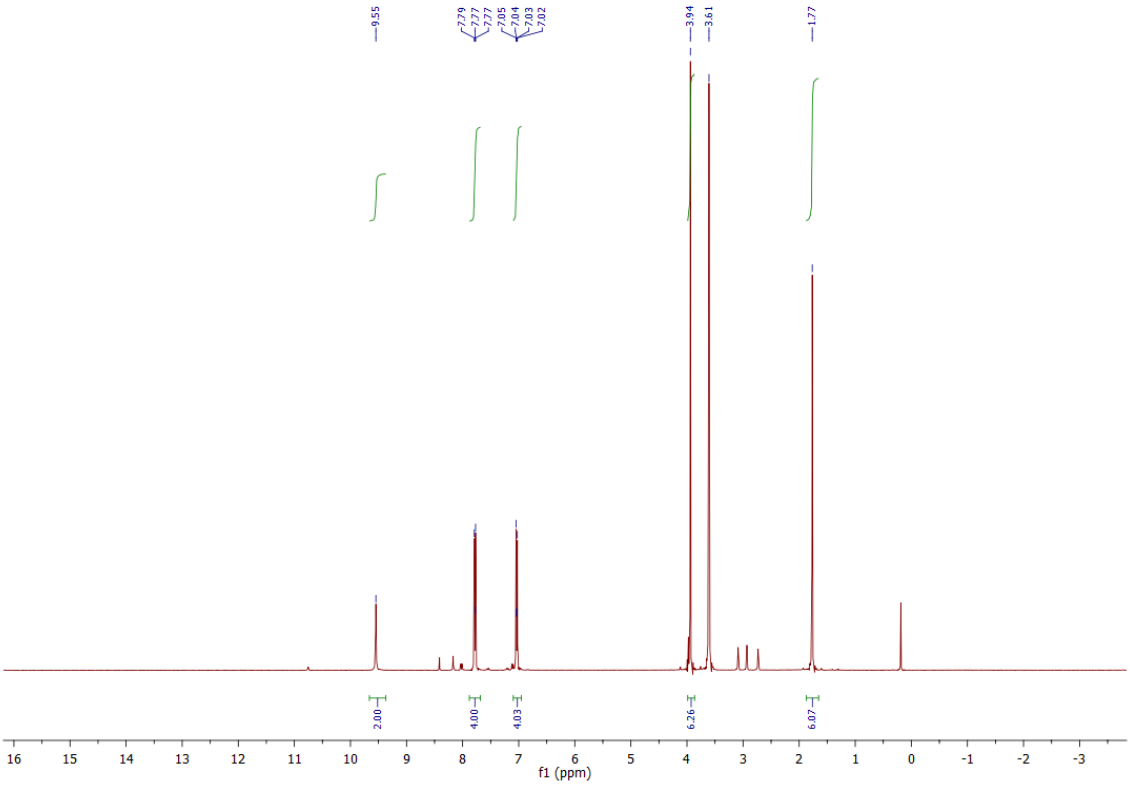

Figure 84 ^{1}H NMR of **10b**

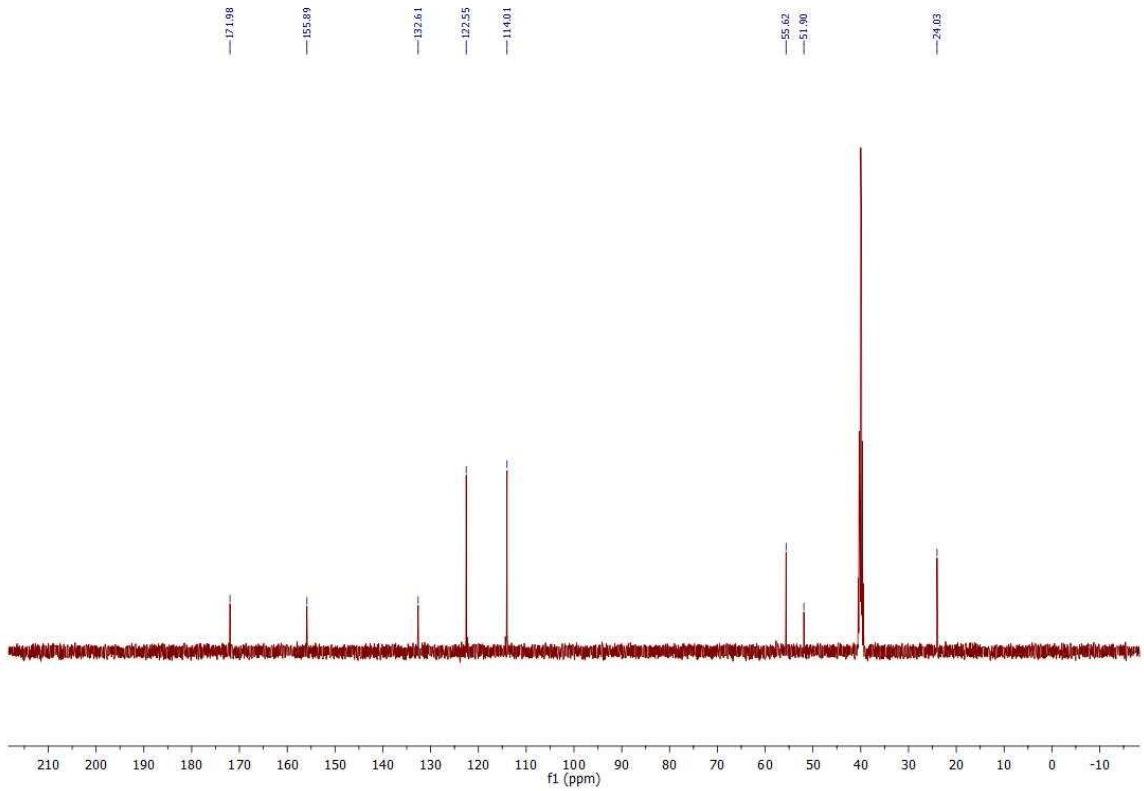

Figure 85 ^{13}C NMR of **10b**

4. Synthesis of Di(p-ClPh)diamide **10e**

p-chloroaniline (3.86 g, 30 mmol) was dissolved in 300 mL diethyl ether in a round bottom flask and purged with nitrogen and covered with a rubber septum. Then dimethylmalonyl dichloride (1.0 mL, 7.6 mmol) was added dropwise via a syringe and a large amount of white precipitate immediately forms. The reaction was stirred for 2 hours. Then 100 mL water was added to the flask and was stirred for 10 minutes. The solution was filtered and the precipitate was washed with another 50 mL water and 100 mL diethyl ether. The product was isolated as a white solid. Yield, 2.20 g, 83%. ^{1}H NMR (400 MHz, DMSO) δ 9.57 (s, 1H), 7.68 (d, J = 8.9 Hz, 2H), 7.33 (dd, J = 7.0, 1.9 Hz, 2H), 1.52 (s, 3H). ^{13}C NMR (126 MHz, DMSO) δ 172.33, 138.54, 128.79, 127.56, 122.37, 52.59, 23.79.

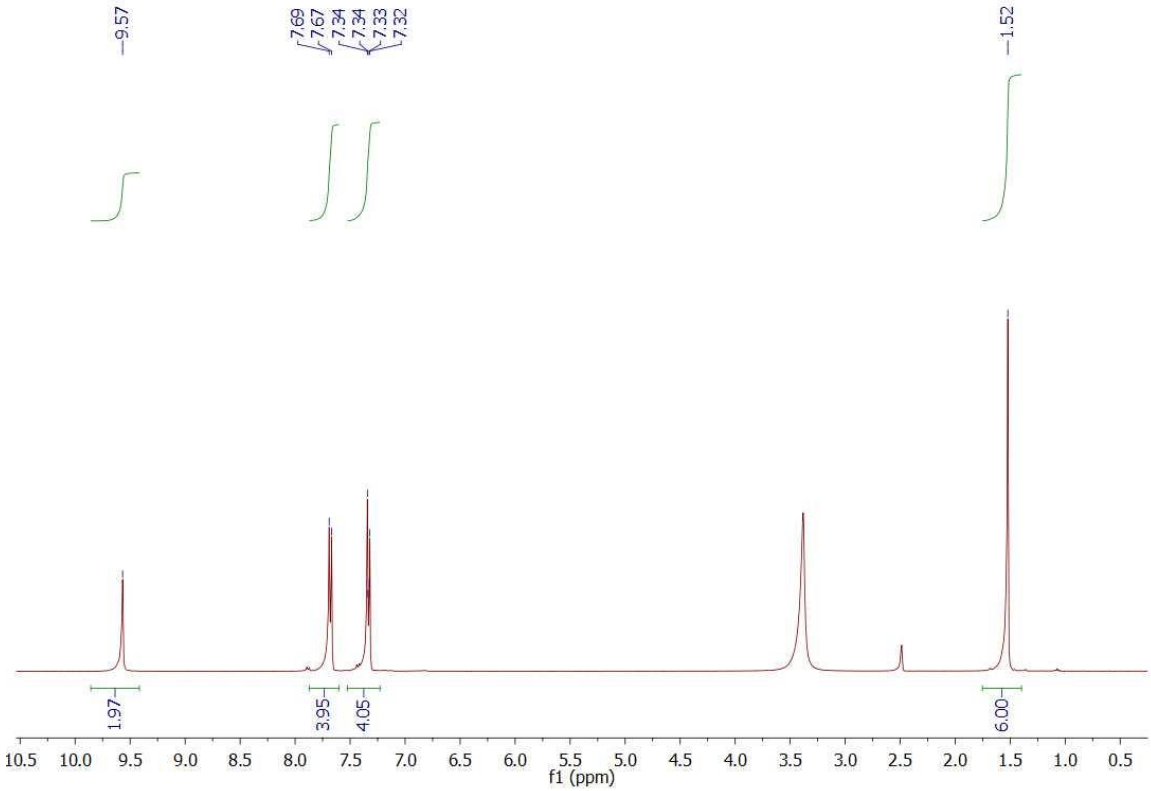

Figure 86 ^{1}H NMR of **10e**

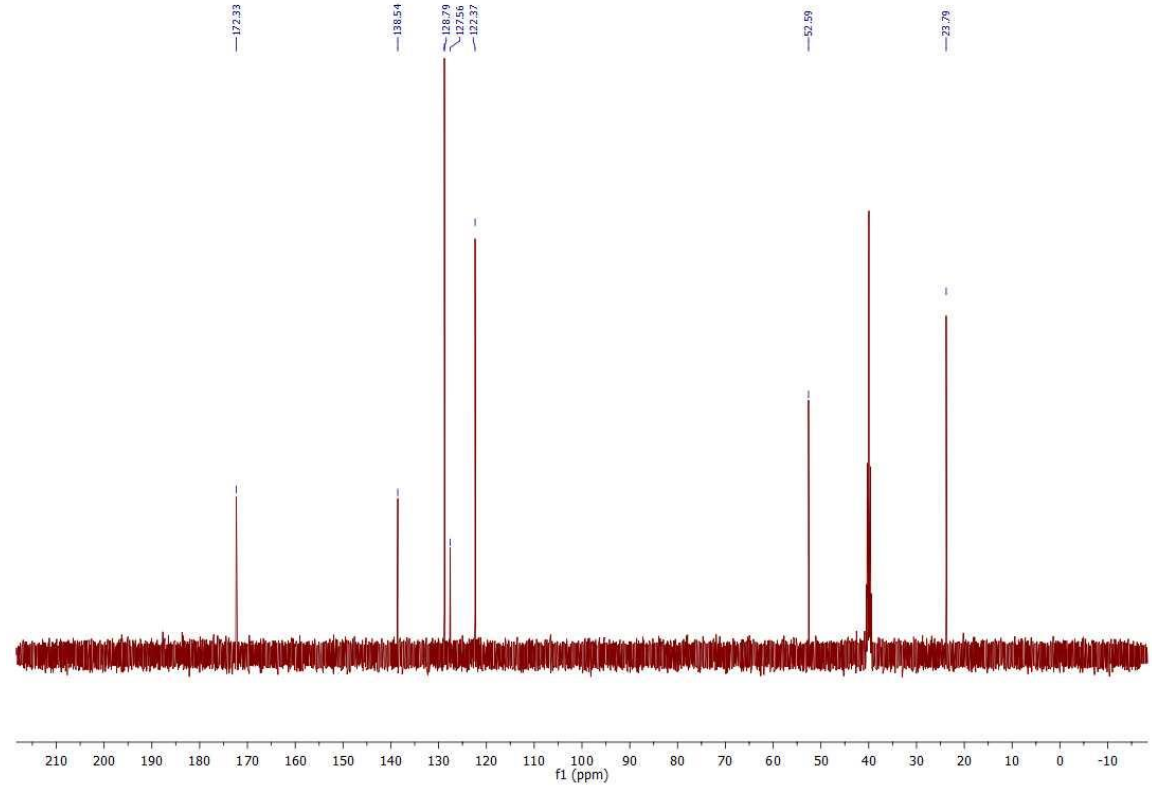

Figure 87 ^{13}C NMR of **10c**

5. Synthesis of Di(p-BrPh)diamide **10f**

p-bromoaniline (5.2 g, 30 mmol) was dissolved in 300 mL diethyl ether in a round bottom flask and purged with nitrogen and covered with a rubber septum. Then dimethylmalonyl dichloride (1.0 mL, 7.6 mmol) was added dropwise via a syringe and a large amount of white precipitate immediately forms. The reaction was stirred for 2 hours. Then 100 mL water was added to the flask and was stirred for 10 minutes. The solution was filtered and the precipitate was washed with another 50 mL water and 100 mL diethyl ether. The product was isolated as a white solid. Yield, 2.87 g, 86%. ^{1}H NMR (400 MHz, DMF) δ 9.77 (s, 1H), 7.75 (d, J = 8.8 Hz, 2H), 7.50 (d, J = 8.7 Hz, 2H), 1.62 (s, 3H). ^{13}C NMR (126 MHz, DMSO) δ 172.31, 139.00, 131.72, 122.71, 115.56, 52.66, 23.78.

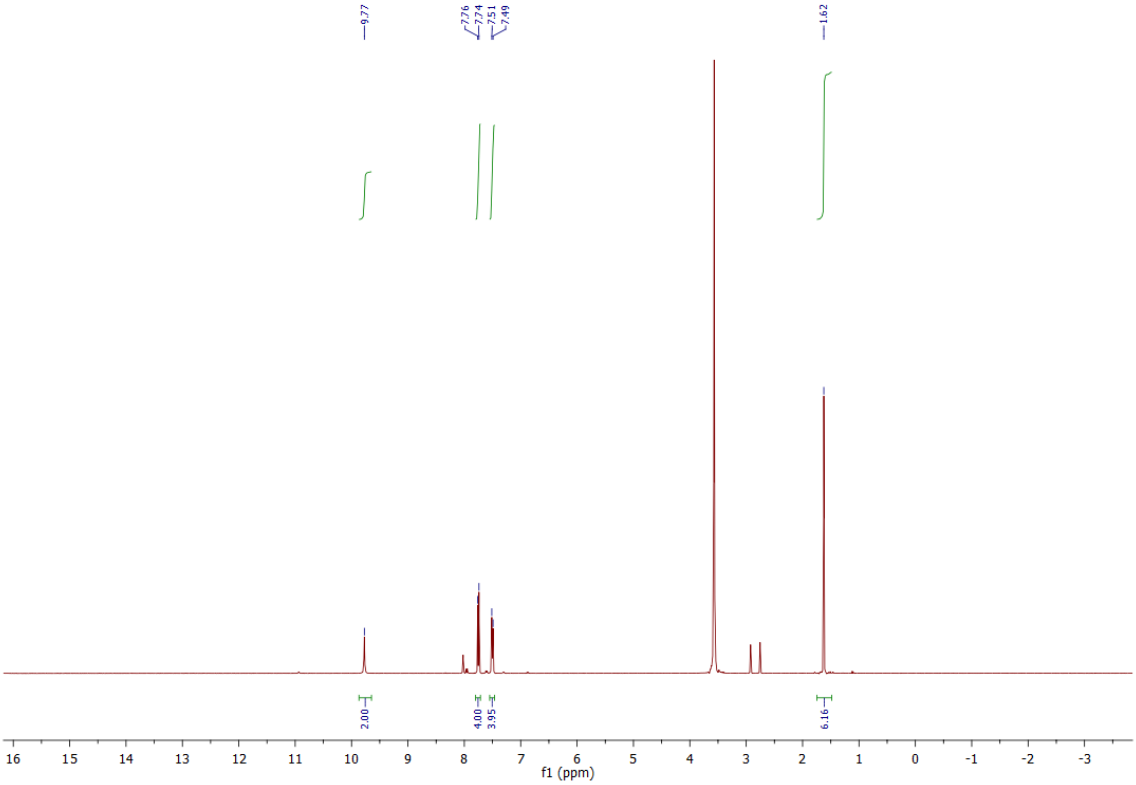

Figure 88 ^{1}H NMR of **10f**

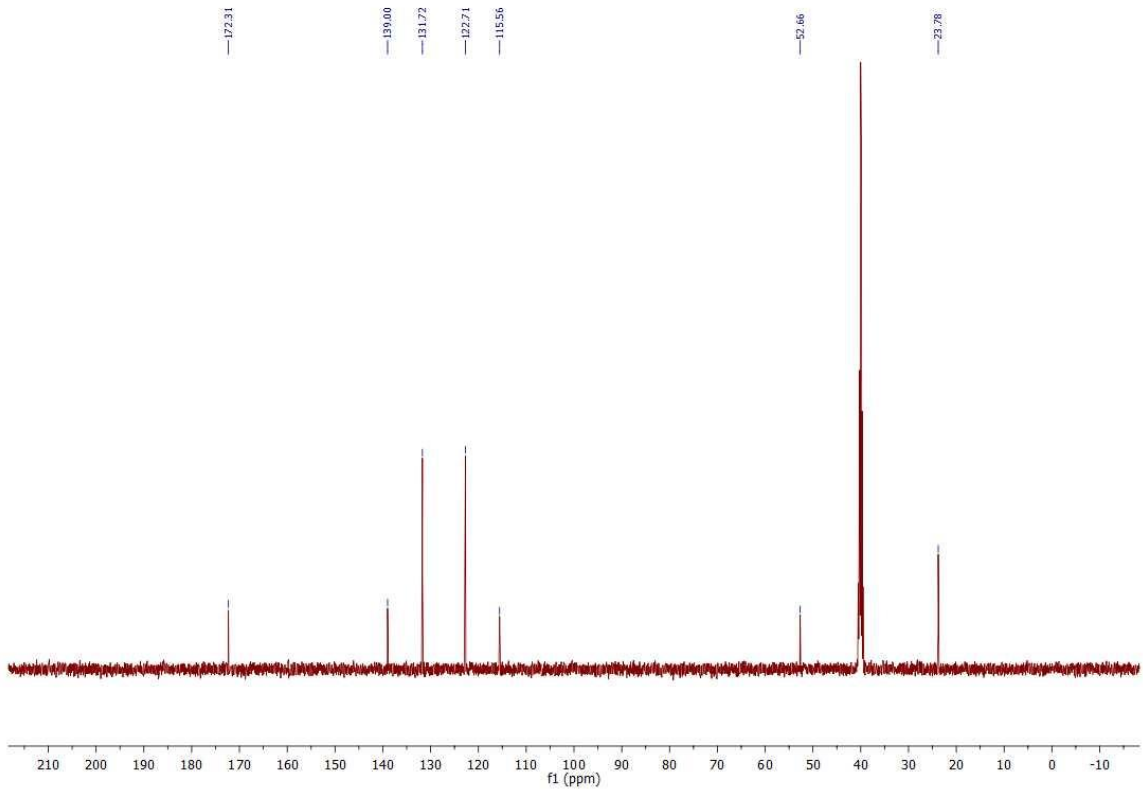

Figure 89 ^{13}C NMR of **10f**

6. Synthesis of Di(p-NO_2-Ph)diamide **10g**

p-nitroaniline (4.18 g, 30 mmol) was dissolved in 200 mL diethyl ether and 100 ml THF in a round bottom flask and purged with nitrogen and covered with a rubber septum. Then dimethylmalonyl dichloride (1.0 mL, 7.6 mmol) was added dropwise via a syringe and a large amount of white precipitate immediately forms. The reaction was stirred for 3 hours. Then 100 mL water was added to the flask and was stirred for 10 minutes. The solution was filtered and the precipitate was washed with another 50 mL water and 100 mL THF. The product was isolated as a white solid. Yield, 1.83 g, 65 %. ^{1}H NMR (400 MHz, DMF) δ 10.33 (s, 1H), 8.32 – 8.24 (m, 2H), 8.09 – 8.03 (m, 2H), 1.69 (s, 3H). ^{13}C NMR (126 MHz, DMSO) δ 172.85, 145.90, 142.84, 125.15, 120.22, 67.49, 53.43, 25.59, 23.52.

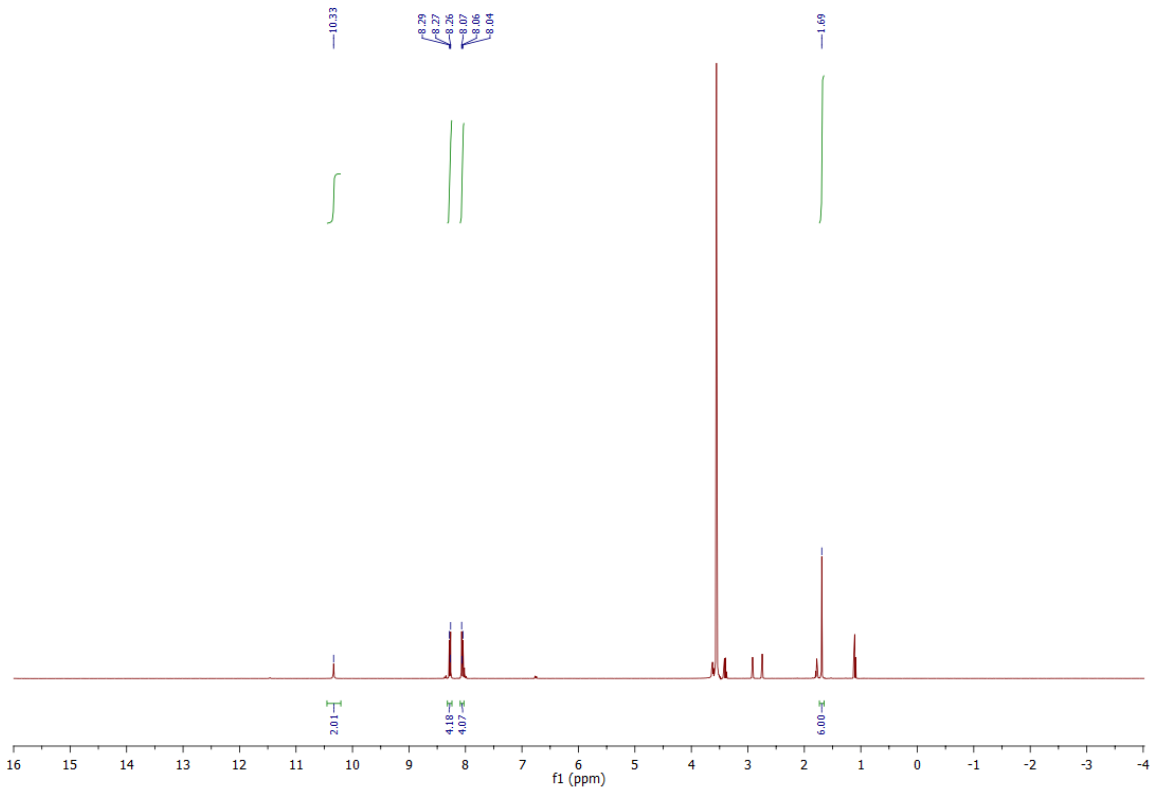

Figure 90 ^{1}H NMR of **10g**

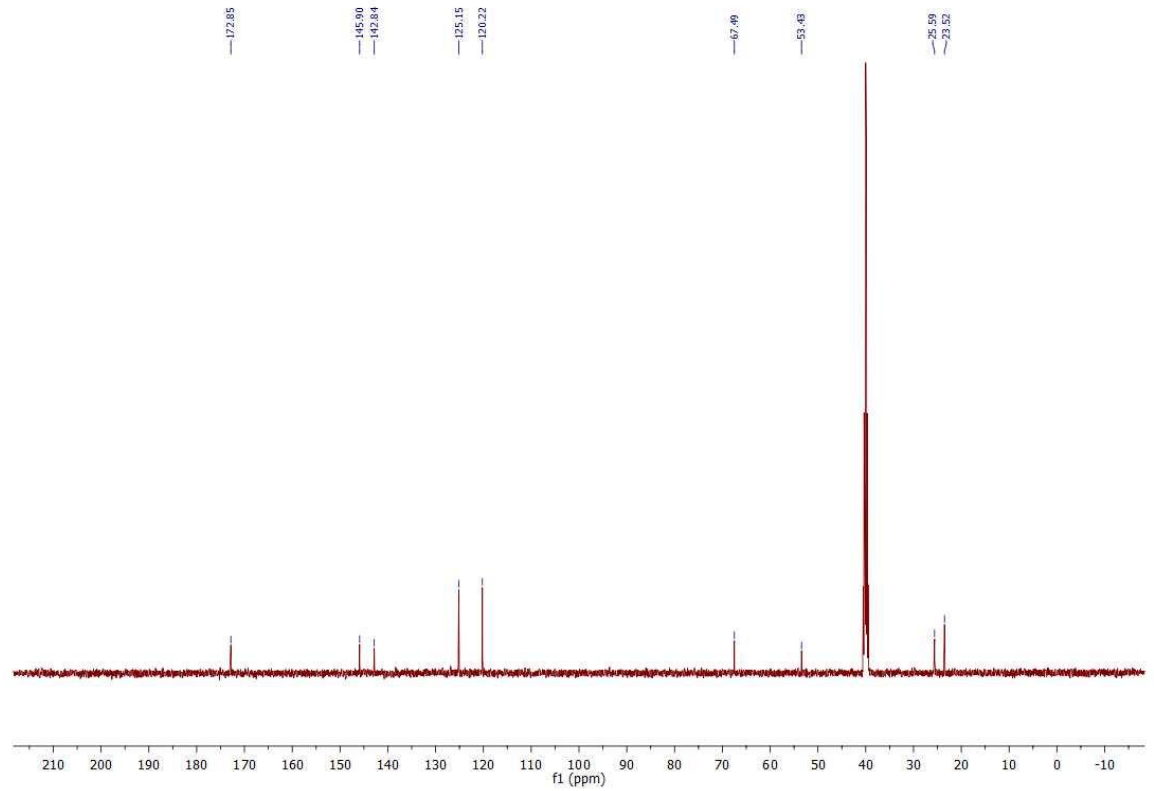

Figure 91 ^{13}C NMR of **10g**

7. Synthesis of Di(p-FPh)diamide **10h**

3.36 g of 4-fluoroaniline was dissolved in 300 mL diethyl ether in a round bottom flask and purged with nitrogen. 1 mL of dimethylmalonyl dichloride was added dropwise via a syringe and stirred for 2 hours. A large amount of white precipitate immediately forms. 100 mL water was added to the flask and was stirred for 10 minutes. The solution was filtered and the precipitate was washed with another 50 mL water and 100 mL diethyl ether. The product was isolated as a white solid. Yield, 1.55 g, 65 %. ^{1}H NMR (400 MHz, $CDCl_3$) δ 8.47 (s, 1H), 7.48 (dd, J = 9.1, 4.8 Hz, 2H), 7.09 – 6.90 (m, 2H), 1.68 (s, 3H). ^{13}C NMR (126 MHz, DMSO) δ 172.19, 159.61, 157.69, 135.93, 122.74, 122.68, 115.52, 115.35, 52.28, 23.91. ^{19}F NMR (471 MHz, DMSO) δ -119.23.

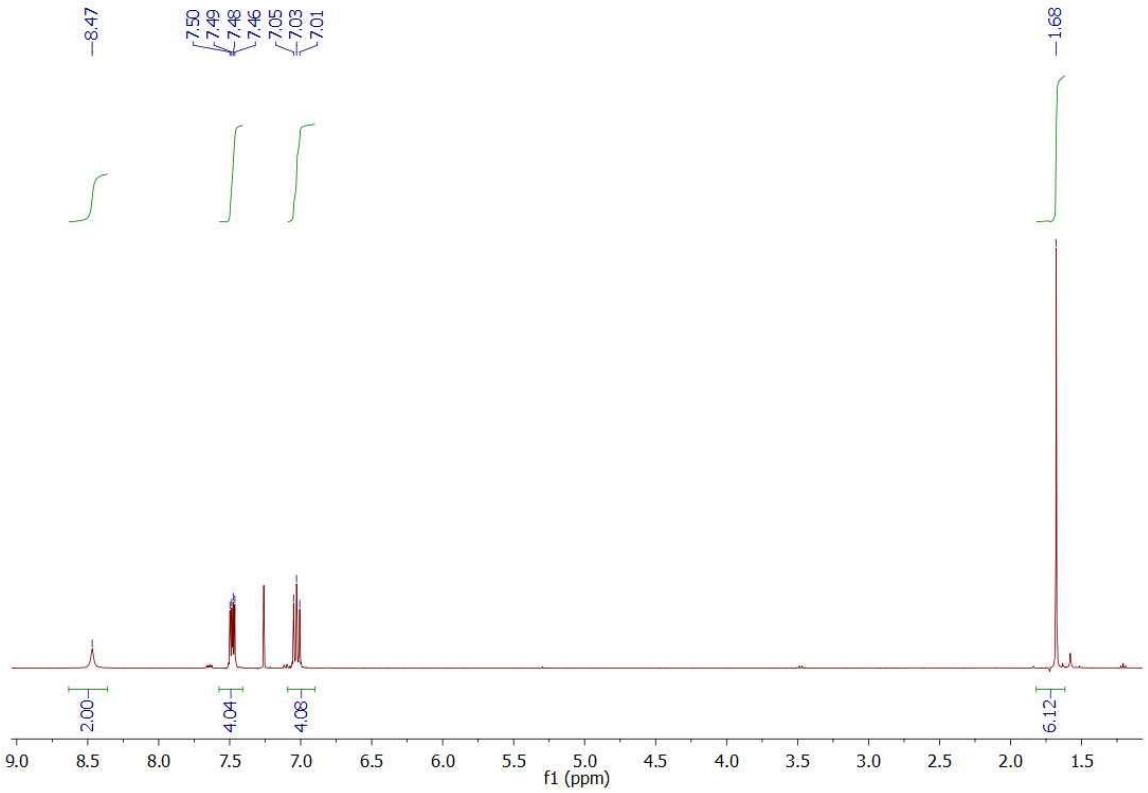

Figure 92 ^{1}H NMR of **10h**

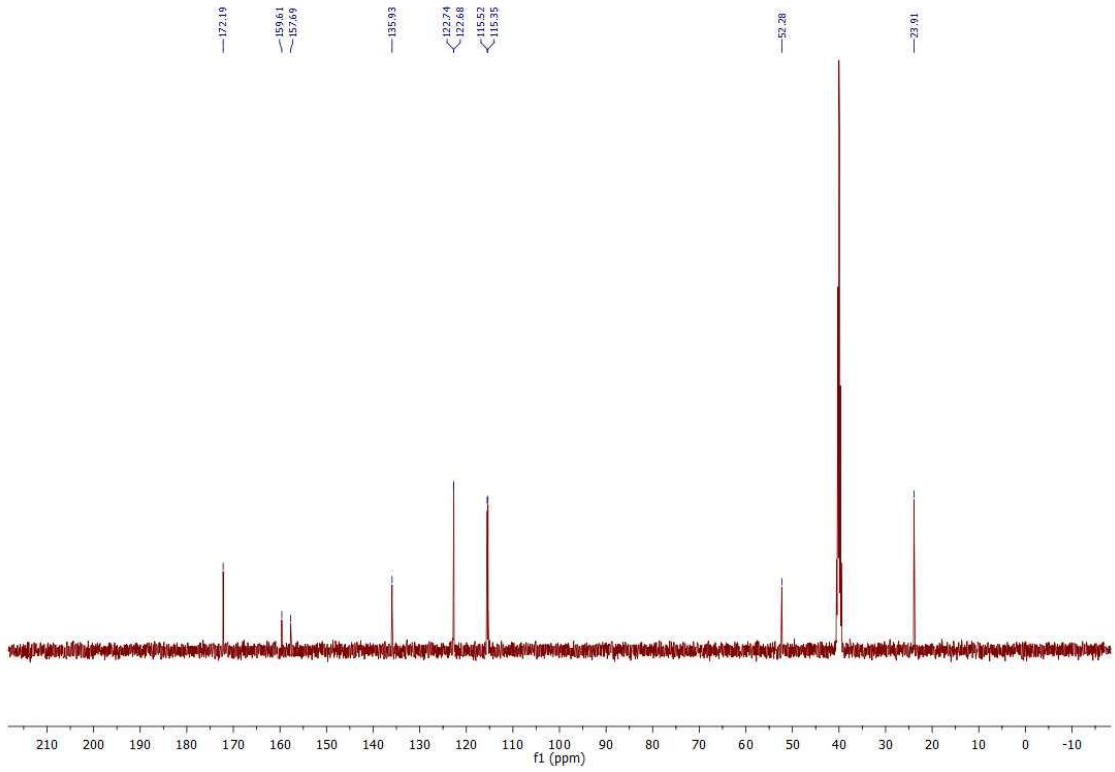

Figure 93 ^{13}C NMR of **10h**

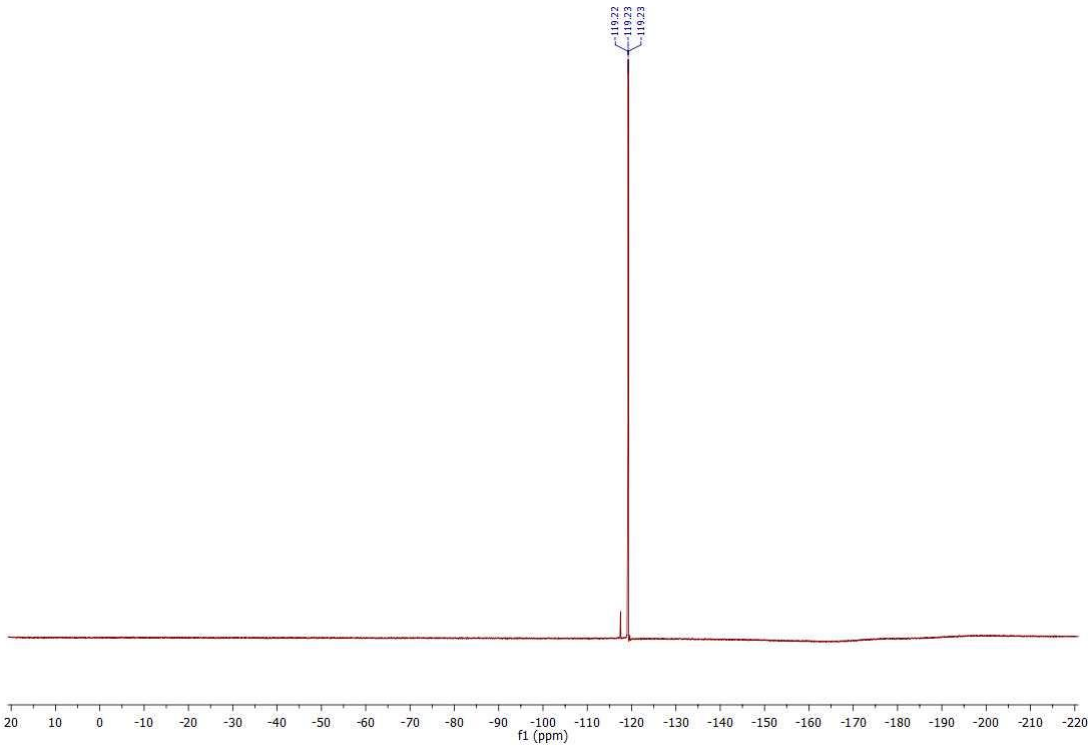

Figure 94 ^{19}F NMR of **10h**

8. Synthesis of imidoyl chloride **11a**

Phosphorus pentachloride (PCl_5) (3.00 g, 14.4 mmol) and **10a** (1.92 g, 6.8 mmol) was added to a Schlenk flask. The flask was equipped with a reflux condenser, purged with nitrogen, and then covered with a rubber septum. Then 50 mL toluene was transferred to the Schlenk flask via cannula. The rubber septum was exchanged for a hose adapter which was connected to an oil bubbler. The reaction was refluxed under an atmosphere of nitrogen for 5 hours or until the evolution of gas stops. The reaction was cooled to room temperature and filtered over celite. Volatiles were removed under reduced pressure overnight. The product was isolated as a yellow solid. Yield, 1.92 g, 88 %. ^{1}H NMR (500 MHz, $CDCl_3$) δ 7.42 – 7.33 (m, 7H), 7.23 – 7.15 (m, 3H), 7.00 – 6.83 (m, 6H), 1.81 (s, 9H). ^{13}C NMR (101 MHz, $CDCl_3$) δ 148.32, 146.77, 128.81, 125.01, 119.66, 59.67, 25.07.

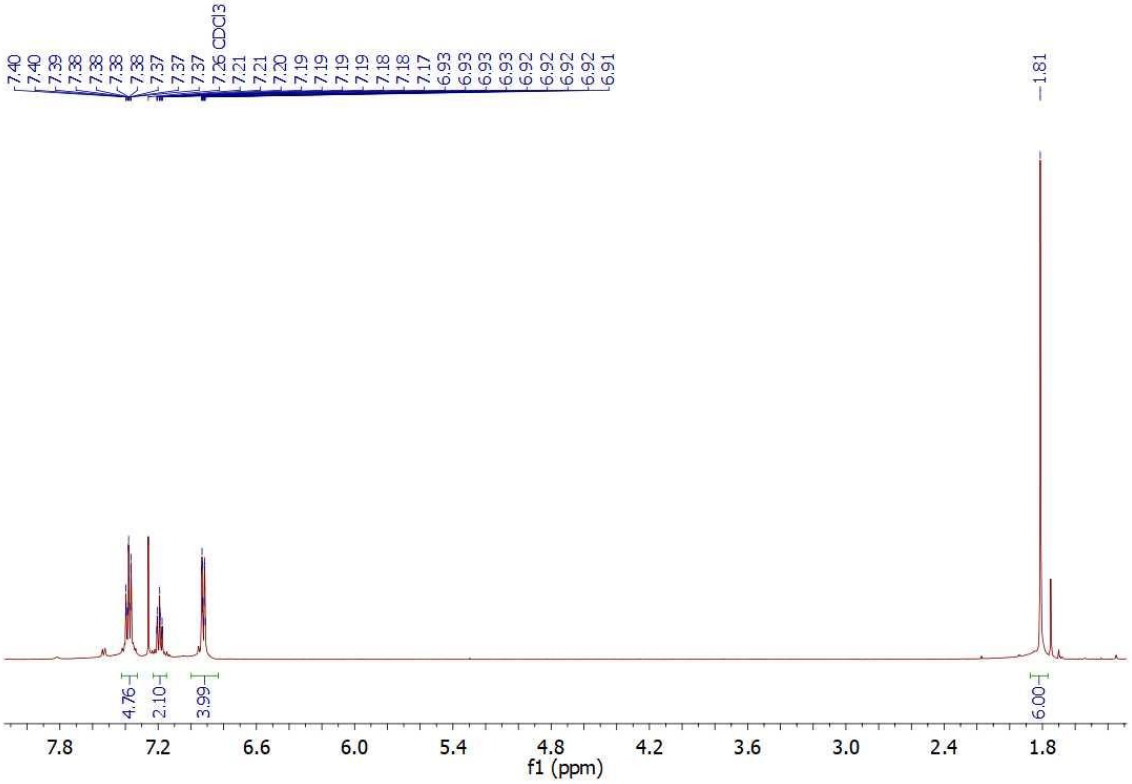

Figure 95 ^{1}H NMR of **11a**

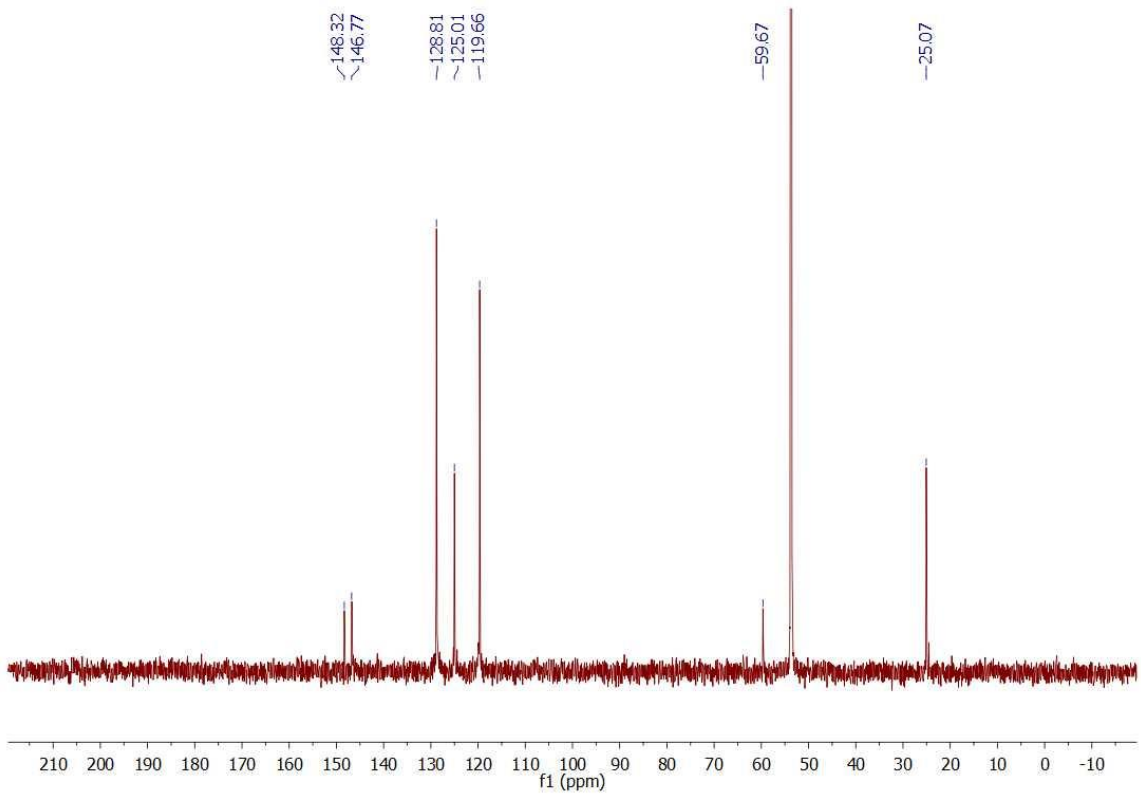

Figure 96 ^{13}C NMR of **11a**

9. Synthesis of tolyl imidoyl chloride **11c**

Phosphorus pentachloride (PCl_5) (1.34 g, 6.43 mmol) and **10c** (1.00 g, 3.22 mmol) was added to a Schlenk flask. The flask was equipped with a reflux condenser, purged with nitrogen, and then covered with a rubber septum. Then 50 mL toluene was transferred to the Schlenk flask via cannula. The rubber septum was exchanged for a hose adapter which was connected to an oil bubbler. The reaction was refluxed under an atmosphere of nitrogen for 5 hours or until the evolution of gas stops. The reaction was cooled to room temperature and filtered over celite. Volatiles were removed under reduced pressure overnight. The product was used without further purification.

10. Synthesis of bromo imidoyl chloride **11f**

Phosphorus pentachloride (PCl_5) (1.00 g, 4.80 mmol) and **10f** (1.00 g, 2.27 mmol) was added to a Schlenk flask. The flask was equipped with a reflux condenser, purged with nitrogen, and then covered with a rubber septum. Then 50 mL toluene was transferred to the Schlenk flask via cannula. The rubber septum was exchanged for a hose adapter which was connected to an oil bubbler. The reaction was refluxed under an atmosphere of nitrogen for 5 hours or until the evolution of gas stops. The reaction was cooled to room temperature and filtered over celite. Volatiles were removed under reduced pressure overnight. The product was used without further purification.

11. Synthesis of DIC-HCl **12a**

Chloroform (25 mL) was added to a Schlenk flask in a glove box containing **11a** (1.00g, 3.13 mmol). Then TMS-formamidine (1.1 g, 3.12 mmol) was dissolved in 2 mL chloroform and added via syringe to the Schlenk flask. The schlenk flask was equipped with a reflux condenser, and the reaction was refluxed under an atmosphere of nitrogen for 5 hours. The solution was concentrated under vacuum to about 10 mL. The product was precipitated with 30 mL hexanes and filtered to give a bright yellow solid. Yield, 1.74 g, 99 %. 1H NMR (400 MHz, CDCl3) δ 10.26 (s, 1H), 7.07 (t, J = 7.8 Hz, 4H), 6.87 (t, J = 7.5 Hz, 2H), 6.73 (s, 4H), 6.49 (d, J = 7.5 Hz, 4H), 2.46 (s, 12H), 2.13 (s, 6H), 1.86 (s, 6H). 13C NMR (101 MHz, CDCl3) δ 159.60, 144.87, 140.62, 134.81, 132.65, 130.22, 128.40, 123.40, 116.19, 53.41, 50.60, 27.61, 20.86, 19.71.

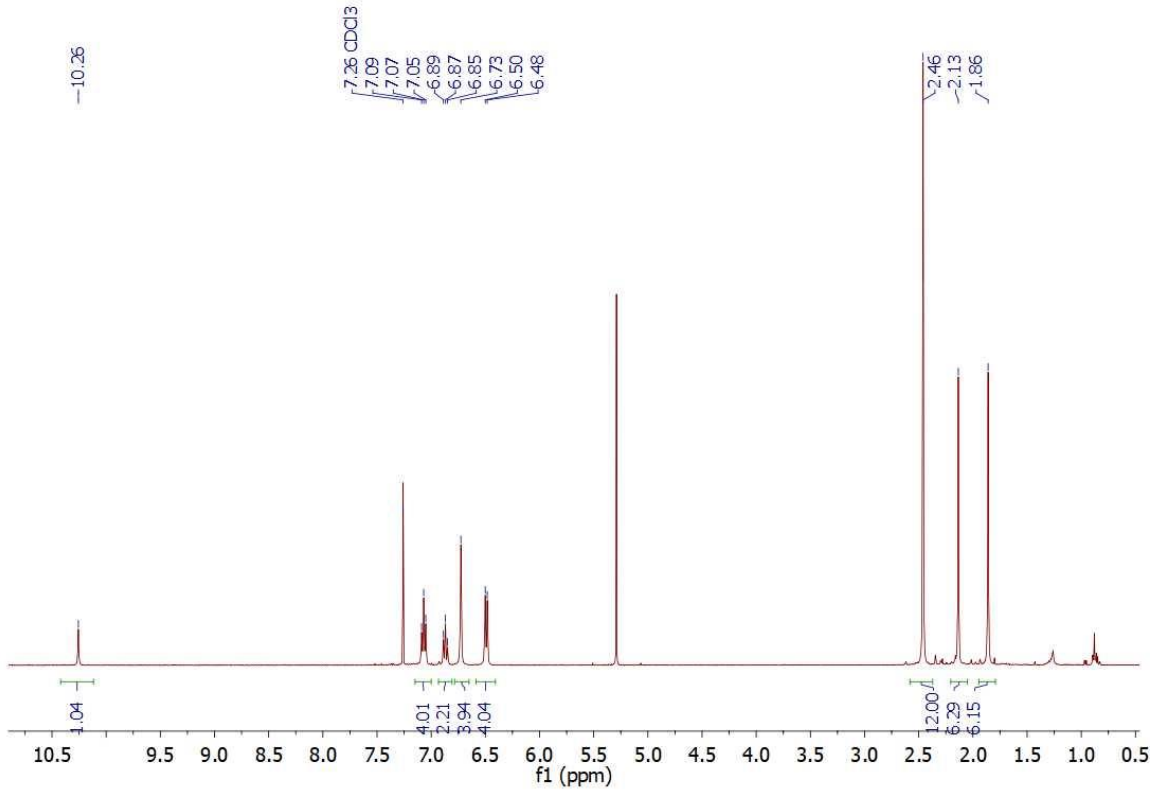

Figure 97 ^{1}H NMR of DICHCl **12a**

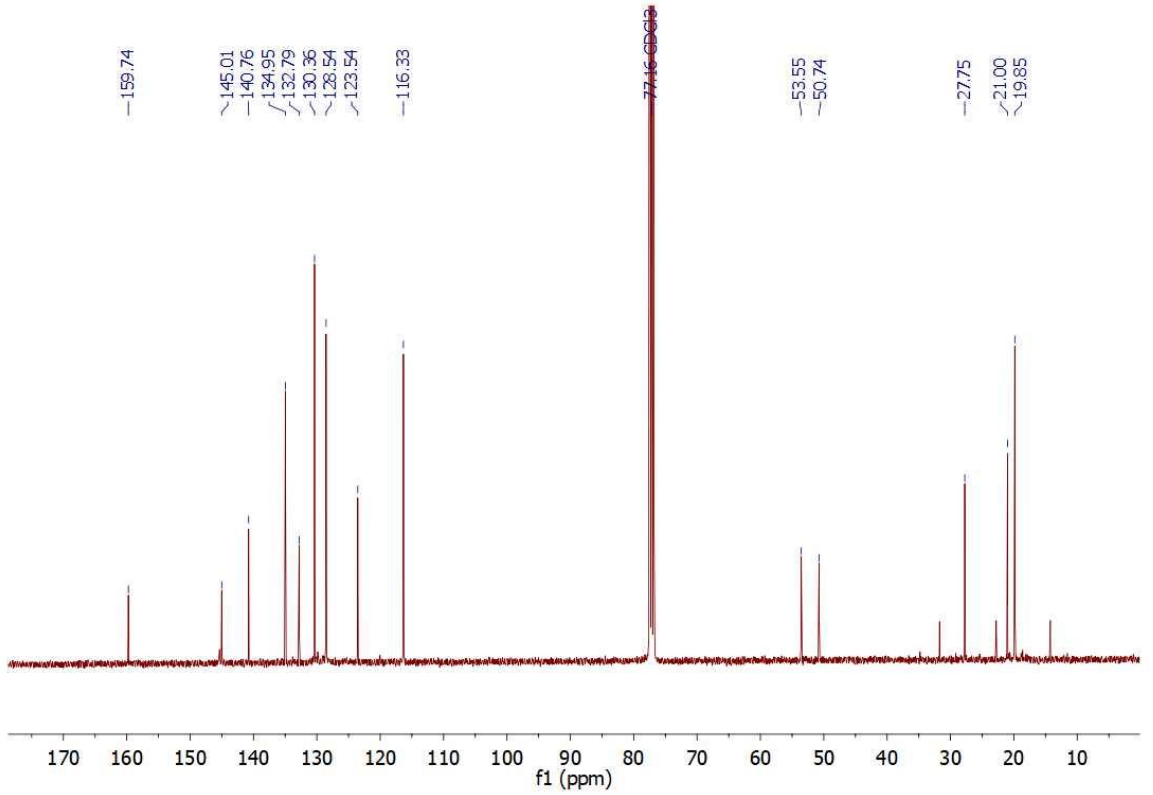

Figure 98 ^{13}C NMR of **13a**

12. Synthesis of DIC(tolyl) HCl **12c**

Chloroform (25 mL) was added to a Schlenk flask in a glove box containing **11c** (1.13g, 3.25 mmol). Then TMS-formamidine (1.15 g, 3.25 mmol) was dissolved in 2 mL chloroform and added via syringe to the Schlenk flask. The schlenk flask was equipped with a reflux condenser, and the reaction was refluxed under an atmosphere of nitrogen for 5 hours. The solution was concentrated under vacuum to about 10 mL. The product was precipitated with 30 mL hexanes and filtered to give a bright yellow solid. The product was used without further purification.

13. Synthesis of DIC(Br) HCl **12f**

Chloroform (25 mL) was added to a Schlenk flask in a glove box containing **11f** (1.08 g, 2.26 mmol). Then TMS-formamidine (0.8 g, 2.27 mmol) was dissolved in 2 mL chloroform and added via syringe to the Schlenk flask. The schlenk flask was equipped with a reflux condenser, and the reaction was refluxed under an atmosphere of nitrogen for 5 hours. The solution was concentrated under vacuum to about 10 mL. The product was precipitated with 30 mL hexanes and filtered to give a bright yellow solid. Yield, 1.38 g, 85 %. ^{1}H NMR (400 MHz, $CDCl_3$) δ 9.53 (s, 2H), 7.18 (d, J = 8.1 Hz, 8H), 6.77 (s, 8H), 6.57 (d, J = 8.3 Hz, 8H), 2.50 (s, 24H), 2.22 (s, 13H), 1.94 (s, 12H). ^{13}C NMR (101 MHz, $CDCl_3$) δ 158.66, 143.86, 141.26, 135.01, 132.86, 131.17, 130.36, 128.09, 127.85, 127.61, 118.28, 116.28, 53.47, 50.77, 28.01, 20.90, 19.82.

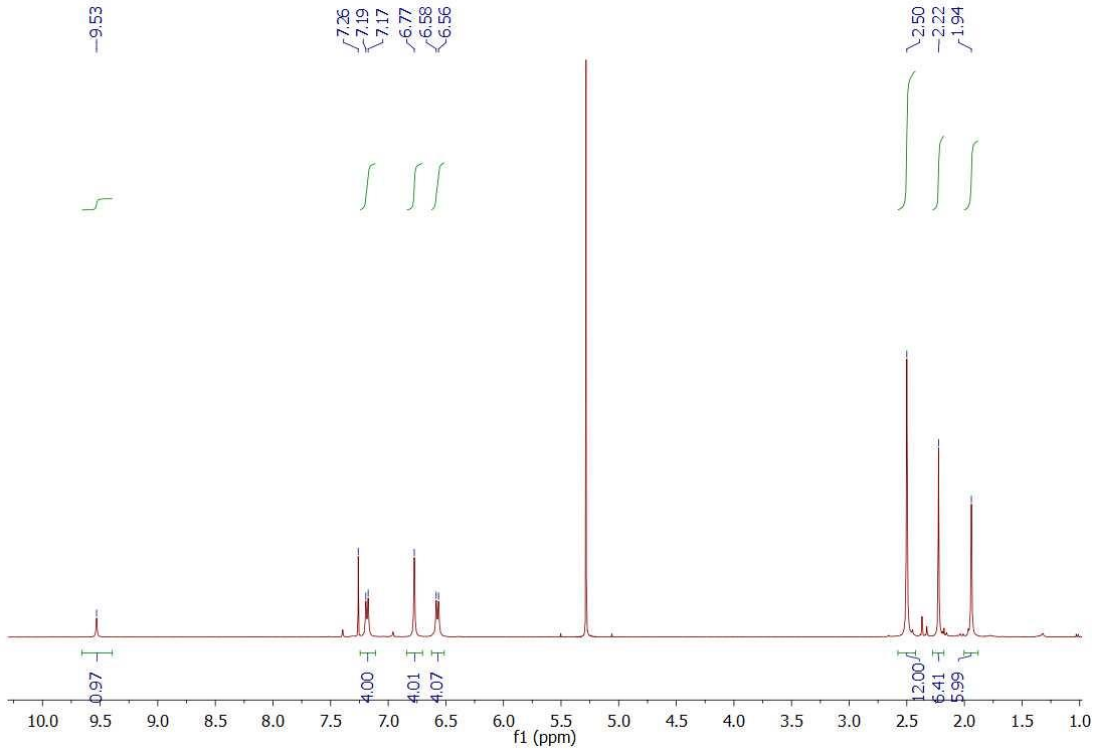

Figure 99 ^{1}H NMR of **12f**

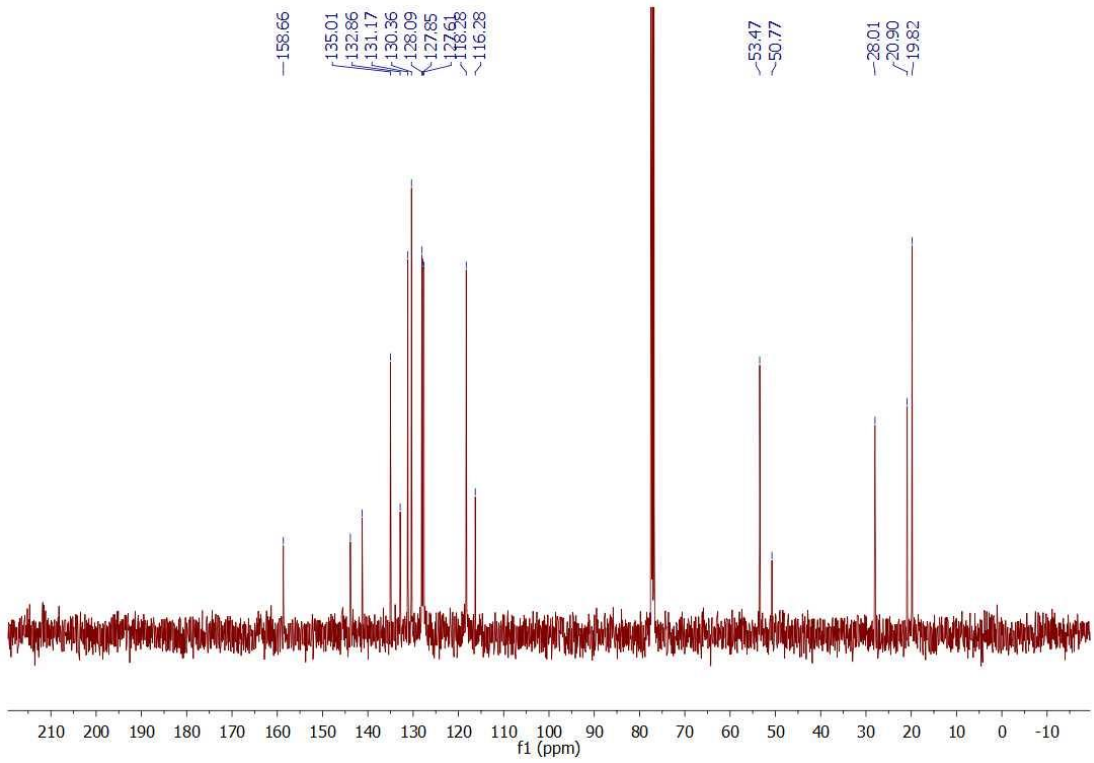

Figure 100 ^{13}C NMR of **12f**

14. Synthesis of DIC free Carbene **13a**

DICHCl **12a** (1.00 g, 1.78 mmol) was dissolved in 25 mL THF in Schlenk flask in a glove box. Then NaHMDS (0.36 g, 196 mmol) was added to the Schlenk flask and was stirred for 30 minutes. Volatiles were removed under vacuum. The residue was redissolved in hexanes and filtered over celite. Volatiles were removed under vacuum and the product was isolated as an off-white solid. Yield, 0.39 g, 42 %. ^{1}H NMR (500 MHz, C_6D_6) δ 6.85 (t, J = 7.7 Hz, 2H), 6.65 (t, J = 7.3 Hz, 1H), 6.57 (s, 2H), 6.41 (d, J = 7.7 Hz, 2H), 2.29 (s, 6H), 2.03 (s, 3H), 1.75 (s, 3H). ^{13}C NMR (101 MHz, C_6D_6) δ 265.49, 261.70, 147.56, 141.54, 136.74, 134.82, 134.65, 129.54, 129.45, 128.67, 128.43, 128.30, 128.19, 128.05, 127.93, 127.81, 126.38, 126.21, 124.36, 121.52, 118.07, 117.64, 49.48, 28.67, 26.32, 20.82, 20.68, 19.43, 19.27, 18.76, 18.67, 3.46, 2.65, 1.41.

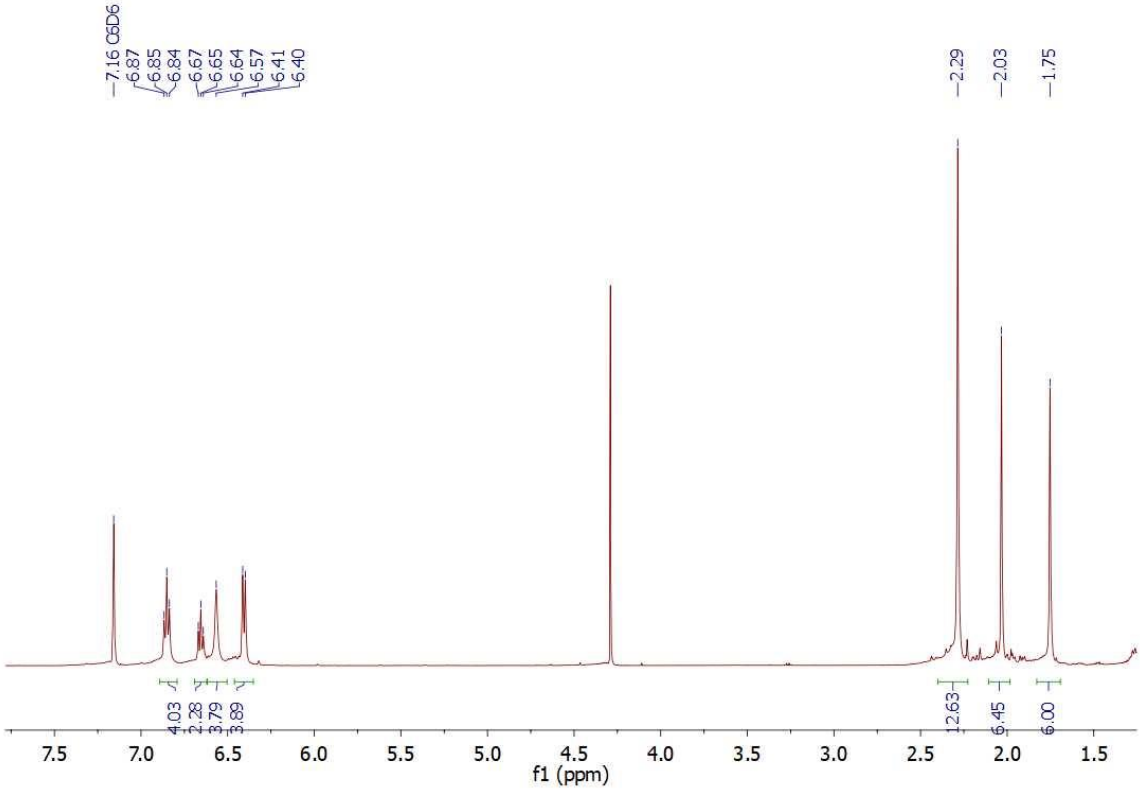

Figure 101 ^{1}H NMR of DIC free carbene **13a**

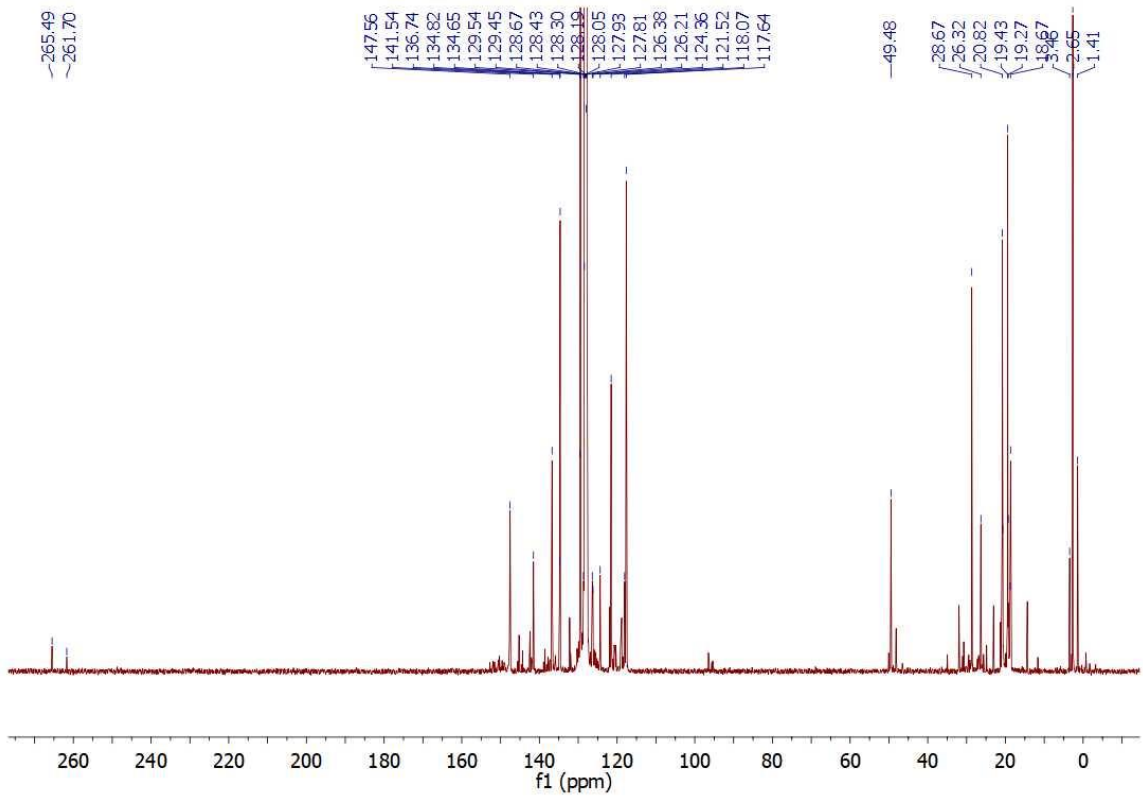

Figure 102 ^{13}C NMR of DIC free carbene **13a**. NMR spectra shows a second isomer of DIC seen by the second peak at 261.7 ppm.

15. Synthesis of DIC-Se **16a**

THF (1 mL) was added to a Schlenk flask in a glove box containing DIC **5a** (100 mg, 0.19 mmol). Then elemental selenium (30 mg, 0.38 mmol) was added to flask and the reaction was stirred overnight. Solvent was removed under vacuum and recrystallized from hexanes to give the product as an orange/pink solid. Yield, 72 mg, 63%. ^{1}H NMR (500 MHz, $CDCl_3$) δ 6.96 (t, J = 7.6 Hz, 2H), 6.74 (t, J = 7.4 Hz, 1H), 6.62 (s, 2H), 6.34 (d, J = 7.7 Hz, 2H), 2.23 (s, 6H), 2.15 (s, 3H), 1.74 (s, 3H). ^{13}C NMR (126 MHz, $CDCl_3$) δ 182.98, 146.82, 138.98, 138.13, 135.13, 129.41, 128.69, 128.57, 128.05, 127.83, 127.71, 121.08, 117.31, 116.82, 48.88, 28.13, 20.96, 19.15, 1.03. ^{77}Se NMR (76 MHz, $CDCl_3$) δ 669.11.

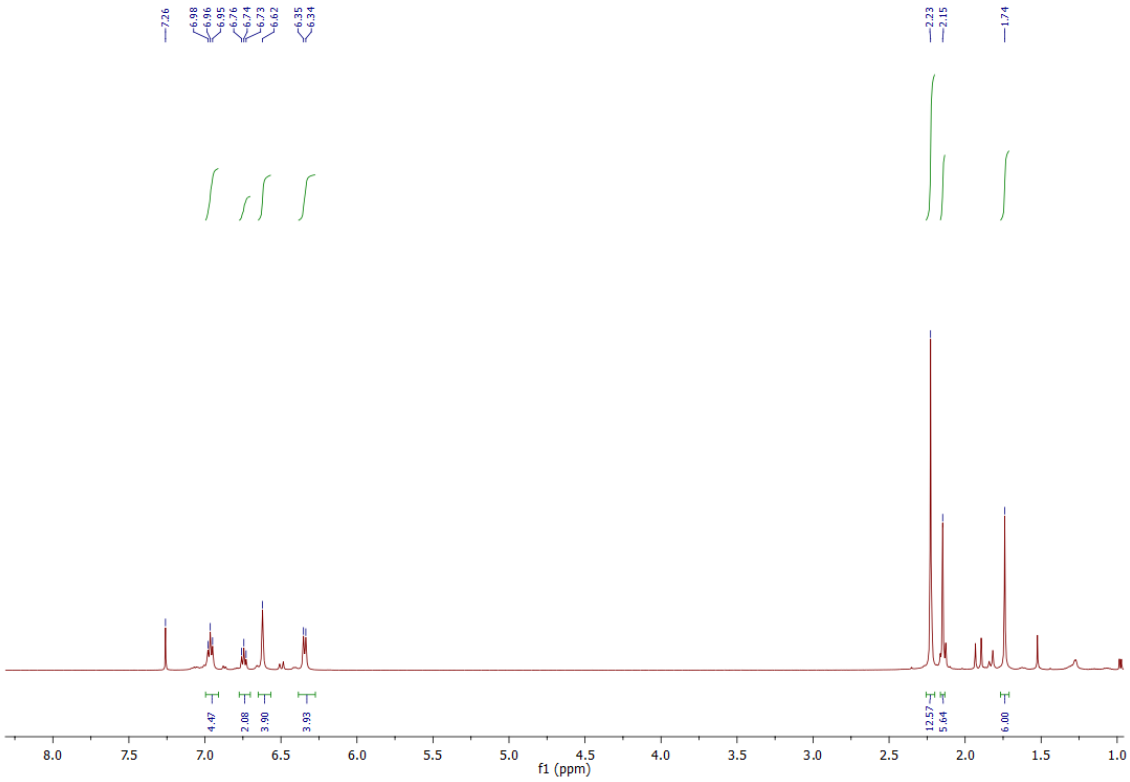

Figure 103 ^{1}H NMR of **16a**

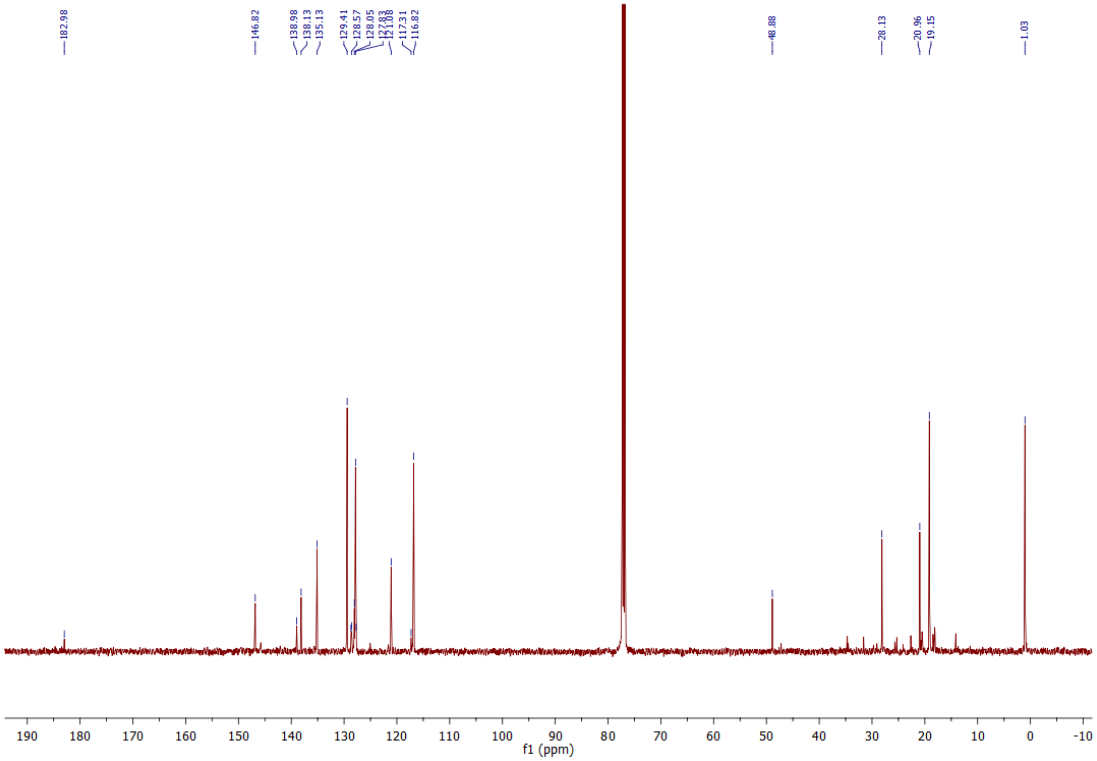

Figure 104 ^{13}C NMR of **16a**

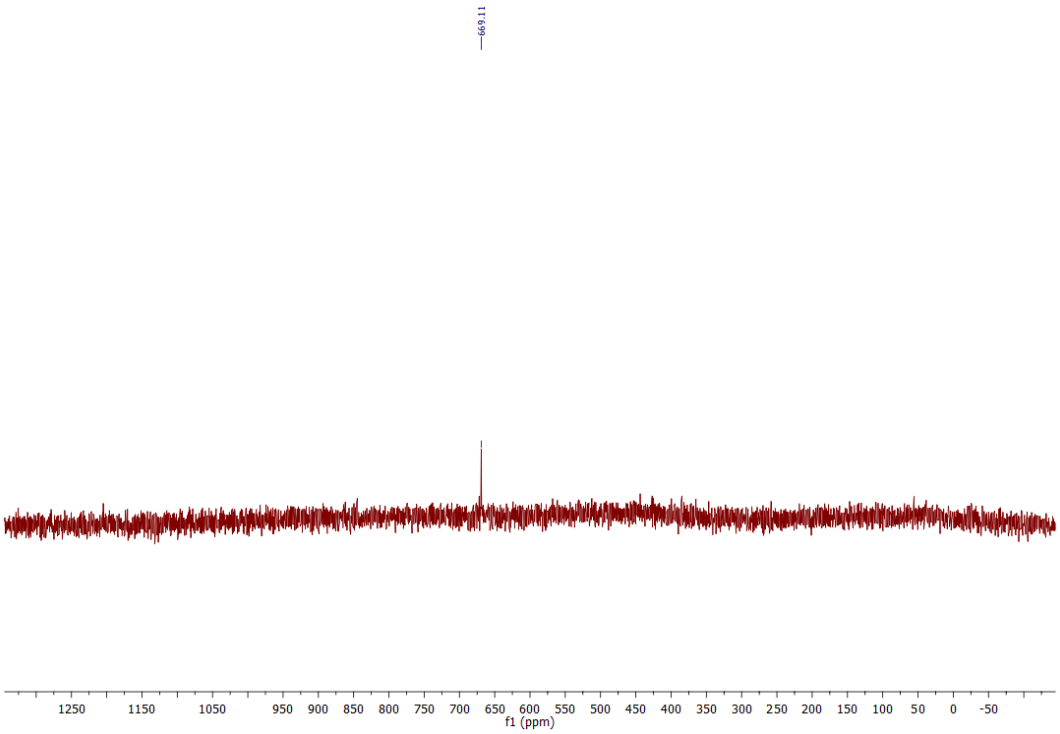

Figure 105 ^{77}Se NMR of DIC selenium adduct **16a**

16. Synthesis of DIC(Tolyl)Se **16c**

Toluene (5 mL) was added to a Schlenk flask in a glove box containing **12c** (100 mg, 0.17 mmol). Then elemental selenium (40 mg, 0.51 mmol) and NaHMDS (34 mg, 0.19 mmol) was added to flask and the reaction was stirred overnight. Solvent was removed under vacuum and recrystallized from hexanes to give the product as an orange/pink solid. 77Se NMR (76 MHz, CDCl3) δ 658.30 (s).

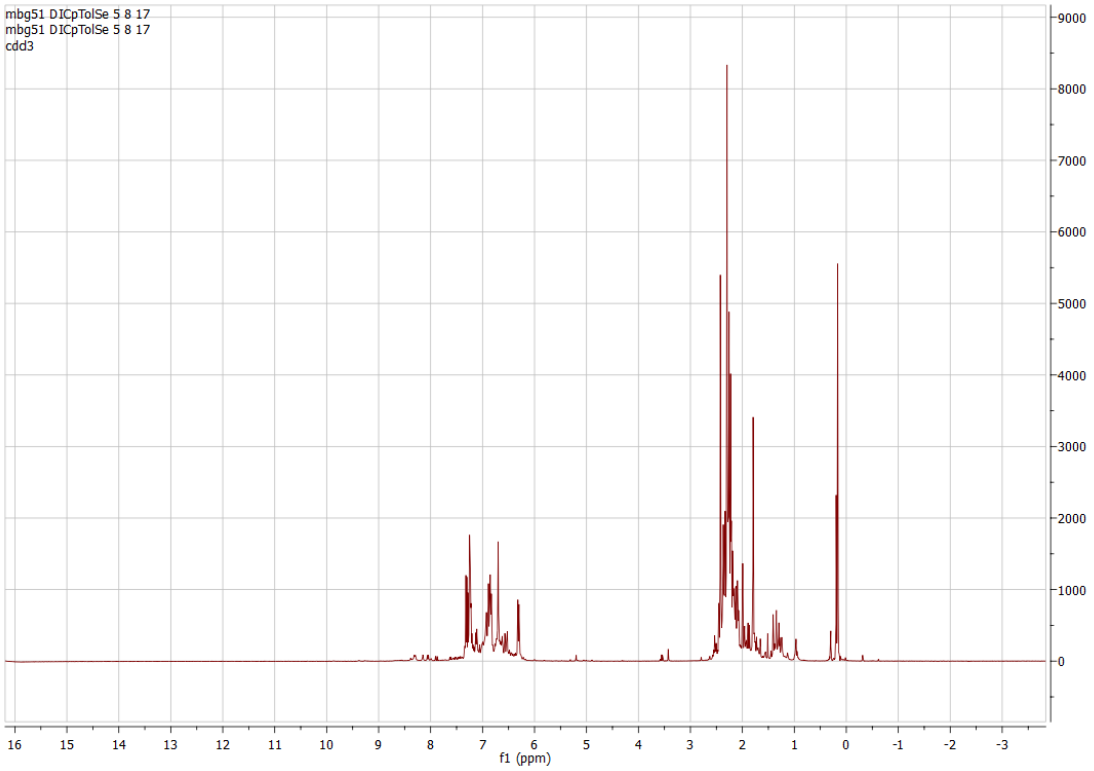

Figure 106 ^{1}H NMR of **16c**

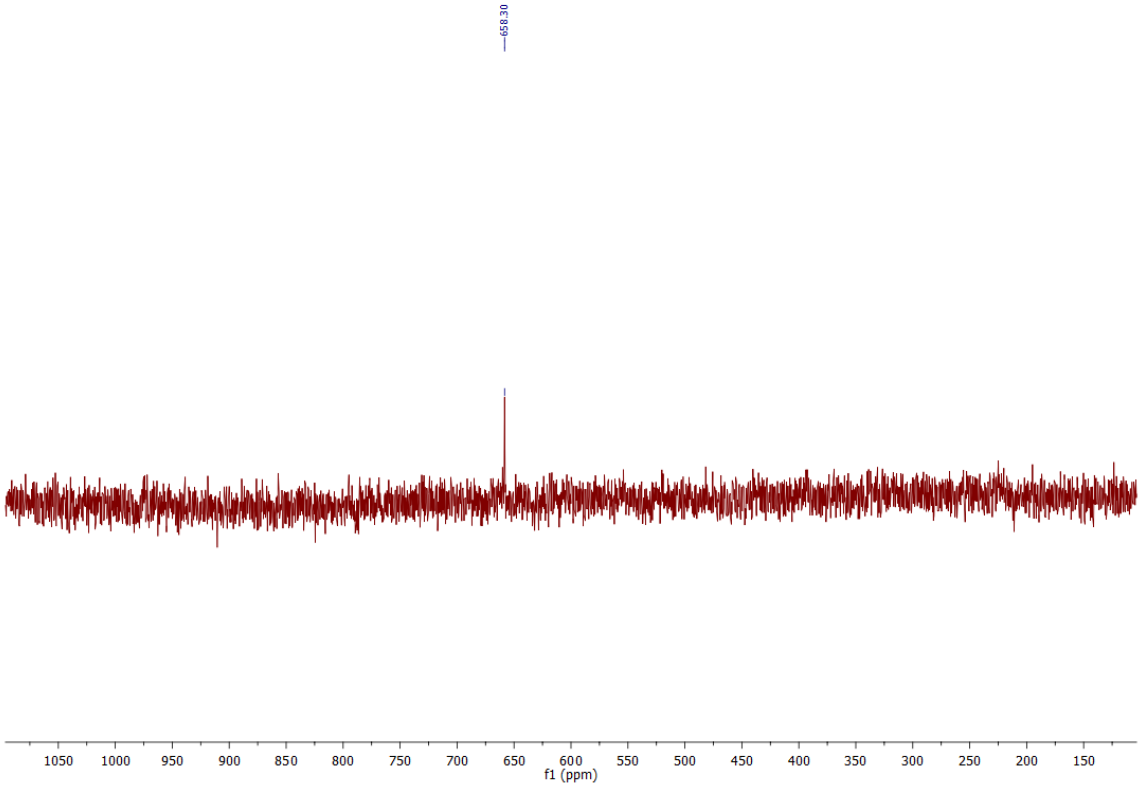

Figure 107 ^{77}Se NMR of **16c**

17. Synthesis of DIC(Br)Se **16f**

Toluene (5 mL) was added to a Schlenk flask in a glove box containing **12c** (100 mg, 0.14 mmol). Then elemental selenium (33 mg, 0.42 mmol) and NaHMDS (28 mg, 0.15 mmol) was added to flask and the reaction was stirred overnight. Solvent was removed under vacuum and recrystallized from hexanes to give the product as an orange/pink solid. Yield, 65 mg, 58%. ^{1}H NMR (400 MHz, $CDCl_3$) δ 7.05 (d, J = 8.6 Hz, 2H), 6.62 (s, 2H), 6.20 (d, J = 8.6 Hz, 2H), 2.20 (s, 9H), 1.78 (s, 3H). ^{13}C NMR (101 MHz, $CDCl_3$) δ 183.15, 145.77, 145.53, 138.84, 138.29, 135.04, 130.32, 129.40, 128.08, 118.29, 113.57, 48.68, 27.86, 20.81, 19.07. ^{77}Se NMR (76 MHz, $CDCl_3$) δ 697.66.

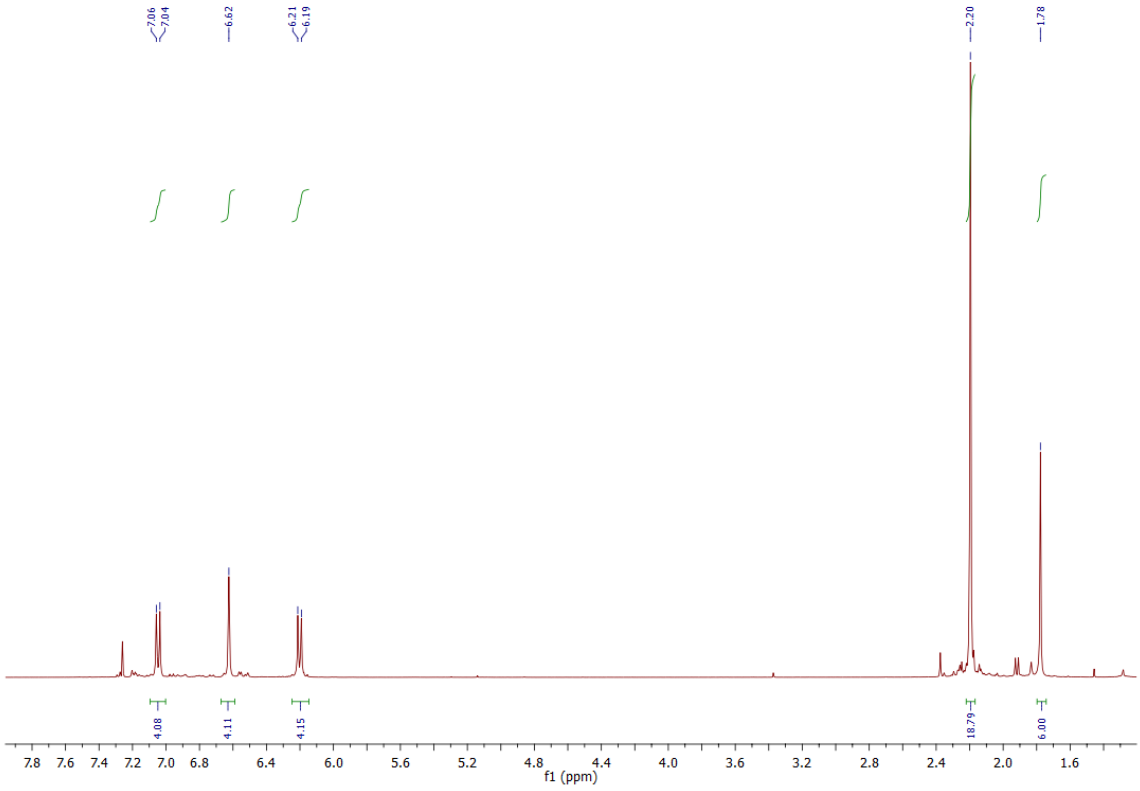

Figure 108 ^{1}H NMR of **16f**

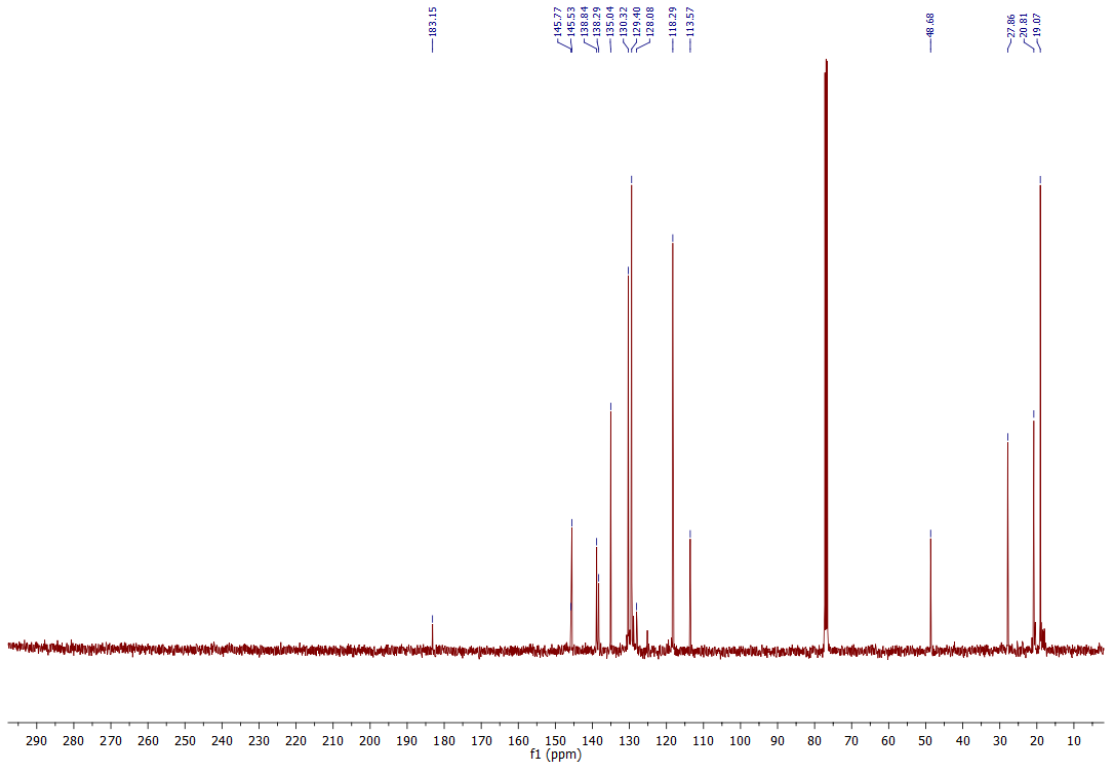

Figure 109 ^{13}C NMR of **16f**

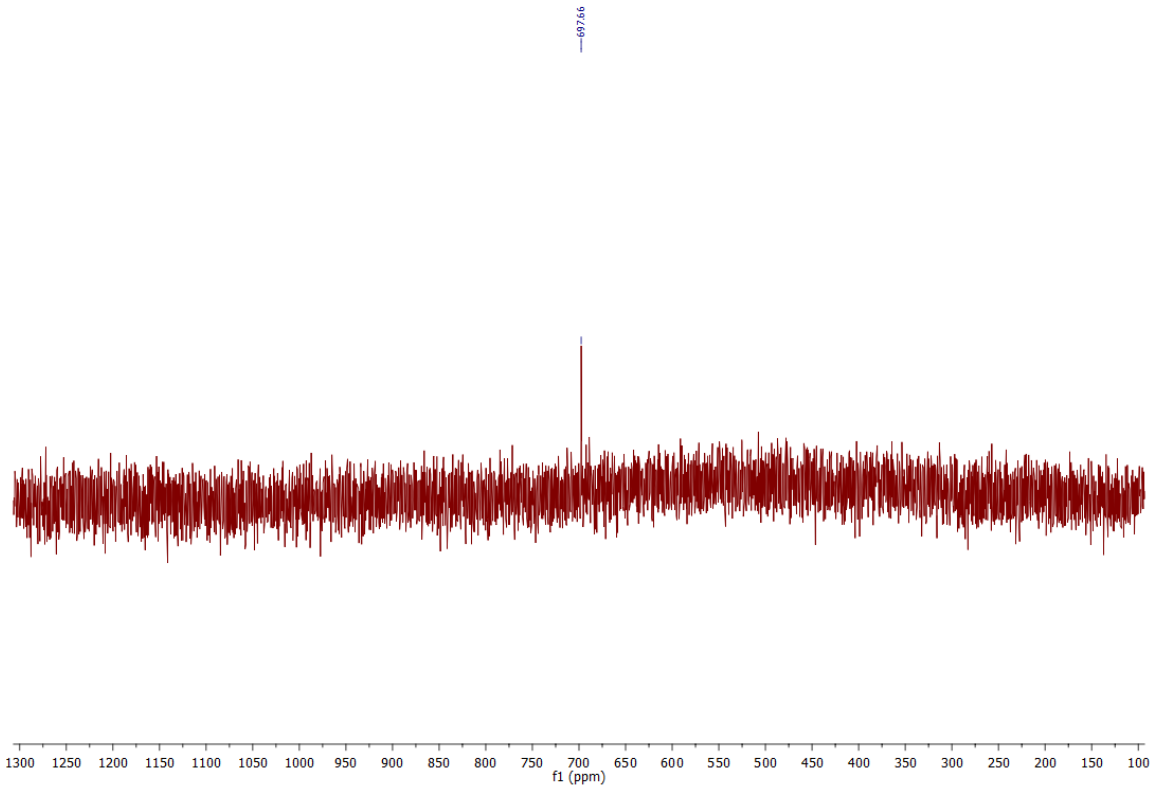

Figure 110 ^{77}Se NMR of **16f**

18. Synthesis of DIC-Ir(COD)Cl **14a**

THF (5 mL) was added to a Schlenk flask in a glove box containing **13a** (36 mg, 0.068 mmol). Then $[Ir(COD)Cl]_2$ (25 mg, 0.37 mmol) was added to flask and the reaction was stirred overnight. Solvent was removed under vacuum and the product was purified by column chromatography (80:20 DCM:Hexanes) to give the product as a red solid. Yield, 46 mg, 72%. ^{1}H NMR (400 MHz, $CDCl_3$) δ 7.05 (t, J = 7.7 Hz, 2H), 6.90 (s, 1H), 6.81 – 6.72 (m, 2H), 6.45 – 6.38 (m, 2H), 4.26 – 4.16 (m, 1H), 2.92 – 2.78 (m, 1H), 2.58 (s, 2H), 2.27 (d, J = 6.6 Hz, 4H), 2.20 (s, 3H), 2.08 (s, 1H), 1.77 (t, J = 7.0 Hz, 1H), 1.71 (s, 2H).

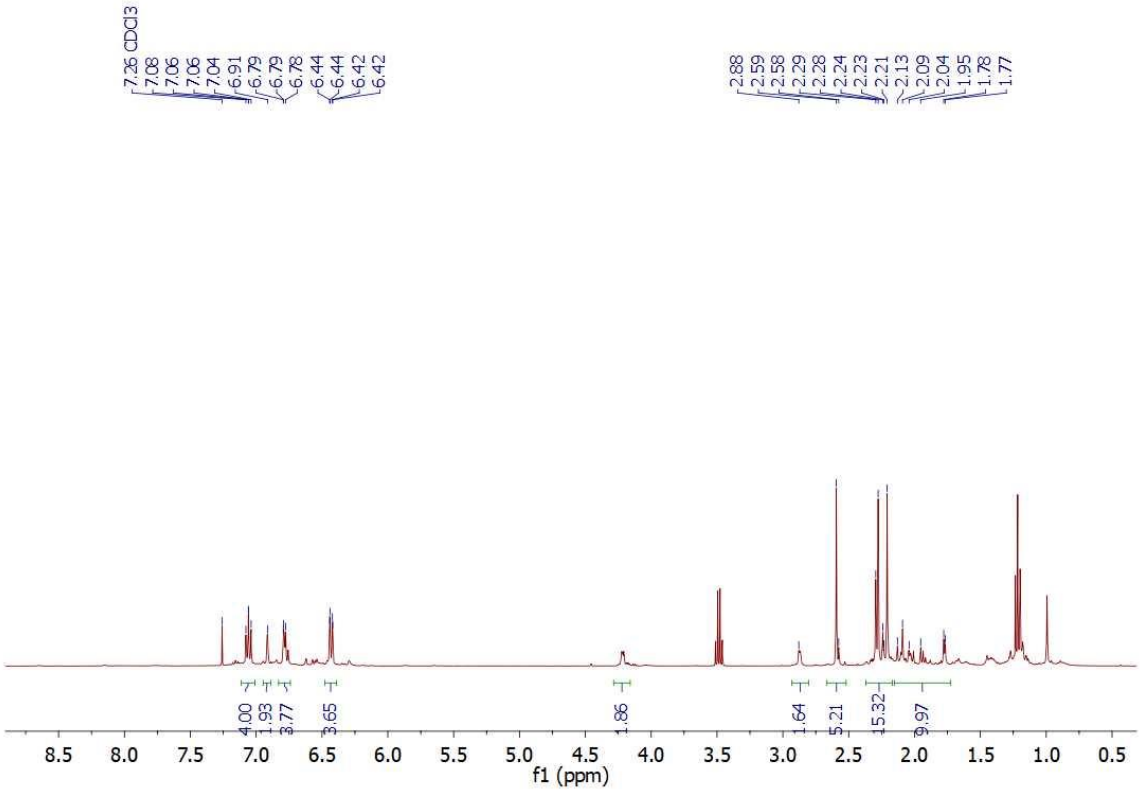

Figure 111 ^{1}H NMR of **14a**

19. Synthesis of DIC-Ir(CO)$_2$Cl **15a**

DCM (10 mL) was added to a vial containing **13a** (46 mg, 0.87 mmol) and a stir bar. Carbon monoxide was bubbled directly into the stirring solution via syringe until all solvent had evaporated. The residue was redissolved in DCM (10 mL) and carbon monoxide bubbled directly through the solution again until all solvent had evaporated. Then hexanes (10 mL) was added to the vial and carbon monoxide was bubbled through again until dry, this was repeated 2 more times. The product was precipitated with DCM and pentane and filtered to give a yellow solid. Yield, 39 mg, 91%. ^{1}H NMR (500 MHz, $CDCl_3$) δ 7.08 (t, J = 7.6 Hz, 4H), 6.84 (s, 4H), 6.75 (s, 2H), 6.44 (d, J = 7.6 Hz, 4H), 2.49 (s, 5H), 2.32 (s, 6H), 2.23 (s, 6H), 1.27 (s, 3H), 1.18 (s, 3H). ^{13}C NMR (126 MHz, $CDCl_3$) δ 211.35, 178.77, 168.86, 146.04, 138.88, 137.78, 135.51, 135.28, 130.06, 129.16, 128.79, 128.47, 122.40, 116.57, 50.03, 31.94, 28.13, 25.01, 21.11, 20.33, 19.51.

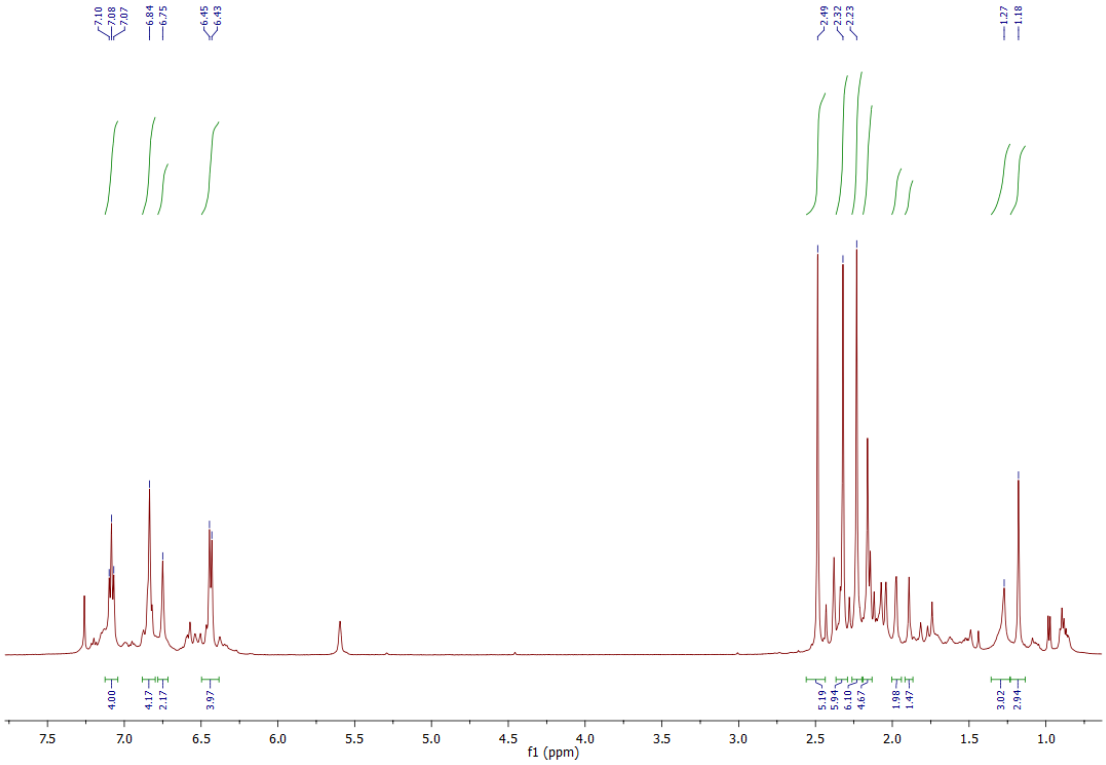

Figure 112 ^{1}H NMR of **15a**

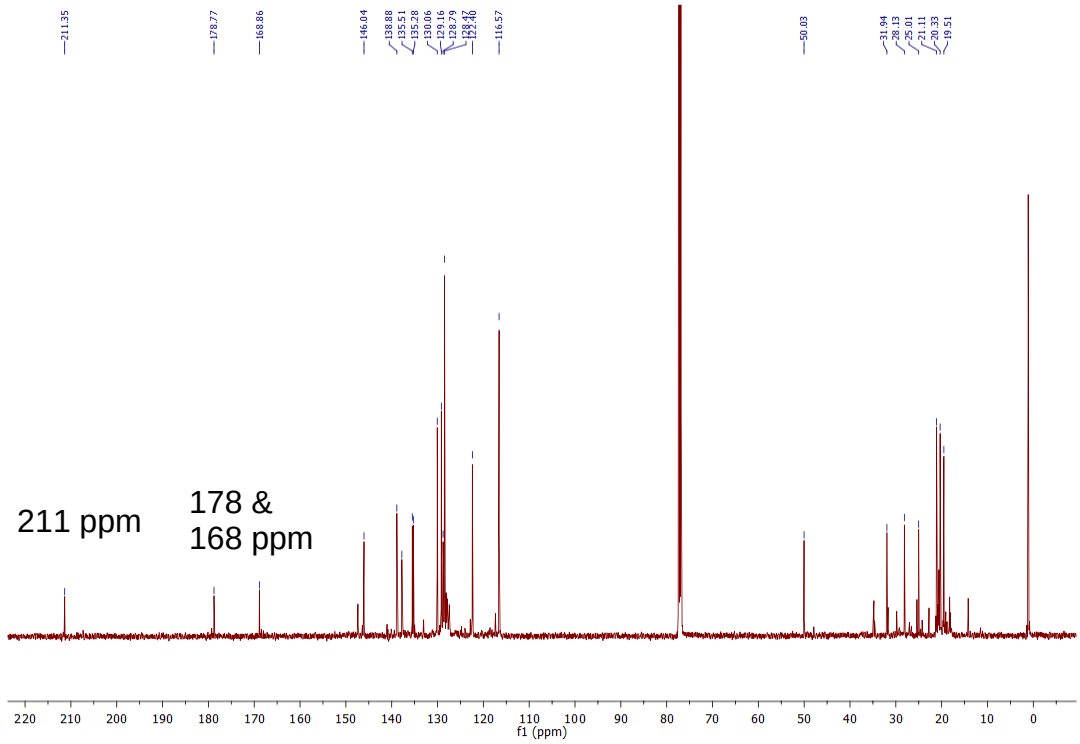

Figure 113 ^{13}C NMR of $(DIC)Ir(CO)_2Cl$ **15a** showing the carbene peak at 211 ppm. and the carbonyl peaks at 168 and 178 ppm.

IV. SYNTHESIS OF AN INDOLE-DERIVED CARBENE (IC) AND AN ABNORMAL DIAMIDOCARBENE (aDAC)

Currently our group is focusing on synthesizing two other new carbenes. Both are structural isomers of two other known carbenes. The first carbene, an indole-derived carbene (IC) is a structural isomer of Bertrand's cyclic(alkyl)aryl carbene (CAArC) and can also be regarded as a benzannulated CAAC, shown in Figure 114.[23] The CAArC features an aryl group incorporated into the heterocyclic ring of the carbene. In Bertrand's carbene the aryl group is adjacent to the carbene carbon, similar to CAmArY. The CAArCs are not stable mostly because there is no steric protection for the carbene. We wanted to investigate the electron withdrawing effect of an aryl group on the nitrogen atom's ability to stabilize the p-orbital of the carbene.

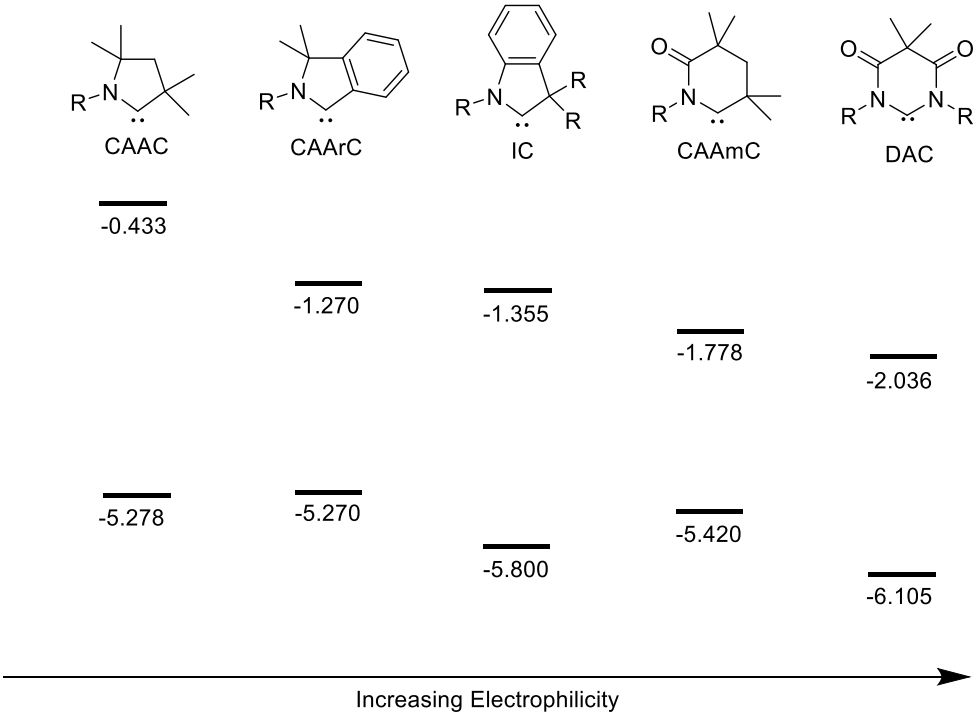

Figure 114 HOMO-LUMO diagram of CAAC, CAArC, IC, CAAmC, and DAC

The addition of the aryl group increases the electrophilicity of the carbene when compared to CAAC, the most similar carbene to the CAArC.[23,55] The IC still incorporates

an aryl group into the ring structure but is located on the back portion of the ring instead of adjacent to the carbene carbon. It also retains the σ-donating sp^3 carbon adjacent to the carbene, which we predict will increase nucleophilicity. The retention of the sp^3 carbon next to the carbene also provides a significant amount of steric protection for the carbene. Since there is only a phenyl attached to the nitrogen atom we hope this is enough protection to allow isolation of this carbene. DFT calculations performed on the IC suggest that it should be a better nucleophile than DAC with a HOMO energy of -5.800 eV. The IC should also be a better electrophile than CAAC with a LUMO energy of -1.355 eV. It's HOMO-LUMO gap of 102.504 kcal/mol lays almost halfway between CAAC (111.7 kcal/mol) and DAC (93.844 kcal/mol) (Figure 114).

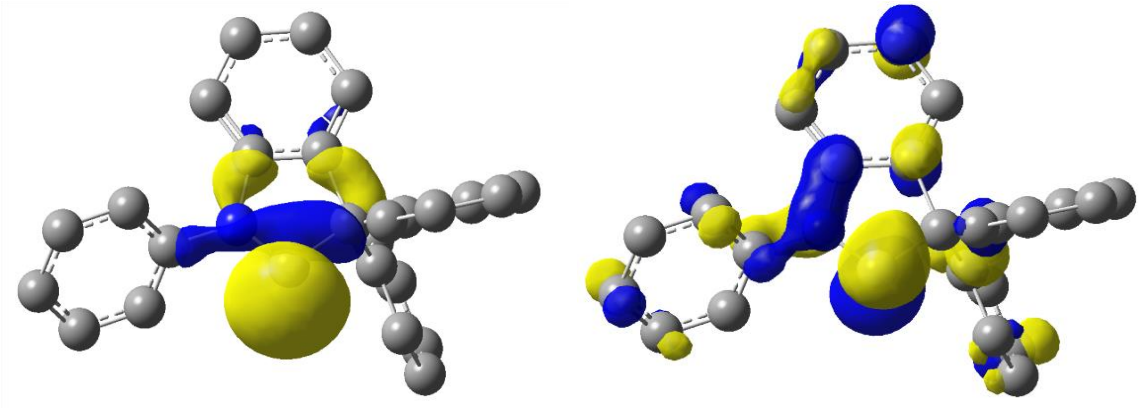

Figure 115 HOMO and LUMO orbital diagrams of the indole carbene (IC)

Initially we attempted the synthesis of IC by starting with commercially available isatin. We attempted multiple methods of substituting the nitrogen. Substitution of alkyl groups was relatively straightforward and gave good yields while arylation of the nitrogen proved to be incredibly difficult. Arylation with diaryliodonium salts gave very low yields. Chan-Lam coupling reactions with isatin and an aryl boronic acid had even lower yields and the results were not reproducible (Figure 116). Due to the difficulty of synthesizing an N-arylisatin, we decided to change our synthetic route.

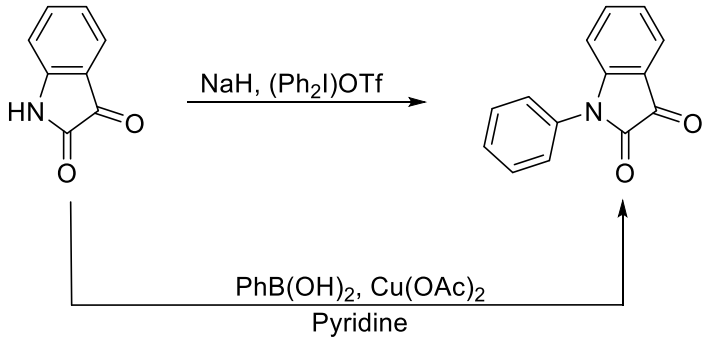

Figure 116 Attempted synthetic routes for arylation of isatin

Condensation of diphenylamine with excess oxalyl chloride in dichloromethane resulted in the formation of diphenylaminooxalylchloride **17** which was used without further purification. N-phenylisatin **18** was synthesized via an intermolecular Friedel-Crafts acylation of **17** with aluminum trichloride.

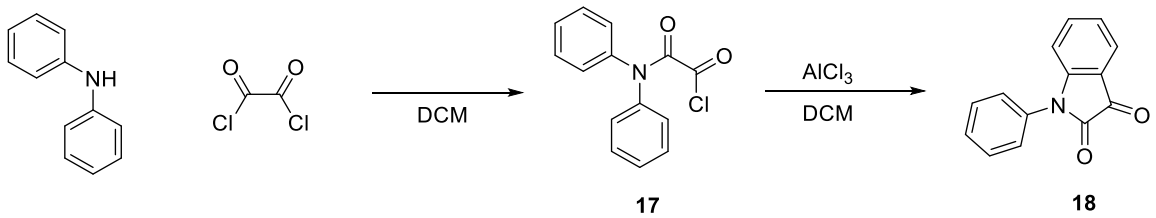

Figure 117 Synthesis of N-phenylisatin

The benzylic carbonyl of N-phenylisatin **18** is very reactive due to the electron withdrawing groups on either side. It was substituted with phenyl groups through electrophilic aromatic substitution. In the presence of triflic acid, **18** forms a carbocation at the benzylic carbon allowing for the EAS of benzene at that position which resulted in N,3,3-triphenylindolone **19**.

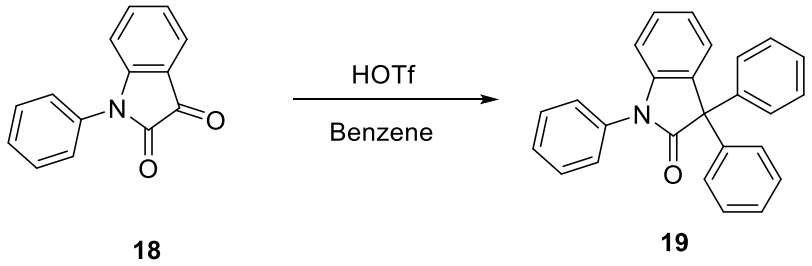

Figure 118 Electrophilic aromatic substitution of **18**

The reduction of the amide to the alcohol proved very challenging as most reducing agents either gave no reaction, over-reduced to the amine, or cleaved the nitrogen carbon bond. Successful reduction of the amide to the alcohol **20** was achieved using one equivalent of $LiAlH_4$ in refluxing THF overnight.

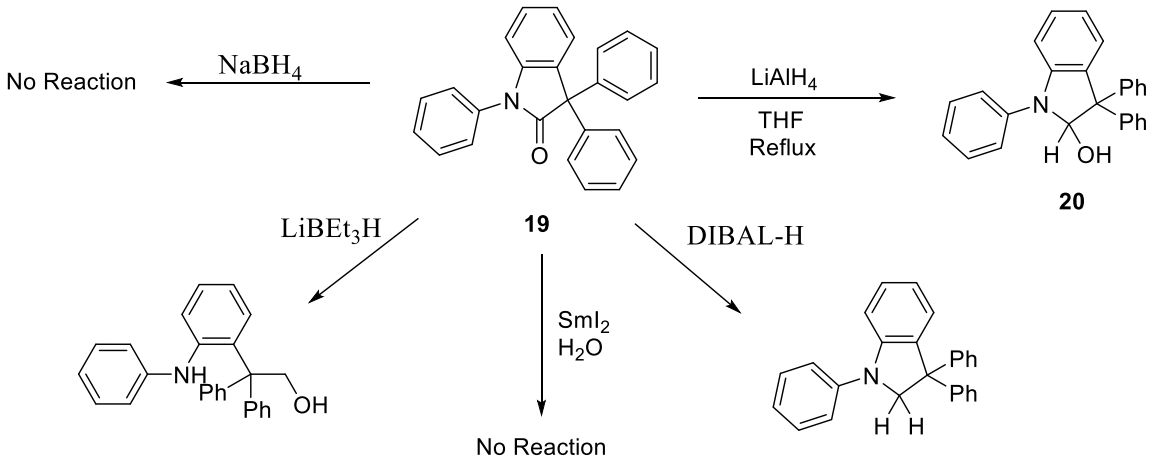

Figure 119 Synthetic attempts to generate the alcohol **20** with various hydride based reducing agents.

Formation of the carbene precursor is currently being attempted. Treatment of **20** with triflic anhydride, triflic acid, or TMS-triflate has resulted in some formation of the iminium triflate salt, but also forms other byproducts that have been difficult to separate. Chlorination attempts with thionyl chloride, oxalyl chloride and PCl_5 have not been successful. Other methods of forming the iminium salt are currently being investigated.

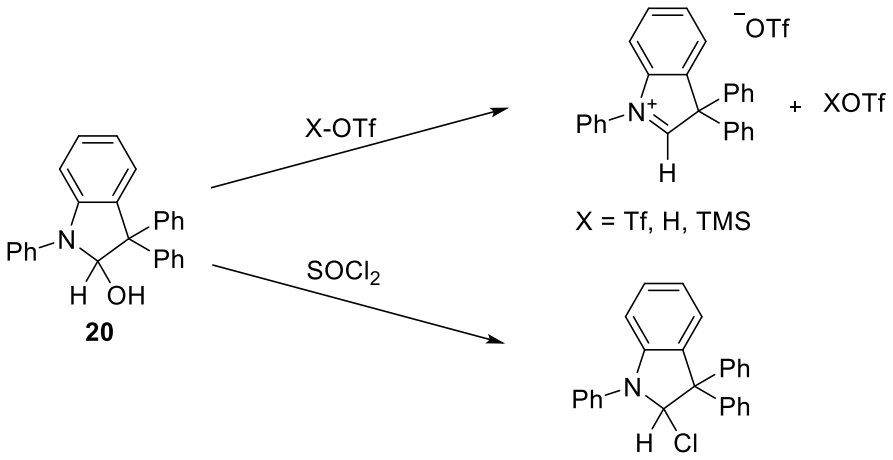

Figure 120 Attempted syntheses of IC precursor

Since the carbene has not been synthesized yet, we cannot say much about its electronic properties. Based on calculations of the energy levels of IC we can predict its relative electrophilicity. Since there is a linear relationship established between the LUMO energy level and selenium NMR we can estimate where we expect the IC–Se adduct's ^{77}Se peak should appear. Calculated from the linear regression equation in Figure 41, the selenium adduct of IC is predicted to have a selenium NMR shift around 608 ppm.

Future investigations of the IC will include synthesizing derivatives by substituting the benzylic position with imino and alkene functional groups (**B** & **C** in Figure 121). Our group will also investigate the effect of the substitution of the aryl group incorporated into the heterocyclic ring to study the tunability of the carbene (**D** & **E** in Figure 121).

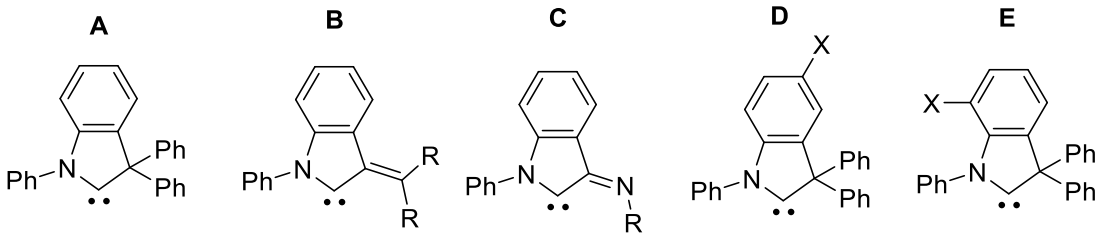

Figure 121 IC derivatives for future study

The other new carbene our group is interested in is the structural isomer of a DAC, the abnormal diamido carbene (aDAC). With Bielawski's CAAmC, replacing one of the nitrogen atoms in a DAC with a quaternary carbon increases the nucleophilicity of the carbene (Figure 122). CAAmC has a HOMO of -5.420 eV while DAC has a HOMO of -6.105. Since CAAmC still retains the amide moiety, it is also still very electrophilic, with a LUMO of -1.778 eV compared to DAC's LUMO of -2.036 eV. The aDAC is essentially an isomerized DAC, with the positions of one of the carbonyls and the carbene carbon switched. This gives us a structure that is very similar to the CAAmC around the carbene center, but features an additional nitrogen and carbonyl in the back of the ring. Since there is an additional nitrogen to delocalize electron density into the carbonyl, there is a slight increase in the LUMO (-1.824 eV) relative to CAAmC (Figure 122). The HOMO energy (-5.821 eV) is lower than we initially expected, but we suspect this may be due to the second carbonyl having an inductive pull effect on the quaternary carbon, reducing the electron density on the carbene carbon. The aDAC also features a HOMO-LUMO gap of 90.36 kcal/mol, slightly smaller than DAC's HOMO-LUMO gap of 93.88 kcal/mol.

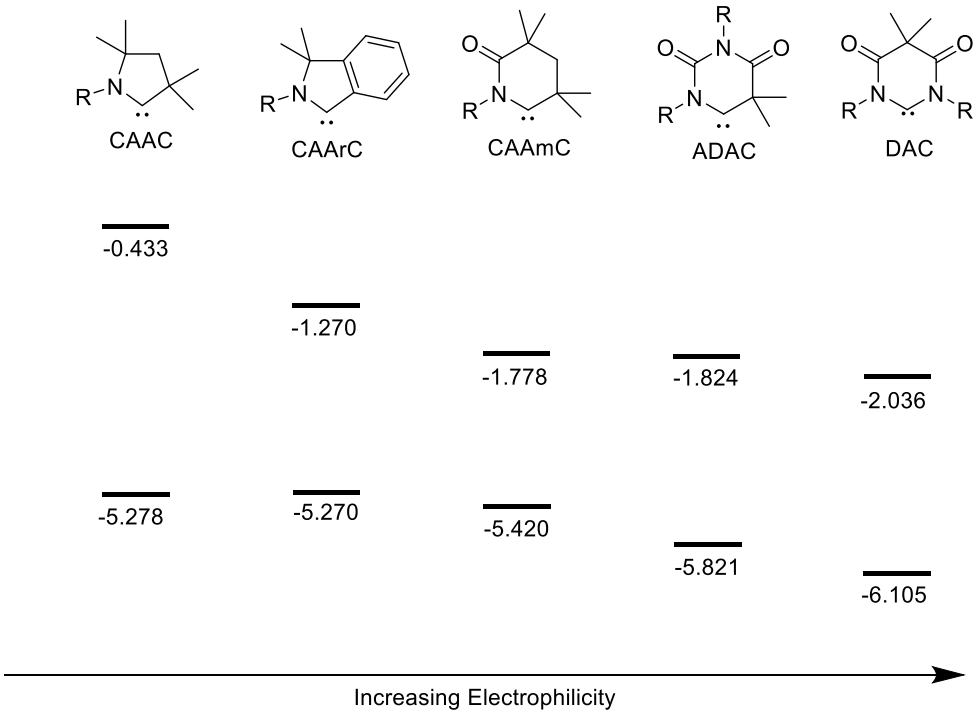

Figure 122 HOMO LUMO diagram of CAAC, CAArC, CAAmC, ADAC, and DAC.

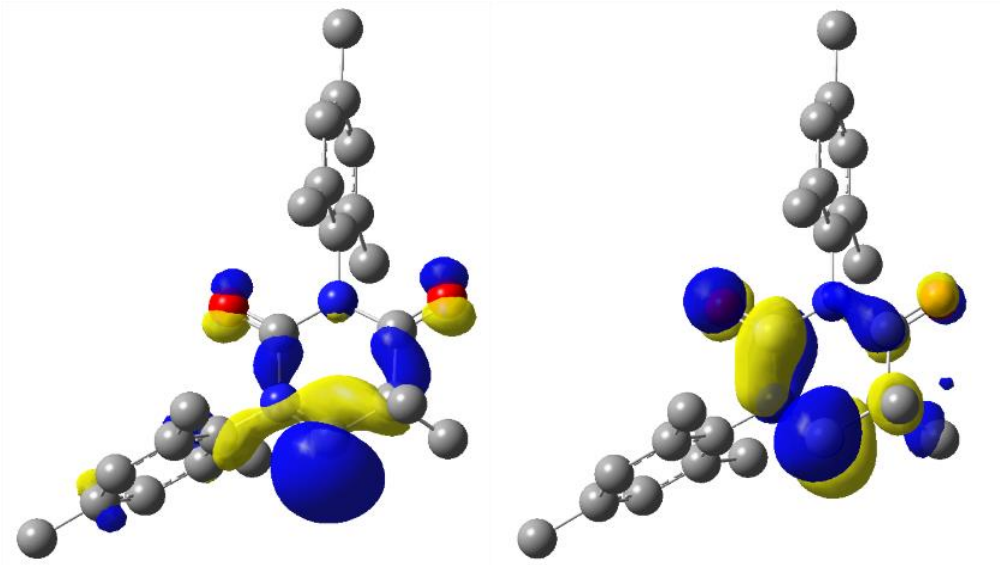

Figure 123 HOMO and LUMO diagrams of the abnormal diamidocarbene (ADAC)

The CAAmC features a Dipp group attached to the nitrogen for steric protection. Generation of the CAAmC results in C–H insertion into the methine on the isopropyl in

the Dipp group.[48] Since the methine groups are more susceptible to C–H insertion relative to the methyl groups in a mesityl, aDAC will be synthesized using mesityl groups.[33,36]

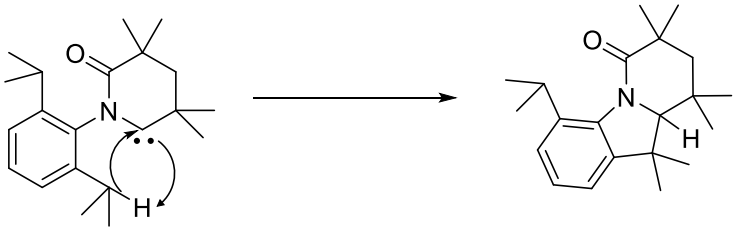

Figure 124 C–H insertion seen in the CAAmC

The synthesis of the aDAC begins by taking the DAC precursor, DACHCl and hydrolyzing the chloride off to give DACHOH **21**. The alcohol product is then oxidized with CrO_3 and acetic acid to give the barbituric acid **22**.

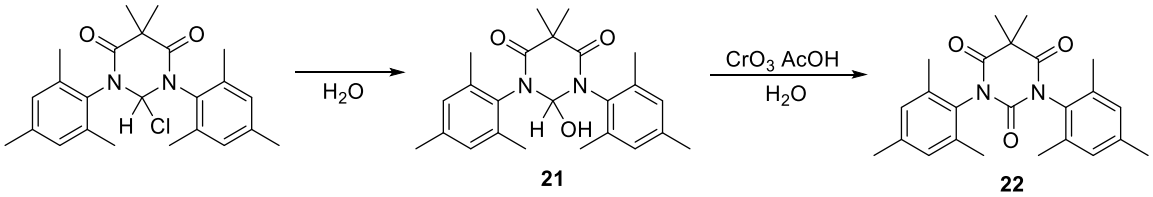

Figure 125 Synthesis of DACOH **21** and dimesitylbarbituric acid **22**

Then using a 0.1 M SmI_2•THF solution, water and oxygen one of the amide carbonyls can be reduced to the alcohol, aDACHOH **23**. The aDACHOH was easily chlorinated with thionyl chloride to give the aDACHCl **24**. Attempts to deprotonate with a variety of strong bases has thus far been unsuccessful. The aDACHOH **21** was also treated with triflic anhydride to give aDACHOTf **25**, but deprotonation of this also was unsuccessful.

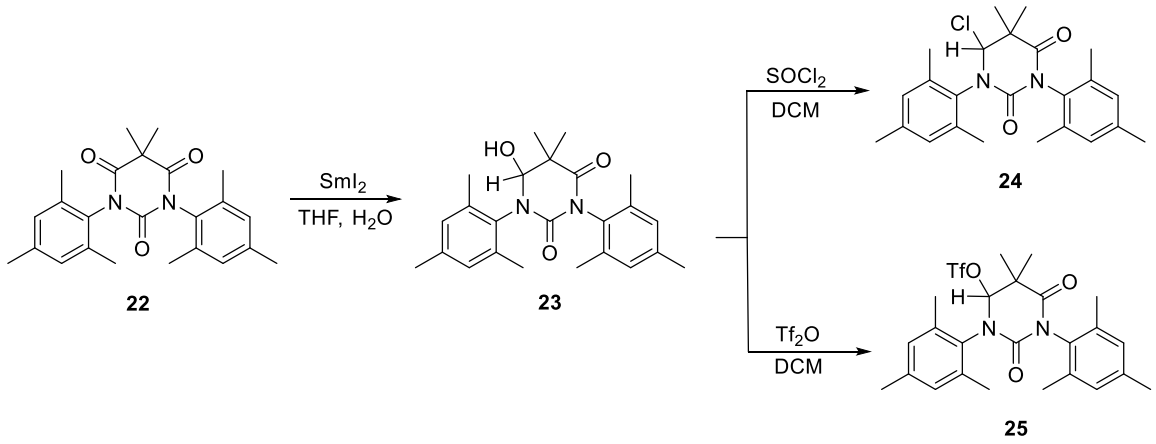

Figure 126 Synthesis of ADACOH **23** and ADACHCl **24**

NMR chemical shifts are related to electron density around an atom, an atom that is more acidic will appear downfield relative to less acidic atoms. Typically, the neutral hydrohalic carbene precursors have proton chemical shifts of ~6.5 ppm while the aDACHCl has a ^{1}H chemical shift of 5.16 ppm, suggesting that proton is less acidic than other similar carbene precursors.[33] We suspect that the reason the aDAC will not undergo deprotonation with NaHMDS is because the proton on the carbene carbon is not acidic enough.

Similar to the indole-derived carbene (IC), we are currently unable to report on the experimentally determined electronic properties. Based on DFT calculations and the linear regression from Figure 41, we predict that the aDAC selenium adduct will have a ^{77}Se NMR chemical shift of ca. 750 ppm.

We are currently investigating other methods of generating the free carbene and other possible carbene precursors that will successfully undergo deprotonation.

Experimental Section

1. Synthesis of N-phenylisatin **18**

Diphenylamine (2.00 g, 11.8 mmol) was dissolved in DCM (100 mL) in a schlenk flask under and atmosphere of nitrogen and equipped with a rubber septum. Then oxalyl chloride (1.1 mL, 12.8 mmol) was added via syringe and stirred for 3 hours. All volatiles were removed under vacuum and the product was redissolved in DCM (100 mL). The flask was cooled to 0° C and 4.5 g $AlCl_3$ was added slowly in portions. This resulted in a brown sludge which was stirred overnight. The reaction was quenched by pouring the contents of the flask over ice resulting in a bright orange precipitate. The product was extracted with DCM and the organic layer was washed with water and saturated NaCl solution, dried over magnesium sulfate and filtered over celite. Volatiles were removed under vacuum to give the product as a bright orange solid. Yield, 1.81 g, 64% ^{1}H NMR (400 MHz, $CDCl_3$) δ 7.70 (ddd, J = 7.5, 1.4, 0.6 Hz, 1H), 7.61 – 7.50 (m, 3H), 7.50 – 7.39 (m, 3H), 7.17 (td, J = 7.5, 0.8 Hz, 1H), 6.90 (dt, J = 8.0, 0.7 Hz, 1H). ^{13}C NMR (101 MHz, DMSO) δ 183.25, 157.92, 151.73, 138.50, 133.82, 130.19, 128.93, 126.97, 125.18, 124.13, 118.13, 111.23.

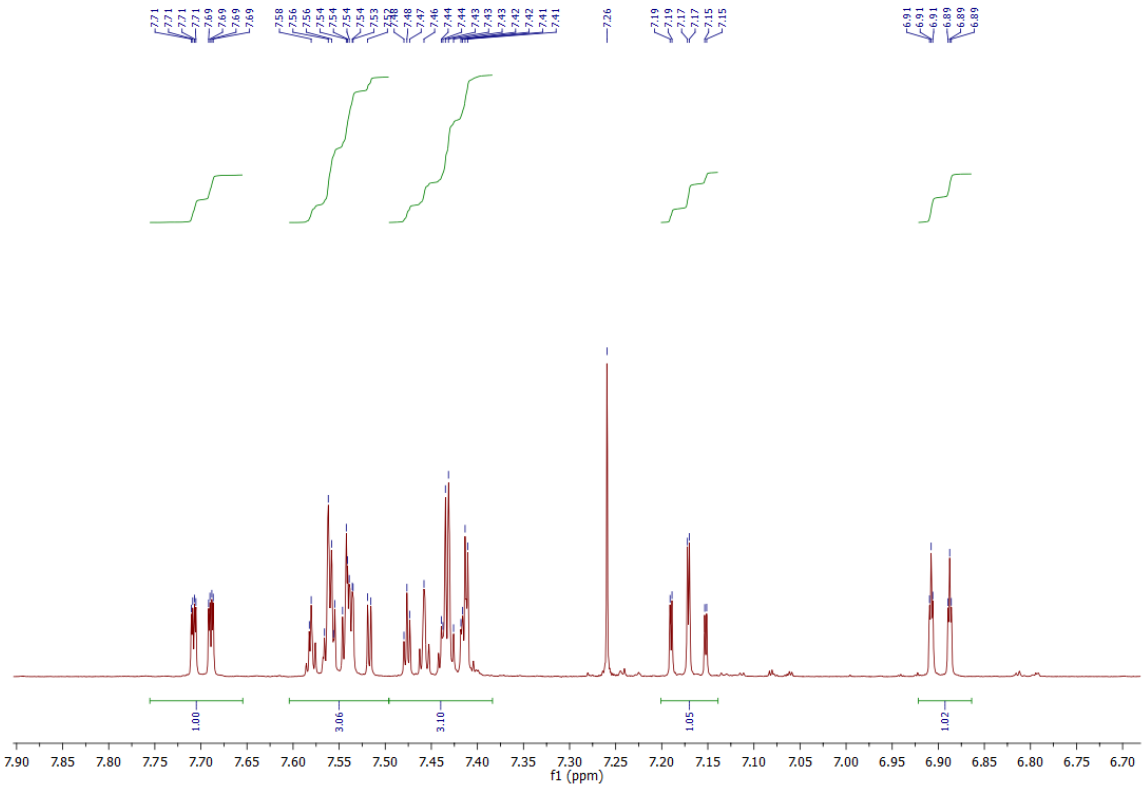

Figure 127 ^{1}H NMR of **18**

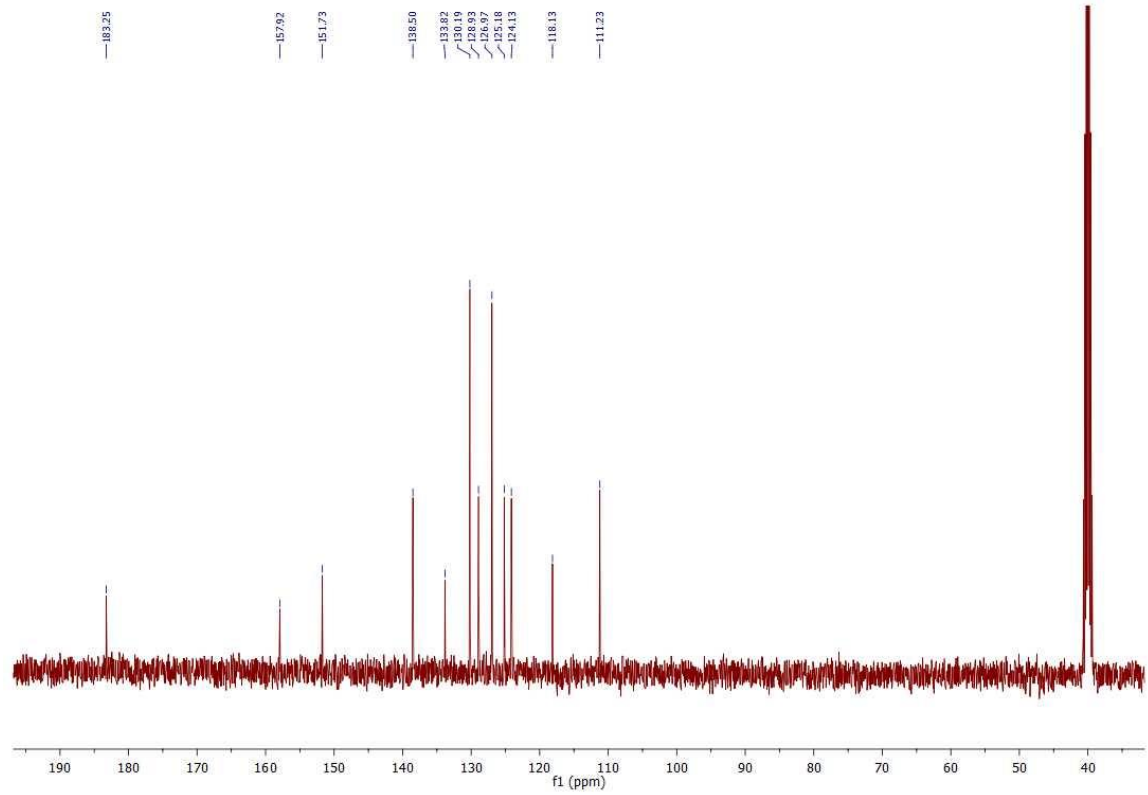

Figure 128 ^{13}C NMR of **18**

2. Synthesis of N,3,3-triphenylindolone **19**

N-Phenylisatin **18** (1.00 g, 4.48 mmol) was added to a round bottom flask with a stir bar and covered with a rubber septum. Then triflic acid (20 mL, 226 mmol) was rapidly added to the flask via syringe and stirred for 15 minutes, the solution turned dark blue. Then benzene (10 mL, 112 mmol) was added to the reaction via syringe and stirred overnight. The reaction was quenched by pouring over ice and stirred for 20 minutes, a white precipitate was formed. The product was extracted with DCM and the organic layers were washed with water and saturated NaCl. The organic layer was concentrated under vacuum and the product was precipitated with pentane. The product is a white crystalline solid. Yield, 1.1 g, 76% ^{1}H NMR (400 MHz, $CDCl_3$) δ 7.58 – 7.49 (m, 2H), 7.49 – 7.38 (m, 3H), 7.38 – 7.19 (m, 12H), 7.12 (td, J = 7.5, 1.1 Hz, 1H), 6.91 (ddd, J = 7.9, 1.1, 0.5 Hz, 1H). ^{13}C NMR (101 MHz, $CDCl_3$) δ 177.00, 143.06, 142.01, 134.57, 132.74, 129.59, 128.56, 128.55, 128.54, 128.53, 128.52, 128.50, 128.19, 128.14, 127.40, 126.81, 126.45, 123.27, 109.89, 62.58.

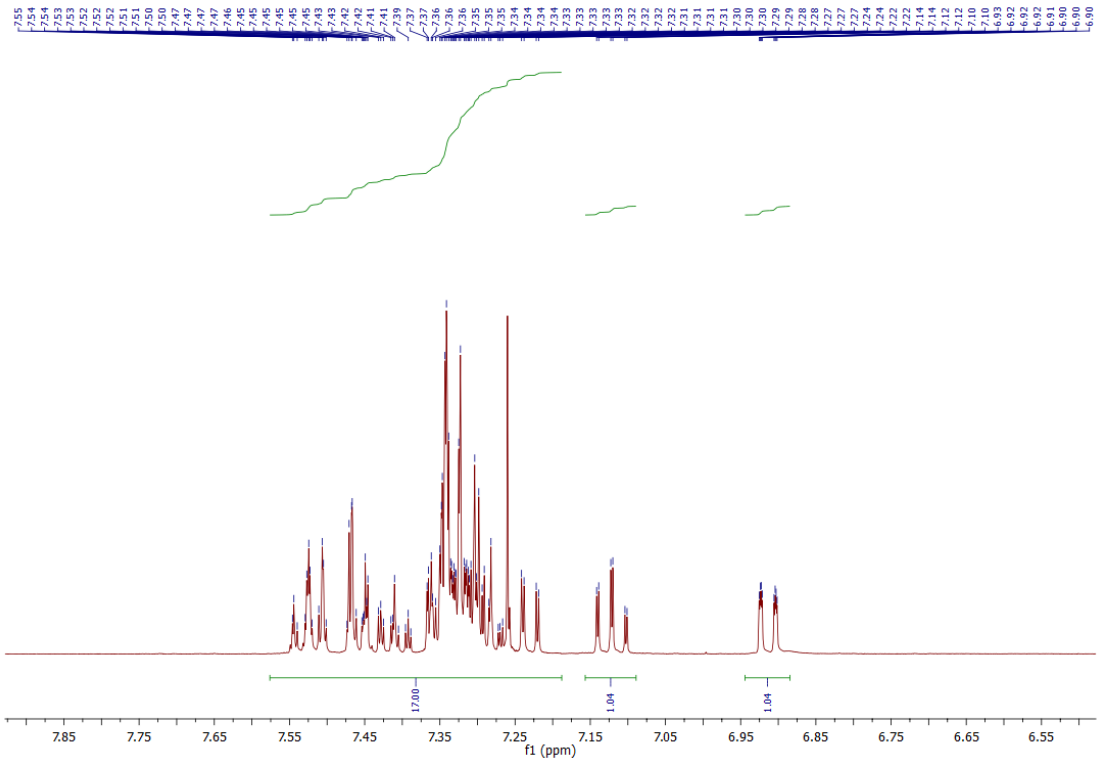

Figure 129 ^{1}H NMR of **19**

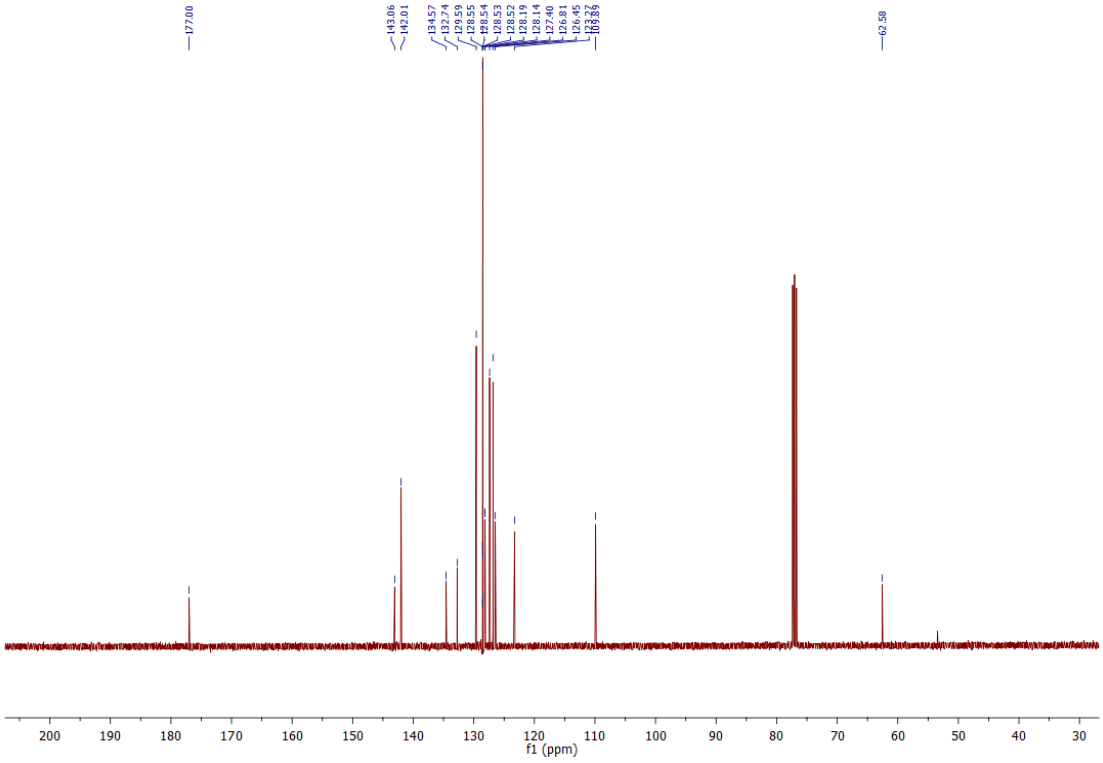

Figure 130 ^{13}C NMR of **19**

3. Synthesis of Triphenylindole-2-ol **20**

N,3,3-triphenylindolone **19 (**500 mg, 1.38 mmol) was added to a schlenk flask with stir bar in the glovebox and dissolved in 30 mL THF. Then $LiAlH_4$ (65 mg, 1.71 mmol) in 10 mL THF was added to the schlenk flask. The Schlenk flask was equipped with a reflux condenser and heated to 50 °C under an atmosphere of nitrogen overnight. The reaction was quenched by slowly adding 30 ml of a 0.1M HCl to the flask. After addition of HCl was complete, the flask was stirred for another 30 minutes. The reaction mixture was filtered over celite and washed with 20 ml THF. The solution was concentrated under vacuum to remove THF. The product was extracted with DCM (20 ml three times). The solution was concentrated to dryness under vacuum. The product was then precipitated with $CHCl_3$/Hexanes and collected via filtration. Yield, 0.285g, 56%. ^{1}H NMR (400 MHz, $CDCl_3$) δ 7.59 – 7.50 (m, 2H), 7.45 – 7.10 (m, 16H), 7.10 – 7.03 (m, 1H), 6.86 (td, J = 7.4, 1.1 Hz, 1H), 5.99 (d, J = 8.0 Hz, 1H), 1.96 (d, J = 8.0 Hz, 1H). ^{13}C NMR (101 MHz, $CDCl_3$) δ 146.29, 145.30, 142.34, 140.64, 138.60, 138.37, 137.50, 135.38, 134.38, 132.06, 131.63, 130.68, 130.67, 129.83, 129.82, 129.48, 128.88, 128.82, 128.81, 128.73, 128.69, 128.56, 128.31, 128.02, 127.96, 127.76, 127.57, 127.42, 127.41, 127.40, 127.21, 127.16, 126.36, 123.80, 123.16, 121.31, 120.95, 120.26, 120.03, 117.17, 111.08, 110.25, 94.71, 64.25.

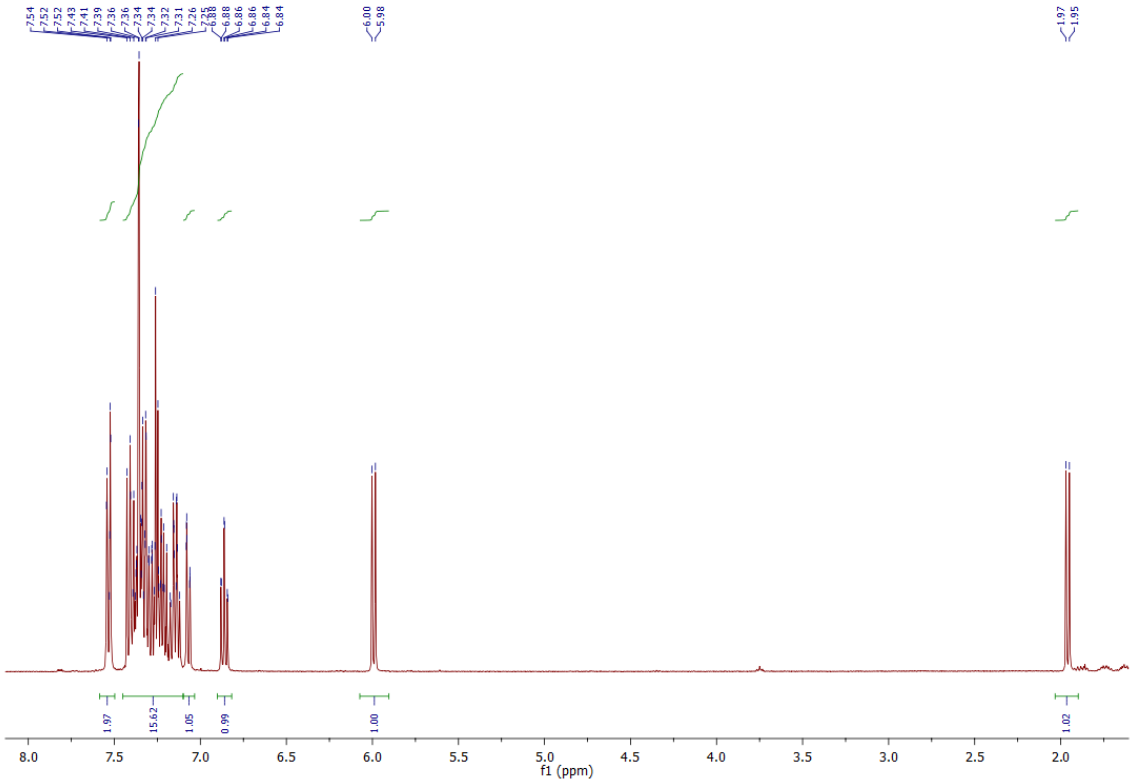

Figure 131 ^{1}H NMR of **20**

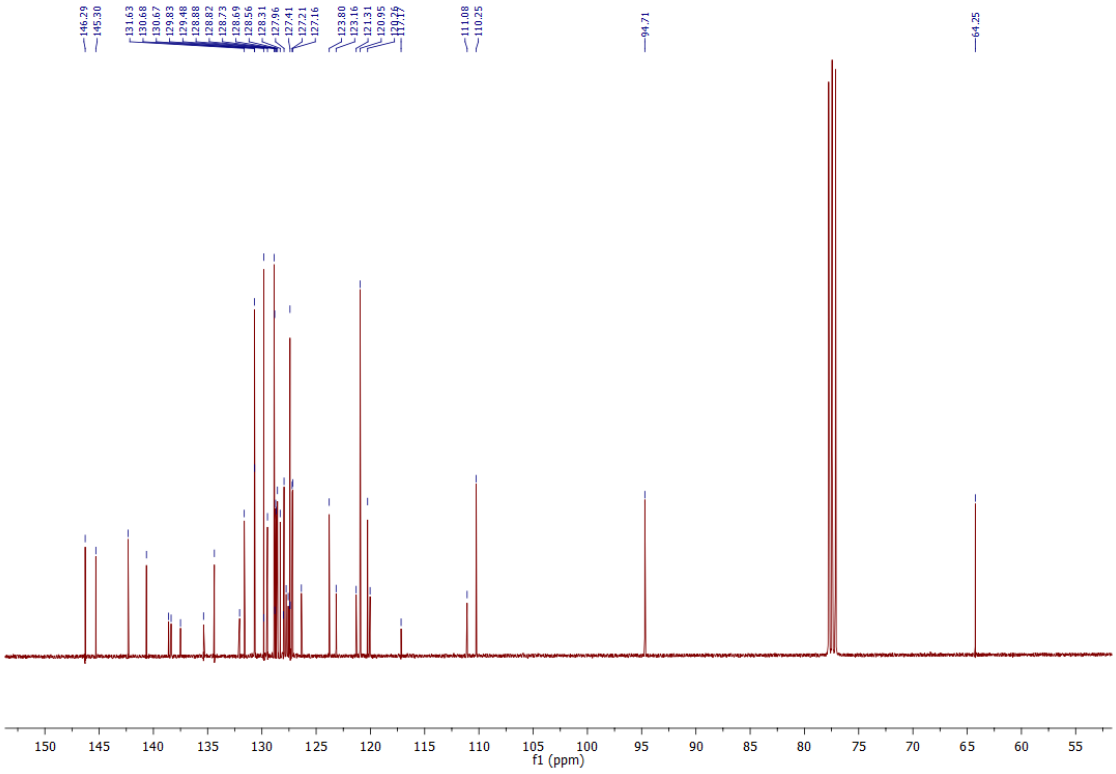

Figure 132 ^{13}C NMR of **20**

4. Synthesis of DACHOH **21**

N,N'-dimesitylformamidine (1.95 g, 6.95 mmol) was dissolved in 30 ml benzene in a round bottom flask under an atmosphere of nitrogen equipped covered with a rubber septum. Then triethylamine (1.4 mL, 10 mmol) was added to the flask via syringe and stirred for 10 minutes. The flask was cooled to 0 °C. Then dimethylmalonyl dichloride (1.0 mL, 7.6 mmol) was added dropwise via syringe. The reaction was warmed to room temperature and stirred for 2 hours. The reaction was then opened to air and 5 mL water was added to the flask. The reaction was stirred for 1 hour. The solution was concentrated to about 20 mL under vacuum and filtered to afford the DACHOH **21** as a white solid. Yield, 2.78 g, 91%. ^{1}H NMR (500 MHz, $CDCl_3$) δ 6.88 (s, 4H), 5.67 (s, 1H), 2.31 – 2.11 (m, 18H), 1.77 (s, 3H), 1.49 (s, 3H). ^{13}C NMR (126 MHz, DMSO) δ 170.63, 138.45, 137.72, 135.39, 134.28, 129.80, 129.44, 88.56, 46.73, 27.95, 21.74, 20.91, 19.07, 18.35.

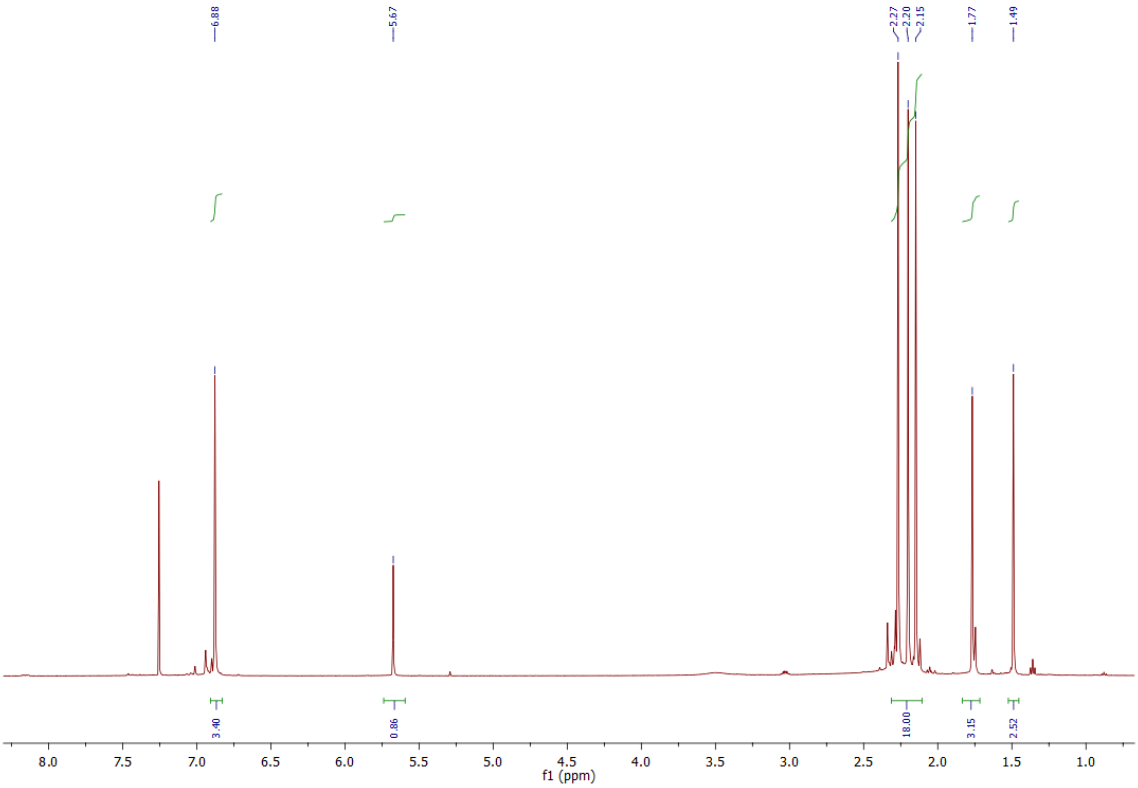

Figure 133 ^{1}H NMR of **21**

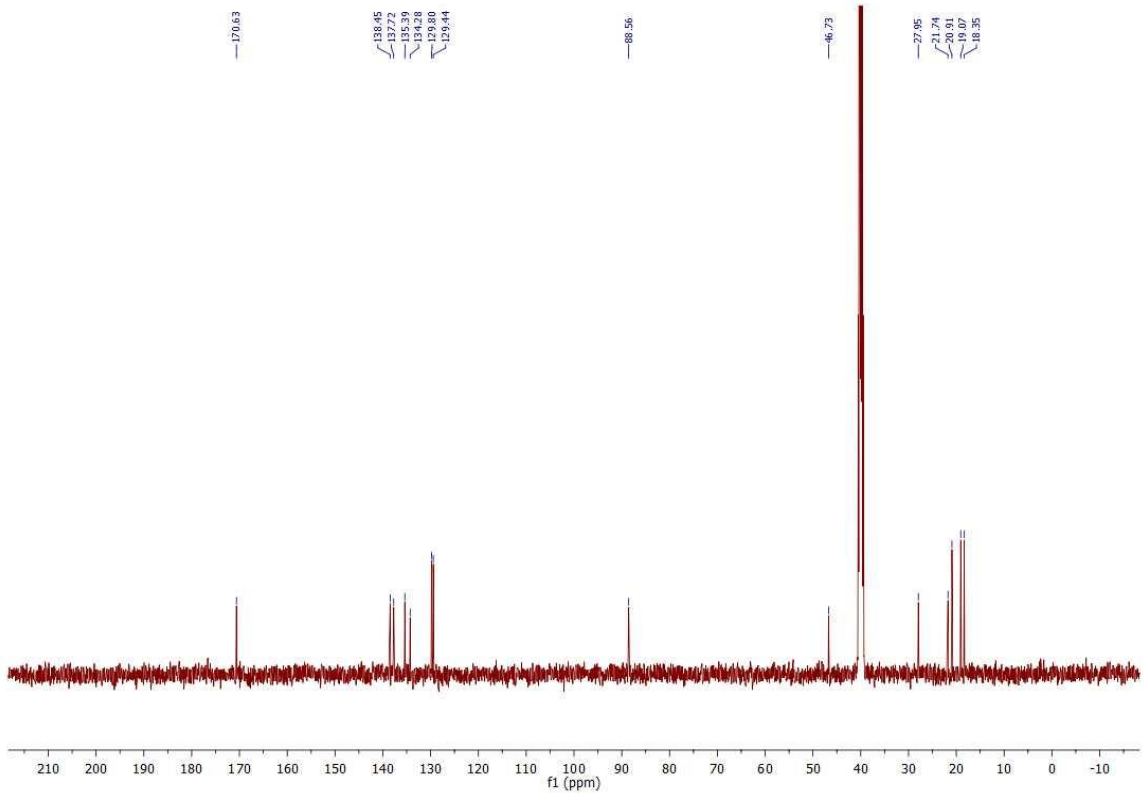

Figure 134 ^{13}C NMR of **21**

5. Synthesis of DAC Urea (Barbituric acid) **22**

Acetic acid (10 mL) was added to a round bottom flask containing **21** (200 mg, 0.51 mmol). Then CrO_3 (250 mg, 2.5 mmol) was dissolved in a minimum amount of water/acetic acid and added to the reaction flask. The reaction was heated to 80 °C and stirred for 3 hours. The solution initially has a brown precipitate and after 3 hours a large amount of white precipitate forms. The precipitate was collected by filtration and washed with water to remove residual chromic acid. Yield, 0.143 g, 71.5%. ^{1}H NMR (400 MHz, $CDCl_3$) δ 6.96 (s, 2H), 2.30 (s, 3H), 2.13 (s, 6H), 1.78 (s, 3H). ^{13}C NMR (101 MHz, $CDCl_3$) δ 171.90, 138.91, 134.86, 130.02, 129.50, 47.90, 25.33, 21.07, 17.57.

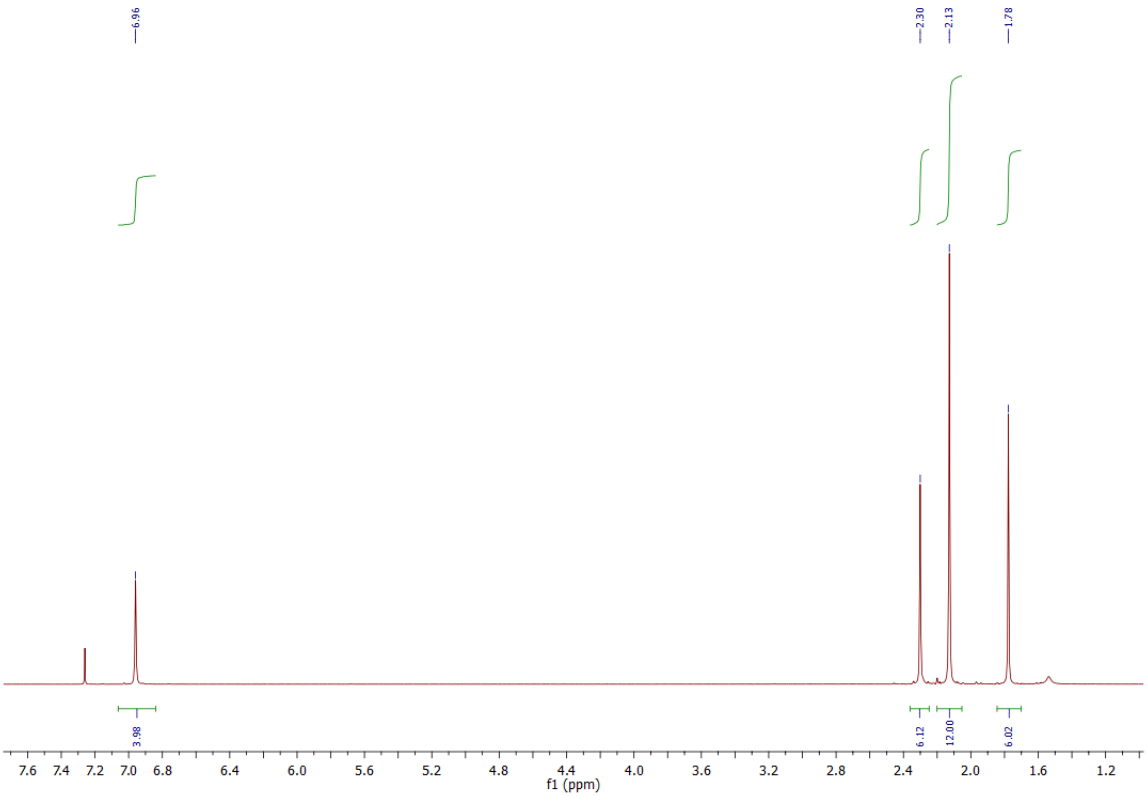

Figure 135 ^{1}H NMR of **22**

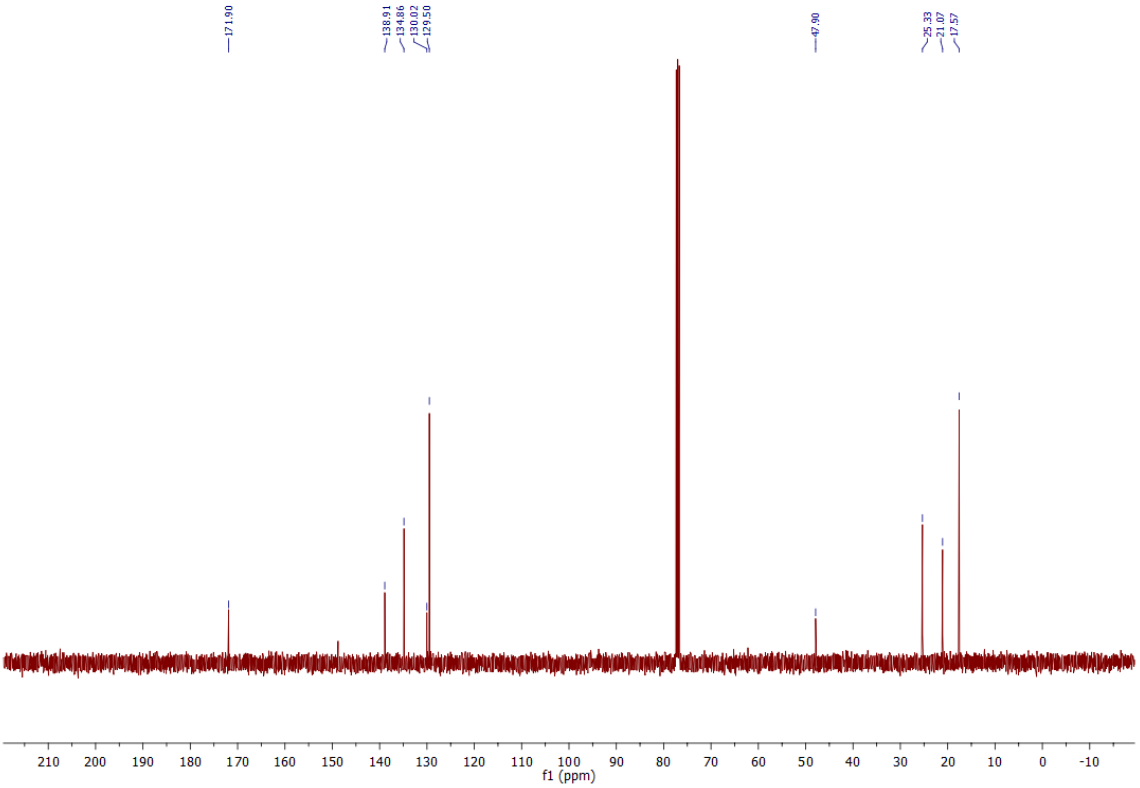

Figure 136 ^{13}C NMR of **22**

6. Synthesis of ADACHOH **23**

THF (20 mL) and H_2O (10 mL) was added to a round bottom flask containing **22** (100 mg, 0.25 mmol). Then 10 mL (4 eq.) of 0.1 M SmI_2 in THF was added rapidly to the solution of **22**. After about 1 minute, air was bubbled into the solution through a cannula for about 5 minutes, solution changes from dark red/purple to yellow with a white precipitate. 50 mL DCM was added to the flask. Then 30 mL of 0.1 M HCl was added to the reaction flask and stirred for 30 minutes to dissolve any left-over Sm metal. The organic layer was separated from the aqueous layer. The aqueous layer was then extracted with 50 mL DCM three times. The organic layers were combined and dried over $MgSO_4$ and filtered over celite. The solution was concentrated to dryness under vacuum. The product was then precipitated using $CHCl_3$ and pentane and collected via filtration. The product **23** was isolated as a white solid. Yield, 65 mg, 65%. ^{1}H NMR (500 MHz, $CDCl_3$) δ 6.91 (dd, J = 25.2, 18.6 Hz, 5H), 4.55 (s, 1H), 2.28 (s, 6H), 2.24 (s, 3H), 2.18 (s, 3H), 2.12 (s, 3H), 2.11 (s, 2H), 2.03 (s, 3H), 1.58 (s, 3H), 1.31 (s, 3H). ^{13}C NMR (126 MHz, DMSO) δ 174.32, 150.64, 138.35, 137.46, 137.31, 136.05, 132.51, 129.89, 129.71, 129.55, 129.09, 129.02, 85.60, 45.30, 25.74, 21.02, 20.96, 20.86, 19.81, 19.76, 18.04, 17.69.

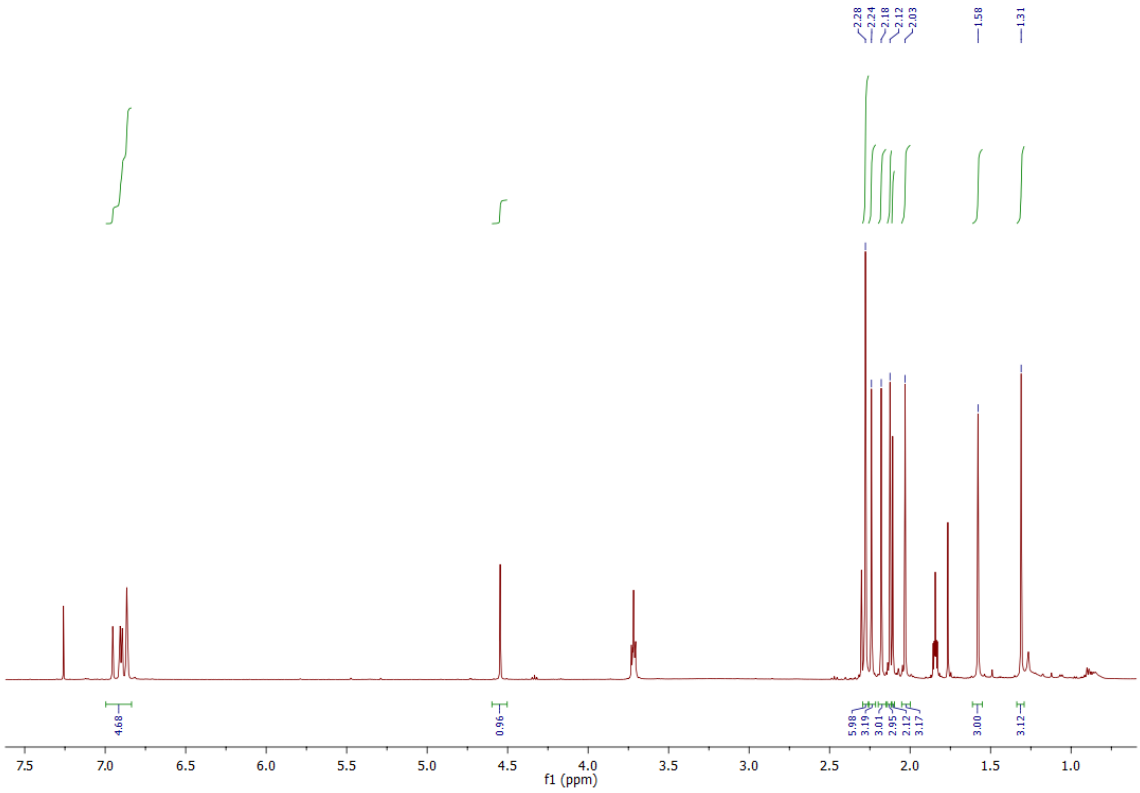

Figure 137 ^{1}H NMR of **23**

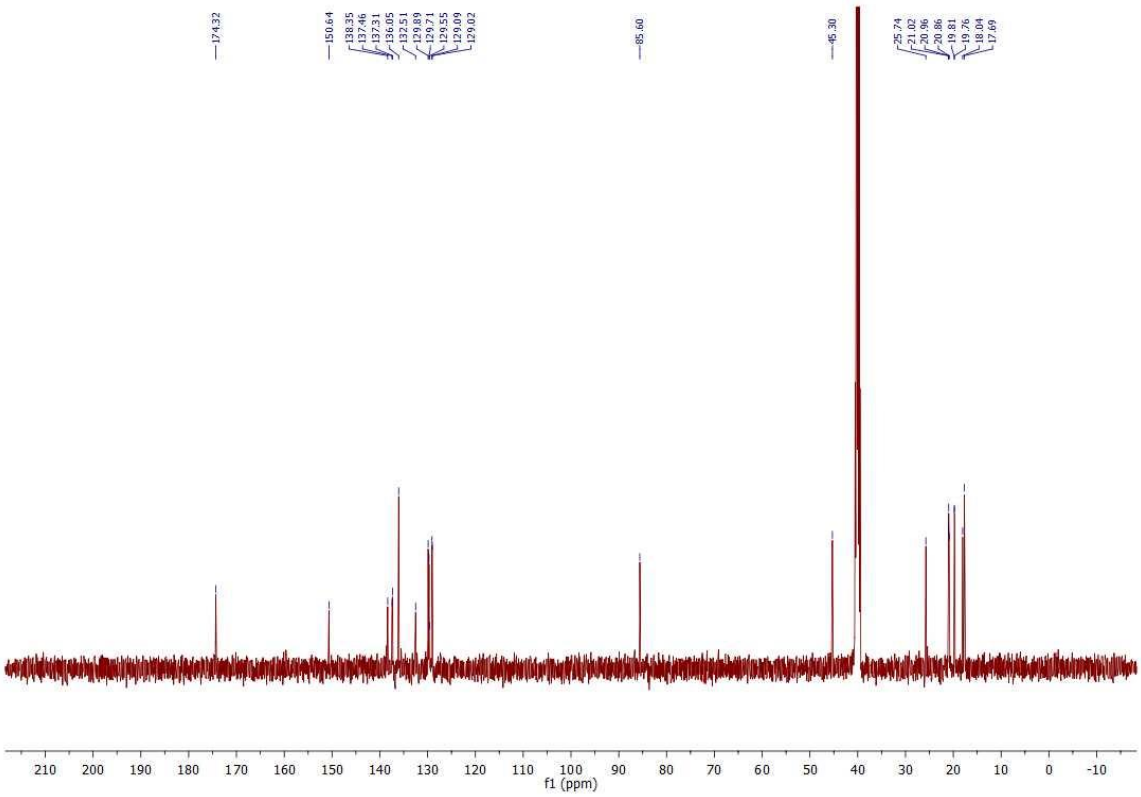

Figure 138 ^{13}C NMR of **23**

7. Synthesis of ADACHCl **24**

DCM (3 mL) was added to a Schlenk flask containing **23** (100 mg, 0.25 mmol) under an atmosphere of nitrogen and equipped with a rubber septum. Then thionyl chloride (1.0 mL, 14 mmol) was added via syringe followed by one drop of DMF via syringe. The reaction was stirred for 3 hours. The solvent was evaporated under vacuum to dryness to afford the product as an orange solid. Yield, 85 mg, 81%. ^{1}H NMR (500 MHz, C_6D_6) δ 6.74 (dd, J = 31.4, 12.3 Hz, 16H), 5.16 (s, 4H), 2.48 (s, 11H), 2.44 (s, 11H), 2.14 (s, 11H), 2.08 (d, J = 7.2 Hz, 24H), 1.93 (s, 11H), 1.41 (s, 14H), 1.34 (s, 11H).

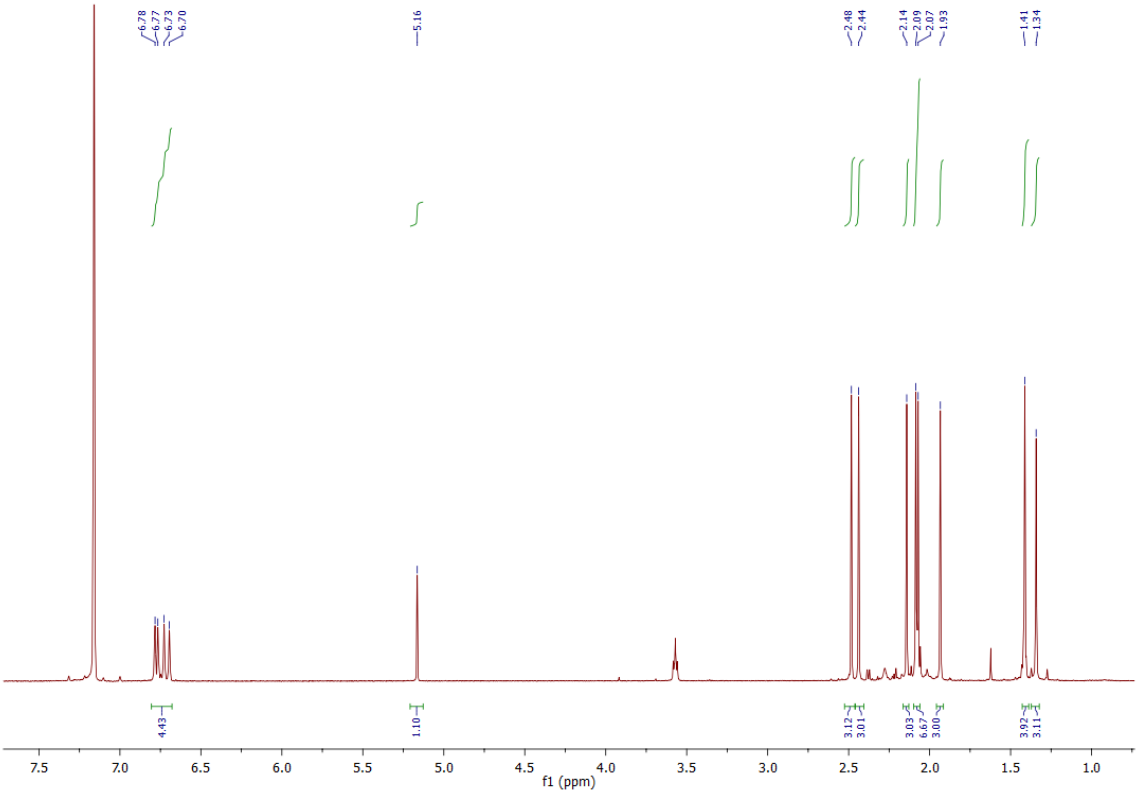

Figure 139 ^{1}H NMR of **24**

8. Synthesis of ADACHOTf **25**

DCM (3 mL) was added to a Schlenk flask containing **23** (100 mg, 0.24 mmol) under an atmosphere of nitrogen and covered with a rubber septum. Then triflic anhydride (0.1

mL, 0.60 mmol) was added via syringe. The reaction was stirred for 3 hours. The solvent was evaporated under vacuum to dryness to afford the product as a white solid. Yield, 85 mg, 81%. ^{1}H NMR (500 MHz, C_6D_6) δ 6.73 (s, 9H), 3.93 (d, J = 19.7 Hz, 2H), 2.25 – 1.99 (m, 41H), 1.30 (s, 8H), 1.21 (s, 8H). ^{19}F NMR (471 MHz, C_6D_6) δ -38.94, -75.23, -77.98.

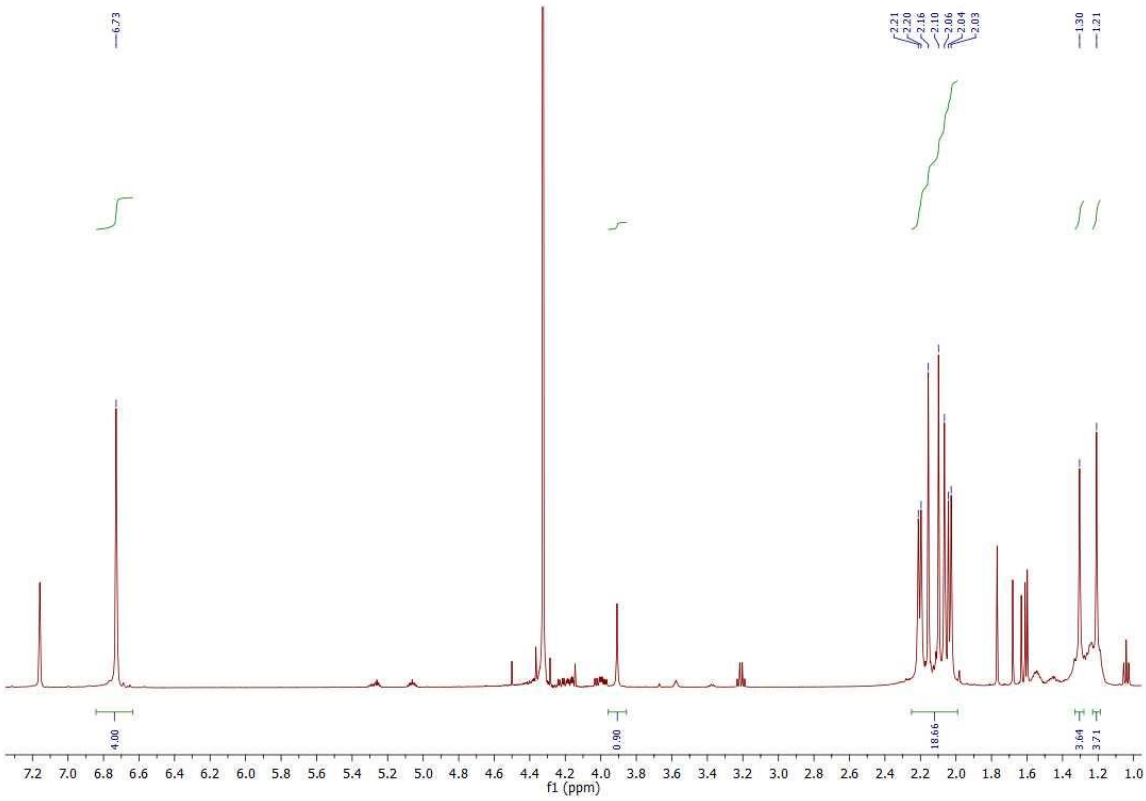

Figure 140 ^{1}H NMR of **25**

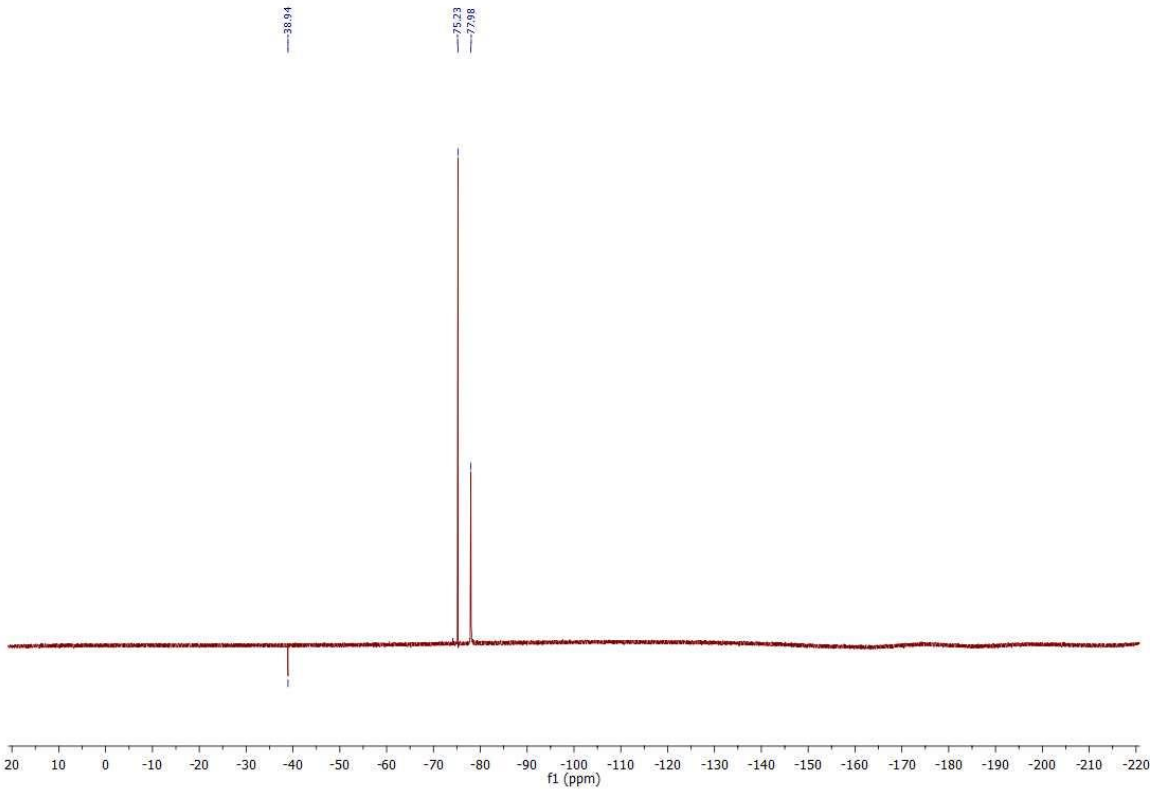

Figure 141 ^{19}F NMR of **25**

V. CONCLUSIONS AND FUTURE WORK

The goal of this project was to develop new electrophilic carbenes with small HOMO-LUMO gaps that may be photoactive. We designed new carbenes by making small modifications to known carbenes. DFT calculations were used to predict changes in the energies of their frontier orbitals. Carbenes with desirable electronic properties were selected for synthesis. This thesis focuses on four of these carbenes: CAmArY, DIC, IC, and aDAC.

CAmArY was found to be the most electrophilic carbene synthesized to date based on DFT analysis and ^{77}Se NMR. The carbene precursor was synthesized in good yields. Unfortunately, CAmArY does not have sufficient steric protection to prevent dimerization upon generation of the carbene. The carbene was successfully trapped with elemental sulfur to form the thioamide. A TEP analysis of CAmArY was attempted, and the CAmArY-Ir[COD]Cl complex was synthesized. When carbonylation of the complex was attempted, the carbene was oxidized to the *N*-Mesitylphthalimide. To our knowledge, this is the only example of this type of reaction and will be explored more in future work. The selenoamide was also synthesized to explore the π-accepting properties of CAmArY via ^{77}Se NMR. The ^{77}Se NMR shift of 1240 ppm is much farther downfield than any reported carbene with the two closest being the CAAmC (1174 ppm) and the five-membered DAC (856 ppm). We are currently exploring methods of increasing the steric protection around the carbene carbon that will allow us to isolate the free carbene.

The second carbene that we selected for synthesis and characterization was the DIC because of its favorable electronic properties. In the series of DICs that we investigated, we found that the frontier orbital energies could be tuned over a wide range

of energies. The DIC precursors were all synthesized in good yields in three steps. The free carbene has been isolated and its electronic properties studied via TEP analysis and ^{77}Se NMR. The TEP analysis suggests that DIC is of similar electron donating ability to MAAC. By substituting the *para*-position of the imino aryl moieties, we can tune the electronic properties of DIC. A Hammett analysis of the LUMO energies as compared to the Hammett parameters gave a linear relationship. We synthesized selected selenium adducts of the DIC derivatives and a plot of their LUMO energies as compared to their ^{77}Se NMR chemical shifts also gave a linear correlation. We are currently synthesizing more derivatives of the DIC to expand our analysis of the tunability of the carbene. We are also exploring the synthesis and characterization of the five-membered DIC and its derivatives.

The indole-derived carbene (IC) and abnormal DAC (aDAC) syntheses are currently being explored. The synthesis of the carbene precursors proved to be very challenging. Both carbenes feature similar HOMO energies, but the aDAC is the more electrophilic of those two. We are currently exploring new methods of synthesizing the carbenes. Future work for the IC will include substituting the benzylic position with other functional groups including, imino and alkene moieties and studying their electronic properties.

CAmArY Dimer

Table 1 Crystal data and structure refinement for CAmArY Dimer.

Identification code	CAmArY Dimer
Empirical formula	$C_{34}H_{30}N_2O_2$
Formula weight	498.60
Temperature/K	293(2)
Crystal system	monoclinic
Space group	$P2_1/n$
a/Å	10.6868(9)
b/Å	16.0711(12)
c/Å	15.0585(13)
α/°	90
β/°	104.704(10)
γ/°	90
Volume/Å^3	2501.6(4)
Z	11
ρ_{calc}g/cm^3	3.641
μ/mm^{-1}	0.226
F(000)	2904.0
Crystal size/mm^3	? × ? × ?
Radiation	MoKα (λ = 0.71073)
2Θ range for data collection/°	3.774 to 67.134
Index ranges	$-15 \leq h \leq 15$, $-24 \leq k \leq 21$, $-22 \leq l \leq 22$
Reflections collected	35758
Independent reflections	9491 [R_{int} = 0.0904, R_{sigma} = 0.1107]
Data/restraints/parameters	9491/0/349
Goodness-of-fit on F^2	1.003
Final R indexes [I>=2σ (I)]	R_1 = 0.0737, wR_2 = 0.1602
Final R indexes [all data]	R_1 = 0.2228, wR_2 = 0.2277
Largest diff. peak/hole / e Å^{-3}	0.26/-0.26

Table 2 Fractional Atomic Coordinates (×10^4) and Equivalent Isotropic Displacement Parameters (Å^2×10^3) for CAmArY-Ir-COD. U_{eq} is defined as 1/3 of of the trace of the orthogonalised U_{IJ} tensor.

Atom	*x*	*y*	*z*	U(eq)
O001	8208.4(15)	3055.8(10)	8099.2(12)	61.0(5)
N002	6497.1(15)	3766(1)	8340.8(11)	38.8(4)
N003	3837.5(16)	5269.2(11)	7564.6(12)	46.9(4)
C004	6143.7(18)	3109.7(12)	8845.1(13)	37.6(4)
C005	5854.7(18)	4509.9(12)	8035.5(13)	37.4(4)
C006	6692.9(18)	4933.6(12)	7574.2(14)	40.2(5)
O007	1723.6(17)	5595.3(15)	7302.4(15)	91.9(7)
C008	4694.7(18)	4725.8(12)	8137.3(13)	37.5(4)
C009	5097.0(19)	2628.9(12)	8477.9(13)	39.9(5)
C00A	7552(2)	3667.7(13)	8000.4(15)	43.6(5)
C00B	6907(2)	2960.5(12)	9701.7(14)	43.2(5)
C00C	2772(2)	4724.0(14)	8522.0(15)	47.3(5)
C00D	3890.4(19)	5702.0(13)	6762.2(14)	42.2(5)
C00E	4007.8(19)	4447.5(12)	8792.7(14)	40.2(5)
C00F	7691.5(19)	4422.2(13)	7543.5(14)	42.8(5)
C00G	4762(2)	2036.7(13)	9015.2(15)	45.9(5)
C00H	3939(2)	6551.3(13)	6796.1(15)	45.4(5)
C00I	6551(2)	2352.6(13)	10201.5(15)	49.4(5)
C00J	3743(2)	5288.1(13)	5957.8(15)	45.7(5)
C00K	3871(2)	6968.3(14)	6007.6(15)	49.3(5)
C00L	4390(2)	4071.7(13)	9626.5(15)	48.8(5)
C00M	8683(2)	4658.7(15)	7196.6(16)	53.5(6)
C00N	3733(2)	6583.0(14)	5195.8(15)	49.1(5)
C00O	5470(2)	1893.0(13)	9883.8(16)	49.2(5)
C00P	3683(2)	5739.0(14)	5183.8(16)	51.7(6)
C00Q	6741(2)	5734.3(14)	7288.2(17)	52.4(6)
C00R	8674(2)	5437.1(16)	6869.2(18)	61.4(7)
C00S	2258(3)	4167.3(15)	9796.0(18)	59.8(6)
C00T	1883(2)	4584.8(15)	9001.4(17)	57.8(6)
C00U	2652(2)	5236.5(16)	7737.8(17)	57.2(6)
C00V	3500(3)	3934.9(15)	10107.2(16)	57.3(6)
C00W	3629(3)	4379.4(14)	5898.6(18)	63.8(7)
C00X	4333(2)	2730.4(15)	7531.5(16)	58.1(6)
C00Y	4104(3)	7017.8(15)	7655.9(16)	61.9(7)
C00Z	7717(2)	5967.6(15)	6925.4(19)	62.5(7)
C010	8086(2)	3446.2(16)	10090.0(18)	66.4(7)
C011	3611(3)	7056.6(17)	4344.6(18)	72.6(8)
C012	5066(3)	1249.0(17)	10451(2)	77.3(8)

Table 3 Anisotropic Displacement Parameters ($Å^2 \times 10^3$) for CAmArY-Ir-COD. The Anisotropic displacement factor exponent takes the form: $-2\pi^2[h^2Å^2U_{11}+2hkÅb^*U_{12}+\ldots]$.

Atom	U_{11}	U_{22}	U_{33}	U_{23}	U_{13}	U_{12}
O001	57.1(10)	46.1(9)	85.8(12)	11.5(8)	29.0(9)	17.8(8)
N002	37.1(9)	33.8(9)	45.3(10)	6.0(7)	9.9(7)	2.6(7)
N003	40.4(10)	47.1(10)	54.6(11)	16.5(8)	14.7(8)	10.2(8)
C004	39.2(10)	31.9(10)	41.2(11)	0.9(8)	9.4(9)	3.3(8)
C005	36.6(10)	33.2(10)	40.0(11)	1.6(8)	5.2(8)	1.3(8)
C006	35.5(10)	38.7(11)	44.1(11)	2.0(9)	6.0(9)	-1.1(8)
O007	47.7(10)	125.7(18)	107.2(16)	65.6(14)	28.9(10)	34.1(11)
C008	35.8(10)	32.5(10)	42.6(11)	2.8(8)	6.8(9)	2.1(8)
C009	42.4(11)	36.2(10)	40.6(11)	-3.9(9)	9.6(9)	0.7(9)
C00A	39.0(11)	39.3(11)	53.1(13)	1.2(10)	12.7(10)	5.6(9)
C00B	48.4(12)	34.0(11)	43.4(12)	0.1(9)	4.8(10)	4.0(9)
C00C	41.6(12)	47.5(12)	53.9(13)	8.7(10)	13.9(10)	2.5(10)
C00D	37.2(10)	45.4(12)	44.3(12)	8.6(9)	10.9(9)	4.7(9)
C00E	44.4(11)	34.2(10)	41.6(11)	-0.1(9)	10.1(9)	0.2(8)
C00F	39.3(11)	40.5(11)	47.7(12)	2.4(9)	9.4(9)	1.3(9)
C00G	48.0(12)	37.2(11)	54.0(13)	-3.9(10)	15.6(11)	-2.9(9)
C00H	44.1(11)	43.5(12)	47.0(12)	6(1)	8.7(10)	8.0(9)
C00I	60.7(14)	41.1(12)	43.1(12)	6.2(10)	7.1(11)	8.1(10)
C00J	41.8(11)	40.1(11)	53.5(13)	3.8(10)	8.9(10)	-2.3(9)
C00K	53.6(13)	39.8(12)	53.5(14)	6.5(10)	11.5(11)	4.5(10)
C00L	56.9(13)	46.3(12)	43.1(12)	0.7(10)	12.6(10)	10.1(10)
C00M	46.2(13)	53.8(14)	63.7(15)	6.9(11)	20.0(11)	3.3(10)
C00N	55.7(13)	44.9(12)	46.4(13)	7.4(10)	12.2(11)	1.8(10)
C00O	60.6(14)	37.6(11)	53.3(14)	4.1(10)	21.5(12)	3.9(10)
C00P	56.3(14)	49.2(13)	48.4(13)	0.2(10)	11.1(11)	-1.5(11)
C00Q	39.6(11)	42.8(12)	73.3(16)	11.0(11)	11.8(11)	-1.0(9)
C00R	45.9(13)	66.1(17)	75.3(17)	16.0(13)	20.9(12)	-5.1(12)
C00S	66.5(16)	53.6(14)	67.7(16)	8.5(12)	32.5(14)	1.6(12)
C00T	48.1(13)	60.0(15)	70.1(16)	9.0(13)	23.9(12)	2.9(11)
C00U	39.5(12)	64.8(15)	69.1(16)	24.3(13)	17.2(11)	13.0(11)
C00V	76.8(17)	52.7(14)	47.0(13)	4.2(11)	24.3(13)	8.0(12)
C00W	73.3(17)	44.9(14)	70.3(17)	0.8(12)	13.0(14)	-6.1(12)
C00X	62.4(15)	58.0(14)	47.9(13)	-4.7(11)	2.8(11)	-12.3(12)
C00Y	76.4(17)	57.2(15)	50.4(14)	-0.6(11)	13.3(13)	16.1(13)
C00Z	46.1(13)	52.5(14)	86.4(19)	23.1(13)	12.2(13)	-4.5(11)
C010	63.7(16)	55.0(15)	64.6(16)	4.8(12)	-12.9(13)	-6.3(12)

C011	104(2)	61.0(17)	57.8(16)	13.1(13)	28.9(15)	5.2(15)
C012	99(2)	63.1(17)	77.3(19)	16.3(14)	35.6(17)	-7.1(15)

Table 4 Bond Lengths for CAmArY Dimer.

Atom	Atom	Length/Å	Atom	Atom	Length/Å
O001	C00A	1.195(2)	C00C	C00U	1.418(3)
N002	C004	1.406(2)	C00D	C00H	1.366(3)
N002	C005	1.397(2)	C00D	C00J	1.356(3)
N002	C00A	1.361(3)	C00E	C00L	1.359(3)
N003	C008	1.395(2)	C00F	C00M	1.349(3)
N003	C00D	1.408(3)	C00G	C00O	1.354(3)
N003	C00U	1.358(3)	C00H	C00K	1.349(3)
C004	C009	1.356(3)	C00H	C00Y	1.467(3)
C004	C00B	1.361(3)	C00I	C00O	1.352(3)
C005	C006	1.437(3)	C00J	C00P	1.360(3)
C005	C008	1.333(3)	C00J	C00W	1.466(3)
C006	C00F	1.357(3)	C00K	C00N	1.345(3)
C006	C00Q	1.362(3)	C00L	C00V	1.351(3)
O007	C00U	1.190(3)	C00M	C00R	1.344(3)
C008	C00E	1.442(3)	C00N	C00P	1.357(3)
C009	C00G	1.355(3)	C00N	C011	1.468(3)
C009	C00X	1.461(3)	C00O	C012	1.474(3)
C00A	C00F	1.421(3)	C00Q	C00Z	1.348(3)
C00B	C00I	1.346(3)	C00R	C00Z	1.351(3)
C00B	C010	1.471(3)	C00S	C00T	1.341(3)
C00C	C00E	1.354(3)	C00S	C00V	1.344(3)
C00C	C00T	1.350(3)			

Table 5 Bond Angles for CAmArY-Ir-COD.

Atom	Atom	Atom	Angle/°	Atom	Atom	Atom	Angle/°
C005	N002	C004	129.99(16)	C00C	C00E	C008	108.60(18)
C00A	N002	C004	118.56(16)	C00C	C00E	C00L	117.7(2)
C00A	N002	C005	111.12(16)	C00L	C00E	C008	133.17(19)
C008	N003	C00D	132.62(17)	C006	C00F	C00A	108.69(18)
C00U	N003	C008	110.81(17)	C00M	C00F	C006	123.0(2)
C00U	N003	C00D	115.26(17)	C00M	C00F	C00A	128.1(2)
C009	C004	N002	120.92(18)	C00O	C00G	C009	121.9(2)
C009	C004	C00B	121.32(19)	C00D	C00H	C00Y	122.6(2)

C00B	C004	N002	117.74(18)	C00K	C00H	C00D	118.1(2)
N002	C005	C006	104.48(16)	C00K	C00H	C00Y	119.4(2)
C008	C005	N002	125.35(18)	C00B	C00I	C00O	122.4(2)
C008	C005	C006	130.11(18)	C00D	C00J	C00P	118.3(2)
C00F	C006	C005	108.76(18)	C00D	C00J	C00W	122.1(2)
C00F	C006	C00Q	117.94(19)	C00P	C00J	C00W	119.6(2)
C00Q	C006	C005	132.7(2)	C00N	C00K	C00H	122.7(2)
N003	C008	C00E	104.41(16)	C00V	C00L	C00E	118.7(2)
C005	C008	N003	125.17(19)	C00R	C00M	C00F	118.1(2)
C005	C008	C00E	130.36(18)	C00K	C00N	C00P	117.8(2)
C004	C009	C00X	122.22(19)	C00K	C00N	C011	121.3(2)
C00G	C009	C004	118.18(19)	C00P	C00N	C011	120.8(2)
C00G	C009	C00X	119.61(19)	C00G	C00O	C012	120.3(2)
O001	C00A	N002	124.4(2)	C00I	C00O	C00G	117.8(2)
O001	C00A	C00F	129.2(2)	C00I	C00O	C012	121.9(2)
N002	C00A	C00F	106.37(17)	C00N	C00P	C00J	121.9(2)
C004	C00B	C010	122.0(2)	C00Z	C00Q	C006	119.1(2)
C00I	C00B	C004	118.1(2)	C00M	C00R	C00Z	119.9(2)
C00I	C00B	C010	119.9(2)	C00T	C00S	C00V	119.7(2)
C00E	C00C	C00U	108.45(19)	C00S	C00T	C00C	117.9(2)
C00T	C00C	C00E	123.3(2)	N003	C00U	C00C	106.90(18)
C00T	C00C	C00U	127.9(2)	O007	C00U	N003	124.3(2)
C00H	C00D	N003	118.1(2)	O007	C00U	C00C	128.8(2)
C00J	C00D	N003	120.24(19)	C00S	C00V	C00L	122.3(2)
C00J	C00D	C00H	121.21(19)	C00Q	C00Z	C00R	121.8(2)

Table 6 Hydrogen Atom Coordinates (Å×10^4) and Isotropic Displacement Parameters (Å^2×10^3) for CAmArY-Ir-COD.

Atom	*x*	*y*	*z*	U(eq)
H00G	4024.07	1719.62	8780.79	55
H00I	7066.9	2244.78	10787.1	59
H00K	3921.37	7546	6026.36	59
H00L	5246.24	3911.98	9861.47	59
H00M	9353.06	4293.31	7184.35	64
H00P	3604.44	5461.17	4630.62	62
H00Q	6108.38	6114.76	7342.45	63
H00R	9327.13	5610.52	6604.12	74
H00S	1660.97	4039.31	10129.97	72
H00T	1036.34	4772.57	8787.39	69
H00V	3756.76	3670.35	10673.67	69

H00A	4439.02	4131.37	6210.3	96
H00B	3409	4213.03	5265.62	96
H00C	2965.75	4198.78	6181.26	96
H00D	3654.04	3126.29	7513.13	87
H00E	3962.06	2204.98	7299.76	87
H00F	4880.14	2926.66	7159.51	87
H00H	3703.76	6718.37	8062.22	93
H00J	3705.88	7554.86	7527.05	93
H00N	5009.38	7085.27	7940.73	93
H00Z	7731.52	6508.24	6707.92	75
H01A	8795.56	3212.78	9890.78	100
H01B	8277.9	3430.24	10748.14	100
H01C	7953.21	4012.39	9884.6	100
H01D	2774.11	7315.07	4170.4	109
H01E	3708.26	6687.43	3865.48	109
H01F	4269.67	7476.95	4441.24	109
H01G	4259.32	1407.53	10572.13	116
H01H	5713.45	1192.54	11020.6	116
H01I	4962.39	727.82	10129	116

Experimental

Single crystals of $C_{34}H_{30}N_2O_2$ **[CAmArY Dimer]** were **[yellow]**. A suitable crystal was selected and **[]** on a **dtrek-CrysAlisPro-abstract goniometer imported rigaku-d*trek images** diffractometer. The crystal was kept at 293(2) K during data collection. Using Olex2 [1], the structure was solved with the ShelXT [2] structure solution program using Intrinsic Phasing and refined with the ShelXL [3] refinement package using Least Squares minimisation.

1. Dolomanov, O.V., Bourhis, L.J., Gildea, R.J, Howard, J.A.K. & Puschmann, H. (2009), J. Appl. Cryst. 42, 339-341.
2. Sheldrick, G.M. (2015). Acta Cryst. A71, 3-8.
3. Sheldrick, G.M. (2015). Acta Cryst. C71, 3-8.

Crystal structure determination of [CAmArY Dimer]

Crystal Data for $C_{34}H_{30}N_2O_2$ (M =498.60 g/mol): monoclinic, space group $P2_1/n$ (no. 14), a = 10.6868(9) Å, b = 16.0711(12) Å, c = 15.0585(13) Å, β = 104.704(10)°, V = 2501.6(4) Å^3, Z = 11, T = 293(2) K, μ(MoKα) = 0.226 mm^{-1},*Dcalc* = 3.641 g/cm^3, 35758 reflections measured (3.774° ≤ 2Θ ≤ 67.134°), 9491 unique (R_{int} = 0.0904, R_{sigma} = 0.1107) which were used in all calculations. The final R_1 was 0.0737 (I > 2σ(I)) and wR_2 was 0.2277 (all data).

Refinement model description

Number of restraints - 0, number of constraints - unknown.

Details:
1. Fixed Uiso
 At 1.2 times of:
  All C(H) groups
 At 1.5 times of:
  All C(H,H,H) groups
2.a Aromatic/amide H refined with riding coordinates:
 C00G(H00G), C00I(H00I), C00K(H00K), C00L(H00L), C00M(H00M), C00P(H00P), C00Q(H00Q), C00R(H00R), C00S(H00S), C00T(H00T), C00V(H00V), C00Z(H00Z)

2.b Idealised Me refined as rotating group:
C00W(H00A,H00B,H00C), C00X(H00D,H00E,H00F), C00Y(H00H,H00J,H00N), C010(H01A, H01B,H01C), C011(H01D,H01E,H01F), C012(H01G,H01H,H01I)

This report has been created with Olex2, compiled on 2017.02.24 svn.r3390 for Rigaku Oxford Diffraction. Please let us know if there are any errors or if you would like to have additional features.

CAmArY Sulfur 829

Table 1 Crystal data and structure refinement for CAmArY Sulfur 829.

Identification code	CAmArY Sulfur 829
Empirical formula	$C_{17}H_{15}NOS$
Formula weight	281.36
Temperature/K	293(2)
Crystal system	orthorhombic
Space group	$P2_12_12_1$
a/Å	8.0730(8)
b/Å	11.6945(12)
c/Å	14.8493(13)
α/°	90
β/°	90
γ/°	90
Volume/Å^3	1401.9(2)
Z	4
ρ_{calc}g/cm^3	1.333
μ/mm^{-1}	0.225
F(000)	592.0
Crystal size/mm^3	? × ? × ?
Radiation	MoKα (λ = 0.71073)
2Θ range for data collection/°	4.434 to 66.926
Index ranges	$-12 \leq h \leq 12$, $-17 \leq k \leq 17$, $-20 \leq l \leq 22$
Reflections collected	19970
Independent reflections	5316 [R_{int} = 0.0645, R_{sigma} = 0.0778]
Data/restraints/parameters	5316/0/184
Goodness-of-fit on F^2	0.969
Final R indexes [I>=2σ (I)]	R_1 = 0.0610, wR_2 = 0.1543
Final R indexes [all data]	R_1 = 0.1851, wR_2 = 0.2153
Largest diff. peak/hole / e Å^{-3}	0.16/-0.33
Flack parameter	0.05(5)

Table 2 Fractional Atomic Coordinates (×10^4) and Equivalent Isotropic Displacement Parameters (Å^2×10^3) for CAmArY Sulfur 829. U_{eq} is defined as 1/3 of of the trace of the orthogonalised U_{IJ} tensor.

Atom	*x*	*y*	*z*	U(eq)
S001	4237.8(18)	5128.3(16)	5687.3(9)	112.9(6)
N002	5959(3)	5447(3)	4258.7(18)	60.6(7)
O003	7965(3)	5549(3)	3182.9(18)	88.8(10)
C004	4699(4)	6026(3)	3790(2)	56.5(8)
C005	8373(5)	4640(3)	4619(3)	65.0(9)
C006	2381(5)	5977(4)	2873(3)	68.2(10)
C007	4578(5)	7181(3)	3878(3)	65.2(10)
C008	7519(5)	5245(4)	3924(3)	66.3(9)
C009	3627(5)	5413(3)	3280(2)	60.4(9)
C00A	7358(5)	4519(3)	5319(3)	65.4(9)
C00B	3296(5)	7701(3)	3441(3)	69.4(10)
C00C	2200(5)	7120(4)	2950(3)	68.7(10)
C00D	7864(6)	4030(4)	6102(3)	83.6(13)
C00E	3811(6)	4168(4)	3175(3)	82.5(13)
C00F	5776(5)	5047(3)	5105(2)	66.1(9)
C00G	9445(7)	3632(4)	6122(4)	92.9(15)
C00H	5744(7)	7830(4)	4424(4)	102.3(16)
C00I	9950(5)	4239(5)	4644(4)	89.0(14)
C00J	800(6)	7708(5)	2506(4)	106.4(17)
C00K	10458(7)	3735(4)	5415(4)	97.1(15)

Table 3 Anisotropic Displacement Parameters (Å^2×10^3) for CAmArY Sulfur 829. The Anisotropic displacement factor exponent takes the form: -2π^2[h^{2}Å^{2}U$_{11}$+2hkÅb*U$_{12}$+…].

Atom	U_{11}	U_{22}	U_{33}	U_{23}	U_{13}	U_{12}
S001	96.1(9)	156.3(14)	86.2(9)	23.9(9)	26.7(7)	13(1)
N002	59.8(16)	71.4(18)	50.7(15)	2.1(14)	1.8(13)	3.9(14)
O003	64.1(16)	143(3)	59.1(16)	21.5(18)	14.9(12)	14.8(18)
C004	54.3(18)	63(2)	51.9(18)	1.2(16)	3.1(15)	3.6(15)
C005	64(2)	64(2)	67(2)	-4.6(19)	-7.8(18)	2.0(17)
C006	69(2)	77(2)	58(2)	-1.1(19)	-7.0(18)	-2(2)
C007	65(2)	65(2)	65(2)	-1.3(18)	5.4(19)	-3.2(17)
C008	59.2(19)	79(2)	61(2)	1.0(19)	1.8(17)	2.8(19)
C009	63(2)	60.6(19)	57.2(19)	-5.7(17)	2.5(17)	0.5(17)
C00A	76(2)	57.6(19)	63(2)	-2.3(17)	-11.0(19)	-1.4(18)
C00B	73(2)	59(2)	77(2)	5.6(19)	0(2)	3.0(19)

C00C	64(2)	76(2)	67(2)	14.7(19)	1.5(19)	6.8(19)
C00D	103(3)	76(3)	72(3)	12(2)	-21(2)	-6(2)
C00E	84(3)	68(2)	95(3)	-20(2)	-4(2)	5(2)
C00F	76(2)	68(2)	55.0(19)	1.3(17)	0.0(18)	-0.1(19)
C00G	109(4)	68(3)	102(4)	7(2)	-48(3)	-4(3)
C00H	106(3)	80(3)	121(4)	-18(3)	-36(3)	-10(3)
C00I	66(2)	100(3)	100(3)	-3(3)	-14(2)	10(2)
C00J	92(3)	114(4)	113(4)	26(3)	-23(4)	20(3)
C00K	83(3)	88(3)	120(4)	-2(3)	-28(3)	9(3)

Table 4 Bond Lengths for CAmArY Sulfur 829.

Atom	Atom	Length/Å	Atom	Atom	Length/Å
S001	C00F	1.517(4)	C006	C00C	1.349(6)
N002	C004	1.406(4)	C007	C00B	1.364(5)
N002	C008	1.374(4)	C007	C00H	1.456(6)
N002	C00F	1.348(5)	C009	C00E	1.472(6)
O003	C008	1.212(4)	C00A	C00D	1.359(6)
C004	C007	1.361(5)	C00A	C00F	1.454(5)
C004	C009	1.355(5)	C00B	C00C	1.333(6)
C005	C008	1.428(5)	C00C	C00J	1.478(6)
C005	C00A	1.332(6)	C00D	C00G	1.359(7)
C005	C00I	1.357(6)	C00G	C00K	1.336(8)
C006	C009	1.347(5)	C00I	C00K	1.352(7)

Table 5 Bond Angles for CAmArY Sulfur 829.

Atom	Atom	Atom	Angle/°	Atom	Atom	Atom	Angle/°
C008	N002	C004	124.5(3)	C006	C009	C004	117.9(3)
C00F	N002	C004	123.3(3)	C006	C009	C00E	120.9(4)
C00F	N002	C008	112.2(3)	C005	C00A	C00D	121.9(4)
C007	C004	N002	118.8(3)	C005	C00A	C00F	108.9(3)
C009	C004	N002	119.0(3)	C00D	C00A	C00F	129.0(4)
C009	C004	C007	122.2(3)	C00C	C00B	C007	122.5(4)
C00A	C005	C008	108.6(3)	C006	C00C	C00J	120.4(4)
C00A	C005	C00I	121.3(4)	C00B	C00C	C006	118.6(4)
C00I	C005	C008	130.1(4)	C00B	C00C	C00J	121.0(4)
C009	C006	C00C	121.9(4)	C00A	C00D	C00G	116.4(5)
C004	C007	C00B	116.8(4)	N002	C00F	S001	126.8(3)
C004	C007	C00H	121.7(4)	N002	C00F	C00A	104.8(3)

C00B	C007	C00H	121.5(4)	C00A	C00F	S001	128.4(3)
N002	C008	C005	105.5(3)	C00K	C00G	C00D	121.8(5)
O003	C008	N002	123.4(4)	C00K	C00I	C005	117.3(5)
O003	C008	C005	131.1(4)	C00G	C00K	C00I	121.3(5)
C004	C009	C00E	121.2(4)				

Table 6 Hydrogen Atom Coordinates (Å×10^4) and Isotropic Displacement Parameters (Å^2×10^3) for CAmArY Sulfur 829.

Atom	*x*	*y*	*z*	U(eq)
H006	1623.14	5567.53	2528.65	82
H00B	3182.78	8489.87	3487.87	83
H00D	7165.19	3970.84	6597.88	100
H00A	4859.11	4002.22	2899.64	124
H00C	2933.66	3879.87	2802.26	124
H00E	3759.14	3808.67	3756.2	124
H00G	9833.1	3279.38	6641.98	111
H00F	5609.38	7627.1	5045.91	153
H00H	5537.15	8633.11	4349.28	153
H00I	6854.65	7658.84	4236.23	153
H00J	10653	4307.7	4150.59	107
H00K	852.18	7578.24	1868.33	160
H00L	863.89	8513.25	2624.82	160
H00M	-225.41	7412.66	2736.85	160
H00N	11532.99	3453.54	5454.47	117

Experimental

Single crystals of $C_{17}H_{15}NOS$ **[CAmArY Sulfur 829]** were **[]**. A suitable crystal was selected and **[]** on a **dtrek-CrysAlisPro-abstract goniometer imported rigaku-d*trek images** diffractometer. The crystal was kept at 293(2) K during data collection. Using Olex2 [1], the structure was solved with the ShelXT [2] structure solution program using Intrinsic Phasing and refined with the ShelXL [3] refinement package using Least Squares minimisation.

1. Dolomanov, O.V., Bourhis, L.J., Gildea, R.J, Howard, J.A.K. & Puschmann, H. (2009), J. Appl. Cryst. 42, 339-341.
2. Sheldrick, G.M. (2015). Acta Cryst. A71, 3-8.
3. Sheldrick, G.M. (2015). Acta Cryst. C71, 3-8.

Crystal structure determination of [CAmArY Sulfur 829]

Crystal Data for $C_{17}H_{15}NOS$ (M =281.36 g/mol): orthorhombic, space group $P2_12_12_1$ (no. 19), a = 8.0730(8) Å, b = 11.6945(12) Å, c = 14.8493(13) Å, V = 1401.9(2) Å^3, Z = 4, T = 293(2) K, μ(MoKα) = 0.225 mm^{-1}, *Dcalc* = 1.333 g/cm^3, 19970 reflections measured (4.434° ≤ 2Θ ≤ 66.926°), 5316 unique (R_{int} = 0.0645, R_{sigma} = 0.0778) which were used in all calculations. The final R_1 was 0.0610 (I > 2σ(I)) and wR_2 was 0.2153 (all data).

Refinement model description

Number of restraints - 0, number of constraints - unknown.

Details:

1. Fixed Uiso
 At 1.2 times of:
  All C(H) groups
 At 1.5 times of:
  All C(H,H,H) groups

2.a Aromatic/amide H refined with riding coordinates:
 C006(H006), C00B(H00B), C00D(H00D), C00G(H00G), C00I(H00J), C00K(H00N)

2.b Idealised Me refined as rotating group:
 C00E(H00A,H00C,H00E), C00H(H00F,H00H,H00I), C00J(H00K,H00L,H00M)

This report has been created with Olex2, compiled on 2017.02.24 svn.r3390 for Rigaku Oxford Diffraction. Please let us know if there are any errors or if you would like to have additional features.

CamarySe

Table 1 Crystal data and structure refinement for CamarySe.

Identification code	CamarySe
Empirical formula	$C_{17}H_{15}NOSe$
Formula weight	328.26
Temperature/K	293(2)
Crystal system	monoclinic
Space group	$P2_1/n$
a/Å	10.019(2)
b/Å	8.6626(17)
c/Å	17.467(5)
α/°	90
β/°	101.67(3)
γ/°	90
Volume/Å^3	1484.7(6)
Z	4
ρ_{calc}g/cm^3	1.469
μ/mm^{-1}	2.524
F(000)	664.0
Crystal size/mm^3	? × ? × ?
Radiation	MoKα (λ = 0.71073)
2Θ range for data collection/°	4.348 to 66.498
Index ranges	$-15 \leq h \leq 13$, $-13 \leq k \leq 12$, $-26 \leq l \leq 25$
Reflections collected	18987
Independent reflections	5521 [R_{int} = 0.1245, R_{sigma} = 0.1293]
Data/restraints/parameters	5521/0/184
Goodness-of-fit on F^2	0.929
Final R indexes [I>=2σ (I)]	R_1 = 0.0703, wR_2 = 0.1778
Final R indexes [all data]	R_1 = 0.2007, wR_2 = 0.2539
Largest diff. peak/hole / e Å^{-3}	0.60/-0.77

Table 2 Fractional Atomic Coordinates (×10^4) and Equivalent Isotropic Displacement Parameters (Å^2×10^3) for CamarySe. U_{eq} is defined as 1/3 of of the trace of the orthogonalised U_{IJ} tensor.

Atom	*x*	*y*	*z*	U(eq)
Se01	5740.2(6)	2137.2(7)	6960.4(3)	73.8(3)
O002	1827(3)	5683(4)	5782.3(18)	61.5(9)
N003	3672(4)	4230(4)	6438.8(18)	44.9(8)
C004	3377(5)	2081(5)	5714(3)	47.7(10)
C005	4240(4)	5409(5)	6981(2)	43.7(9)
C006	3941(5)	5394(6)	7716(2)	49.7(10)
C007	4246(5)	2826(5)	6376(3)	47.9(10)
C008	2481(5)	4472(6)	5859(2)	53.1(11)
C009	2341(5)	3058(5)	5411(2)	49.7(11)
C00A	5081(5)	6466(6)	6742(3)	51.3(10)
C00B	5393(5)	7616(6)	8016(3)	55.6(12)
C00C	4553(5)	6541(6)	8224(3)	56.4(12)
C00D	3030(6)	4214(7)	7953(3)	67.5(14)
C00E	5650(5)	7597(6)	7269(3)	59.5(13)
C00F	1339(6)	2655(7)	4768(3)	63.7(14)
C00G	3484(6)	644(6)	5398(3)	63.3(13)
C00H	5390(6)	6441(7)	5938(3)	71.9(15)
C00I	2494(7)	233(7)	4751(3)	81.4(18)
C00J	1474(7)	1230(8)	4443(3)	80.2(18)
C00K	6010(6)	8854(8)	8575(3)	79.9(17)

Table 3 Anisotropic Displacement Parameters (Å^2×10^3) for CamarySe. The Anisotropic displacement factor exponent takes the form: -2π^2[h^{2}Å^2U_{11}+2hkÅb*U_{12}+…].

Atom	U_{11}	U_{22}	U_{33}	U_{23}	U_{13}	U_{12}
Se01	63.1(4)	65.9(5)	86.1(5)	-0.2(3)	-0.2(3)	15.9(3)
O002	47.1(18)	68(2)	62.1(19)	-10.6(16)	-7.5(14)	21.0(17)
N003	48(2)	45(2)	42.4(18)	-0.6(15)	10.0(15)	1.4(16)
C004	51(3)	48(3)	47(2)	-4.5(18)	14.3(19)	-8(2)
C005	41(2)	43(2)	47(2)	-4.8(18)	6.7(17)	3.1(19)
C006	49(2)	55(3)	45(2)	-3(2)	8.1(19)	5(2)
C007	47(2)	49(3)	52(3)	0.0(19)	19(2)	-2(2)
C008	50(3)	62(3)	46(2)	1(2)	7.5(19)	1(2)
C009	51(3)	55(3)	45(2)	0(2)	15(2)	-6(2)
C00A	48(3)	48(3)	57(3)	5(2)	10(2)	2(2)
C00B	46(3)	55(3)	62(3)	-11(2)	0(2)	7(2)

C00C	54(3)	63(3)	54(3)	-9(2)	16(2)	6(3)
C00D	73(4)	75(4)	60(3)	-2(3)	27(3)	-15(3)
C00E	54(3)	49(3)	76(3)	-3(2)	14(2)	-7(2)
C00F	65(3)	72(4)	50(3)	-1(2)	2(2)	-17(3)
C00G	76(4)	55(3)	61(3)	-3(2)	20(3)	-4(3)
C00H	86(4)	68(4)	69(3)	5(3)	32(3)	-11(3)
C00I	116(5)	60(4)	73(4)	-23(3)	30(4)	-27(4)
C00J	94(5)	75(4)	67(4)	-14(3)	5(3)	-28(4)
C00K	74(4)	76(4)	84(4)	-32(3)	4(3)	-10(3)

Table 4 Bond Lengths for CamarySe.

Atom	Atom	Length/Å	Atom	Atom	Length/Å
Se01	C007	1.738(5)	C006	C00D	1.485(7)
O002	C008	1.229(6)	C008	C009	1.446(6)
N003	C005	1.431(5)	C009	C00F	1.391(7)
N003	C007	1.359(6)	C00A	C00E	1.386(7)
N003	C008	1.416(6)	C00A	C00H	1.498(6)
C004	C007	1.451(6)	C00B	C00C	1.354(7)
C004	C009	1.361(7)	C00B	C00E	1.381(8)
C004	C00G	1.375(6)	C00B	C00K	1.496(7)
C005	C006	1.375(6)	C00F	C00J	1.377(8)
C005	C00A	1.366(6)	C00G	C00I	1.391(8)
C006	C00C	1.389(7)	C00I	C00J	1.363(9)

Table 5 Bond Angles for CamarySe.

Atom	Atom	Atom	Angle/°	Atom	Atom	Atom	Angle/°
C007	N003	C005	125.1(4)	N003	C008	C009	103.7(4)
C007	N003	C008	112.6(4)	C004	C009	C008	109.5(4)
C008	N003	C005	122.1(4)	C004	C009	C00F	121.8(5)
C009	C004	C007	108.7(4)	C00F	C009	C008	128.7(5)
C009	C004	C00G	121.5(5)	C005	C00A	C00E	117.8(4)
C00G	C004	C007	129.8(5)	C005	C00A	C00H	122.3(4)
C006	C005	N003	118.6(4)	C00E	C00A	C00H	119.8(5)
C00A	C005	N003	117.6(4)	C00C	C00B	C00E	119.3(4)
C00A	C005	C006	123.8(4)	C00C	C00B	C00K	121.0(5)
C005	C006	C00C	116.0(4)	C00E	C00B	C00K	119.6(5)
C005	C006	C00D	121.9(4)	C00B	C00C	C006	122.6(4)
C00C	C006	C00D	122.1(4)	C00B	C00E	C00A	120.4(5)

N003 C007 Se01	126.0(4)	C00J C00F C009	116.3(6)
N003 C007 C004	105.5(4)	C004 C00G C00I	117.2(6)
C004 C007 Se01	128.5(4)	C00J C00I C00G	120.9(5)
O002 C008 N003	123.9(4)	C00I C00J C00F	122.3(5)
O002 C008 C009	132.3(4)		

Table 6 Hydrogen Atom Coordinates (Å×10^4) and Isotropic Displacement Parameters (Å^2×10^3) for CamarySe.

Atom	*x*	*y*	*z*	U(eq)
H00C	4379.24	6570.17	8726.98	68
H00A	2115.33	4370.97	7667.77	101
H00B	3050.47	4303.73	8503.22	101
H00D	3334.16	3202.71	7841.92	101
H00E	6207.97	8348	7117.87	71
H00F	618.21	3312.01	4568.71	76
H00G	4188.96	-25.7	5608.51	76
H00H	5768.84	5456.53	5846.05	108
H00I	6033.18	7240.93	5894.42	108
H00J	4565.49	6608.88	5558.18	108
H00K	2527.67	-735.71	4526.27	98
H00L	847.48	937.89	3998.18	96
H00M	5493.61	9788.25	8459.49	120
H00N	6933.67	9032.5	8523.3	120
H00O	5999.17	8534.26	9099.6	120

Experimental

Single crystals of $C_{17}H_{15}NOSe$ **[CamarySe]** were **[]**. A suitable crystal was selected and **[]** on a **dtrek-CrysAlisPro-abstract goniometer imported rigaku-d*trek images** diffractometer. The crystal was kept at 293(2) K during data collection. Using Olex2 [1], the structure was solved with the olex2.solve [2] structure solution program using Charge Flipping and refined with the ShelXL [3] refinement package using Least Squares minimisation.

1. Dolomanov, O.V., Bourhis, L.J., Gildea, R.J, Howard, J.A.K. & Puschmann, H. (2009), J. Appl. Cryst. 42, 339-341.
2. Bourhis, L.J., Dolomanov, O.V., Gildea, R.J., Howard, J.A.K., Puschmann, H. (2015). Acta Cryst. A71, 59-75.
3. Sheldrick, G.M. (2015). Acta Cryst. C71, 3-8.

Crystal structure determination of [CamarySe]

Crystal Data for $C_{17}H_{15}NOSe$ (M =328.26 g/mol): monoclinic, space group $P2_1/n$ (no. 14), a = 10.019(2) Å, b = 8.6626(17) Å, c = 17.467(5) Å, β = 101.67(3)°, V = 1484.7(6) Å^3, Z = 4, T = 293(2) K, μ(MoKα) = 2.524 mm^{-1}, *Dcalc* = 1.469 g/cm^3, 18987 reflections measured (4.348° ≤ 2Θ ≤ 66.498°), 5521 unique (R_{int} = 0.1245, R_{sigma} = 0.1293) which were used in all calculations. The final R_1 was 0.0703 (I > 2σ(I)) and wR_2 was 0.2539 (all data).

Refinement model description

Number of restraints - 0, number of constraints - unknown.

Details:

1. Fixed Uiso
 At 1.2 times of:
  All C(H) groups
 At 1.5 times of:
  All C(H,H,H) groups

2.a Aromatic/amide H refined with riding coordinates:
 C00C(H00C), C00E(H00E), C00F(H00F), C00G(H00G), C00I(H00K), C00J(H00L)

2.b Idealised Me refined as rotating group:
 C00D(H00A,H00B,H00D), C00H(H00H,H00I,H00J), C00K(H00M,H00N,H00O)

This report has been created with Olex2, compiled on 2017.02.24 svn.r3390 for Rigaku Oxford Diffraction. Please let us know if there are any errors or if you would like to have additional features.

2,4,6-trimethylphenylphthalimide

Table 1 Crystal data and structure refinement for 2,4,6-trimethylphenylphthalimide.

Identification code	2,4,6-trimethylphenylphthalimide
Empirical formula	$C_{22.67}N_{1.33}O_{2.67}H_{0.33}$
Formula weight	333.91
Temperature/K	293(2)
Crystal system	orthorhombic
Space group	$P2_12_12_1$
a/Å	8.176(5)
b/Å	12.123(6)
c/Å	14.592(9)
α/°	90
β/°	90
γ/°	90
Volume/Å^3	1446.3(14)
Z	3
ρ_{calc}g/cm^3	1.150
μ/mm^{-1}	0.078
F(000)	501.0
Crystal size/mm^3	? × ? × ?
Radiation	MoKα (λ = 0.71073)
2Θ range for data collection/°	4.368 to 66.516
Index ranges	$-12 \leq h \leq 12$, $-18 \leq k \leq 18$, $-22 \leq l \leq 22$
Reflections collected	20127
Independent reflections	5445 [R_{int} = 0.4129, R_{sigma} = 0.6714]
Data/restraints/parameters	5445/0/184
Goodness-of-fit on F^2	0.872
Final R indexes [I>=2σ (I)]	R_1 = 0.0989, wR_2 = 0.1878
Final R indexes [all data]	R_1 = 0.4664, wR_2 = 0.3438
Largest diff. peak/hole / e Å^{-3}	0.14/-0.14
Flack parameter	0.5(10)

Table 2 Fractional Atomic Coordinates (×10^4) and Equivalent Isotropic Displacement Parameters (Å^2×10^3) for 2,4,6-trimethylphenylphthalimide. U_{eq} is defined as 1/3 of of the trace of the orthogonalised U_{IJ} tensor.

Atom	*x*	*y*	*z*	U(eq)
O001	8077(8)	5779(6)	6685(5)	84(2)
N002	5856(9)	5468(6)	5720(5)	63(2)
O003	4267(9)	4876(6)	4504(5)	97(3)
C004	4629(10)	6104(8)	6204(6)	53(2)
C005	7497(12)	5367(8)	6006(7)	64(3)
C006	7166(11)	4412(8)	4627(6)	61(2)
C007	2282(11)	6189(9)	7166(7)	64(3)
C008	4653(11)	7245(9)	6097(6)	61(2)
C009	2227(12)	7325(9)	7052(7)	68(3)
C00A	3417(12)	7839(8)	6535(6)	64(3)
C00B	5570(14)	4909(8)	4889(7)	67(3)
C00C	3501(11)	5571(8)	6747(6)	63(3)
C00D	8310(12)	4682(7)	5283(6)	62(3)
C00E	9227(15)	3531(8)	3764(8)	80(3)
C00F	7610(14)	3854(9)	3855(8)	77(3)
C00G	9940(12)	4377(9)	5196(8)	74(3)
C00H	10374(14)	3785(9)	4416(8)	81(3)
C00I	3572(12)	4329(8)	6900(7)	88(3)
C00J	5932(13)	7818(9)	5514(7)	90(4)
C00K	834(12)	7995(9)	7483(7)	97(4)

Table 3 Anisotropic Displacement Parameters (Å^2×10^3) for 2,4,6-trimethylphenylphthalimide. The Anisotropic displacement factor exponent takes the form: $-2\pi^2[h^2Å^2U_{11}+2hkÅb^*U_{12}+\ldots]$.

Atom	U_{11}	U_{22}	U_{33}	U_{23}	U_{13}	U_{12}
O001	62(4)	124(6)	66(5)	-27(5)	-12(4)	7(4)
N002	52(5)	71(5)	66(5)	-11(4)	-4(4)	6(4)
O003	65(5)	134(7)	92(5)	-32(5)	-25(4)	3(5)
C004	52(6)	58(6)	50(5)	-4(5)	-9(5)	4(5)
C005	58(6)	72(7)	61(7)	6(5)	-6(5)	-1(5)
C006	62(6)	70(6)	52(6)	-8(5)	-6(5)	-2(5)
C007	49(6)	69(7)	74(7)	1(6)	-3(5)	-2(5)
C008	55(6)	68(7)	59(6)	2(5)	-1(5)	2(5)
C009	55(6)	80(8)	68(7)	-18(6)	-4(5)	3(6)
C00A	74(7)	51(6)	67(7)	-6(5)	-6(6)	4(5)
C00B	68(7)	65(6)	68(7)	-14(5)	-7(6)	3(6)

C00C	55(6)	69(7)	64(6)	2(6)	-4(5)	-6(5)
C00D	66(7)	60(6)	59(6)	1(5)	2(5)	2(5)
C00E	92(8)	68(7)	80(7)	-19(5)	28(7)	-14(6)
C00F	71(7)	78(7)	82(8)	-5(6)	2(6)	-11(6)
C00G	59(7)	82(7)	80(7)	-4(6)	-4(5)	4(6)
C00H	67(7)	80(7)	95(9)	-3(7)	13(7)	15(6)
C00I	68(7)	78(8)	117(9)	16(7)	-10(6)	0(6)
C00J	86(8)	90(8)	92(8)	13(6)	26(7)	-3(7)
C00K	73(7)	110(9)	108(9)	-30(7)	8(7)	22(7)

Table 4 Bond Lengths for 2,4,6-trimethylphenylphthalimide.

Atom	Atom	Length/Å	Atom	Atom	Length/Å
O001	C005	1.207(10)	C007	C009	1.387(12)
N002	C004	1.450(10)	C007	C00C	1.388(13)
N002	C005	1.411(11)	C008	C00A	1.396(12)
N002	C00B	1.408(11)	C008	C00J	1.516(12)
O003	C00B	1.206(11)	C009	C00A	1.381(12)
C004	C008	1.391(11)	C009	C00K	1.534(12)
C004	C00C	1.377(11)	C00C	C00I	1.523(13)
C005	C00D	1.498(13)	C00D	C00G	1.389(12)
C006	C00B	1.487(13)	C00E	C00F	1.385(14)
C006	C00D	1.378(12)	C00E	C00H	1.371(14)
C006	C00F	1.363(13)	C00G	C00H	1.392(13)

Table 5 Bond Angles for 2,4,6-trimethylphenylphthalimide.

Atom	Atom	Atom	Angle/°	Atom	Atom	Atom	Angle/°
C005	N002	C004	124.1(7)	C00A	C009	C007	119.4(10)
C00B	N002	C004	124.1(8)	C00A	C009	C00K	120.6(10)
C00B	N002	C005	111.8(8)	C009	C00A	C008	121.8(9)
C008	C004	N002	117.6(8)	N002	C00B	C006	105.7(9)
C00C	C004	N002	119.6(8)	O003	C00B	N002	124.3(9)
C00C	C004	C008	122.7(9)	O003	C00B	C006	129.9(9)
O001	C005	N002	125.5(9)	C004	C00C	C007	118.7(9)
O001	C005	C00D	129.3(9)	C004	C00C	C00I	121.5(9)
N002	C005	C00D	105.2(8)	C007	C00C	C00I	119.8(9)
C00D	C006	C00B	108.7(8)	C006	C00D	C005	108.6(8)
C00F	C006	C00B	130.4(9)	C006	C00D	C00G	121.7(10)
C00F	C006	C00D	120.7(10)	C00G	C00D	C005	129.6(10)

C009 C007 C00C	120.4(9)	C00H C00E C00F	121.5(10)
C004 C008 C00A	116.8(9)	C006 C00F C00E	118.3(10)
C004 C008 C00J	121.9(9)	C00D C00G C00H	117.1(10)
C00A C008 C00J	121.3(9)	C00E C00H C00G	120.6(10)
C007 C009 C00K	120.0(10)		

Table 6 Hydrogen Atom Coordinates (Å×10^4) and Isotropic Displacement Parameters (Å^2×10^3) for 2,4,6-trimethylphenylphthalimide.

Atom	*x*	*y*	*z*	U(eq)
H007	1498.11	5839.78	7524.89	77
H00A	3394.86	8602.86	6476.21	77
H00E	9541.87	3133.59	3248.22	96
H00F	6847.09	3694.58	3401.27	93
H00G	10709.18	4560.2	5640.73	88
H00H	11451.3	3559.38	4336.43	97
H00B	3549.81	3958.13	6318.84	132
H00C	2647.44	4102.04	7259.22	132
H00D	4562.38	4144.41	7217.95	132
H00I	7001.96	7575.53	5695.74	134
H00J	5847.72	8601.25	5596.92	134
H00K	5756.01	7639.2	4880.84	134
H00L	-178.53	7811.37	7186.12	146
H00M	1050.04	8767.63	7407.89	146
H00N	757	7823.95	8123.86	146

Experimental

Single crystals of $C_{22.67}N_{1.33}O_{2.67}H_{0.33}$ **[2,4,6-trimethylphenylphthalimide]** were **[]**. A suitable crystal was selected and **[]** on a **dtrek-CrysAlisPro-abstract goniometer imported rigaku-d*trek images** diffractometer. The crystal was kept at 293(2) K during data collection. Using Olex2 [1], the structure was solved with the ShelXT [2] structure solution program using Intrinsic Phasing and refined with the ShelXL [3] refinement package using Least Squares minimisation.

1. Dolomanov, O.V., Bourhis, L.J., Gildea, R.J, Howard, J.A.K. & Puschmann, H. (2009), J. Appl. Cryst. 42, 339-341.
2. Sheldrick, G.M. (2015). Acta Cryst. A71, 3-8.
3. Sheldrick, G.M. (2015). Acta Cryst. C71, 3-8.

Crystal structure determination of [2,4,6-trimethylphenylphthalimide]

Crystal Data for $C_{22.666667}N_{1.333333}O_{2.666667}H_{0.333333}$ (M =333.91 g/mol): orthorhombic, space group $P2_12_12_1$ (no. 19), a = 8.176(5) Å, b = 12.123(6) Å, c = 14.592(9) Å, V = 1446.3(14) Å^3, Z = 3, T = 293(2) K, μ(MoKα) = 0.078 mm^{-1},*Dcalc* = 1.150 g/cm^3, 20127 reflections measured (4.368° ≤ 2Θ ≤ 66.516°), 5445 unique (R_{int} = 0.4129, R_{sigma} = 0.6714) which were used in all calculations. The final R_1 was 0.0989 (I > 2σ(I)) and wR_2 was 0.3438 (all data).

Refinement model description

Number of restraints - 0, number of constraints - unknown.

Details:

1. Fixed Uiso
 At 1.2 times of:
  All C(H) groups
 At 1.5 times of:
  All C(H,H,H) groups

2.a Aromatic/amide H refined with riding coordinates:
 C007(H007), C00A(H00A), C00E(H00E), C00F(H00F), C00G(H00G), C00H(H00H)

2.b Idealised Me refined as rotating group:
 C00I(H00B,H00C,H00D), C00J(H00I,H00J,H00K), C00K(H00L,H00M,H00N)

This report has been created with Olex2, compiled on 2017.02.24 svn.r3390 for Rigaku Oxford Diffraction. Please let us know if there are any errors or if you would like to have additional features.

DIC-Se-2

Table 1 Crystal data and structure refinement for DIC-Se-2.

Identification code	DIC-Se-2
Empirical formula	$C_{36}H_{38}N_4Se$
Formula weight	605.66
Temperature/K	293(2)
Crystal system	triclinic
Space group	P-1
a/Å	14.8268(14)
b/Å	15.2222(16)
c/Å	15.6260(17)
α/°	68.583(10)
β/°	89.820(8)
γ/°	82.100(8)
Volume/Å^3	3247.8(6)
Z	4
ρ_{calc}g/cm^3	1.239
μ/mm^{-1}	1.186
F(000)	1264.0
Crystal size/mm^3	? × ? × ?
Radiation	MoKα (λ = 0.71073)
2Θ range for data collection/°	3.21 to 67.14
Index ranges	$-22 \leq h \leq 22$, $-22 \leq k \leq 22$, $-24 \leq l \leq 22$
Reflections collected	47494
Independent reflections	23624 [R_{int} = 0.1068, R_{sigma} = 0.2380]
Data/restraints/parameters	23624/0/755
Goodness-of-fit on F^2	0.896
Final R indexes [I>=2σ (I)]	R_1 = 0.0683, wR_2 = 0.1248
Final R indexes [all data]	R_1 = 0.2732, wR_2 = 0.2004
Largest diff. peak/hole / e Å^{-3}	0.35/-0.64

Table 2 Fractional Atomic Coordinates (×10^4) and Equivalent Isotropic Displacement Parameters (Å^2×10^3) for DIC-Se-2. U_{eq} is defined as 1/3 of of the trace of the orthogonalised U_{IJ} tensor.

Atom	*x*	*y*	*z*	U(eq)
Se01	337.1(3)	6927.2(3)	3183.5(4)	71.59(18)
Se02	2650.0(4)	-1106.1(4)	6323.1(3)	73.15(18)
N003	2080(2)	7201(2)	3371(2)	45.6(8)
N004	1915.2(19)	5749(2)	3313(2)	42.7(8)
N005	3583(2)	7490(2)	3386(2)	49.8(8)
N006	3010(2)	-899(2)	7938(2)	53.7(9)
N007	3059(2)	4635(2)	3400(2)	50.8(8)
N008	2807(2)	493(3)	6667(2)	52.7(9)
N009	2960(2)	1878(3)	6744(2)	54.7(9)
C00A	3015(3)	6950(3)	3529(3)	42.7(9)
N00B	3374(3)	-735(3)	9328(3)	70.5(11)
C00C	2823(2)	5381(3)	3530(3)	43.5(9)
C00D	3339(2)	5903(3)	3954(3)	45.1(9)
C00E	1677(3)	8128(3)	3307(3)	49.9(10)
C00F	2778(3)	967(3)	5695(3)	49.7(10)
C00G	1339(3)	5160(3)	3130(3)	46.7(10)
C00H	3527(3)	1524(3)	4352(3)	52.5(10)
C00I	2856(3)	2658(3)	6981(3)	53.7(11)
C00J	3510(3)	8467(3)	2973(3)	51.8(11)
C00K	3569(3)	1014(3)	5264(3)	48.6(10)
C00L	1518(3)	6599(3)	3305(3)	48.7(10)
C00M	3892(3)	4053(3)	3678(3)	52.5(11)
C00N	3173(3)	-1908(3)	8304(3)	54.4(11)
C00O	2741(3)	1983(3)	3879(3)	54.1(11)
C00P	1177(3)	5248(3)	2260(3)	55.9(11)
C00Q	1470(3)	8811(3)	2462(3)	59.1(12)
C00R	3163(3)	5568(3)	4963(3)	59.2(11)
C00S	2012(3)	3109(3)	7020(3)	60.5(12)
C00T	2818(3)	1063(3)	7180(3)	57.2(11)
C00U	4344(2)	5736(3)	3851(3)	58.9(12)
C00V	1967(3)	1913(3)	4336(3)	58.7(12)
C00W	3582(3)	3082(3)	7062(3)	61.0(12)
C00X	1961(3)	1404(3)	5249(3)	56.3(11)
C00Y	2827(3)	-452(3)	7019(3)	56.9(11)
C00Z	1525(3)	8295(3)	4089(3)	58.8(11)
C010	4025(3)	-2360(3)	8338(3)	56.6(11)
C011	4039(3)	3453(3)	4558(3)	57.9(11)
C012	3826(4)	-1608(4)	9865(3)	61.9(12)

C013	949(3)	4540(3)	3839(3)	56.3(11)
C014	4441(3)	539(3)	5770(3)	64.9(12)
C015	361(3)	4028(3)	3644(4)	66.5(13)
C016	3053(3)	-413(3)	8525(3)	61.5(12)
C017	3380(3)	-2321(4)	10394(3)	67.8(13)
C018	2465(3)	-2387(4)	8629(3)	65.2(12)
C019	585(3)	4714(3)	2096(4)	68.0(13)
C01A	3465(3)	3911(3)	7199(3)	68.6(13)
C01B	2607(3)	605(3)	8159(3)	67.0(13)
C01C	168(3)	4106(3)	2785(4)	72.2(14)
C01D	2629(4)	4339(3)	7253(3)	71.5(13)
C01E	4837(3)	2874(3)	4838(4)	69.9(14)
C01F	953(3)	9887(4)	3192(5)	71.5(14)
C01G	4519(3)	4039(3)	3060(3)	67.3(13)
C01H	5475(3)	2883(4)	4232(4)	79.8(16)
C01I	1902(3)	3938(3)	7158(3)	72.1(14)
C01J	1100(3)	9693(3)	2429(4)	71.6(14)
C01K	3377(3)	9053(3)	3441(4)	65.6(13)
C01L	1600(3)	8637(3)	1609(3)	79.1(15)
C01M	4171(4)	-3319(4)	8754(3)	72.1(14)
C01N	4776(3)	-1834(3)	7924(3)	73.3(14)
C01O	3848(4)	-3132(4)	10983(3)	79.8(15)
C01P	2717(3)	2573(3)	2894(3)	76.1(14)
C01Q	2646(4)	-3349(4)	9017(3)	80.5(15)
C01R	1168(3)	4403(3)	4801(3)	76.5(14)
C01S	1104(3)	1335(4)	5726(3)	80.7(15)
C01T	3705(3)	8824(4)	2075(4)	73.9(14)
C01U	5324(3)	3442(4)	3351(4)	79.1(15)
C01V	1716(3)	7528(3)	5002(3)	78.6(15)
C01W	3386(3)	10009(4)	2989(5)	84.9(17)
C01X	4740(4)	-1703(4)	9983(4)	80.5(15)
C01Y	1162(3)	9189(4)	4010(4)	71.8(14)
C01Z	3492(4)	-3817(4)	9094(4)	79.7(15)
C020	1623(3)	5901(4)	1491(3)	81.8(15)
C021	4745(4)	-3239(4)	11072(4)	88.3(16)
C022	5199(4)	-2534(5)	10581(4)	88.7(17)
C023	3536(4)	10340(4)	2093(5)	100(2)
C024	1590(4)	610(4)	8198(4)	107(2)
C025	565(4)	10865(3)	3137(5)	114(2)
C026	1531(3)	-1899(4)	8576(4)	91.7(17)
C027	-484(4)	3541(4)	2580(4)	103.3(19)
C028	2930(5)	1097(4)	8737(3)	114(2)

C029	3698(4)	9767(4)	1631(4)	100.0(19)
C02A	3663(5)	-4878(4)	9565(5)	130(2)

Table 3 Anisotropic Displacement Parameters ($Å^2 \times 10^3$) for DIC-Se-2. The Anisotropic displacement factor exponent takes the form: $-2\pi^2[h^2Å^2U_{11}+2hkÅb^*U_{12}+\ldots]$.

Atom	U_{11}	U_{22}	U_{33}	U_{23}	U_{13}	U_{12}
Se01	38.6(3)	64.2(3)	115.6(4)	-39.1(3)	-0.4(2)	-2.3(2)
Se02	90.3(4)	69.4(3)	67.3(3)	-36.0(3)	-7.0(3)	-6.0(3)
N003	38.4(18)	41.0(19)	59(2)	-21.3(17)	0.2(15)	-3.2(15)
N004	35.7(18)	40.8(18)	53(2)	-18.5(16)	-0.9(15)	-6.8(15)
N005	45(2)	42(2)	61(2)	-16.0(18)	-1.9(16)	-8.5(16)
N006	54(2)	55(2)	55(2)	-26(2)	4.2(17)	-1.2(17)
N007	40.1(19)	49(2)	66(2)	-27.2(19)	-5.9(16)	-0.3(16)
N008	55(2)	57(2)	50(2)	-28(2)	2.4(17)	1.0(18)
N009	50(2)	62(2)	59(2)	-31(2)	-2.4(17)	-2.1(19)
C00A	41(2)	44(2)	46(2)	-21(2)	-1.4(18)	-1.3(19)
N00B	90(3)	70(3)	52(3)	-28(2)	4(2)	1(2)
C00C	37(2)	43(2)	49(2)	-15(2)	-0.8(18)	-5.9(18)
C00D	40(2)	42(2)	55(3)	-20(2)	-1.7(19)	-3.7(18)
C00E	40(2)	44(2)	67(3)	-24(2)	-6(2)	1.1(19)
C00F	53(3)	54(3)	45(3)	-25(2)	0(2)	2(2)
C00G	41(2)	45(2)	56(3)	-19(2)	-2(2)	-8.3(19)
C00H	53(3)	54(3)	58(3)	-30(2)	6(2)	-6(2)
C00I	59(3)	55(3)	51(3)	-28(2)	-2(2)	0(2)
C00J	43(2)	40(2)	69(3)	-16(2)	-6(2)	-6.9(19)
C00K	49(3)	51(3)	50(3)	-26(2)	-2(2)	-1(2)
C00L	47(2)	39(2)	59(3)	-18(2)	0(2)	-3.0(19)
C00M	49(3)	46(3)	71(3)	-34(3)	-6(2)	-1(2)
C00N	55(3)	56(3)	57(3)	-26(2)	-1(2)	-7(2)
C00O	61(3)	53(3)	50(3)	-24(2)	-4(2)	-2(2)
C00P	46(3)	55(3)	68(3)	-24(2)	-1(2)	-8(2)
C00Q	51(3)	55(3)	76(3)	-31(3)	-8(2)	-2(2)
C00R	70(3)	53(3)	52(3)	-17(2)	-7(2)	-8(2)
C00S	40(2)	67(3)	75(3)	-30(3)	-8(2)	2(2)
C00T	50(3)	67(3)	58(3)	-35(3)	0(2)	10(2)
C00U	37(2)	51(3)	93(3)	-35(3)	-6(2)	3.4(19)
C00V	55(3)	57(3)	66(3)	-30(3)	-17(2)	6(2)
C00W	51(3)	69(3)	65(3)	-30(3)	-6(2)	-1(2)
C00X	44(3)	64(3)	64(3)	-32(3)	-1(2)	4(2)

C00Y	52(3)	68(3)	54(3)	-32(3)	5(2)	4(2)
C00Z	45(2)	63(3)	77(3)	-37(3)	2(2)	-3(2)
C010	60(3)	58(3)	54(3)	-26(2)	3(2)	0(2)
C011	54(3)	53(3)	73(3)	-33(3)	-5(2)	-4(2)
C012	69(3)	66(3)	54(3)	-27(3)	-4(3)	-4(3)
C013	47(3)	46(3)	71(3)	-17(2)	-1(2)	-3(2)
C014	53(3)	75(3)	67(3)	-31(3)	-4(2)	8(2)
C015	51(3)	47(3)	97(4)	-21(3)	-3(3)	-8(2)
C016	68(3)	62(3)	59(3)	-29(3)	7(2)	-3(2)
C017	69(3)	78(4)	60(3)	-30(3)	2(3)	-11(3)
C018	58(3)	74(3)	69(3)	-32(3)	-2(2)	-11(3)
C019	59(3)	72(3)	82(4)	-40(3)	-17(3)	-6(3)
C01A	63(3)	79(4)	72(3)	-35(3)	-3(3)	-13(3)
C01B	93(4)	56(3)	48(3)	-21(2)	7(3)	7(3)
C01C	54(3)	55(3)	112(5)	-37(3)	-12(3)	-8(2)
C01D	82(4)	64(3)	75(3)	-35(3)	0(3)	-6(3)
C01E	71(3)	55(3)	86(4)	-34(3)	-22(3)	6(3)
C01F	47(3)	64(3)	115(4)	-49(4)	-10(3)	0(2)
C01G	60(3)	75(3)	74(3)	-43(3)	-2(3)	7(3)
C01H	58(3)	84(4)	113(5)	-64(4)	-24(3)	15(3)
C01I	66(3)	66(3)	83(4)	-33(3)	0(3)	9(3)
C01J	59(3)	52(3)	101(4)	-28(3)	-23(3)	2(2)
C01K	50(3)	59(3)	93(4)	-34(3)	-20(2)	-6(2)
C01L	91(4)	67(3)	72(3)	-19(3)	-14(3)	-7(3)
C01M	76(4)	68(3)	70(3)	-27(3)	0(3)	1(3)
C01N	55(3)	85(4)	76(3)	-27(3)	12(2)	-2(3)
C01O	84(4)	85(4)	65(3)	-18(3)	0(3)	-23(3)
C01P	98(4)	67(3)	56(3)	-19(3)	-11(3)	1(3)
C01Q	93(4)	80(4)	73(4)	-28(3)	2(3)	-30(3)
C01R	68(3)	88(4)	65(3)	-12(3)	9(3)	-26(3)
C01S	52(3)	100(4)	87(4)	-37(3)	5(3)	4(3)
C01T	76(3)	61(3)	85(4)	-25(3)	5(3)	-18(3)
C01U	54(3)	103(4)	97(4)	-63(4)	0(3)	4(3)
C01V	86(4)	85(4)	71(3)	-41(3)	6(3)	2(3)
C01W	71(4)	60(4)	135(5)	-54(4)	-33(4)	1(3)
C01X	90(4)	93(4)	68(4)	-34(3)	6(3)	-31(3)
C01Y	54(3)	79(4)	103(4)	-61(4)	1(3)	0(3)
C01Z	97(4)	60(3)	78(4)	-23(3)	-10(3)	-3(3)
C020	81(4)	103(4)	65(3)	-30(3)	3(3)	-28(3)
C021	92(5)	93(4)	73(4)	-24(3)	-10(3)	-7(4)
C022	63(4)	119(5)	87(4)	-42(4)	-6(3)	-10(4)
C023	96(5)	63(4)	128(6)	-13(4)	-24(4)	-27(3)

C024	104(5)	95(4)	97(4)	-19(4)	48(4)	22(3)
C025	103(5)	66(3)	189(7)	-76(4)	-33(4)	21(3)
C026	61(3)	106(4)	105(4)	-32(4)	11(3)	-21(3)
C027	83(4)	92(4)	157(6)	-64(4)	-11(4)	-35(3)
C028	216(7)	73(4)	60(3)	-40(3)	-8(4)	5(4)
C029	116(5)	77(4)	93(5)	-8(4)	4(4)	-36(4)
C02A	149(6)	63(4)	157(6)	-18(4)	-2(5)	-14(4)

Table 4 Bond Lengths for DIC-Se-2.

Atom	Atom	Length/Å	Atom	Atom	Length/Å
Se01	C00L	1.745(4)	C00P	C019	1.359(6)
Se02	C00Y	1.762(4)	C00P	C020	1.474(6)
N003	C00A	1.384(4)	C00Q	C01J	1.362(6)
N003	C00E	1.422(4)	C00Q	C01L	1.458(6)
N003	C00L	1.350(5)	C00S	C01I	1.345(6)
N004	C00C	1.377(4)	C00T	C01B	1.484(6)
N004	C00G	1.420(4)	C00V	C00X	1.353(6)
N004	C00L	1.342(4)	C00W	C01A	1.345(6)
N005	C00A	1.221(4)	C00X	C01S	1.468(6)
N005	C00J	1.376(5)	C00Z	C01V	1.474(6)
N006	C00N	1.415(5)	C00Z	C01Y	1.353(6)
N006	C00Y	1.355(5)	C010	C01M	1.350(6)
N006	C016	1.378(5)	C010	C01N	1.470(6)
N007	C00C	1.228(4)	C011	C01E	1.343(6)
N007	C00M	1.386(5)	C012	C017	1.356(6)
N008	C00F	1.422(5)	C012	C01X	1.348(6)
N008	C00T	1.381(5)	C013	C015	1.351(6)
N008	C00Y	1.335(5)	C013	C01R	1.470(6)
N009	C00I	1.357(5)	C015	C01C	1.333(6)
N009	C00T	1.225(5)	C016	C01B	1.498(6)
C00A	C00D	1.493(5)	C017	C01O	1.338(6)
N00B	C012	1.366(5)	C018	C01Q	1.353(6)
N00B	C016	1.238(5)	C018	C026	1.465(6)
C00C	C00D	1.488(5)	C019	C01C	1.350(6)
C00D	C00R	1.504(5)	C01A	C01D	1.336(6)
C00D	C00U	1.496(5)	C01B	C024	1.507(7)
C00E	C00Q	1.352(6)	C01B	C028	1.484(6)
C00E	C00Z	1.348(6)	C01C	C027	1.486(6)
C00F	C00K	1.348(5)	C01D	C01I	1.344(6)
C00F	C00X	1.357(5)	C01E	C01H	1.334(7)

C00G	C00P	1.336(5)	C01F	C01J	1.339(6)
C00G	C013	1.354(5)	C01F	C01Y	1.334(6)
C00H	C00K	1.347(5)	C01F	C025	1.492(6)
C00H	C00O	1.341(5)	C01G	C01U	1.364(6)
C00I	C00S	1.355(5)	C01H	C01U	1.329(7)
C00I	C00W	1.357(6)	C01K	C01W	1.368(6)
C00J	C01K	1.340(6)	C01M	C01Z	1.335(7)
C00J	C01T	1.353(6)	C01O	C021	1.319(7)
C00K	C014	1.467(5)	C01Q	C01Z	1.336(7)
C00M	C011	1.343(6)	C01T	C029	1.345(6)
C00M	C01G	1.342(6)	C01W	C023	1.333(7)
C00N	C010	1.344(5)	C01X	C022	1.357(7)
C00N	C018	1.353(6)	C01Z	C02A	1.496(7)
C00O	C00V	1.345(6)	C021	C022	1.336(7)
C00O	C01P	1.469(5)	C023	C029	1.319(8)

Table 5 Bond Angles for DIC-Se-2.

Atom	Atom	Atom	Angle/°	Atom	Atom	Atom	Angle/°
C00A	N003	C00E	118.9(3)	N009	C00T	N008	114.8(4)
C00L	N003	C00A	123.5(3)	N009	C00T	C01B	130.4(4)
C00L	N003	C00E	117.6(3)	C00O	C00V	C00X	122.3(4)
C00C	N004	C00G	117.4(3)	C01A	C00W	C00I	120.9(4)
C00L	N004	C00C	125.6(3)	C00F	C00X	C01S	122.2(4)
C00L	N004	C00G	117.0(3)	C00V	C00X	C00F	116.9(4)
C00A	N005	C00J	131.7(3)	C00V	C00X	C01S	120.9(4)
C00Y	N006	C00N	118.2(4)	N006	C00Y	Se02	120.8(3)
C00Y	N006	C016	122.9(4)	N008	C00Y	Se02	121.9(3)
C016	N006	C00N	118.9(4)	N008	C00Y	N006	117.2(4)
C00C	N007	C00M	126.0(3)	C00E	C00Z	C01V	121.6(4)
C00T	N008	C00F	116.1(4)	C00E	C00Z	C01Y	117.7(5)
C00Y	N008	C00F	119.0(3)	C01Y	C00Z	C01V	120.7(5)
C00Y	N008	C00T	124.9(4)	C00N	C010	C01M	118.0(5)
C00T	N009	C00I	130.0(4)	C00N	C010	C01N	121.4(4)
N003	C00A	C00D	115.1(3)	C01M	C010	C01N	120.6(4)
N005	C00A	N003	126.9(4)	C01E	C011	C00M	120.2(5)
N005	C00A	C00D	117.9(3)	C017	C012	N00B	121.9(5)
C016	N00B	C012	132.3(4)	C01X	C012	N00B	118.0(5)
N004	C00C	C00D	114.9(3)	C01X	C012	C017	119.2(5)
N007	C00C	N004	114.6(3)	C00G	C013	C01R	121.7(4)
N007	C00C	C00D	130.3(3)	C015	C013	C00G	118.1(4)

C00A	C00D	C00R	108.6(3)	C015	C013	C01R	120.1(4)
C00A	C00D	C00U	108.5(3)	C01C	C015	C013	122.1(5)
C00C	C00D	C00A	110.1(3)	N006	C016	C01B	115.5(4)
C00C	C00D	C00R	108.1(3)	N00B	C016	N006	127.5(4)
C00C	C00D	C00U	112.8(3)	N00B	C016	C01B	116.8(4)
C00U	C00D	C00R	108.6(3)	C01O	C017	C012	120.1(5)
C00Q	C00E	N003	118.7(4)	C00N	C018	C01Q	117.4(5)
C00Z	C00E	N003	118.8(4)	C00N	C018	C026	122.3(5)
C00Z	C00E	C00Q	122.5(4)	C01Q	C018	C026	120.2(5)
C00K	C00F	N008	118.7(4)	C01C	C019	C00P	121.7(5)
C00K	C00F	C00X	122.8(4)	C01D	C01A	C00W	120.5(5)
C00X	C00F	N008	118.4(4)	C00T	C01B	C016	109.5(4)
C00P	C00G	N004	119.2(4)	C00T	C01B	C024	107.9(4)
C00P	C00G	C013	121.7(4)	C016	C01B	C024	107.7(4)
C013	C00G	N004	119.1(4)	C028	C01B	C00T	111.9(4)
C00O	C00H	C00K	122.5(4)	C028	C01B	C016	108.7(4)
N009	C00I	C00W	121.1(4)	C028	C01B	C024	111.0(4)
C00S	C00I	N009	120.4(4)	C015	C01C	C019	118.2(5)
C00S	C00I	C00W	117.9(4)	C015	C01C	C027	121.5(5)
C01K	C00J	N005	123.2(4)	C019	C01C	C027	120.3(5)
C01K	C00J	C01T	119.3(4)	C01A	C01D	C01I	119.3(5)
C01T	C00J	N005	117.0(4)	C01H	C01E	C011	119.6(5)
C00F	C00K	C014	121.2(4)	C01J	C01F	C025	121.1(5)
C00H	C00K	C00F	117.3(4)	C01Y	C01F	C01J	118.8(4)
C00H	C00K	C014	121.5(4)	C01Y	C01F	C025	120.1(5)
N003	C00L	Se01	121.5(3)	C00M	C01G	C01U	119.0(5)
N004	C00L	Se01	121.9(3)	C01U	C01H	C01E	120.9(5)
N004	C00L	N003	116.6(3)	C01D	C01I	C00S	120.6(5)
C011	C00M	N007	119.3(4)	C01F	C01J	C00Q	122.1(5)
C01G	C00M	N007	120.3(4)	C00J	C01K	C01W	119.4(5)
C01G	C00M	C011	120.2(4)	C01Z	C01M	C010	121.7(5)
C010	C00N	N006	119.3(4)	C021	C01O	C017	120.6(5)
C010	C00N	C018	122.1(4)	C01Z	C01Q	C018	121.9(5)
C018	C00N	N006	118.6(4)	C029	C01T	C00J	120.9(5)
C00H	C00O	C00V	118.2(4)	C01H	C01U	C01G	119.9(5)
C00H	C00O	C01P	121.6(4)	C023	C01W	C01K	119.4(6)
C00V	C00O	C01P	120.3(4)	C012	C01X	C022	119.4(5)
C00G	C00P	C019	118.1(4)	C01F	C01Y	C00Z	121.9(5)
C00G	C00P	C020	121.7(4)	C01M	C01Z	C02A	121.3(6)
C019	C00P	C020	120.2(4)	C01Q	C01Z	C01M	118.9(5)
C00E	C00Q	C01J	116.9(4)	C01Q	C01Z	C02A	119.8(6)
C00E	C00Q	C01L	123.4(4)	C01O	C021	C022	120.4(6)

C01J	C00Q	C01L	119.6(5)	C021	C022	C01X	120.2(5)
C01I	C00S	C00I	120.7(4)	C029	C023	C01W	121.8(6)
N008	C00T	C01B	114.7(4)	C023	C029	C01T	119.1(6)

Table 6 Hydrogen Atom Coordinates (Å×10^4) and Isotropic Displacement Parameters (Å^2×10^3) for DIC-Se-2.

Atom	*x*	*y*	*z*	U(eq)
H00H	4063.2	1558.29	4039.48	63
H00A	3471.77	5914.12	5246.74	89
H00B	3384.06	4898.82	5248.54	89
H00C	2519.22	5677.36	5039.38	89
H00S	1501.97	2841.67	6950.44	73
H00D	4463.29	5904.06	3210.6	88
H00E	4574.59	5074.52	4178.14	88
H00F	4640.41	6120.74	4097.35	88
H00V	1417.94	2226.45	4013.59	70
H00W	4167.54	2794.43	7021.36	73
H011	3586.79	3438.04	4974.84	69
H01O	4506.56	731.13	6284.75	97
H01P	4931.92	714.94	5369.94	97
H01Q	4454.49	-139.91	5987.6	97
H015	81.51	3607.86	4124.66	80
H017	2746.42	-2246.8	10347.21	81
H019	462.75	4769.41	1493.17	82
H01R	3970.99	4189.88	7256.21	82
H01S	2551.62	4908.21	7356.74	86
H01E	4943.76	2468.49	5450.19	84
H01G	4406.55	4430.5	2444.14	81
H01H	6032.73	2492.81	4429.81	96
H01V	1318.3	4236.84	7186.67	87
H01J	943.28	10176.01	1858.09	86
H01K	3280.66	8811.41	4067.3	79
H01A	2131.08	8172.33	1683.11	119
H01B	1678.06	9221.03	1119.24	119
H01C	1074.87	8401.9	1463.57	119
H01X	4760.35	-3641.7	8805.11	87
H01Z	4792.54	-1751.97	7285.08	110
H	5342.82	-2185.56	8237.28	110
HA	4681.7	-1219.78	7977.78	110
H01	3538.44	-3623.88	11332.71	96

H0AA	2454.18	3216.12	2800.19	114
HB	2354.77	2322.01	2554.87	114
HC	3325.84	2567.37	2683.72	114
H1AA	2169.17	-3695.43	9237.59	97
H01D	1796.48	4128.82	4958.13	115
H01F	787.1	3982.13	5198.29	115
H01I	1064.17	5007.14	4874.34	115
H2AA	1077.52	680.8	6101.6	121
HD	598.42	1571.21	5281.05	121
HE	1075.41	1708.48	6108.11	121
H01T	3844.69	8412.87	1760.62	89
H01U	5767.13	3427	2931.61	95
H01L	1413.63	7001.14	5028.84	118
H01M	1498.85	7763.65	5468.26	118
H01N	2361.86	7321.36	5102.21	118
H01W	3288.23	10423.94	3304.01	102
H3AA	5052.13	-1203.59	9656.98	97
H01Y	1055.84	9319.46	4540.81	86
H02A	1527.76	6527.52	1515.25	123
H02B	1367.5	5924.97	917.39	123
H02C	2265.36	5674.92	1538.32	123
H021	5063.47	-3808.4	11478.16	106
H022	5830.85	-2613.84	10649.2	106
H023	3525.56	10992.13	1785.12	120
H02J	1289.73	1254.12	8034.3	161
H02K	1445.03	235.93	8810.74	161
H02L	1388.55	344.54	7774.54	161
H02D	467.53	11282.45	2502.62	171
H02E	983.02	11099.52	3439.95	171
H02F	-4.67	10843.35	3431.55	171
H02M	1507.44	-1493.38	8926.43	138
H02N	1127.76	-2363.07	8822.85	138
H02O	1346.83	-1520.25	7945.71	138
H02G	-275.79	2873.49	2897.52	155
H02H	-524.48	3681.63	1929.37	155
H02I	-1074.44	3704.65	2781.28	155
H02P	3573.37	1111.4	8678.21	171
H02Q	2813.56	759.54	9369.16	171
H02R	2613.72	1737.38	8538.82	171
H029	3807.29	10010.99	1007.57	120
H02S	3345.48	-5165.48	9226.01	194
H02T	3449.2	-5052.86	10177.32	194

H02U	4305.38	-5098.24	9595.41	194

Table 7 Solvent masks information for DIC-Se-2.

Number	X	Y	Z	Volume	Electron count	Content
1	0.000	-0.845	0.000	443.5	102.0	?
2	0.265	0.656	0.701	11.3	0.0	?
3	0.735	0.344	0.299	11.3	0.1	?

Experimental

Single crystals of $C_{36}H_{38}N_4Se$ **[DIC-Se-2]** were **[]**. A suitable crystal was selected and **[]** on a **dtrek-CrysAlisPro-abstract goniometer imported rigaku-d*trek images** diffractometer. The crystal was kept at 293(2) K during data collection. Using Olex2 [1], the structure was solved with the ShelXT [2] structure solution program using Intrinsic Phasing and refined with the ShelXL [3] refinement package using Least Squares minimisation.

1. Dolomanov, O.V., Bourhis, L.J., Gildea, R.J, Howard, J.A.K. & Puschmann, H. (2009), J. Appl. Cryst. 42, 339-341.
2. Sheldrick, G.M. (2015). Acta Cryst. A71, 3-8.
3. Sheldrick, G.M. (2015). Acta Cryst. C71, 3-8.

Crystal structure determination of [DIC-Se-2]

Crystal Data for $C_{36}H_{38}N_4Se$ (M =605.66 g/mol): triclinic, space group P-1 (no. 2), a = 14.8268(14) Å, b = 15.2222(16) Å, c = 15.6260(17) Å, α = 68.583(10)°, β = 89.820(8)°, γ = 82.100(8)°, V = 3247.8(6) Å^3, Z = 4, T = 293(2) K, μ(MoKα) = 1.186 mm^{-1}, $Dcalc$ = 1.239 g/cm^3, 47494 reflections measured (3.21° ≤ 2Θ ≤ 67.14°), 23624 unique (R_{int} = 0.1068, R_{sigma} = 0.2380) which were used in all calculations. The final R_1 was 0.0683 (I > 2σ(I)) and wR_2 was 0.2004 (all data).

Refinement model description

Number of restraints - 0, number of constraints - unknown.

Details:

1. Fixed Uiso
 At 1.2 times of:
  All C(H) groups
 At 1.5 times of:
  All C(H,H,H) groups

2.a Aromatic/amide H refined with riding coordinates:
 C00H(H00H), C00S(H00S), C00V(H00V), C00W(H00W), C011(H011), C015(H015), C017(H017), C019(H019), C01A(H01R), C01D(H01S), C01E(H01E), C01G(H01G), C01H(H01H), C01I(H01V), C01J(H01J), C01K(H01K), C01M(H01X), C01O(H01), C01Q(H1AA), C01T(H01T), C01U(H01U), C01W(H01W), C01X(H3AA), C01Y(H01Y), C021(H021), C022(H022), C023(H023), C029(H029)

2.b Idealised Me refined as rotating group:
 C00R(H00A,H00B,H00C), C00U(H00D,H00E,H00F), C014(H01O,H01P,H01Q), C01L(H01A, H01B,H01C), C01N(H01Z,H,HA), C01P(H0AA,HB,HC), C01R(H01D,H01F,H01I), C01S(H2AA, HD,HE), C01V(H01L,H01M,H01N), C020(H02A,H02B,H02C), C024(H02J,H02K,H02L), C025(H02D,H02E,H02F), C026(H02M,H02N,H02O), C027(H02G,H02H,H02I), C028(H02P, H02Q,H02R), C02A(H02S,H02T,H02U)

This report has been created with Olex2, compiled on 2017.02.24 svn.r3390 for Rigaku Oxford Diffraction. Please let us know if there are any errors or if you would like to have additional features

DICIr(CO2)Cl

Table 1 Crystal data and structure refinement for DICIr(CO2)Cl.

Identification code	DICIr(CO2)Cl
Empirical formula	$C_{38}H_{38}N_4O_2ClIr$
Formula weight	810.37
Temperature/K	293(2)
Crystal system	monoclinic
Space group	$P2_1/n$
a/Å	15.7014(6)
b/Å	15.7693(7)
c/Å	15.7391(6)
α/°	90
β/°	103.507(4)
γ/°	90
Volume/Å^3	3789.2(3)
Z	8
ρ_{calc}g/cm^3	2.841
μ/mm^{-1}	7.259
F(000)	3232.0
Crystal size/mm^3	? × ? × ?
Radiation	MoKα (λ = 0.71073)
2Θ range for data collection/°	3.298 to 52.742
Index ranges	$-19 \leq h \leq 19$, $-19 \leq k \leq 19$, $-19 \leq l \leq 19$
Reflections collected	36079
Independent reflections	7745 [R_{int} = 0.0849, R_{sigma} = 0.0662]
Data/restraints/parameters	7745/0/423
Goodness-of-fit on F^2	1.031
Final R indexes [I>=2σ (I)]	R_1 = 0.0392, wR_2 = 0.0781
Final R indexes [all data]	R_1 = 0.0755, wR_2 = 0.0911
Largest diff. peak/hole / e Å^{-3}	1.59/-0.66

Table 2 Fractional Atomic Coordinates (×10^4) and Equivalent Isotropic Displacement Parameters (Å^2×10^3) for DICIr(CO2)Cl. U_{eq} is defined as 1/3 of of the trace of the orthogonalised U_{IJ} tensor.

Atom	*x*	*y*	*z*	U(eq)
Ir01	1170.4(2)	4317.4(2)	1604.1(2)	42.13(8)
Cl02	2111.7(10)	3170.1(10)	2058(1)	60.1(4)
N004	2096(3)	5234(3)	3231(3)	35.3(10)
N005	2795(3)	5344(3)	2112(3)	37.3(10)
N006	4025(3)	6084(3)	2207(3)	42.8(11)
N007	2544(3)	5940(3)	4481(3)	42.4(11)
O009	-32(3)	3144(3)	405(3)	80.8(15)
O00A	-159(3)	5641(3)	1103(4)	88.5(17)
C00B	3545(3)	5738(3)	2633(3)	39.0(12)
C00C	2774(3)	5661(3)	3833(3)	38.0(12)
C00D	2110(3)	5066(3)	2404(3)	37.1(12)
C00E	2720(3)	5302(4)	1178(3)	41.5(13)
C00F	650(4)	5702(4)	3336(4)	49.7(14)
C00G	2238(3)	5932(4)	670(3)	43.9(14)
C00H	1287(3)	5082(4)	3491(3)	41.1(13)
C00I	3009(3)	6390(4)	5209(3)	44.2(14)
C00J	1180(4)	4328(4)	3903(4)	49.1(14)
C00K	-303(4)	4750(5)	3864(4)	63.1(19)
C00L	4852(4)	6461(4)	2490(3)	48.4(14)
C00M	3126(4)	4662(4)	835(4)	49.6(15)
C00N	3658(3)	5606(3)	3603(3)	39.2(13)
C00O	369(4)	4189(4)	4068(4)	58.8(17)
C00P	3350(4)	5969(4)	5973(4)	54.5(16)
C00Q	423(4)	3584(4)	870(4)	56.9(16)
C00R	-142(4)	5508(5)	3522(4)	61.0(18)
C00S	3758(4)	4069(4)	1388(4)	64.1(18)
C00T	371(4)	5150(4)	1296(4)	56.8(17)
C00U	2103(4)	5852(4)	-218(4)	60.7(18)
C00V	4925(4)	7325(4)	2479(4)	58.7(17)
C00W	2953(4)	4622(4)	-62(4)	63.1(18)
C00X	3982(4)	4685(4)	3803(4)	58.2(16)
C00Y	4302(3)	6230(4)	4134(3)	55.1(17)
C00Z	1919(4)	3718(4)	4193(4)	66.6(18)
C010	5736(5)	7689(5)	2672(4)	73(2)
C011	3005(4)	7256(4)	5208(4)	64.6(18)
C012	804(4)	6563(4)	3010(4)	66.8(18)
C013	1883(4)	6679(3)	1061(4)	51.0(15)
C014	2433(4)	5195(5)	-603(4)	61.8(17)

C015	5601(4)	5978(4)	2682(4)	63.1(18)
C016	3703(4)	6415(5)	6711(4)	71(2)
C017	6479(5)	7212(6)	2882(5)	86(2)
C018	-1182(4)	4533(5)	4042(5)	96(3)
C019	3715(5)	7260(5)	6706(5)	84(2)
C01A	6407(4)	6365(6)	2877(5)	84(2)
C01B	3375(5)	7689(5)	5948(5)	85(2)
C01C	2263(6)	5115(5)	-1584(4)	97(3)

Table 3 Anisotropic Displacement Parameters ($Å^2 \times 10^3$) for DICIr(CO2)Cl. The Anisotropic displacement factor exponent takes the form: -$2\pi^2[h^2Å^2U_{11}+2hkÅb^*U_{12}+\ldots]$.

Atom	U_{11}	U_{22}	U_{33}	U_{23}	U_{13}	U_{12}
Ir01	39.71(13)	48.09(14)	34.74(12)	-2.41(11)	0.89(9)	-0.67(12)
Cl02	56.6(10)	57.6(9)	60.3(9)	-5.7(8)	1.8(7)	9.8(8)
N004	30(2)	42(3)	33(2)	2(2)	4.9(18)	1(2)
N005	34(2)	48(3)	28(2)	3(2)	3.5(19)	-1(2)
N006	42(3)	46(3)	41(3)	0(2)	12(2)	-1(2)
N007	41(3)	51(3)	34(2)	-4(2)	6(2)	-7(2)
O009	70(3)	72(3)	80(3)	-18(3)	-26(3)	2(3)
O00A	65(3)	68(3)	115(4)	8(3)	-16(3)	17(3)
C00B	34(3)	40(3)	41(3)	-1(3)	5(2)	-1(3)
C00C	36(3)	39(3)	35(3)	9(3)	0(2)	-1(3)
C00D	38(3)	40(3)	35(3)	1(2)	12(2)	11(3)
C00E	36(3)	54(3)	34(3)	-1(3)	8(2)	-6(3)
C00F	37(3)	70(4)	41(3)	-4(3)	5(2)	2(3)
C00G	41(3)	55(4)	35(3)	1(3)	6(2)	-6(3)
C00H	32(3)	60(4)	30(3)	-10(3)	6(2)	-7(3)
C00I	42(3)	54(4)	34(3)	-2(3)	5(2)	-9(3)
C00J	52(4)	56(4)	42(3)	-10(3)	16(3)	-16(3)
C00K	41(4)	103(6)	47(4)	-28(4)	14(3)	-18(4)
C00L	42(3)	60(4)	41(3)	8(3)	6(3)	-3(3)
C00M	51(4)	59(4)	39(3)	0(3)	13(3)	3(3)
C00N	34(3)	53(3)	29(3)	4(2)	4(2)	-2(3)
C00O	68(5)	67(4)	45(4)	-18(3)	20(3)	-29(4)
C00P	54(4)	58(4)	47(4)	-8(3)	2(3)	-7(3)
C00Q	42(4)	69(4)	55(4)	4(3)	0(3)	5(3)
C00R	41(4)	91(6)	50(4)	-20(4)	8(3)	7(4)
C00S	70(4)	75(4)	52(4)	9(3)	23(3)	27(4)
C00T	55(4)	56(4)	53(4)	-1(3)	0(3)	-10(3)

C00U	66(4)	76(5)	36(3)	6(3)	5(3)	9(4)
C00V	49(4)	69(5)	56(4)	9(3)	8(3)	-2(3)
C00W	70(5)	76(5)	49(4)	-8(3)	24(3)	7(4)
C00X	44(4)	71(4)	59(4)	15(3)	11(3)	18(3)
C00Y	33(3)	91(5)	40(3)	-5(3)	5(2)	-19(3)
C00Z	82(5)	57(4)	68(4)	12(3)	32(4)	6(4)
C010	74(5)	70(5)	74(5)	0(4)	17(4)	-20(4)
C011	75(5)	56(4)	55(4)	0(3)	1(3)	-3(4)
C012	53(4)	76(5)	70(4)	3(4)	10(3)	15(4)
C013	50(4)	50(4)	49(3)	0(3)	3(3)	0(3)
C014	69(4)	79(5)	37(3)	-2(3)	13(3)	3(4)
C015	47(4)	61(4)	83(5)	4(4)	18(3)	8(3)
C016	75(5)	91(6)	41(4)	-2(4)	-2(3)	-10(4)
C017	49(5)	121(7)	88(6)	-5(5)	15(4)	-27(5)
C018	56(4)	163(8)	78(5)	-35(5)	31(4)	-43(5)
C019	78(5)	99(6)	63(5)	-36(5)	-4(4)	-22(5)
C01A	38(4)	115(7)	101(6)	-5(5)	16(4)	6(4)
C01B	102(6)	63(5)	84(6)	-21(4)	12(5)	-13(4)
C01C	131(7)	123(7)	38(4)	-8(4)	20(4)	21(6)

Table 4 Bond Lengths for DICIr(CO2)Cl.

Atom	Atom	Length/Å	Atom	Atom	Length/Å
Ir01	Cl02	2.3399(15)	C00H	C00J	1.382(7)
Ir01	C00D	2.070(5)	C00I	C00P	1.369(7)
Ir01	C00Q	1.848(6)	C00I	C011	1.367(8)
Ir01	C00T	1.803(7)	C00J	C00O	1.376(8)
N004	C00C	1.418(6)	C00J	C00Z	1.495(8)
N004	C00D	1.334(6)	C00K	C00O	1.357(9)
N004	C00H	1.444(6)	C00K	C00R	1.358(9)
N005	C00B	1.412(6)	C00K	C018	1.511(8)
N005	C00D	1.337(6)	C00L	C00V	1.368(8)
N005	C00E	1.449(6)	C00L	C015	1.374(8)
N006	C00B	1.245(6)	C00M	C00S	1.486(8)
N006	C00L	1.403(7)	C00M	C00W	1.376(8)
N007	C00C	1.239(6)	C00N	C00X	1.548(7)
N007	C00I	1.399(6)	C00N	C00Y	1.515(7)
O009	C00Q	1.133(7)	C00P	C016	1.360(8)
O00A	C00T	1.125(7)	C00U	C014	1.362(8)
C00B	C00N	1.510(7)	C00V	C010	1.366(8)
C00C	C00N	1.515(7)	C00W	C014	1.373(8)

C00E	C00G	1.385(7)	C010	C017	1.363(10)
C00E	C00M	1.370(7)	C011	C01B	1.359(8)
C00F	C00H	1.378(7)	C014	C01C	1.510(8)
C00F	C00R	1.376(8)	C015	C01A	1.373(9)
C00F	C012	1.492(8)	C016	C019	1.332(9)
C00G	C00U	1.369(7)	C017	C01A	1.340(10)
C00G	C013	1.495(7)	C019	C01B	1.366(10)

Table 5 Bond Angles for DICIr(CO2)Cl.

Atom	Atom	Atom	Angle/°	Atom	Atom	Atom	Angle/°
C00D	Ir01	Cl02	86.87(14)	C00H	C00J	C00Z	121.7(5)
C00Q	Ir01	Cl02	88.33(19)	C00O	C00J	C00H	116.4(6)
C00Q	Ir01	C00D	174.3(2)	C00O	C00J	C00Z	121.8(6)
C00T	Ir01	Cl02	174.7(2)	C00O	C00K	C00R	117.5(6)
C00T	Ir01	C00D	95.8(2)	C00O	C00K	C018	120.1(7)
C00T	Ir01	C00Q	89.3(3)	C00R	C00K	C018	122.4(7)
C00C	N004	C00H	117.5(4)	C00V	C00L	N006	119.4(5)
C00D	N004	C00C	124.5(4)	C00V	C00L	C015	119.0(6)
C00D	N004	C00H	117.4(4)	C015	C00L	N006	121.1(6)
C00B	N005	C00E	117.9(4)	C00E	C00M	C00S	122.7(5)
C00D	N005	C00B	125.0(4)	C00E	C00M	C00W	116.1(6)
C00D	N005	C00E	116.9(4)	C00W	C00M	C00S	121.1(6)
C00B	N006	C00L	130.2(5)	C00B	C00N	C00C	109.6(4)
C00C	N007	C00I	131.1(5)	C00B	C00N	C00X	106.8(4)
N005	C00B	C00N	114.3(4)	C00B	C00N	C00Y	111.9(4)
N006	C00B	N005	114.1(5)	C00C	C00N	C00X	106.3(4)
N006	C00B	C00N	131.5(5)	C00Y	C00N	C00C	111.3(4)
N004	C00C	C00N	113.5(4)	C00Y	C00N	C00X	110.6(4)
N007	C00C	N004	113.7(5)	C00K	C00O	C00J	123.6(6)
N007	C00C	C00N	132.5(5)	C016	C00P	C00I	119.8(6)
N004	C00D	Ir01	122.4(4)	O009	C00Q	Ir01	178.5(6)
N004	C00D	N005	117.8(5)	C00K	C00R	C00F	122.7(6)
N005	C00D	Ir01	119.6(4)	O00A	C00T	Ir01	176.6(6)
C00G	C00E	N005	117.2(5)	C014	C00U	C00G	122.7(6)
C00M	C00E	N005	119.9(5)	C010	C00V	C00L	119.5(6)
C00M	C00E	C00G	122.9(5)	C014	C00W	C00M	123.5(6)
C00H	C00F	C012	122.5(5)	C017	C010	C00V	121.5(7)
C00R	C00F	C00H	117.3(6)	C01B	C011	C00I	120.0(6)
C00R	C00F	C012	120.1(6)	C00U	C014	C00W	117.3(6)
C00E	C00G	C013	122.3(5)	C00U	C014	C01C	121.6(6)

C00U	C00G	C00E	117.1(5)	C00W	C014	C01C	121.1(6)
C00U	C00G	C013	120.6(5)	C01A	C015	C00L	119.9(7)
C00F	C00H	N004	118.8(5)	C019	C016	C00P	121.1(7)
C00F	C00H	C00J	122.0(5)	C01A	C017	C010	118.8(7)
C00J	C00H	N004	119.2(5)	C016	C019	C01B	119.8(7)
C00P	C00I	N007	119.8(5)	C017	C01A	C015	121.1(7)
C011	C00I	N007	120.3(5)	C011	C01B	C019	120.1(7)
C011	C00I	C00P	119.1(5)				

Table 6 Hydrogen Atom Coordinates (Å×10^4) and Isotropic Displacement Parameters (Å^2×10^3) for DICIr(CO2)Cl.

Atom	*x*	*y*	*z*	U(eq)
H00O	275.7	3682.13	4334.73	71
H00P	3340.58	5379.2	5988.43	65
H00R	-584.72	5912.03	3407.79	73
H00A	4330.32	4321.1	1524.57	96
H00B	3773.98	3548.14	1076.97	96
H00C	3576.75	3956.75	1918.64	96
H00U	1771.52	6262.17	-572.09	73
H00V	4425.24	7661.67	2340.45	70
H00W	3201.15	4181.87	-316.08	76
H00D	3587.29	4300.75	3432.68	87
H00E	4003.8	4555.36	4403.67	87
H00F	4556.88	4625.87	3696.31	87
H00G	4864.43	6158.31	4000.98	83
H00H	4353.5	6128.64	4745.4	83
H00I	4097.98	6797.8	3992.2	83
H00J	2196.03	3613.64	3719.37	100
H00K	1697.61	3193.92	4365.8	100
H00L	2338.97	3952.98	4678.56	100
H010	5782.89	8277.07	2659.92	87
H011	2747.58	7550.1	4700.27	78
H01A	718.18	6982.16	3425.08	100
H01B	400.05	6662.76	2459.64	100
H01C	1392.97	6599.52	2936.8	100
H01D	1345.59	6523.36	1210.54	77
H01E	1775.84	7135.29	645.94	77
H01F	2301.11	6857.58	1577.69	77
H015	5562.37	5389.1	2679.52	76
H016	3939.3	6126.16	7226.91	86

H017	7027.09	7469.39	3025.21	103
H01G	-1471.79	4121.27	3623.81	145
H01H	-1534.66	5036.35	3993.59	145
H01I	-1099.06	4304.55	4620.41	145
H019	3954.7	7556.56	7216.62	100
H01J	6910.56	6034.14	3009.12	101
H01K	3398.05	8277.85	5939.81	102
H01L	1648.81	5187.95	-1836.19	146
H01M	2444.16	4564.54	-1733.11	146
H01N	2587.67	5543.01	-1807.57	146

Table 7 Solvent masks information for DICIr(CO2)Cl.

Number	X	Y	Z	Volume	Electron count	Content
1	0.000	0.000	0.500	307.3	86.5	?
2	-0.083	0.194	0.937	27.8	0.0	?
3	0.083	0.806	0.063	27.8	0.0	?
4	0.500	0.500	1.000	307.3	86.5	?
5	0.417	0.306	0.437	27.8	0.0	?
6	0.583	0.694	0.563	27.8	0.0	?

Experimental

Single crystals of $C_{38}H_{38}N_4O_2ClIr$ **[DICIr(CO2)Cl]** were **[]**. A suitable crystal was selected and **[]** on a **dtrek-CrysAlisPro-abstract goniometer imported rigaku-d*trek images** diffractometer. The crystal was kept at 293(2) K during data collection. Using Olex2 [1], the structure was solved with the ShelXT [2] structure solution program using Intrinsic Phasing and refined with the ShelXL [3] refinement package using Least Squares minimisation.

1. Dolomanov, O.V., Bourhis, L.J., Gildea, R.J, Howard, J.A.K. & Puschmann, H. (2009), J. Appl. Cryst. 42, 339-341.
2. Sheldrick, G.M. (2015). Acta Cryst. A71, 3-8.
3. Sheldrick, G.M. (2015). Acta Cryst. C71, 3-8.

Crystal structure determination of [DICIr(CO2)Cl]

Crystal Data for $C_{38}H_{38}N_4O_2ClIr$ (M =810.37 g/mol): monoclinic, space group $P2_1/n$ (no. 14), a = 15.7014(6) Å, b = 15.7693(7) Å, c = 15.7391(6) Å, β = 103.507(4)°, V = 3789.2(3) Å^3, Z = 8, T = 293(2) K, μ(MoKα) = 7.259 mm^{-1}, *Dcalc* = 2.841 g/cm^3, 36079 reflections measured (3.298° ≤ 2Θ ≤ 52.742°), 7745 unique (R_{int} = 0.0849, R_{sigma} = 0.0662) which were used in all calculations. The final R_1 was 0.0392 (I > 2σ(I)) and wR_2 was 0.0911 (all data).

Refinement model description

Number of restraints - 0, number of constraints - unknown.

Details:

1. Fixed Uiso

At 1.2 times of:

All C(H) groups

At 1.5 times of:

All C(H,H,H) groups
2.a Aromatic/amide H refined with riding coordinates:
C00O(H00O), C00P(H00P), C00R(H00R), C00U(H00U), C00V(H00V), C00W(H00W), C010(H010), C011(H011), C015(H015), C016(H016), C017(H017), C019(H019), C01A(H01J), C01B(H01K)
2.b Idealised Me refined as rotating group:
C00S(H00A,H00B,H00C), C00X(H00D,H00E,H00F), C00Y(H00G,H00H,H00I), C00Z(H00J, H00K,H00L), C012(H01A,H01B,H01C), C013(H01D,H01E,H01F), C018(H01G,H01H,H01I), C01C(H01L,H01M,H01N)

This report has been created with Olex2, compiled on 2017.02.24 svn.r3390 for Rigaku Oxford Diffraction. Please let us know if there are any errors or if you would like to have additional features.

LITERATURE CITED

(1) Bertrand, G. U. Y. *Stable Singlet Carbenes*; 2004.

(2) Tomioka, H.; Iwamoto, E.; Itakura, H.; Hirai, K. Generation and Characterization of a Fairly Stable Triplet Carbene. *Nature* **2001**, *412* (6847), 626–628.

(3) Hirai, K.; Hirai, K.; Itoh, T.; Itoh, T.; Tomioka, H.; Tomioka, H. Persistent Triplet Carbenes. *Chem. Rev.* **2009**, *109* (8), 3275–3332.

(4) Gu, S. Y.; Su, M. D. Theoretical Designs for Triplet Ground-State Carbenes: A Target for Experimental Studies. *Chem. Phys. Lett.* **2007**, *443* (4–6), 211–215.

(5) Lavallo, V.; Mafhouz, J.; Canac, Y.; Donnadieu, B.; Schoeller, W. W.; Bertrand, G. Synthesis, Reactivity, and Ligand Properties of a Stable Alkyl Carbene. *J. Am. Chem. Soc.* **2004**, *126* (28), 8670–8671.

(6) Alder, R. W.; Butts, C. P.; Orpen, A. G. Stable Aminooxy-and Aminothiocarbenes. *J. Am. Chem. …* **1998**, No. 8, 11526–11527.

(7) Teuma, E.; Lyon-Saunier, C.; Gornitzka, H.; Mignani, G.; Baceiredo, A.; Bertrand, G. A Stable (Amino)(Phosphino)Carbene as Bidentate Ligand for Palladium and Nickel Complexes: Synthesis, Structure, and Catalytic Activity. *J. Organomet. Chem.* **2005**, *690* (24–25), 5541–5545.

(8) Alder, R. W.; Allen, P. R.; Murray, M.; Orpen, A. G. Bis(Diisopropylamino)Carbene. *Angew. Chemie Int. Ed. English* **1996**, *35* (10), 1121–1123.

(9) Wisniak, J. Eugène Melchior Peligot. *Para Quitarle El Polvo* **2009**, *20* (1), 61–69.

(10) Pauling, L. The Nature of the Chemical Bond. Application of Results Obtained from the Quantum Mechanics and from a Theory of Paramagnetic Susceptibility to the Structure of Molecules. *J. Am. Chem. Soc.* **1931**, *53* (4), 1367–1400.

(11) Priv, V. Neues Uber Carbene. **1961**, No. 5.

(12) Barynmaalz, D.; Siiure, D.; Hyacinthengeruch, V.; Untereuchungen, M.; Mittheilung, V.; Kohlenwaeseretoffee, B.; Toluol, M.; Xvii, D. B.; Xviii, D. B. Buchner Und Th. Curtius: Ueber Die Einwirkun# von DiasoessigBther. 2377–2379.

(13) Breslow, R. On the Mechanism of Thiamine Action. IV. 1 Evidence from Studies on Model Systems. *J. Am. Chem. Soc.* **1958**, *80* (14), 3719–3726.

(14) Dirocco, D. A.; Oberg, K. M.; Rovis, T. Isolable Analogues of the Breslow Intermediate Derived from Chiral Triazolylidene Carbenes. *J. Am. Chem. Soc.* **2012**, *134* (14), 6143–6145.

(15) Wanzlick, H.-W.; Schikora, E. Ein Neuer Zugang Zur Carben-Chemie. *Angew. Chemie* **1960**, *72* (14), 494–494.

(16) Wanzlick, H.-W.; Schikora, E. Ein Nucleophiles Carben. *Chem. Ber.* **1961**, *94*, 2389–2393.

(17) Igau, A.; Grutzmacher, H.; Baceiredo, A.; Bertrand, G. Analogous α,α'-Bis-Carbenoid Triply Bonded Species: Synthesis of a Stable Λ3-Phosphinocarbene- Λ5-Phosphaacetylene. *J. Am. Chem. Soc.* **1988**, *110* (10), 6463–6466.

(18) Arduengo, A. J.; Kline, M.; Harlow, R. L. A Stable Crystalline Carbene. *J. Am. Chem. Soc.* **1991**, *113* (1), 361–363.

(19) Arduengo, III, A. J.; Krafczyk, R. Auf Der Suche Nach Stabilen Carbenen. *Chemie Unserer Zeit* **1998**, *32* (1), 6.

(20) Kelly III, R. a.; Clavier, H.; Giudice, S.; Scott, N. M.; Stevens, E. D.; Bordner, J.; Samardjiev, I.; Hoff, C. D.; Cavallo, L.; Nolan, S. P. Determination of N-Heterocyclic Carbene (NHC) Steric and Electronic Parameters Using the [(NHC)Ir(CO) 2 Cl] System. *Organometallics* **2008**, *27* (2), 202–210.

(21) Arduengo, A. J.; Dias, H. V. R.; Harlow, R. L.; Kline, M. Electronic Stabilization of Nucleophilic Carbenes. *J. Am. Chem. Soc.* **1992**, *114* (14), 5530–5534.

(22) Lavallo, V.; Canac, Y.; Präsang, C.; Donnadieu, B.; Bertrand, G. Stable Cyclic (Alkyl)(Amino)Carbenes as Rigid or Flexible, Bulky, Electron-Rich Ligands for Transition-Metal Catalysts: A Quaternary Carbon Atom Makes the Difference. *Angew. Chemie - Int. Ed.* **2005**, *44* (35), 5705–5709.

(23) Rao, B.; Tang, H.; Zeng, X.; Liu, L.; Melaimi, M.; Bertrand, G. Cyclic (Amino)(Aryl)Carbenes (CAArCs) as Strong σ-Donating and π-Accepting Ligands for Transition Metals. *Angew. Chemie - Int. Ed.* **2015**, *54* (49), 14915–14919.

(24) Pauling, L. The Structure of Singlet Carbene Molecules. *J. Chem. Soc. Chem. Commun.* **1980**, No. 15, 688–689.

(25) No Title. *Synthesis (Stuttg).* **1993**, *16*, 561.

(26) Lennard-Jones, L. E. T h e Electronic Structure of some Diatomic Molecules. *Trans. Faraday Soc.* **1929**, *25* (668), 668–686.

(27) Carter, E. A.; Goddard, W. A. Correlation-Consistent Singlet-Triplet Gaps in Substituted Carbenes. *J. Chem. Phys.* **1988**, *88* (3), 1752–1763.

(28) Iwamoto, E.; Hirai, K.; Tomioka, H. A Triplet Carbene Surviving a Week in Solution at Room Temperature. *J. Am. Chem. Soc.* **2003**, *125* (48), 14664–14665.

(29) Arduengo, A. J.; Davidson, F.; Dias, H. V. R.; Goerlich, J. R.; Khasnis, D.; Marshall, W. J.; Prakasha, T. K. An Air Stable Carbene and Mixed Carbene “Dimers.” *J. Am. Chem. Soc.* **1997**, *119* (52), 12742–12749.

(30) Organ, M. G.; Abdel-Hadi, M.; Avola, S.; Dubovyk, I.; Hadei, N.; Kantchev, E. A. B.; O'Brien, C. J.; Sayah, M.; Valente, C. Pd-Catalyzed Aryl Amination Mediated by Well Defined, N-Heterocyclic Carbene (NHC)-Pd Precatalysts, PEPPSI. *Chem. - A Eur. J.* **2008**, *14* (8), 2443–2452.

(31) Nguyen, S. B. T.; Johnson, L. K.; Grubbs, R. H. Ring-Opening Metathesis Polymerization (ROMP) of Norbornene by a Group VIII Carbene Complex in Protic Media. *J. Am. …* **1992**, *114* (8), 3974–3975.

(32) Jones, G. O.; Chang, Y. A.; Horn, H. W.; Acharya, A. K.; Rice, J. E.; Hedrick, J. L.; Waymouth, R. M. N-Heterocyclic Carbene-Catalyzed Ring Opening Polymerization of ε-Caprolactone with and without Alcohol Initiators: Insights from Theory and Experiment. *J. Phys. Chem. B* **2015**, *119* (17), 5728–5737.

(33) Hudnall, T. W.; Bielawski, C. W. An N,N???-Diamidocarbene: Studies in C-H Insertion, Reversible Carbonylation, and Transition-Metal Coordination Chemistry. *J. Am. Chem. Soc.* **2009**, *131* (44), 16039–16041.

(34) Frey, G. D.; Lavallo, V.; Donnadieu, B.; Schoeller, W. W.; Bertrand, G. Facile Splitting of Hydrogen and Ammonia by Nucleophilic Activation at a Single Carbon Center. *Science (80-.).* **2007**, *316* (5823), 439–441.

(35) Moerdyk, J. P.; Bielawski, C. W. Reductive Generation of Stable, Five-Membered N,N′-Diamidocarbenes. *Chem. Commun.* **2014**, *50* (35), 4551–4553.

(36) Moerdyk, J. P.; Schilter, D.; Bielawski, C. W. N,N'-Diamidocarbenes: Isolable Divalent Carbons with Bona Fide Carbene Reactivity. *Acc. Chem. Res.* **2016**, *49* (8), 1458–1468.

(37) Huisgen, R. Altes Und Neues Über Aliphatische Diazoverbindungen. *Angew. Chemie* **1955**, No. 17, 439–463.

(38) Scholl, M.; Ding, S.; Lee, C. W.; Grubbs, R. H. Synthesis and Activity of a New Generation of Ruthenium-Based Olefin Metathesis Catalysts Coordinated with 1,3-Dimesityl-4,5-Dihydroimidazol-2-Ylidene Ligands. *Org. Lett.* **1999**, *1* (6), 953–956.

(39) Base, L.; Carbene, C.; Moore, J. L.; Rovis, T. *Asymmetric Organocatalysis*; 2009; Vol. 291.

(40) Wei, S.; Wei, X. G.; Su, X.; You, J.; Ren, Y. Insight into the Role of the Counteranion of an Imidazolium Salt in Organocatalysis: A Combined Experimental and Computational Study. *Chem. - A Eur. J.* **2011**, *17* (21), 5965–5971.

(41) Nyce, G.; Glauser, T.; Connor, E. F.; Möck, A.; Waymouth, R. M.; Hedrick, J. L. In Situ Generation of Carbenes: A General and Vesatile Plattform for Organocatalytic Living Polymerization. *J. Am. Chem. Soc.* **2003**, *125* (5), 3046–3056.

(42) Ledet, A. D.; Hudnall, T. W. Reduction of a Diamidocarbene-Supported Borenium Cation: Isolation of a Neutral Boryl-Substituted Radical and a Carbene-Stabilized Aminoborylene. *Dalt. Trans.* **2016**.

(43) Lavallo, V.; Canac, Y.; Donnadieu, B.; Schoeller, W. W.; Bertrand, G. CO Fixation to Stable Acyclic and Cyclic Alkyl Amino Carbenes: Stable Amino Ketenes with a Small HOMO-LUMO Gap. *Angew. Chemie - Int. Ed.* **2006**, *45* (21), 3488–3491.

(44) Hudnall, T. W.; Moerdyk, J. P.; Bielawski, C. W. Ammonia N – H Activation by a N , N 0 -Diamidocarbene W. *Chem. Commun.* **2010**, No. 46, 4288–4290.

(45) Turner, Z. R. Chemically Non-Innocent Cyclic (Alkyl)(Amino)Carbenes: Ligand Rearrangement, C−H and C−F Bond Activation. *Chem. - A Eur. J.* **2016**, *22* (32), 11461–11468.

(46) Krysiak, J.; Kato, T.; Gornitzka, H.; Baceiredo, A.; Mikolajczyk, M.; Bertrand, G. The First Asymmetric Cyclopropanation Reactions Involving a Stable Carbene. *J. Org. Chem.* **2001**, *66* (24), 8240–8242.

(47) Moerdyk, J. P.; Bielawski, C. W. Diamidocarbenes as Versatile and Reversible [2+1] Cycloaddition Reagents. *Nat. Chem.* **2012**, *4* (4), 275–280.

(48) McCarty, Z. R.; Lastovickova, D. N.; Bielawski, C. W. A Cyclic (Alkyl)(Amido)Carbene: Synthesis, Study and Utility as a Desulfurization Reagent. *Chem. Commun.* **2016**, *52* (31), 5447–5450.

(49) Maas, G. Ruthenium-Catalysed Carbenoid Cyclopropanation Reactions with Diazo Compounds. *Chem. Soc. Rev.* **2004**, *33* (3), 183.

(50) Perera, T. A.; Reinheimer, E. W.; Hudnall, T. W. Photochemically Switching Diamidocarbene Spin States Leads to Reversible Büchner Ring Expansions. *J. Am. Chem. Soc.* **2017**, jacs.7b09264.

(51) Verlinden, K.; Buhl, H.; Frank, W.; Ganter, C. Determining the Ligand Properties of N-Heterocyclic Carbenes from 77Se NMR Parameters. *Eur. J. Inorg. Chem.* **2015**, *2015* (14), 2416–2425.

(52) Tolman, C. A. Steric Effects of Phosphorus Ligands in Organometallic Chemistry and Homogeneous Catalysis. *Chem. Rev.* **1977**, *77* (3), 313–348.

(53) Back, O.; Henry-Ellinger, M.; Martin, C. D.; Martin, D.; Bertrand, G. 31P NMR Chemical Shifts of Carbene-Phosphinidene Adducts as an Indicator of the π-Accepting Properties of Carbenes. *Angew. Chemie - Int. Ed.* **2013**, *52* (10), 2939–2943.

(54) Rodrigues, R. R.; Dorsey, C. L.; Arceneaux, C. A.; Hudnall, T. W. Phosphaalkene vs. Phosphinidene: The Nature of the P–C Bond in Carbonyl-Decorated Carbene → PPh Adducts. *Chem. Commun.* **2014**, *50* (2), 162–164.

(55) Liske, A.; Verlinden, K.; Buhl, H.; Schaper, K.; Ganter, C. Determining the π - Acceptor Properties of N - Heterocyclic Carbenes by Measuring the 77 Se NMR Chemical Shifts of Their Selenium Adducts. *Organometallics* **2013**, *32*, 5269.

(56) Gaussian 09, Revision A.02, M. J. Frisch, G. W. Trucks, H. B. Schlegel, G. E. Scuseria, M. A. Robb, J. R. Cheeseman, G. Scalmani, V. Barone, G. A. Petersson, H. Nakatsuji, X. Li, M. Caricato, A. Marenich, J. Bloino, B. G. Janesko, R. Gomperts, B. Mennucci, H. P. Hratchian, J. V. Ortiz, A. F. Izmaylov, J. L. Sonnenberg, D. Williams-Young, F. Ding, F. Lipparini, F. Egidi, J. Goings, B. Peng, A. Petrone, T. Henderson, D. Ranasinghe, V. G. Zakrzewski, J. Gao, N. Rega, G. Zheng, W. Liang, M. Hada, M. Ehara, K. Toyota, R. Fukuda, J. Hasegawa, M. Ishida, T. Nakajima, Y. Honda, O. Kitao, H. Nakai, T. Vreven, K. Throssell, J. A. Montgomery, Jr., J. E. Peralta, F. Ogliaro, M. Bearpark, J. J. Heyd, E. Brothers, K. N. Kudin, V. N. Staroverov, T. Keith, R. Kobayashi, J. Normand, K. Raghavachari, A. Rendell, J. C. Burant, S. S. Iyengar, J. Tomasi, M. Cossi, J. M. Millam, M. Klene, C. Adamo, R. Cammi, J. W. Ochterski, R. L. Martin, K. Morokuma, O. Farkas, J. B. Foresman, and D. J. Fox, Gaussian, Inc., Wallingford CT, 2016.

(57) Makhlou, A.; Wahl, M.; Frank, W.; Ganter, C. A New Mixed Amino − Amido N-Heterocyclic Carbene Based on Anthranilic Acid. *Organometallics* **2013**, *32* (4), 854–861.

(58) Blake, G. A.; Moerdyk, J. P.; Bielawski, C. W. Tuning the Electronic Properties of Carbenes: A Systematic Comparison of Neighboring Amino versus Amido Groups. *Organometallics* **2012**, *31* (8), 3373–3378.

(59) Dragisich, V.; Wulff, W. D.; Hoogsteen, K. Imino Carbene Complexes of Tungsten and Chromium as Synthons for Nitrile Ylides in Reactions with Alkynes, Alkenes, Nitriles, and Aldehydes. *Organometallics* **1990**, *9* (11), 2867–2870.